Behavior of Riveted Connections in Steel Truss Bridges

Saura M. Jost

A thesis submitted in partial fulfillment of the
requirements for the degree of

Master of Science in Civil Engineering

University of Washington

2012

Committee Members:

Jeffrey W. Berman

Charles W. Roeder

Dawn E. Lehman

Program Authorized to Offer Degree:
Civil and Environmental Engineering

University of Washington

Abstract

Behavior of Riveted Connections in Steel Truss Bridges

Saura M. Jost

Chair of Supervisory Committee:

Professor Jeffrey W. Berman

Department of Civil and Environmental Engineering

Current recommendations provided by the Federal Highway Administration (FHWA) for load rating of steel truss bridges were shown to be overly conservative in estimating the rivet capacity in shear by researchers from the University of Washington. Many steel truss bridges in place were constructed during the mid 20th century and require such load rating to determine if retrofitting, tear down, or a live loading limit is necessary. Past research on riveted connections has not included tests on as-built riveted connections, but rather shop fabricated specimens. Therefore, an enhanced understanding of ultimate rivet shear strength in gusset plates and the relation to connection length could improve the current procedure.

Experiments on secondary riveted joints with various connection lengths were tested in a Universal Testing Machine (UTM) to determine the average ultimate shear strength of the rivets. The riveted connection was assembled with supporting members to improve capacity and stability and allow for testing of longer connections through shear failure. The test setup used for this investigation placed each rivet under a uniform load. This differed from previous research performed by Fisher and Rumpf (1967) on lap splices. Their loading mechanism caused the average ultimate strength of the rivets to decrease as connection length increases, and therefore a reduction factor was recommended by AASHTO for connections greater than 50 inches. The results of this test program in combination of past research will serve as an upper and lower bound, respectively, for connection behavior.

Results showed that the average ultimate rivet shear strength was not a function of connection length under the designed load mechanism. The average ultimate rivet shear

strength was larger than the values used in the load rating procedure and past research. The connecting elements deformed prior to failure of the rivets, which is a result of the rivets being stronger than the nominal values from the time of construction. This suggest that for gusset plate connections loaded in a distributed manner, that a reduction factor for ultimate rivet strength may not be needed, and there is potential that current reduction factors for longer connections could be reduced.

Acknowledgements

Dedication

For RLW & BB.

Table of Contents

List of Figures

ix

List of Tables

Chapter 1: Introduction

1.1   Statement of Problem

Following the collapse of the I-35W Bridge in Minneapolis, MN, there was motivation to investigate gusset plate connections in steel truss bridges from the same era across the country. Research on load rating of gusset plate connections performed by the University of Washington determined that rivet shear strength controlled the capacity of many of the connections that were evaluated. One key finding was that the recommended rivet shear strengths given in the AASHTO Manual for Bridge Evaluation (2011) were considerably lower than the ultimate rivet shear strengths found in the literature. The low strength recommendations suggested that the rivets needed replacement; however, when historical test data was considered, it was found that replacement was not necessary. This could lead to expensive rivet replacement, unnecessarily. Past research performed by Fisher and Rumpf (1967) lead to an inclusion of a reduction factor in current calculations for riveted joints longer than 50 in. This reduction factor could also lead to an estimate of connection strength that is lower than the actual strength. The Washington State Department of Transportation's (WSDOT) observations and past research on connection length effect prompt a need to determine rivet shear strength and its relation to connection length from the actual steel bridges through experimental research.

1.2   Objectives

WSDOT has salvaged components from three Washington State steel truss bridges that were built in the 1930s. WSDOT has made these available to researchers at the University of Washington, providing an opportunity to examine the objectives listed below. These components include miscellaneous riveted connections, individual rivets, and full truss bridge joints.

The objectives of the research program described in this thesis were developed to leverage the available vintage bridge components and address the problem statement above.

Specifically the goals are to:

- Perform experiments on aged riveted joints to provide an explanation for the length effect of riveted connections
- Determine the actual shear strengths of rivets and compare them to current FHWA recommendations, AASHTO Manual for Bridge Evaluation, and past research

Achieving these objectives will lead to the following outcomes:

- Adjustments to current methods used in design and evaluation of riveted connections
- More accurate data on as-built structures for bridge evaluations

The bridges in the research program are representative of many in place across the country, and a better understanding of the controlling mechanisms in such bridges will provide insight to the behavior of older riveted structures. Achieving these objectives will save the U.S. Department of Transportation significant time and money on inspection and maintenance costs by improving the efficiency of the load rating procedure for steel truss bridges.

1.3   Scope of Work

The research began with a comprehensive literature review of past experiments on rivets and riveted joints with a focus on joint length. In addition, material properties of the vintage grades of structural and rivet steel were gathered to predict the strength of the connecting elements and rivets under load. Current methods of evaluating riveted connections provided by the FHWA and AASHTO were also reviewed to investigate how connections are currently evaluated.

The experimental program consisted of testing riveted joints of various lengths from 10 - 79 inches (corresponding to a connection length of 2 - 18 rivets). They were tested using the universal testing machines (UTM) in the University of Washington Structures Lab.

The bridge components were modified and assembled into a configuration that loaded the rivets in shear. Two separate test configurations were designed to allow for testing of connections of varying length. Shorter connections were tested in a 300-kip UTM, while the longer connections were tested in a 2400-kip UTM.

1.4   Organization of Thesis

This thesis begins with a literature review of past research and design guidelines for riveted connections in Chapter 2. Chapter 3 outlines the development of the test specimen design, the expected behavior of the specimen, and test setup. Chapter 4 provides material test results and a summary of the experimental observations for each test. Chapter 5 includes an analysis and discussion of results. Chapter 6 gives recommendations and conclusions based on experimental results. A list of references and appendices are included following the final chapter. Appendix A includes the ASTM Historical Standards that were used to determine the nominal and expected strengths of the rivet and structural steel from the time of construction. Appendix B includes additional graphs from the bridge study analyzing the yielding in gusset plate connections from Section 3.4.5. Appendix C includes a set of sample calculations for the test specimen design. Appendix D includes the shop drawings for the test specimens. Appendix E includes additional data from the experiments.

Chapter 2: Literature Review

2.1 General

The following chapter summarizes literature on riveted joints and rivet fasteners including experimental research and design guidelines. The first section gives background information on rivets and the installation process. The subsequent sections summarize experiments from the literature dating from 1905-2010 by describing the test program and objectives, material test data, test specimen configuration, and relevant conclusions. For some experimental programs, the rivet ultimate strength versus connection length is plotted, as this is the primary motivation of the experiments discussed later in this thesis. The final section summarizes the rivet evaluation section of the current FHWA and AASHTO guidelines for load rating of bridges followed by a summary of the literature review.

2.2 Rivet Background Information

2.2.1 General

At the turn of the 20th century when iron and steel were introduced, rivets became the preferred fastener because of the clamping force they provided. However, the axial force in the rivets, which provides the clamping force, varied considerably, making them difficult to evaluate. The use of such fasteners has declined as more consistent high-strength bolts became available in the early 1930s (D'Aniello, Portioli, & Landolfo, 2011).

In the present day, riveted connections are rarely used in the field or in machine shops, but they are still of interest. Many steel bridges and railroads built in the beginning of the 20th century are still in place, and understanding riveted connections is important to evaluate and retrofit these structures. Specifications from 1986 recognized three structural rivet steels as described in Table 2.1 (adapted from (Kulak, Fisher, & Struik, 1987)).

Table 2.1 Rivet Structural Steels (Kulak, Fisher, & Struik, 1987)

ASTM A502	Composition	Use
Grade 1	Carbon Rivet Steel	General purpose
Grade 2	Carbon-Manganese Rivet Steel	Can be used with high-strength carbon and high-strength low alloy structural steels
Grade 3	Carbon-Manganese Rivet Steel	Grade 2 with enhanced corrosion resistance

2.2.2   Installation process

To install a rivet, it is inserted into matching holes that are 1/16 in. greater than the nominal diameter of the un-driven-rivet. The rivet head is formed on the projecting end of the shank, and the opposite head is formed by either squeezing with a pressure riveter (often done in the shop) or by accelerated pounding with a pneumatic hammer (in the shop or field). As a result, the hole clearance decreases due to the increase in the diameter of the driven-rivet. Typically for short grip rivets the hole is filled completely, but for larger grip lengths, the hole clearance becomes larger (Kulak, Fisher, & Struik, 1987). Figure 2.1 depicts an installed rivet.
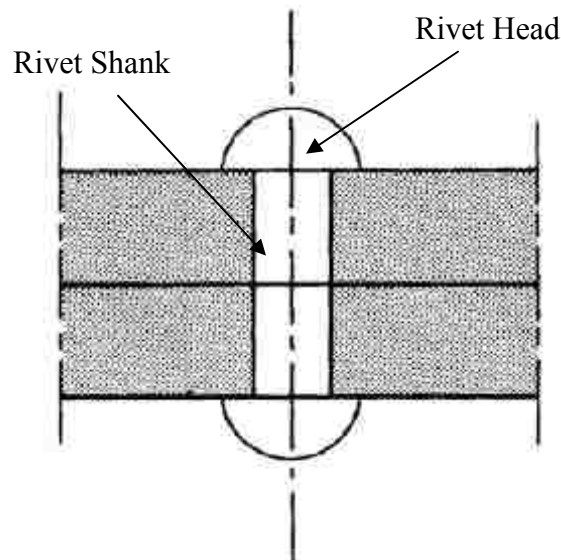
Figure 2.1 Installed Rivet (Kulak, Fisher, & Struik, 1987)

In the shop, rivets can be driven hot by heating them to 1800 °F (most common) or cold. The plies draw together with installation bolts and rivet equipment. As the rivet cools the plies are squeezed together creating a residual clamping force in the rivet. This causes the rivet to shrink in diameter and longitudinally. Hot-driven rivets are capable of developing clamping forces near the yield force of the rivet. The magnitude of this clamping force also depends on the joint stiffness, the driving method, pressure, time, and the finishing temperature. This clamping force is essential to the slip resistance of the connection but does not influence the ultimate strength of the connection.

2.3 Review of Relevant Literature

The literature reviewed in the following section was selected on the basis that it involved experiments on riveted connections by loading in shear or it compiled historical information on rivet shear strength. Where appropriate, rivet ultimate strength data was plotted versus connection length when rivet shear was the failure mechanism.

2.3.1 American Railway Engineering and Maintenance-of-Way Association (1905)

The American Railway Engineering and Maintenance-of-Way Association (AREMA) performed tests on various types of riveted joints. Ninety tests were performed consisting of five tests on each of 18 connection types. The 18 connection types consisted of a single shear lap splice in lengths of one to three rivets, a double shear butt splice with 2-6 rivets in a line, a double shear butt splice with 6-10 rivets in a line with a single filler plate and two-filler plates, and various staggered rivet patterns with two to four filler plates. Figure 2.2, Figure 2.3, and Figure 2.4, show the various connection types.

In the test specimens, rivet holes were punched with a 15/16 in. diameter and a die of 1 in. diameter with no reaming except to make the holes. The contact surface was painted with graphite paint. Prior to being driven with a stationary pressure riveter, the rivets had a 7/8 in. diameter.
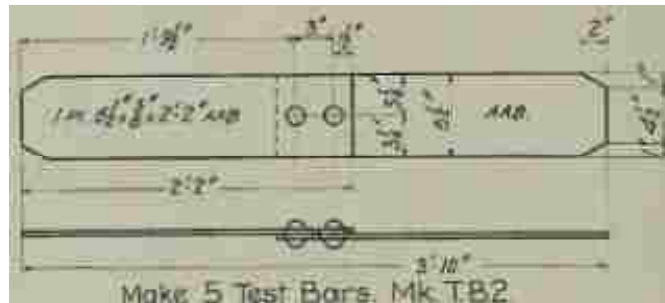
Figure 2.2 Lap Splice Joint (AREMA, 1905)
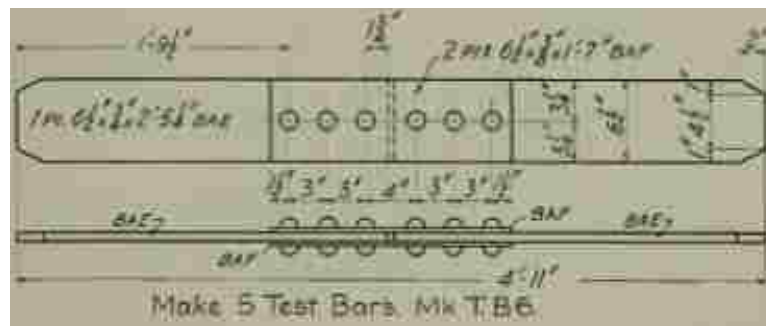
Figure 2.3 Butt Splice Joint (AREMA, 1905)
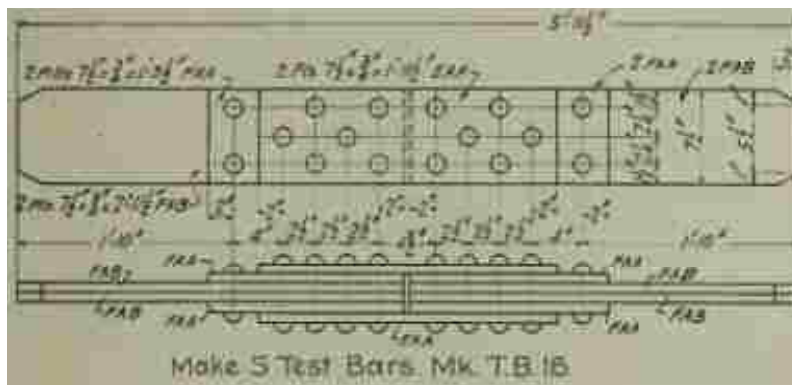
Figure 2.4 Splice Joint with Filler Plates and Staggered Pattern (AREMA, 1905)

The specimens were tested in a 400-kip screw power driven Riehle lever machine, and the ends of specimens were held in head blocks by wedges. Micro-extensometers were attached to the end of the splice plates and a 1-kip (1000 pound) load was applied until they were able to read. As the load was increased incrementally, readings from the micro-extensometers were taken until the maximum load was attained.

From these tests, the following conclusions were made regarding riveted connection behavior:

1. The friction between surfaces held in contact by the rivets provided resistance for the joint against shear deformation.

2. The yield point of the joint occurred when the shearing forces equaled friction resistance of the surfaces held in contact.

3. At the yield point, slipping of surfaces in contact caused the riveted joint to deform. This was due to the space left between the rivet and edge of the hole after a hot driven-rivet cools and decreases in size.

4. Once the rivet began bearing against the edge of the hole after slip, deformation of the rivet body took place, and the resistance rapidly increased until the rivet reached its ultimate shear strength.

5. Lap joints with an unsymmetrical distribution of rivets deflected sideways under strain, which placed the rivets in tension and reduced their clamping force holding the surfaces together.

6. The strength of a riveted joint was reduced when filler plates were inserted between main plates, but the full strength could be obtained by connecting the fillers to main plates with additional rivets.

7. The strength of a riveted joint with a rivet grip more than four times the rivet diameter decreased as the grip length increased.

8. If the rivet grip is larger than four times the diameter, the number of rivets should be increased by at least 1% for each 1/16 in. increase in grip. This will obtain the same strength as a joint with the same length and a grip shorter than four times the diameter.

9. A riveted joint with forces in the same direction can safely be loaded beyond yield until rivets bear on the rivet holes. However, with alternated forces in the opposite direction, it is unsafe to strain the joint up to the yield point.

10. Holes in component pieces must match and the driving tool should distress the rivet throughout its length so that the rivet hole is filled to obtain the minimum slip at yield.

The ultimate rivet shear strength data from each of the 90 tests is presented in Table 2.2 (gathered from (AREMA, 1905)). Test specimens TB1-3 were single shear splices and all remaining tests were butt splices.

Table 2.2 Ultimate Rivet Shear Strengths (AREMA, 1905)

Test	No. Rivets	Pitch [in.]	Joint Length [in.]	Average Ultimate Rivet Shear $V_{u,avg}$ [psi]					Avg. [ksi]
				1	2	3	4	5	
TB1	1	0	0	53218	36587	54879	54547	55711	51.0
TB2	2	3	3	47563	48395	48229	48062	49070	48.3
TB3	3	3	6	45734	44902	45457	47120	45734	45.8
TB4	2	0	0	53467	50723	52120	52386	51555	52.1
TB5	4	3	3	50139	50430	50555	50888	52385	50.9
TB6	6	3	6	48507	45336	47370	47883	45541	46.9
TB7	6	3	6	50031	47841	45707	50890	49172	48.7
TB8	8	3	9	48782	48949	49476	50446	49892	49.5
TB9	10	3	12	48782	48937	48782	50446	56843	50.8
TB10	6	3	6	46289	50779	45041	52109	47480	48.3
TB11	8	3	9	48782	44015	50058	51416	50779	49.0
TB12	10	3	12	53911	41577	41577	41577	41577	44.0
TB13	4	5	7.5	48783	54687	49240	48506	51485	50.5
TB14	4	5	7.5	46912	46566	44002	47674	45110	46.1
TB15	6	4.5	11.5	49199	48021	46843	48090	46843	47.8
TB16	6	4.5	11.5	48409	45041	45873	50030	48506	47.6
TB17	6	4.5	11.5	45388	44625	44348	45457	44903	44.9
TB18	6	4.333	15.5	45457	46288	47259	46330	46150	46.3

Figure 2.5 shows the average ultimate shear strength of the five tests performed from each of the 18 connection types. The legend specifies the type of splice and pitch of rivets, where "Single_Shear_Splice_3_in." corresponds to the test of a tension splice in single shear with rivets spaced at three inches center-to-center. In addition, the data were plotted with the strength of the rivets predicted by current AASHTO recommendations, where the ultimate rivet shear strength was approximated as 67% of the ultimate rivet tensile strength. In addition, the formula includes a reduction factor that depends on connection length (AASHTO, American Association of State Highway and Transportation Officials, 2011) from Eq. 2-9. The ultimate shear strength appears to decrease overall as connection length

increases, as predicted by AASHTO, however, the longest connection is only 15.5 in. The approximate average shear stress for all 90 tests was 48.25 ksi.
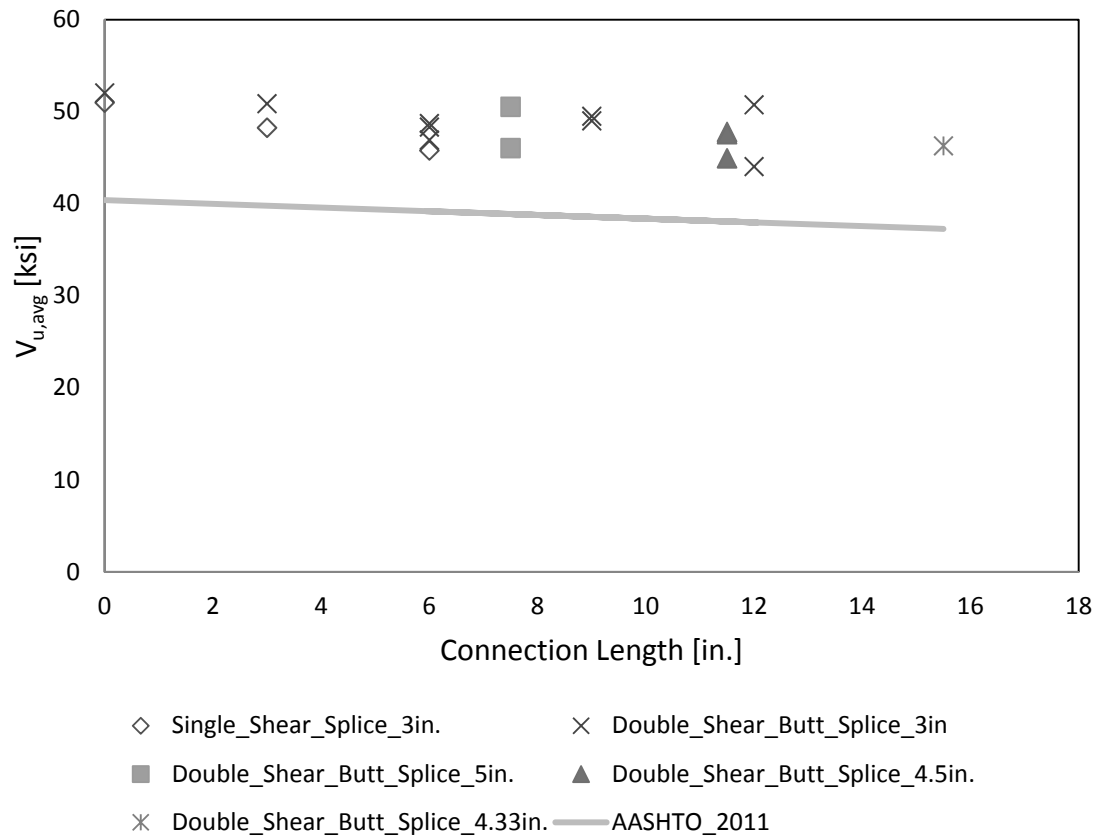
Figure 2.5 Average Ultimate Rivet Shear Strength vs. Connection Length (AREMA, 1905)

In addition to connection length, the grip of the rivets (L_g) also varied between tests. The average rivet shear strength was also plotted versus the connection length normalized by the rivet grip to determine if the grip had an effect as shown in Figure 2.6. This plot shows that the rivet shear strength decreases for larger rivet grips but does not vary significantly.
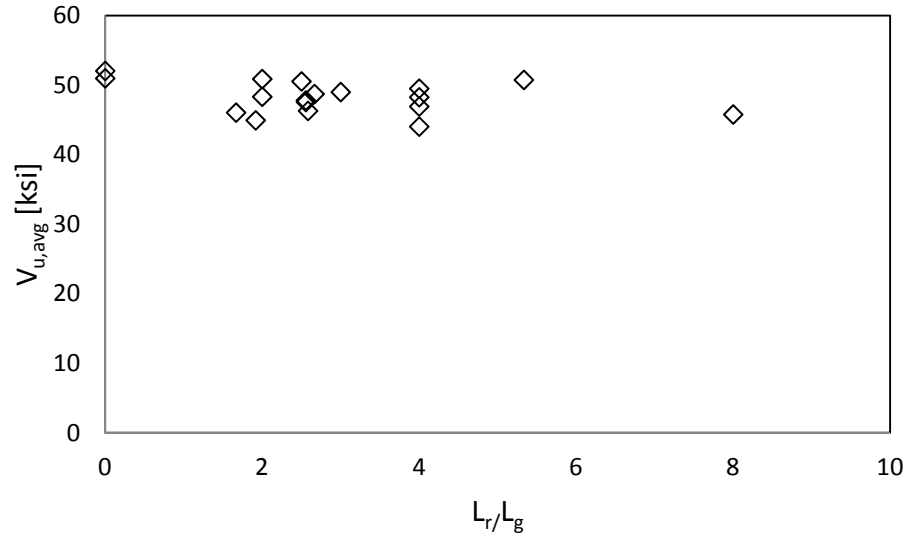
Figure 2.6 Average Ultimate Rivet Shear Strength vs. L_r/L_g (AREMA, 1905)

Another parameter studied was the effect of rivet pitch on the connection length effect. Figure 2.7 plots the average rivet shear strength against the connection length divided by the rivet pitch (p). This plot shows that the rivet strength does not vary significantly with rivet pitch. This relationship was also found in other data presented in this literature review where pitch or rivet grip was varied.
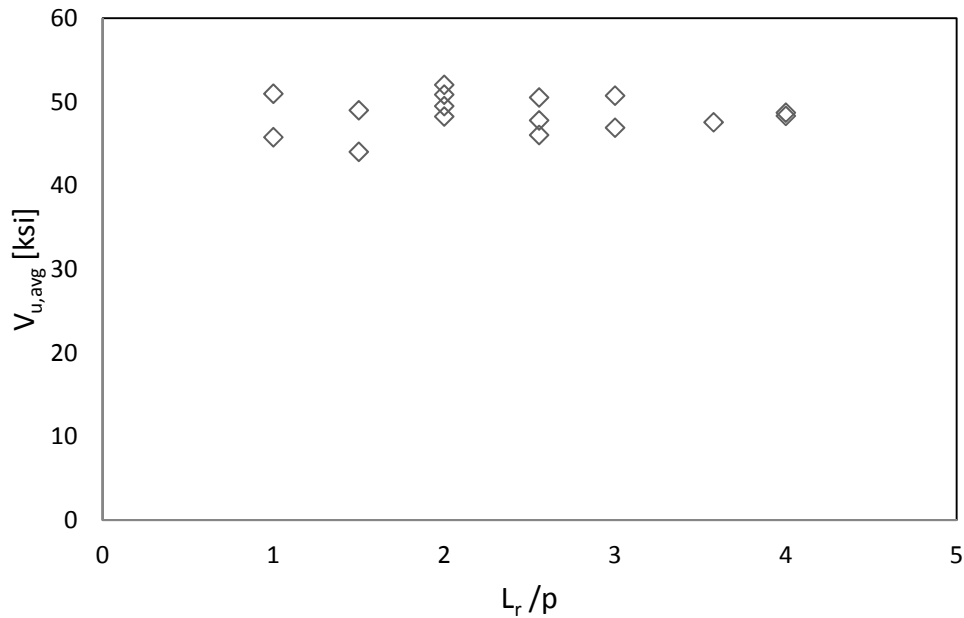
Figure 2.7 Average Ultimate Rivet Shear Strength vs. L_r/p (AREMA, 1905)

2.3.2 Talbot and Moore (1911)

Talbot and Moore performed equivalent tests to AREMA except they tested nickel-steel (Ni-steel) and chrome-nickel-steel (Cr-Ni-steel) riveted joints. This was motivated by the Board of Engineers of the Quebec Bridge's consideration of using nickel-steel to reconstruct a bridge over the St. Lawrence River that had collapsed during construction.

Five or more of each of the 18 connection types (same as AREMA tests) were tested in tension using Ni-steel. For Cr-Ni-steel, 56 tests were performed in tension. In addition, 16 Ni-steel and 16 Cr-Ni-steel joints were tested in tension, compression, and alternate tension and compression.

Some of the Ni-steel joints used rivets that were formed using a hydro-pneumatic riveter while others were made using a hand-pneumatic hammer. In contrast, all of the Cr-Ni-steel joints utilized a hydro-pneumatic riveter to form the rivets. The material properties for the rivets (tensile yielding, ultimate tensile strength) were gathered from the tension tests as shown below in Table 2.3 (Talbot & Moore, 1911). The bottom row shows an approximation for the ultimate rivet shear strength taken as the ultimate tensile strength divided by $\sqrt{3}$.

Table 2.3 Rivet Material Properties (Talbot & Moore, 1911)

Property	Ni- Steel	Cr-Ni Steel
F_y (ksi)	45	38.4
F_u (ksi)	68.5	59
Approx. Shear Strength (ksi)	39.55	34.06

From these tests, the following observations and conclusions were made by Talbot and Moore (1911):

1. Slip of the joint occurred at loads within ordinary working shear stress of the rivet.
2. A regular increase in slip of the joint occurred to a marked load where the average shear stress in the rivet was 35 ksi for the Ni-steel riveted joints. At this point in the test, bending of the rivet occurred.
3. All riveted joints failed by shearing of the rivets, and the ultimate shear stress did not differ significantly between Ni-steel and Cr-nickel-steel rivets.

4. The resistance of a joint up to first noticeable slip of the rivet was more dependent on the workmanship of riveting rather than the quality of rivet material. In addition, it is likely that grip length also had an influence.

5. The yield point of a riveted joint is defined as the load at which a marked increase of force occurs and it was found to be close to the first bending of the rivet. For longer-rivets, the importance of resistance to bending is higher.

6. The strength of the riveted material, which is influenced by the relative hardness of rivets and plates, determines the ultimate shear strength of the riveted joints.

7. The ratio of the yield to the ultimate shear strength of the riveted joint was about the same as the ratio between yield and ultimate tensile strength of the plate material.

8. For-riveted joints designed for ultimate strength it was found that the strength of the rivet material and plate could be improved by considering special steels.

9. For-riveted joints designed for clamping force of rivets (without bending) it was found that special steels will not improve strength as they perform similarly to carbon-steel rivets up to first slip.

The results of the tests, which were identical in geometry to those conducted by AREMA, are given in Table 2.4 (gathered from (Talbot & Moore, 1911)). The average ultimate rivet shear strength was calculated for each of the 18 tests specimens as the average of the shop and field riveted specimens.

Table 2.4 Ultimate Rivet Shear Tests for Nickel-steel and Chrome-Nickel steel (Talbot & Moore, 1911)

Test Specimen	No. Rivets/Row	Connection Length [in.]	Average Ultimate Rivet Shear $V_{u,avg}$ [psi]	
			Ni-steel	Cr-Ni Steel
TB1	1	0	60140	55550
TB2	2	3	58080	56330
TB3	3	6	56120	55100
TB4	2	4	57720	56650
TB5	4	10	55120	54970
TB6	6	16	56960	54910
TB7	6	16	56460	51950
TB8	8	22	58460	53280
TB9	10	28	57880	54260
TB10	6	16	54760	48190
TB11	8	22	57160	51860
TB12	10	28	58200	52350
TB13	4	19.5	57000	52500
TB14	4	19.5	52440	48570
TB15	6	27.5	55340	51120
TB16	6	27.5	55860	52010
TB17	6	27.5	55140	50470
TB18	6	35.5	55320	51050
		Average	**56564**	**52840**

Figure 2.8 shows the variation of ultimate shear strength with connection length for Ni-steel and the same plot for Cr-Ni steel is shown in Figure 2.9, and both include the strength calculated by AASHTO. It appears that ultimate rivet shear strength decreases overall as connection length increases more than AASHTO would predict both steel types. In addition, Ni-steel has a larger strength than Ni-Cr-steel, and the average ultimate shear strength for Ni-steel and Ni-Cr steel were 56.56 ksi and 52.84 ksi, respectively.
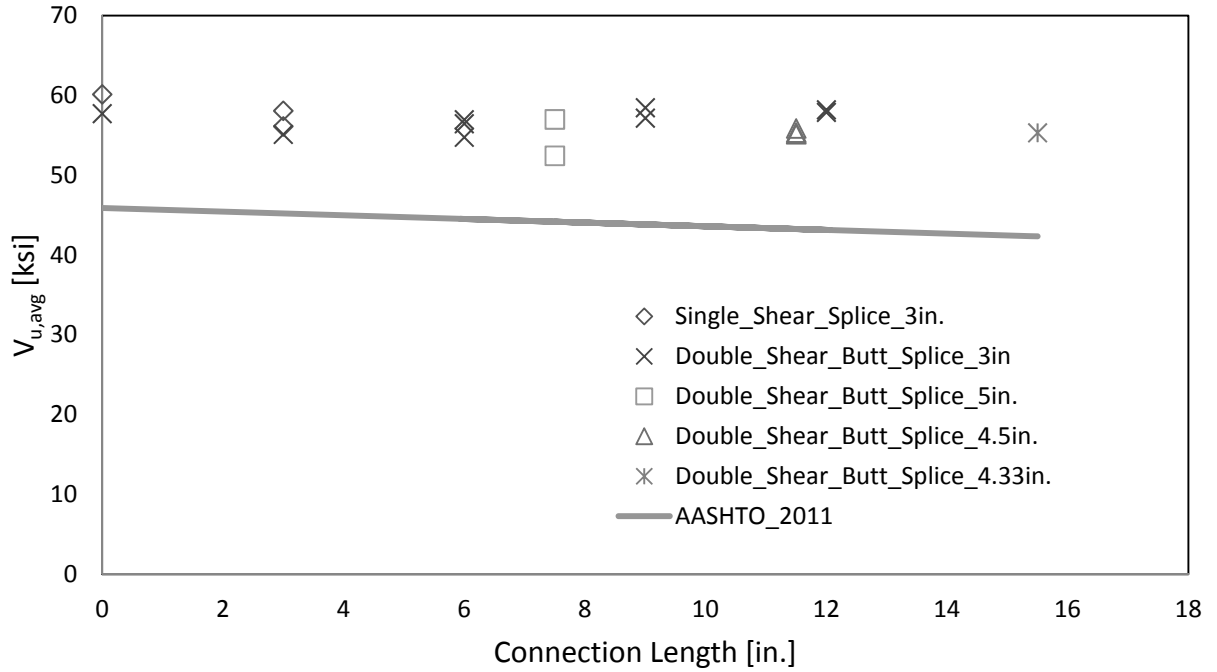
Figure 2.8 Ultimate Shear Strength Ni-Steel vs. Connection Length (Talbot & Moore, 1911)
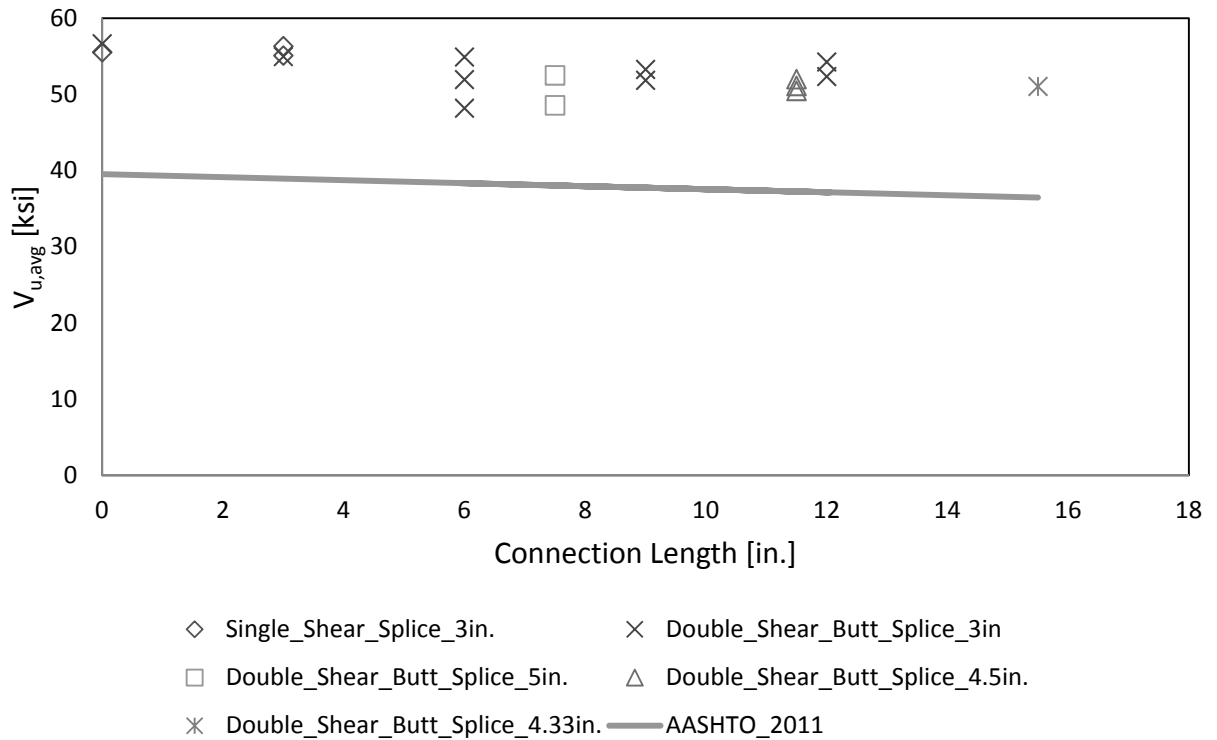
Figure 2.9 Ultimate Shear Strength Cr-Ni-Steel vs. Connection Length (Talbot & Moore, 1911)

2.3.3 Davis, Woodruff, and Davis (1939)

Davis, Woodruff, and Davis performed experiments on large riveted joints, and varied the
joint length, splice type, plate and rivet steel, pitch, and rivet pattern. The goals of the
research were to:

1. Determine the strength of riveted connections with as many as 28 transverse rows of
   rivets

2. Compare the behavior of joints having plates made of carbon, silicon, or nickel steel

3. Compare the behavior of joints having plates of carbon, silicon, or nickel steel

4. Compare the behavior of butt and shingle joints

5. Examine the partition of load among transverse rows of rivets

6. Determine effect of net section of plates

7. Investigate the slip of joint during loading

8. Determine a relationship between tensile stress in plates and shearing stress in rivets

Forty pairs of joints were tested, and the maximum joint length was nine rivets at either end.
The rivet and plate steel were made of softer materials than those used in buildings and
bridges at the time. They were rolled to the specifications of the San Francisco-Oakland Bay
Bridge at Carnegie Illinois Steel Corp. The rivets were driven with a hydraulic machine.
Each test name was given a series letter: A, B, C, D, F, and varied by if they were designed
to fail in plate or-rivets, by joint type (lap, butt, and shingle), number of plates, and rivet and
plate steel type.

From these tests, the following were concluded:

1. Ultimate load decreased as rivet length increased.

2. There was an insignificant effect on strength with rivet pitch.

3. Manganese-steel rivets performed better with regard to ultimate strength than carbon-steel.

4. For joints that were designed to fail in the rivets, there was not a correlation with plate material.

5. Strength of the rivet surface in double shear was as low as 80% of strength in single shear.

6. Riveted joint strength was not directly proportional to net section area as typically expected. It was ineffective to use fewer-rivets in the end row and disadvantageous to use wide spacing of end row rivets. When a full number of rivets were used in a row, the efficiency was 10% higher when the gage was four-rivet diameters compared to three. There was a better correlation with observed strength when the net section calculated by deducting the projected sectional areas of the rivet holes in the first two rows than that computed by standard specifications.

7. Insignificant difference between efficiency in butt and shingle splices.

8. The following phases of load and slip were observed (1) At low loads, partition of load was controlled by warping of plates, initial tension in the rivets, and the character of the faying surfaces. (2) After slip occurred throughout joint, shearing stresses became equalized among the rivets in various rows. (3) Rivets in the end rows experienced stresses larger than the average ultimate stress. (4) The partition of load among rivets became uniform. (5) Plastic flow in plates was large enough to cause excessive deformation of end rivets.

The results for the carbon-steel rivets listing the average rivet shear strength, connection length, and rivet pitch, are shown in Table 2.5 for the carbon-steel rivets and Table 2.6 for the manganese-steel rivets. The specimens, which were designed to fail in the rivets (series A or B) rather than the plates, are listed. The specimen names denote the failure mechanism, rivet, and plate type. For example, "ACC" means the specimen was designed to fail in the rivets (series A), has a rivet type of carbon-steel (C), and a plate type of carbon-steel (C). Manganese-steel is denoted by "M," Silicon-steel by "S," and Nickel-steel by "N."

Table 2.5 Ultimate Rivet Shear Tests for Carbon-steel (Davis, Woodruff, & Davis, 1939)

Specimen	$V_{u,avg}$ [ksi]	L_c [in]	Pitch [in.]
ACC18	55.7	28.5	5.25
ACC36	55.1	56.5	5.25
ACC54	50	84.5	5.25
ASC36	54	46.5	4
ASC54	51.1	69.5	4
BCC-20a	56.4	19	3
BCC-20b	58.6	26.5	4.5
BCC-20c	57.2	34	6

Table 2.6 Ultimate Rivet Shear Tests for Manganese-steel (Davis, Woodruff, & Davis, 1939)

Specimen	$V_{u,avg}$ [ksi]	L_c [in]	Pitch [in.]
ACM12	75.9	19.75	4
ACM24	77.4	39	5.25
ACM36	71.4	58.25	5.25
ASM12	72.4	19.75	5.25
ASM24	78	39	5.25
ASM36	72.7	58.25	5.25
ANM12	74.7	19.75	5.25
ANM24	77.7	39	5.25
ANM36	75.7	58.25	5.25

The average rivet shear strength versus connection length for the carbon-steel is shown in Figure 2.10 and manganese-steel is shown in Figure 2.11. Both plots depict longer connections, but do not show as much of a decrease in strength as AASHTO.
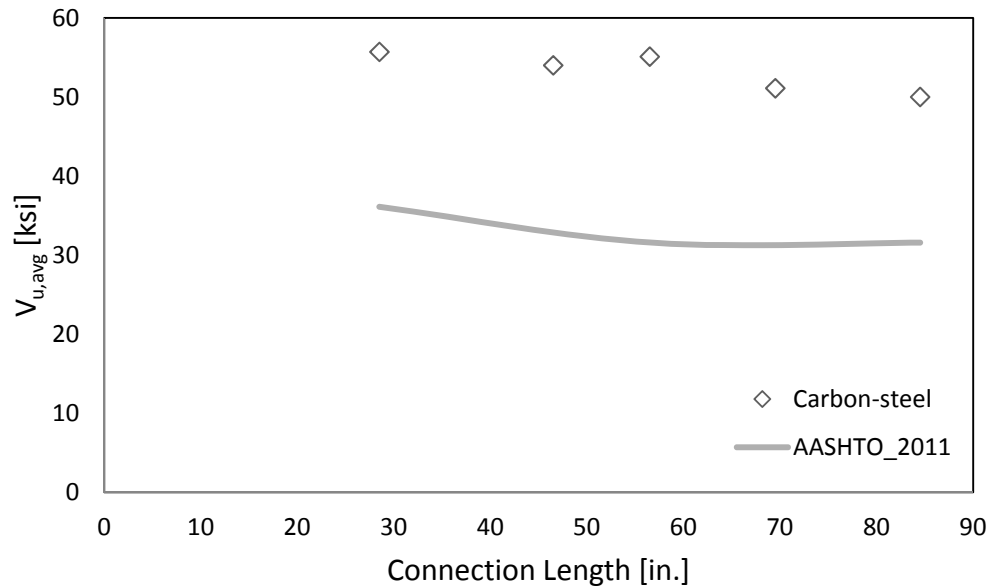
Figure 2.10 Ultimate Shear Strength C-Steel vs. Connection Length (Davis, Woodruff, & Davis, 1939)
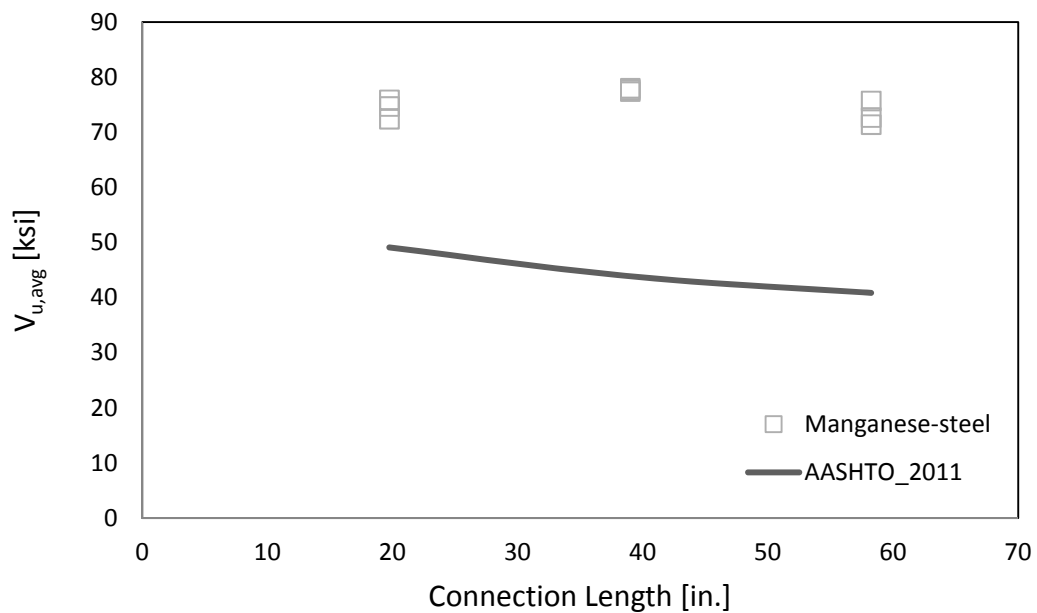
Figure 2.11 Ultimate Shear Strength Mn-Steel vs. Connection Length (Davis, Woodruff, & Davis, 1939)

2.3.4 Wilson, Bruckner and McCrackin (1942)

The goals of research performed by Wilson, Bruckner, and McCrackin (1942) were to determine the material properties of three low-alloy structural steels (named A, B, C in accordance with ASTM Tentative Specifications A242-41T) and to determine the behavior of structural joints fabricated with these steels.

For each material type, the experiments used the same type of plates and rivets in the riveted joint. The material properties to be determined were as follows: chemical composition, physical properties of materials, initial tension, tensile strength, hardness and shearing strength of driven rivets, strength of plates without joints, joints in plates fabricated with riveting, and joints in plates fabricated by welding. The chemical composition of the low-alloy structural steels varied for the rivets tested (Table 2.7 gathered from (Wilson, Bruckner, & McCrackin, 1942)). Prevalent elements are bolded. Steel alloy A has the most Nickel (Ni) along with Copper (Cu), while Steel alloy B is the only alloy with Chromium (Cr) and with the least amount of Ni, and Steel alloy C has the most Manganese (Mn) and some Ni. The material properties for each type of rivet are given in Table 2.8 for the as-rolled and annealed conditions as the average of three material tests.

Table 2.7 Chemical Composition for Low-Alloy Steels (Wilson, Bruckner, & McCrackin, 1942)

Low-alloy Steel	C	Mn	P	S	Si	Cu	Ni	Cr
A	0.169	**0.512**	0.009	0.033	0.013	**0.89**	**1.84**	0
B	0.088	0.371	0.093	0.031	0.307	0.38	**0.55**	**0.784**
C	0.21	**1.47**	0.013	0.031	0.184	0.25	**0.52**	0

Table 2.8 Material Properties for Steel Alloys (Wilson, Bruckner, & McCrackin, 1942)

Property	Steel Alloy					
	A		B		C	
	as rolled	annealed	as rolled	annealed	as rolled	annealed
F_y (ksi)	53	52.35	49.1	42.9	53.77	81.5
F_u (ksi)	74.73	74.12	69.1	65	49.07	76.33

Figure 2.12 depicts the test apparatus for the single and double shear tests that were performed on un-driven-rivets. Figure 2.13 depicts the joints that were tested with driven-rivets in single and double shear.
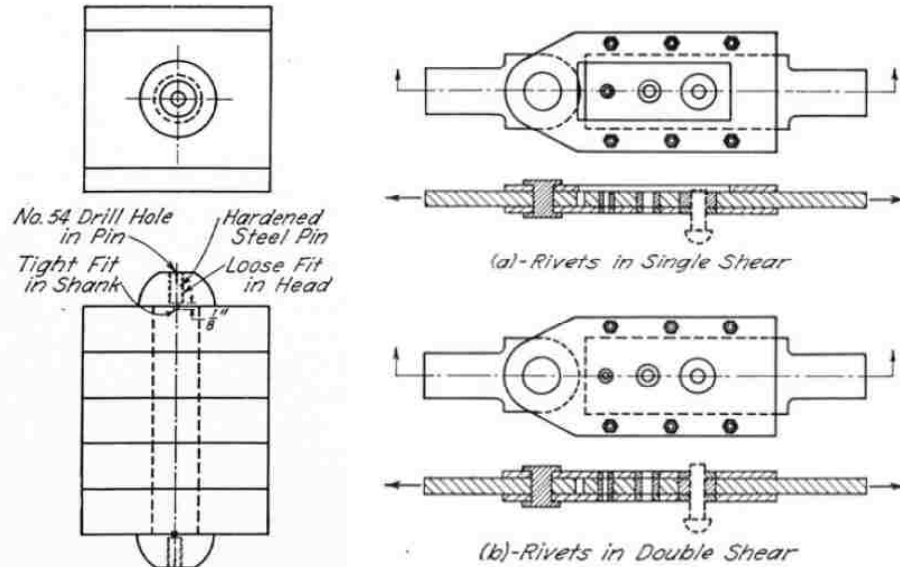
Figure 2.12 Prepared Rivet for Tension Test (left) Shear Test Apparatus for Un-driven-rivets (right) (Wilson, Bruckner, & McCrackin, 1942)
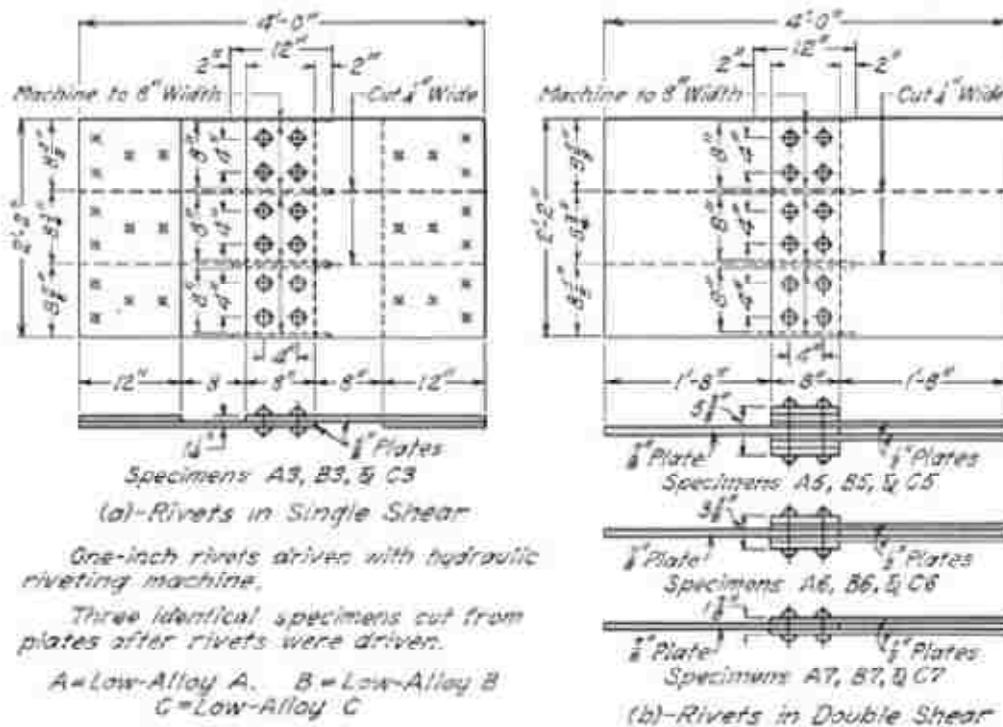
Figure 2.13 Joints Tested in Single Shear (a) and Double Shear (b) (Wilson, Bruckner, & McCrackin, 1942)

Table 2.9 presents the results of the ultimate shear strength test for single shear and double shear un-driven and driven rivets for each type of steel alloy (gathered from (Wilson, Bruckner, & McCrackin, 1942)). Each result is an average of three tests. The un-driven single shear tests had a grip length of 1.25 in. The un-driven double shear tests had three grip lengths: 1 3/8 in., 1 5/8 in., and 5 3/8 in. The rivets for both single and double shear were 1 in. in diameter and driven with a hydraulic riveting machine. For the driven rivet tests, the rivets were 1 in. in diameter, driven with a hydraulic riveting machine, and had a grip of 1¼ in for single shear. Table 2.10 compares the results of the shear to tension ratio for single and double shear and un-driven rivets for each rivet type. This shows that the ratio of rivet shear to tension is between 0.67-0.70.

Table 2.9 Ultimate Shear Strength Summary (Wilson, Bruckner, & McCrackin, 1942)

Steel Alloy	Un-Driven-rivets		Driven-rivets	
	Single Shear [ksi]	Double Shear [ksi]	Single Shear [ksi]	Double Shear [ksi]
A	50.18	48.64	63.92	63.83
B	50.13	47.34	64.82	61.25
C	56.94	54.44	75.96	71.27

Table 2.10 Comparison of Three-Alloys in Shear (Wilson, Bruckner, & McCrackin, 1942)

Ratio	Rivet A	Rivet B	Rivet C
Single Shear: Tension Un-driven	0.67	0.73	0.69
Double Shear: Tension Un-driven	0.65	0.69	0.66
Machine Driven:Un-driven Single Shear	1.13	1.15	1.18

Based on these tests, the following were concluded:

1. The initial tension in the rivets increased with grip from values below 13 ksi (2 in. grip) to 40 ksi (5 in. grip).
   - For short rivets (2 in. grip), tension was greater when driven with a pneumatic hand riveting hammer rather than a hydraulic machine.
   - For long rivets (5 in.), the tension was less for those driven with a pneumatic hammer versus a hydraulic machine.
   - There was no relation between initial tension and the rivet material except for the short rivets where the initial tension was less for alloy C followed by A then B.

2. The tensile strength was greater by 29% for driven vs. un-driven-rivets.
   - Rivet type B with a 3 in. grip had an increase in tensile strength when driven with a hydraulic riveting machine instead of a hand driven pneumatic hammer.
   - This led to a decrease in the ductility of the rivet, but no brittle fractures were observed.

3. Rivets with a 5 in. grip were able to fill the holes just beneath the rivet head but not in middle of the rivet shaft.

4. The net section of plates of small riveted joints developed unit strength 10% greater than the coupons tested, and the unit strength without the joints did not differ from the coupons for all three alloys.

5. Minimum shear that led to substantial slip was smaller for shorter rivets than for longer rivets.

6. Minimum shear leading to a substantial slip for rivet material was greater for-rivet B than C and for-rivet A than B, but not by a significant amount.

2.3.5 Munse and Cox (1956)

Munse and Cox (1956) tested rivets in combined shear and tension as only shear or tension
alone were provided for in the design specification at the time. They utilized a shear-tension
ratio to describe the behavior.

To assemble the testing apparatus, high button-head hot-driven-rivets (at 2000°F) were used
and were driven into pairs of round blocks in a fabrication shop using a hydraulic press
riveter. The loading blocks were attached to a pull plate in the test apparatus, which could
simulate shear and tensile load. Seven ratios of shear-tension ranging from direct tension to
direct shear were performed in this apparatus (see Figure 2.14).
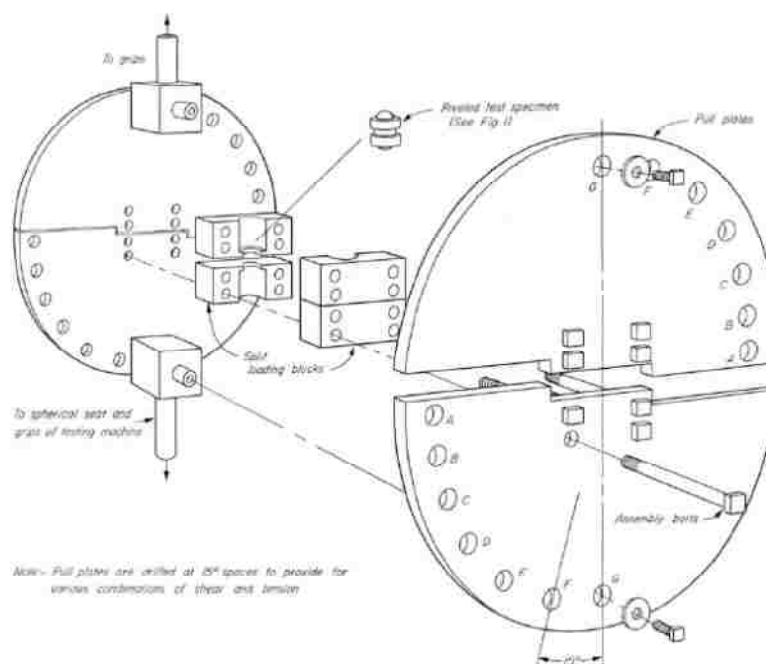
Figure 2.14 Test Apparatus for Shear-Tension Tests

The material properties for-rivets (killed, semi-killed, rimmed) used in the preliminary tests
are given in Table 2.11 (gathered from (Munse & Cox, 1956)). The material test is based on
hand-pneumatic driven 7/8 in. diameter-rivets with a grip length of 2 in., and the value given
is the average of two tests and based on the nominal rivet area. The yield and ultimate tension
strengths for the rivets used in the primary tests were based on ASTM A-141 for hot and cold
driven, 7/8 in. diameter rivets and are given in

Table 2.12 (gathered from (Munse & Cox, 1956)).

Table 2.11 Rivet Material Properties for Preliminary Tests (Munse & Cox, 1956)

	Killed	**Semi-Killed**	**Rimmed**
F_y [ksi]	51.45	42.4	46.06
F_u [ksi]	80.36	73.6	76.9

Table 2.12 Rivet Material Properties for Primary Tests (Munse & Cox, 1956)

	Tensile Strength
F_y [ksi]	28
F_u [ksi]	52

Preliminary tests determined the following:

1. There was a less than 5% difference between the ultimate strength of rivets that were killed, semi-killed, and rimmed steels subjected to identical heating and driving conditions.
2. There was a small effect when the furnace temperature (1800-1950 °F) and driving times (7-30 seconds) were varied.
3. For a 2 in. grip, the initial tension was equal to the approximate yield point of the rivets.

4. The length of soaking time before driving affected the ultimate strength. Figure 2.15 below shows the interaction curve for the preliminary tests.
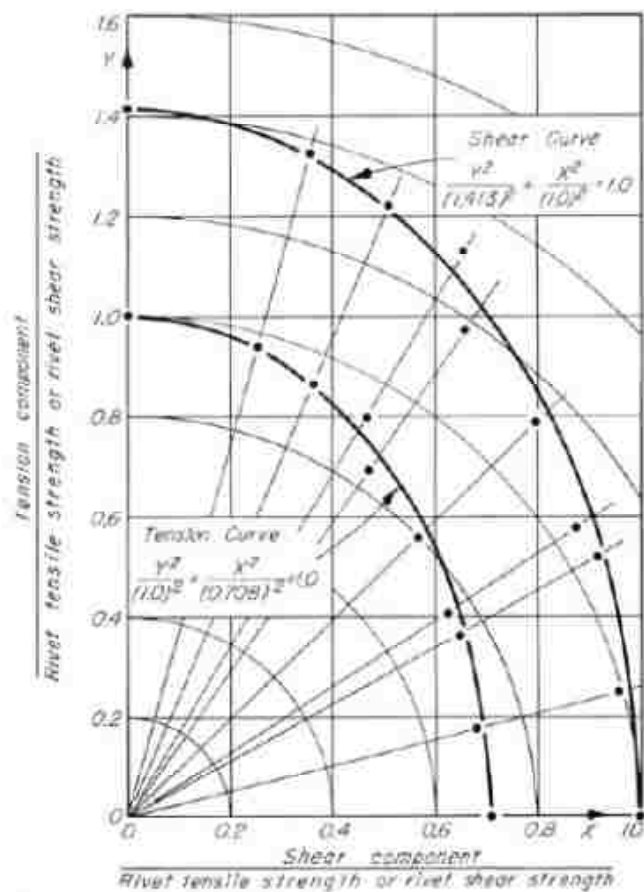
Figure 2.15 Interaction Curve for Shear-Tension Ratios Preliminary Tests (Munse & Cox, 1956)

The primary tests were conducted on-rivets with a diameter of 3/4 in., 7/8 in., and 1 in. They varied by grip length, hot versus cold formed, and hand pneumatic or machine driven. Table 2.13 summarizes the average ultimate shear strength (only shear: tension ratio of 1.0:0) based on nominal rivet diameter for each series (gathered from (Munse & Cox, 1956)). The average ultimate shear strength of the rivets was 51.58 ksi.

Table 2.13 Summary of Primary Tests for Pure Shear (Munse & Cox, 1956)

Series	Grip Length [in.]	Driven	Formed	Ultimate Shear Strength [ksi]
1	1	Hand-Pneumatic	Cold	54.77
2	1	Hand-Pneumatic	Hot	52.85
3	5	Hand-Pneumatic	Cold	50.73
4	5	Hand-Pneumatic	Hot	51.20
5	2	Hand-Pneumatic	Cold	53.11
6	3	Hand-Pneumatic	Cold	52.26
9	5	Machine	Cold	48.82
10	5	Machine	Hot	48.94
			Average	**51.58**

Primary tests determined the following:

1. Ultimate strength of rivets was reduced by 8% when the grip was increased from 1 in. to 5 in.
2. Using hot versus cold formed rivets had little or no effect on the ultimate strength at various shear to tension ratios.
3. Machined driven-rivets were slightly weaker than hand-pneumatic rivets, which Munse and Cox hypothesized may have been due to the difference in soaking conditions.
4. Concerning rivet diameter, the ultimate strength varied by less than 7%.
5. As the shear to tension ratio increased, the energy-absorbing cap of rivets under static load decreased.

6. The following non-dimensional elliptical interaction curve was developed to
   determine the ultimate strength:

$$S = r \times S_s \qquad (2.1)$$

$$r = 1.333 \sqrt{\frac{1 + m^2}{1.333^2 + m^2}} \qquad (2.2)$$

where: S = ultimate strength of the rivet subject to tension and shear

m = ratio of tensile component of force to shear component of force

S_s = ultimate strength of rivet in direct shear

Figure 2.16 below depicts the interaction curve described by the above equations for shear
and tension.
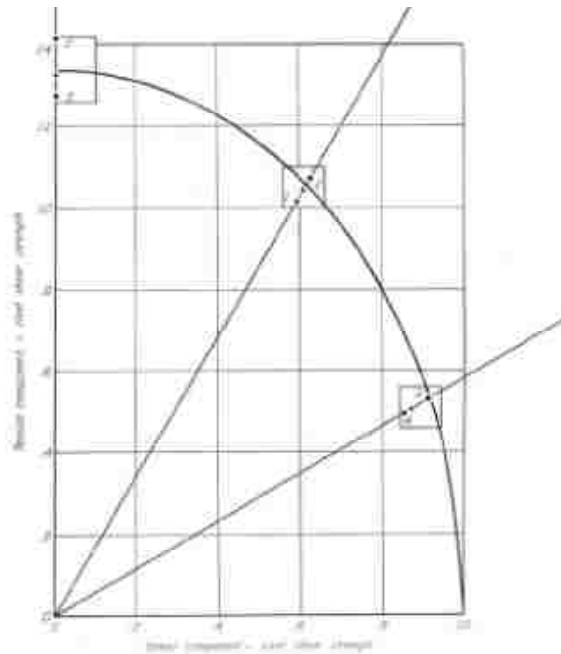
Figure 2.16 Interaction Curve for-rivets of Primary Tests (Munse & Cox, 1956)

2.3.6 Dlugosz (1962)

Dlugosz (1962) performed the fourth series of long joint tests (denoted the DR series) at Lehigh University. The goals of the research were to determine the effects of joint length, investigate unbuttoning and the redistribution of rivet forces under load, and the overall ductility of riveted joints.

Three joints were tested with varying connection lengths (see Figure 2.17). They were fabricated at Bethlehem Steel Co. from halves of double shear butt joints. The plate material was ASTM A7. The rivets were ASTM A141, and had a diameter of 7/8 in., a 3.5 in. pitch, and a grip of 4 in. A net section tension area to shear area ratio of 1:0.75 was maintained by adjusting the plate width.
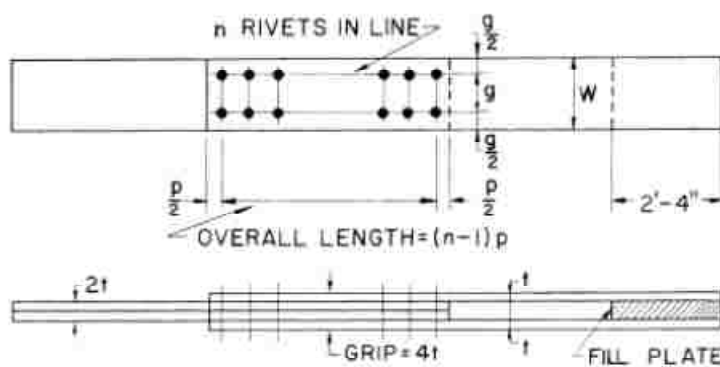
MARK	n	t	WIDTH IN.	GAGE IN.	g/d_h	A_{riv} nom SQ. IN.	A_{net} SQ. IN.	$\frac{T}{S}$
DR 71	7	2"	8.48	4.24	4.52	16.83	13.21	1:0.78
DR 101	10	2"	11.12	5.56	594	24.04	18.49	1:0.77
DR 131	13	2"	13.78	6.89	7.35	31.25	23.81	1:0.76

Figure 2.17 Dimensions of Lap Joints (Dlugosz, 1962)

Material tests on plate coupons were performed in a 120-kip mechanical screw type-testing machine, and un-driven-rivets were tested in double shear in a shear jig. The material properties are summarized in Table 2.14 denotes the maximum strength of the rivet for a single shear plane loaded in double shear. The lap joints were tested to failure in a 5 million pound hydraulic testing machine at 100-kip increments. Table 2.15 summarizes the results.

Table 2.14 Material Properties for-rivets and Plates(Dlugosz, 1962)

	ASTM A141 Rivets	ASTM A7 Plate
F_y (tensile) [ksi]	36.10	28.50
F_u (tensile) [ksi]	57.67	60.00
Ultimate Shear (double shear) [ksi]	55.30	

Table 2.15 Results of Lap Joint Tests (Dlugosz, 1962)

ITEM	UNITS	DR 71	DR 101	DR 131
PATTERN ALL holes drilled $\frac{15}{16}$" ALL pitches $3\frac{1}{2}$" Gage = $\frac{1}{2}$"				
RIVETS				
No. in line		7	10	13
No. of $\frac{7}{8}$" A141 rivets		14	20	26
Nom. shear area	sq. in.	16.83	24.04	31.25
PLATES				
Nom. width	in.	8.46	11.12	13.78
Nom. thickness	in.	2	2	2
Nom. gross area	sq. in.	16.96	22.24	27.56
Nom. net area	sq. in.	13.21	18.49	23.81
Actual net area	sq. in.	13.18	18.47	23.73
% Deviation in net area	%	-0.21	-0.11	-0.34
T/S RATIO (A_g/A_N)				
Nominal		1:0.78	1:0.77	1:0.76
Actual		1:0.78	1:0.77	1:0.76
WORKING LOAD ($\begin{matrix}T=20,000\\S=15,000\end{matrix}$)	kips	252	361	469
SLIP LOAD (First Major)		444	518	830
Nom. rivet shear	ksi	26.4	21.6	26.6
Nom. tension, net section	ksi	33.6	28.0	34.9
TYPE OF FAILURE		rivet	rivet	rivet
Load at failure	kips	738	942	1216
Nom. rivet shear	ksi	43.9	39.2	38.9
Nom. tens.—net section	ksi	55.9	51.0	51.0
Act. tens.—net section	ksi	56.0	51.0	51.2
UNBUTTONING FACTOR U		0.836	0.747	0.741

From these tests, the following were concluded:

1. The unbuttoning factor decreases from 0.84 (7 rows of rivets) to 0.74 (13 rows of rivets) as the number of rivets increases. The unbuttoning factor (U) captures the ductility of the joint by expressing the joint length effect on connection with ultimate strength, where the more ductile a joint is the more ability it has to redistribute load. The equation shows that for longer joints, U decreases as fasteners are less capable of redistributing load.

$$U = \frac{\tau_{avg}}{\tau_1} \qquad (2.3)$$

where: τ_{avg} = nominal shear stress at time first rivet fails

τ_1 = average nominal shear strength of a single rivet of the same lot

2. The difference between the predicted (based on theoretical result) and ultimate load was 2.55%.
3. A theoretical analysis determined that a drop in ultimate strength by 13.9% occurred when the pitch was increased from 2.5 in. to 6 in.
4. The design assumption that rivets completely fill holes was not correct because slip occurred in all joints.
5. The design assumption of equal load sharing between rivets was not correct because equalization of load among fasteners did not occur, and there was more inequality with longer connections.
6. As joint length increased, the average shear stress in the rivets at joint failure decreased.

The length effect is plotted in Figure 2.18 in addition to the strengths calculated by AASHTO. This shows that the strength decreases similar to the trend to AASHTO but is not as reduced.
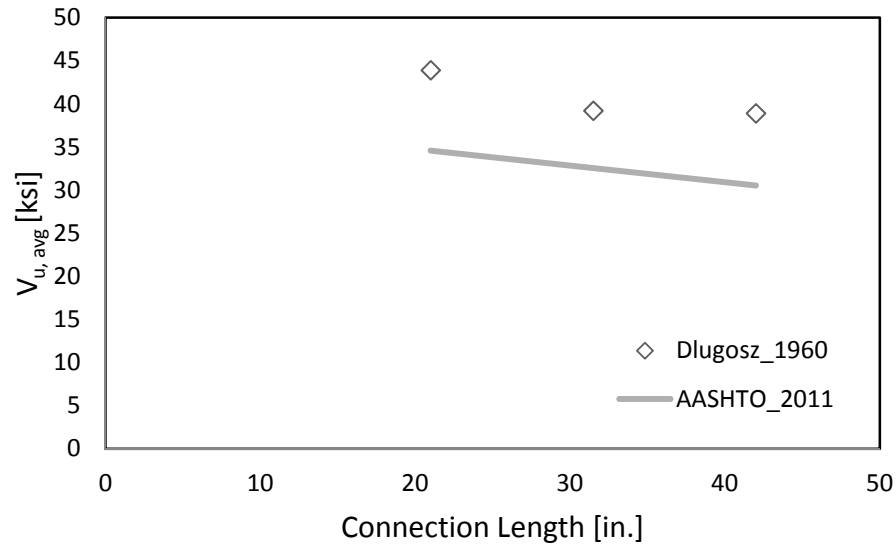
Figure 2.18 Ultimate Rivet Shear Strength vs. Joint Length (Dlugosz, 1962)

2.3.7   Fisher and Rumpf (1967)

Fisher and Rumpf used mathematical models based on past literature of riveted and bolted joints to develop a theoretical solution for unequal distributions of load among bolts in double-lap tension splices. The concept of "balance design" in riveted connections was also compared to the same condition for bolted connections. Balance design means that the tensile capacity of the net section of the connecting element will equal the ultimate shear strength of the fasteners. This is because the tensile strength of low carbon steel plates (ASTM-A7) was equal to the tensile strength of rivets made of the same material. In addition, past research has shown that rivets have approximately 75% of their tensile strength in shear. However, the shear strength of a bolt is higher than that of a rivet and does not have the same ratio in comparison to the connecting plates. These models were investigated by applying them to test results they performed on full sized connections. Nineteen tests were performed: eight with 7/8" A325 bolts, A7 steel plate, and a tension area to shear ratio of (1:1.10) and eleven with 7/8" A325 bolts, A440 steel plate, tension area to shear ratio (1:1.0). The ratio between tensile stress on the net section of the plate to the average shear stress on the nominal area of fasteners is described as the shear: tension (A_s: A_n) ratio. Figure 2.19 depicts the lap joint and key deformations in the plates and bolts.
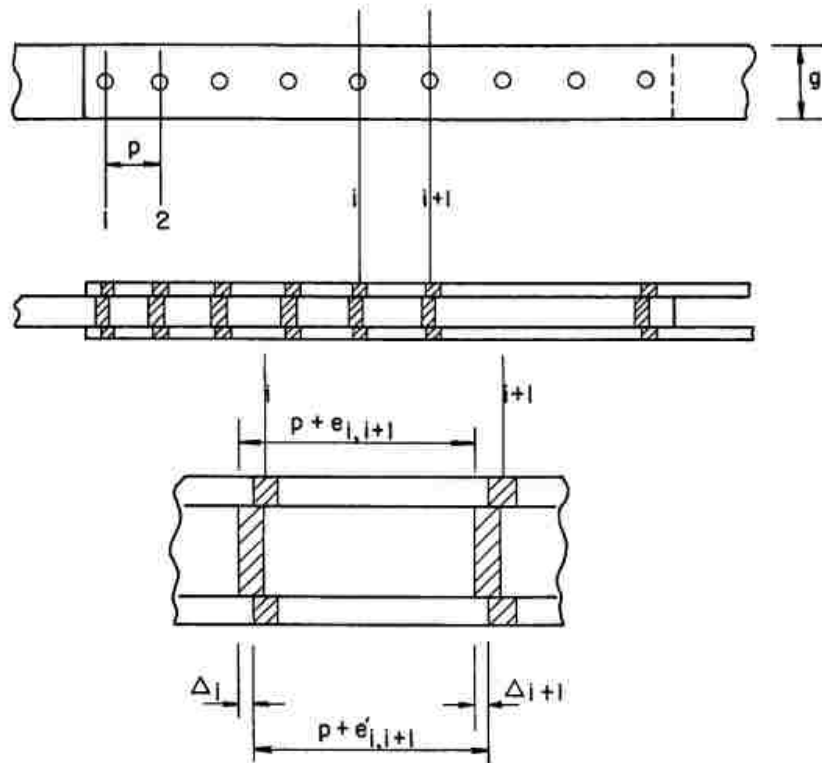
Figure 2.19 Joint Deformation in Plates and Bolts (Fisher & Rumpf, 1967)

The theoretical solution was developed by satisfying the following basic conditions: equilibrium (statics) of the load on the bolt group, continuity (compatibility of total deformation throughout elastic/inelastic ranges), initial conditions (ultimate strength of plate, and ultimate strength of critical fastener). The following assumptions were made: once major slip has occurred, fasteners transmit the entire applied load through bearing, frictional forces in the region between slip and ultimate load were neglected, analytical expressions are applicable to the component elements of expressions for stress-strain relationships, and fasteners had equal diameter.

The individual component strengths were used in the development of the theoretical solution. To estimate the plate strength in the connection, a coupon of the plate material with holes was tested in tension. To estimate the fastener strength, bolts were tested in double shear by loading plates in a tension and compression jig. The single bolts had approximately 5% less shear strength in tension than when loaded in compression. The load elongation relationships for the connection components were inputted into the equilibrium equations.

To determine the partition of loading between each bolt, the hole offset was calculated as the sum of the total fastener deformation (shear, bending, and bearing of fasteners and plate bearing deformation), and elongation of the hole radius in the main and lap plates (taken from plate calibration measurements). This deformation was used to partition loading, but the stress in each rivet was computed from the theoretical solution.

To compare the experimental results to the theoretical predictions (as shown in Figure 2.20), the total deformation was computed using the following equation (Fisher & Rumpf, 1967):

$$DEF. = Slip + \sum_{i=1}^{n} e_{i,i+1} + e_{ol} + e_{nx} \qquad (2.4)$$

where: slip = measured deformations at each end of the joint between the end bolts and points X (including actual joint slip and inelastic deformation)

$e_{i,i+1}$ = computed main plate elongations within the joint proper

e_{ol} and e_{nx} = measured plate elongations between the end bolts and points X
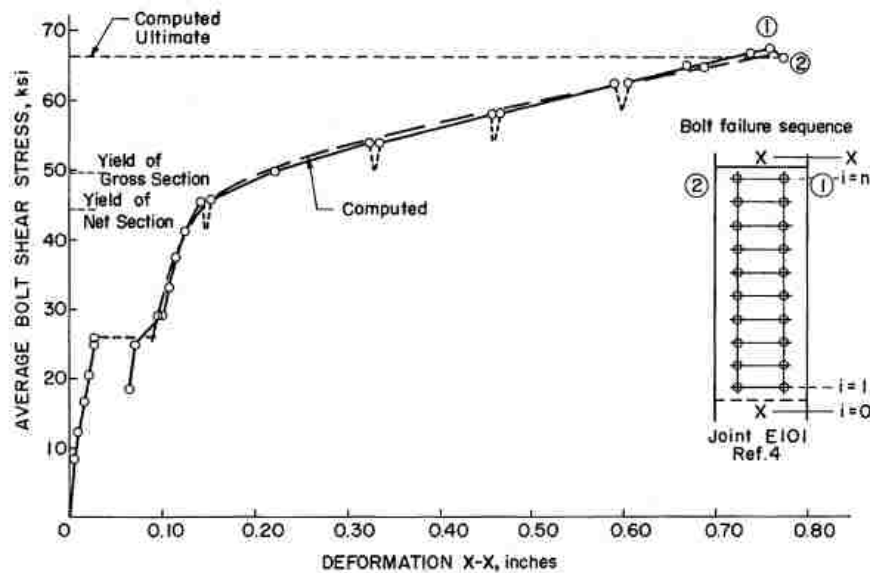
Figure 2.20 Comparison of Computed and Experimental Joint Deformation (Fisher & Rumpf, 1967)

Based on this research, the following were concluded:

1. A theoretical solution for load partitioning in double-lap plate splices was developed. The solution was in two pieces was valid for the range of behavior between major joint slip and ultimate load and was applicable to elastic and inelastic regions.
2. The theoretical solution was verified with experimental test results with the greatest difference being approximately 4%.
3. There was a decrease in the average ultimate shear strength as joint length increases, which was greater for A7 than A440 for "balanced" joints.
4. The average shear strength of fasteners in longer joints increased as net plate area increased.

2.3.8   Kulak, Fisher, and Struik (1987)

Kulak, Fisher, and Struik (1987) provided criteria to improve then current design procedures for bolted and riveted joints. The book focused on providing a background on the types of fasteners, connections, loading conditions, and design procedures. The behavior of individual fasteners under various loading conditions was examined. The types of connections considered were symmetric butt splices, lap splices, truss type connections, and some special types of joints and other miscellaneous considerations.

Chapter 3 of Kulak, Fisher and Struik (1987) provides information on the behavior of rivet fasteners in tension and shear along with design recommendations. They concluded the following:

1. For rivets in shear, the average shear to tension strength was 0.75.
2. A double shear test of A502 Grade 1 rivets showed a slight decrease in the strength of rivets in single shear compared to double shear. This is due to the eccentricity of the applied load, which causes out of plane forces and secondary stresses in the rivet. This result implies that in single shear, the load is not pure shear unless the rivet is restrained in single shear.
3. Driving rivets increased the tensile and therefore the shear strength.

For rivets in tension, it was recommended that the strength might exceed un-driven-rivet strength by 10-20% depending on the rivet material, driving method, and grip length. The following equations were developed:

For-rivets in tension:

$$B_u = A_b \times \sigma_u$$ (2.5)

where: A_b = cross sectional area of bolt and

σ_u = tensile strength (60 ksi A502 Grade 1, 80 ksi A502 Grade 2 or 3)

For-rivets in shear:

$$T_u = 0.75 \times \sigma_u$$ (2.6)

The ratio of 0.75 is independent of rivet grade, installation procedure, diameter, and grip length. The shear resistance is directly proportional to the available shear area and number of critical shear planes, therefore, the maximum shear resistance is:

$$S_u = 0.75 \times m \times A_b \times \sigma_u$$ (2.7)

where: m = number of critical shear planes that pass through the rivet

A_b = cross sectional area of un-driven-rivet

The behavior of symmetric butt splices is of interest because it relates to the issue of connection length, and was discussed in Chapter 5 of Kulak, Fisher and Struik (1987). Observations of butt splice behavior from their review of test results for joint behavior up to slip include:

1. Slip-resistant joints have a low probability of slip during the life of the structure. The joint is located where major slip would jeopardize the serviceability of structure and designed under un-factored loads.

2. The factors that affect slip resistance included the following: joint geometry, number of faying surfaces, joint stiffness, type of steel, surface preparation and treatment, bolt clamping force, and grip length.

3. External load was perpendicular to the fastener axis and transmitted by frictional forces on contact area of plates being fastened.

4. This frictional resistance was dependent on the fastener preload and the slip resistance of faying surfaces. The maximum capacity was reached when the frictional resistance was exceeded and slip of joint occurred bringing plates into bearing against the bolts s (depicted in Figure 2.21 under Case 2).
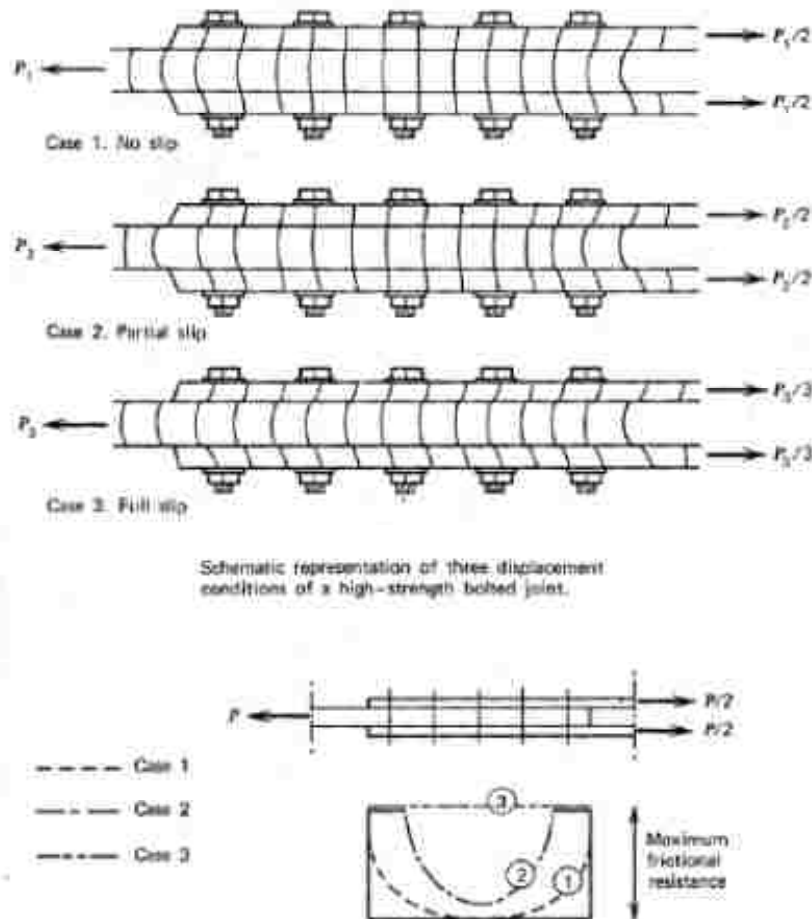
Figure 2.21 Schematic of Displacement Conditions and Friction Forces (Kulak, Fisher, & Struik, 1987)

5. After a major slip occurred, the fasteners were in bearing. The load was transferred by shear and bearing so, the connection became "bearing type." Shear strength of fasteners and local bearing stresses in plate were critical as opposed to fastener preload as illustrated in Figure 2.21 Case 3.

6. Upon major slip, the end bolts beared against the main and splice plates and as load was increased, the end bolts and holes deformed further until succeeding bolts came into bearing, which continued until all bolts, were in bearing. (See Figure 2.22)

   - Increasing load caused bolts to deform in proportion to the force, and such deformation depended on plate elongation between two rows of bolts. There were differential elongations at ends of joints, so the end bolts carried greater load than those in the interior.

   - Leveling out of load occurred if bolts had good shear ductility.

- End pitches had large displacement and differential elongation leading to bolt failure in shear.
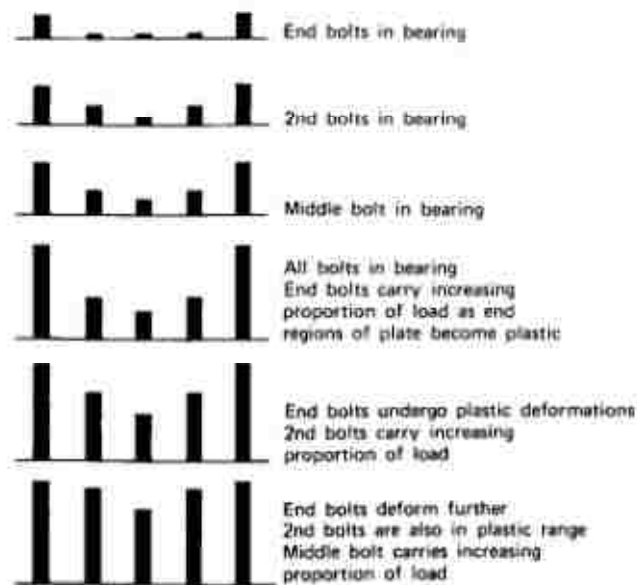
Figure 2.22 Bolt Forces After Major Slip Occurs (Kulak, Fisher, & Struik, 1987)

7. Short connections almost completely equalized the load before bolt failure, which led to simultaneous shearing of bolts.

8. In long connections, end fasteners reached critical shear deformation and failed before full strength of each fastener was achieved. The remaining bolts could not take much more load without causing failure and fracture in sequential fashion, called "unzipping."

9. Joint length influenced the ultimate strength of the joint, which determined whether simultaneous shearing or unzipping would occur. The average fastener shear at ultimate load versus joint length is shown in Figure 2.23. Longer joints decreased in average bolt shear strength compared to a single fastener. Short joints were negligible up to 10 in., as bolts provided the same strength as a single fastener.
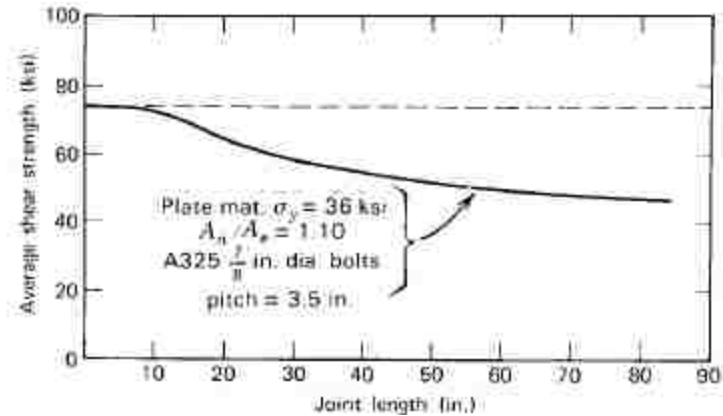
Figure 2.23 Effect of Joint Length on Ultimate Strength(Kulak, Fisher, & Struik, 1987)

10. In addition, for shorter connections, the forces were able to redistribute more evenly, but in longer connections, the fasteners at the ends carried twice the force as those in the center. This trend is shown in Figure 2.24-Figure 2.26. The un-shaded portion of the bars represents the shear stress upon yielding of the gross section of the plate and the shaded portion is the additional stress that the rivets can take up to the ultimate load. For a smaller number of fasteners, this additional stress is uniform, but as the number of fasteners increases, more of the load is taken by the outer fasteners.
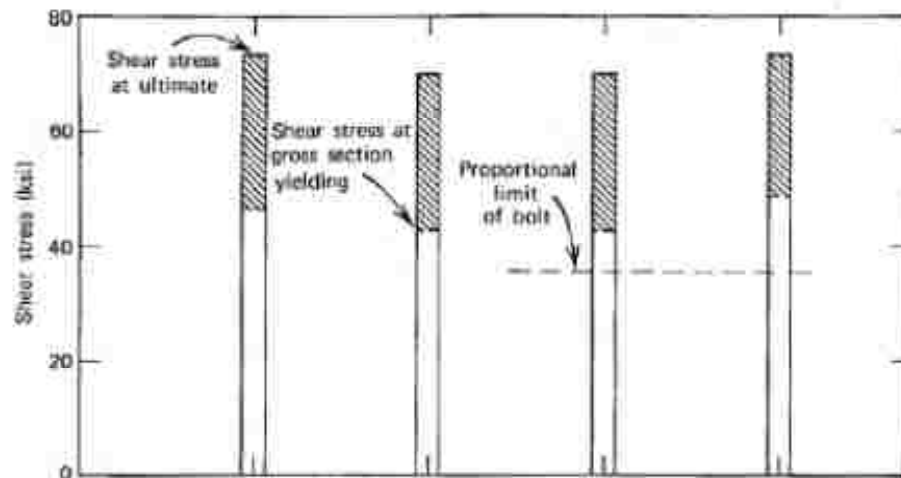
Figure 2.24 Load Partition for Four Fasteners in Line (Kulak, Fisher, & Struik, 1987)
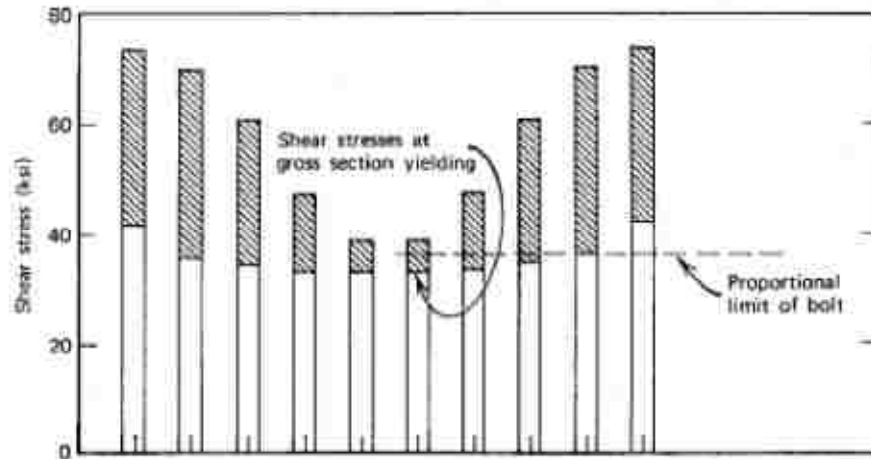
Figure 2.25 Load Partition for 10 Fasteners in a Line (Kulak, Fisher, & Struik, 1987)
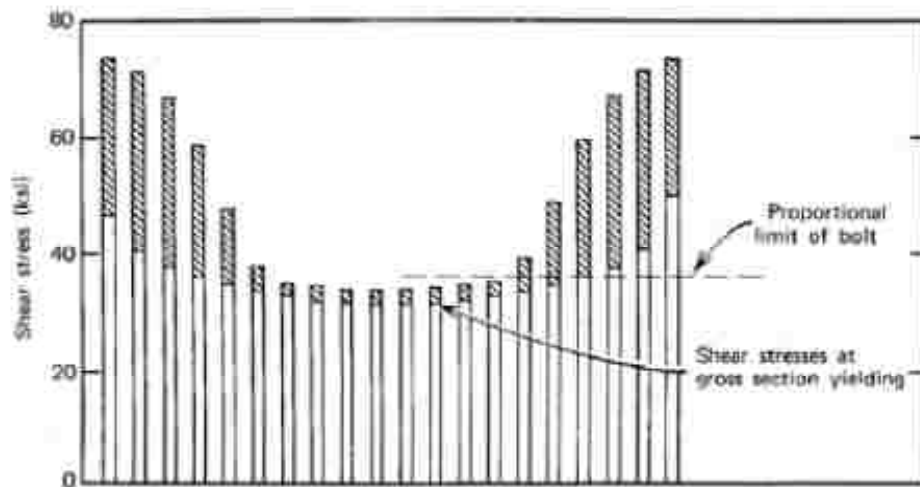
Figure 2.26 Load Partition for 20 Fasteners in a Line (Kulak, Fisher, & Struik, 1987)

Although the figures above relate to high-strength bolts, the concept of a reduction factor and the overall trend is applicable to rivets. The behavior is consistent with the theoretical solution developed by Fisher & Rumpf (1967) for the partition of loads in fasteners.

2.3.9   Roeder, Leon, and Preece (1994)

Roeder, Leon, and Preece (1994), examined the seismic behavior of riveted connections with the goal of improving understanding of that behavior and developing models to predict it.

Some preliminary tests were performed on-rivets to determine their shear strength. At the University of Washington (UW), two double shear tests were performed on a single rivet, and the ultimate shear strength was determined to be 41 ksi. At the University of Minnesota (UMN), tests were performed on spliced connections with three ¾ in. diameter Grade 1 A502 rivets in double shear, and the capacity was approximately 56.59 ksi.

2.3.10 D'Aniello, Portioli, Fiorino, and Landolfo (2010)

D'Aniello, Portioli, Fiorino, and Landolfo (2010), performed lap-shear tests on riveted connections of aged metal structures inspired by the large volume of existing railroads in Europe. The rivet strengths were compared to the predicted shear strengths to evaluate the provisions of EN 1993:1-8. According to EN 1993: 1-8, riveted connections can only be of bearing type, not slip resistant.

The test specimens were selected by the Steel Division of RFI and consisted of connections used for lattice roofing and bridges. The following material tests were performed: tensile coupon tests, Brinnel hardness tests (BH), chemical analysis, and Charpy-V notch (CVN).

The testing scope consisted of testing different materials, geometries, and configurations, and comparing existing results with predicted response according to modern codes. Riveted connections varied in connection length, rivet diameter, and loading (single or double shear). Figure 2.27 depicts the connection types. For the experimental tests, the following parameters were examined: load eccentricity, net area, plate width, joint length, and rivet clamping force. In total, 64 lap shear tests were performed by loading in tension under a displacement control until failure. A diagram of the setup in the testing machine is depicted in Figure 2.28.

S-16-10-1			U-16-10-2		
U-16-10-1			U-16-10-4		
S-19-10-1			S-19-10-2		
U-19-10-1			U-19-10-2_90		
S-19-12-1			U-19-10-2_60		
U-19-12-1			S-19-10-4		
S-22-10-1			U-19-10-4_90		
U-22-10-1			U-19-10-4_60		
S-22-12-1			S-22-12-2		
U-22-12-1			U-22-12-2		
			S-22-12-4		
			U-22-12-4		

Figure 2.27 Riveted Specimens (D'Aniello, Portioli, & Landolfo, 2011)
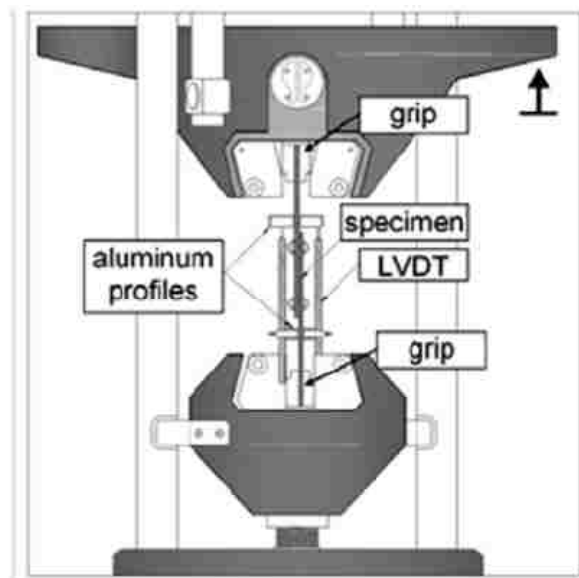
Figure 2.28 Test Setup (D'Aniello, Portioli, & Landolfo, 2011)

The following were the primary results:

1. The failure modes included rivet shear, bearing at rivet holes of thinner plates, and failure in tension on net section.

2. For symmetrical loading, the failure modes were rivet shear and bearing.

3. For unsymmetrical loading, the failure modes were rivet shear and tension and out of plane deformation due to bending (shorter connections, less observed in longer connections).

4. Spacing of rivets did not influence shear strength.

5. Strength did not increase linearly as the number of rivets increased. Instead, the strength, on average, decreased at a decreasing rate as shown in Table 2.16

6. For longer joints, the redistribution of rivet force did not occur, and yielding on the gross section was observed.

7. For longer joints with a larger A_n/A_g ratio, there less of a decrease in average shear strength as joint length increased.

8. Short lap joints (up to 2 rivets) were not affected by joint length.

9. For larger A_n/A_g shear capacity was improved by doubling the number of shear planes. This did not affect the strength for small A_n/A_g ratios.

The rivet shear strength was calculated from the test results by extracting tests in which rivet shear was the failure mechanism (some specimens failed in bearing or tension on net section) and dividing by the number of rivets and rivet area. Ultimate rivet shear stress was also compared to connection length. The data (adapted from (D'Aniello, Portioli, & Landolfo, 2011)) is summarized in Table 2.16 . Figure 2.29 shows that as ultimate rivet shear strength decreases as connection length increases for single shear, at about the same rate as AASHTO's prediction, however, the predicted strengths are still much less than the experiment results.

Table 2.16 Experimental Test Results (D'Aniello, Portioli, & Landolfo, 2011)

Specimen	No. Rivets/ Row	Single/ Double Shear	Connection Length [in.]	F_u [kip]	Rivet Dia. [in.]	$V_{u,avg}$ [ksi]
U-16-10-1	1	single	0	18.03	0.630	57.87
U-19-10-1	1	single	0	22.81	0.748	51.91
U-19-12-1	1	single	0	26.43	0.748	60.15
U-22-10-1	1	single	0	32.55	0.866	55.24
U-22-12-1	1	double	0	31.53	0.866	53.51
U-16-10-2	2	single	5.512	34.88	0.630	55.96
U-16-10-4	4	single	14.173	47.22	0.630	37.88
U-22-12-2	2	double	3.543	61.01	0.866	51.77
					Average	**53.04**
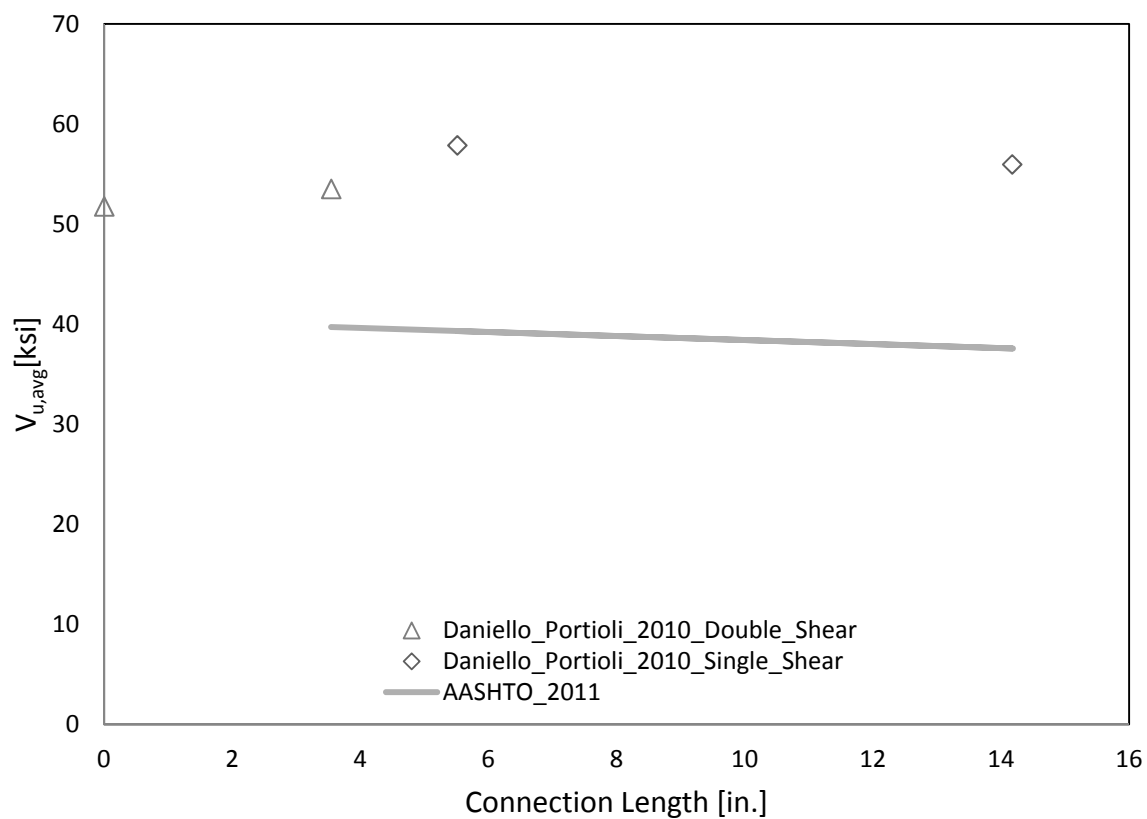
Figure 2.29 Ultimate Rivet Shear Strength vs. Connection Length (D'Aniello, Portioli, & Landolfo, 2011)

2.4 Review of Current Federal Highway Administration (FHWA) Guidelines for Evaluating the Strength of Riveted Connections

2.4.1 General

FHWA released the Guide to Evaluation of Bolted and Riveted Gusset Plate Connections (denoted the FHWA Guide) which provides guidelines to bridge owners in meeting the requirements of the FHWA Technical Advisory T 5140.29 Load-carrying Capacity Considerations of Gusset Plates in Non-load-path Redundant Steel Truss Bridges. It is for use with AASHTO Load Resistance Factored Rating (LRFR) or Load Factored Rating (LFR). This section describes the recommendations for fastener resistance.

2.4.2 Resistance of Fasteners

These recommendations assume that the steel truss bridge is non-load-path-redundant. This means failure of a main component will likely lead to collapse of the bridge. It is also assumed that the plates and fasteners determine the strength, and the resistance is the smaller of the fastener and gusset resistance. In concentrically loaded bolted and riveted gusset connections, the axial load in each connected member is distributed equally to all fasteners at the strength limit state.

The factored shear resistance of one rivet is described by the following equation:

$$iR = iFmA_r \tag{2.8}$$

where: iF = Factored shear strength of one rivet. The values in Table 2.18 may be used for iF based on the year of construction for unknown-rivet types, or on the type of rivets.

m= the number of shear planes

A_r = cross-sectional area of the rivet before driving

For connections with a length greater than 50 in., the resistance shall be taken as 0.8 multiplied by the equation above. Table 2.17 and Table 2.18 summarizes the recommendations (gathered from (FHWA, 2009)).

Table 2.17 FHWA Design Recommendations (FHWA, 2009)

	iF (ksi)
Constructed prior to 1936 or of unknown origin	18
Construction after 1936 but of unknown origin	21
ASTM A 502 Grade I	27
ASTM A 502 Grade II	32

Table 2.18 Design Recommendations (AASHTO, American Association of State Highway and Transportation Officials, 2011)

	iF (ksi)
Constructed prior to 1936 or of unknown origin	34.5
Construction after 1936 but of unknown origin	34
ASTM A 502 Grade I	34
ASTM A 502 Grade II	48

Furthermore, the 2011 revisions of the AASHTO Manual for Bridge Evaluation, the following equation was recommended which reduces the factored shear strength of the rivet for longer connection lengths.

Factored resistance of rivets in shear shall be taken as (Equation 6A.6.12.5.1-1 from (AASHTO, American Association of State Highway and Transportation Officials, 2011)):

$$R_n = \varphi_s F_u R_1 R_2 R_3 m A_r \qquad (2.9)$$

where: φ_s = resistance factor for rivets in shear, taken as 0.80

F_u = rivet Ultimate Tensile Strength [ksi]

R_1 = shear/tension ratio, taken as 0.67

R_2 = joint length factor, taken as 1-(0.25L/50) for 0<L≤50 and 0.75 for L>50 in.

L = connection length between extreme fasteners in each of the spliced parts measured parallel to the line of axial force, for splices, the 50 in. length is measured between the extreme bolts on only one side of the connection.(in.)

m = the number of faying surfaces

A_r = cross sectional area of the rivet before driving (in^2)

This equation was motivated by the research of Fisher and Rumpf (1967) described in Section 2.3.7). It will be used to determine how the ultimate rivet strength varies with connection length in comparison to the results of the test program.

2.5 Effective Rivet Yield

This concept was developed by Davis et al. (1939) to determine the yield point of a rivet, which indicates the onset of nonlinear behavior of the riveted connection. The method uses the average rivet shear stress versus deformation plot to identify four stages of behavior (see Table 2.19). Figure 2.30 divides an average rivet stress versus joint set plot into these four stages. The effective rivet yield (ERY) is identified when the slope of the average rivet stress versus joint set becomes half of the slope from Stage III (see Figure 2.31).

Table 2.19 Stages to Determine ERY (Olson, 2010)

	Occurrence/Behavior
Stage I:	Rivets have not slipped and load is transferred between faying surfaces via friction
Stage II:	Rivets slip
Stage III:	Rivets bear on rivet holes while connecting elements behave elastically
Stage III:	Yielding begins in rivets and/or connecting elements
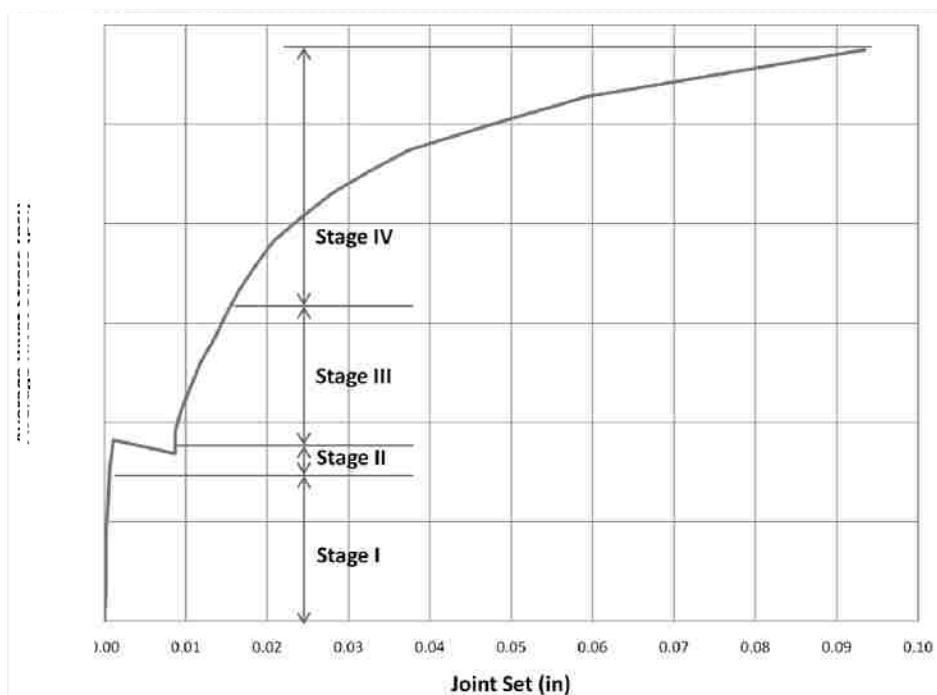
Figure 2.30 Average Rivet Stress vs. Joint Set for ERY (Olson, 2010)
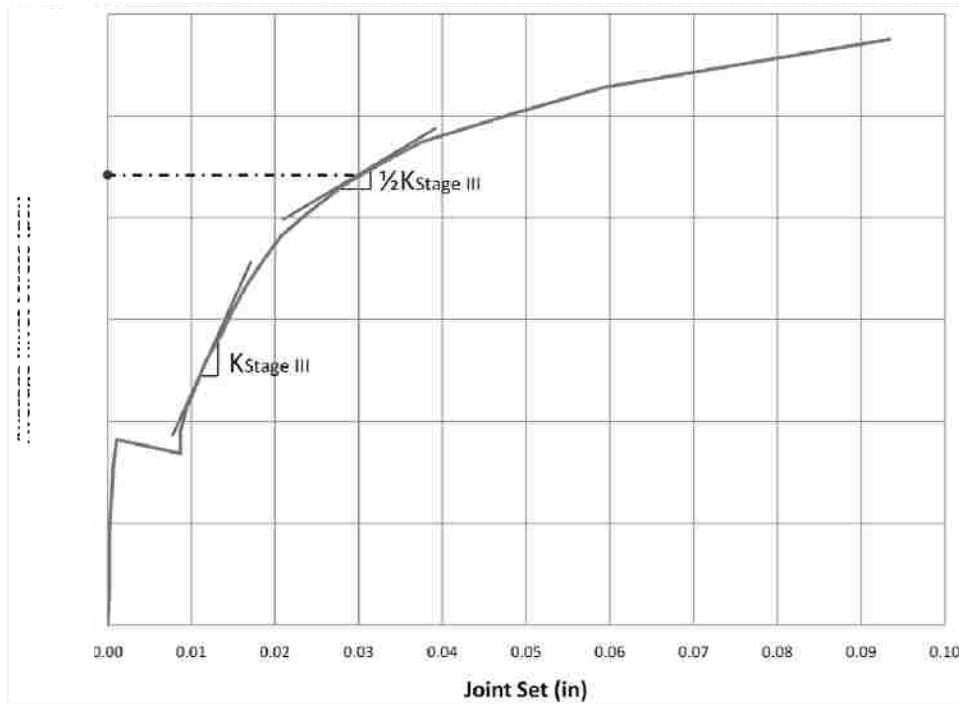
Figure 2.31 Calculation for ERY (Olson, 2010)

2.6   Summary of Literature Review

The literature reviewed has provided information on the behavior of riveted connections as they appear in older structures. In addition, data on rivet shear strength and joint length effect have been gathered.

The findings were recurrent in the literature:

Riveted connection behavior upon loading

1. The strength of the riveted material determines the ultimate shear strength of the riveted joints.
2. The factors that affect slip resistance include the following: joint geometry, number of faying surfaces, joint stiffness, type of steel, surface preparation and treatment, fastener clamping force, and grip length.
3. After the yield point (shear force equals the friction resistance of surfaces held in contact), the slipping of the surfaces in contact cause the riveted joint to deform.
4. The rivet bears against the end of the hole and deformation of the rivet body takes place.
5. Excessive deformation of end rivets occurs due to plastic flow in connection.
6. If sufficient ductility exists, this deformation leads to failure of the rivets in shear. Due to this behavior, the failure modes of riveted connections include rivet shear, bearing at rivet holes of thinner plates, and failure in tension on net section.

Riveted connection behavior and joint length

1. Average ultimate shear stress in the rivets decreased as joint length increased but not as much as AASHTO (2011) currently predicts.
2. There was an insignificant effect on rivet strength with rivet pitch.
3. Short connections can almost completely equalize the load before fastener failure, which led to simultaneous shearing of bolts.
4. In long connections, end fasteners reached critical shear deformation and fail before full strength of each fastener is achieved.
5. Remaining fasteners cannot take much more load without causing failure and fracture in sequential fashion, called "unzipping."

2.6.1 Comparison of Design Recommendations and Relevant Research

There are significant differences between the rivet strength found in the literature and the current FHWA and AASHTO recommendations used for load rating of bridges. Table 2.20 summarizes the average ultimate rivet shear strengths from the literature reviewed where splice connections were tested in tension.

Table 2.21 normalizes the average ultimate rivet shear strength to the corresponding FHWA recommendation from Table 2.18. For rivets with more carbon, the range is from 41-57 ksi and for low alloys 52-74 ksi. However, the recommendations from FHWA suggest 27 ksi should be used, while the ultimate strength could be as high as approximately 57 ksi according to Table 2.20. On average, the actual rivet strengths are 2-3 times larger than the FHWA recommendations from 2009 and 1-2 times larger for recommendations from 2010. This shows that the current recommendations are conservative by approximately for the selection of rivets, leading to an underestimation of design strength for the connection.

Table 2.20 Summary of Average Rivet Ultimate Shear Strength Based on Literature Splice Tests

Literature	$V_{u,avg}$ [ksi]	Rivet Dia. [in.]	Composition	No. of Tests	Std. Dev [ksi]
AREMA 1904	48.25	0.875	C-steel	90	2.28
Talbot & Moore 1911	56.56	0.875	Ni- steel	18	1.77
	52.84	0.875	Cr-Ni steel	18	2.48
Davis, Davis, & Woodruff 1939	55.17	0.875	C-steel	10	2.74
	75.10	0.875	Mn-steel	9	2.46
Dlugosz 1960	40.67	0.875	ASTM A141	3	2.80
Roeder, Leon, & Preece 1994	56.59	0.75	Grade 1 A502	6	-
D'Aniello, Portioli, Fiorino, & Landolfo 2010	53.04	varies (0.630-0.860)	EN 1993:1-8	8	6.76

Table 2.21 Normalized Average Rivet Ultimate Shear Strength to FHWA Recommendations

Literature	Vu_{avg}/V_u FHWA (2009)	Vu_{avg}/V_u AASHTO (2010)
AREMA 1904	2.7	1.4
Talbot & Moore 1911	3.1	1.6
	2.9	1.5
Davis, Davis, & Woodruff 1939	2.6	1.6
	3.6	2.2
Dlugosz 1960	1.5	1.2
Roeder, Leon, & Preece 1994	2.1	1.7

Table 2.22 summarizes the material tests for-rivets used in the connections, and the third column normalizes the average rivet ultimate strength to the expected strength from material tests. Overall, the rivet in a connection appears to achieve about 74% of a single rivet in double shear.

Table 2.22 Summary of Ultimate Rivet Shear Strength Based on Literature Material Tests

Literature	V_u [ksi]	$V_{u,avg}/V_u$	Single/Double Shear?
Davis, Davis, & Woodruff 1939	42.10	0.763	Double
	54.50	0.726	
Wilson, Bruckner, & McCrackin 1942	63.92	-	Single
	64.82	-	
	75.96	-	
	63.83	-	Double
	61.25	-	
	71.27	-	
Munse & Cox 1952	51.58	-	Single
Dlugosz 1960	55.30	1.360	Double
Roeder, Leon, & Preece 1994	41.00	0.725	Double

Another recurring goal in the research reviewed, was to capture the effect of joint length on average ultimate rivet shear stress. The average rivet shear strength for a connection was normalized by the approximate rivet strength based on the tensile strength of the rivets (from Eq 2-9) for each experiment. Figure 2.32 shows that the rivet shear strength is much more than 67% of the tensile rivet strength as assumed by AASHTO.

The current recommendations from AASHTO, which incorporate a reduction factor for longer connections, were also plotted with the data from the literature review. This shows that the data follows similar trend as AASHTO for shorter connections as the strength decreases linearly, but overall predicts a strength that is 20% lower. This could be a combination of the lack of a length effect in the literature and the assumption of the shear strength in the rivets as 67% of the tensile strength.
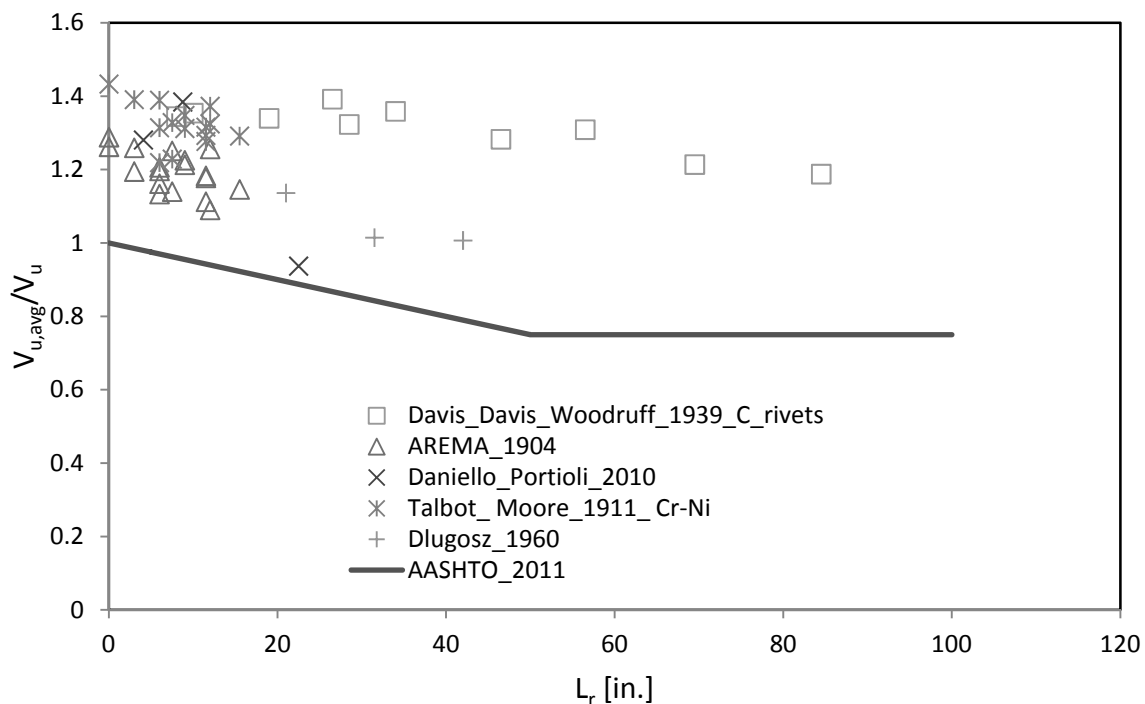
Figure 2.32 Summary of Normalized Ultimate Rivet Shear Strength vs. Joint Length from Literature

Although the data in Figure 2.32 was plotted versus connection length, within each test other parameters were also varied which include the following: rivet grip, loading in single or double shear, rivet pitch, rivet material, and rivet diameter (only in D'Aniello et. al 2011). In order to isolate the effect of connection length on average rivet shear strength, each parameter was considered separately. Many of the connections varied in rivet grip and pitch for a given connection length, however, Section 2.3.1 shows that this did not affect the rivet shear strength significantly. Figure 2.33 shows the data including the shortest grip for each connection length for only carbon steel rivets (the rivet pitch did not vary as much as grip for a given test and was not plotted separately). This shows that the rivet strength was approximately 30% higher than the AASHTO prediction, and the connection length appears

to decrease linearly at a lower slope. The data follows in similar trend for rivets of other materials (manganese, chrome-nickel, and nickel alloys) as shown in Figure 2.34. This shows that for a similar material and grip that the connection length effect is still less than AASHTO predictions.
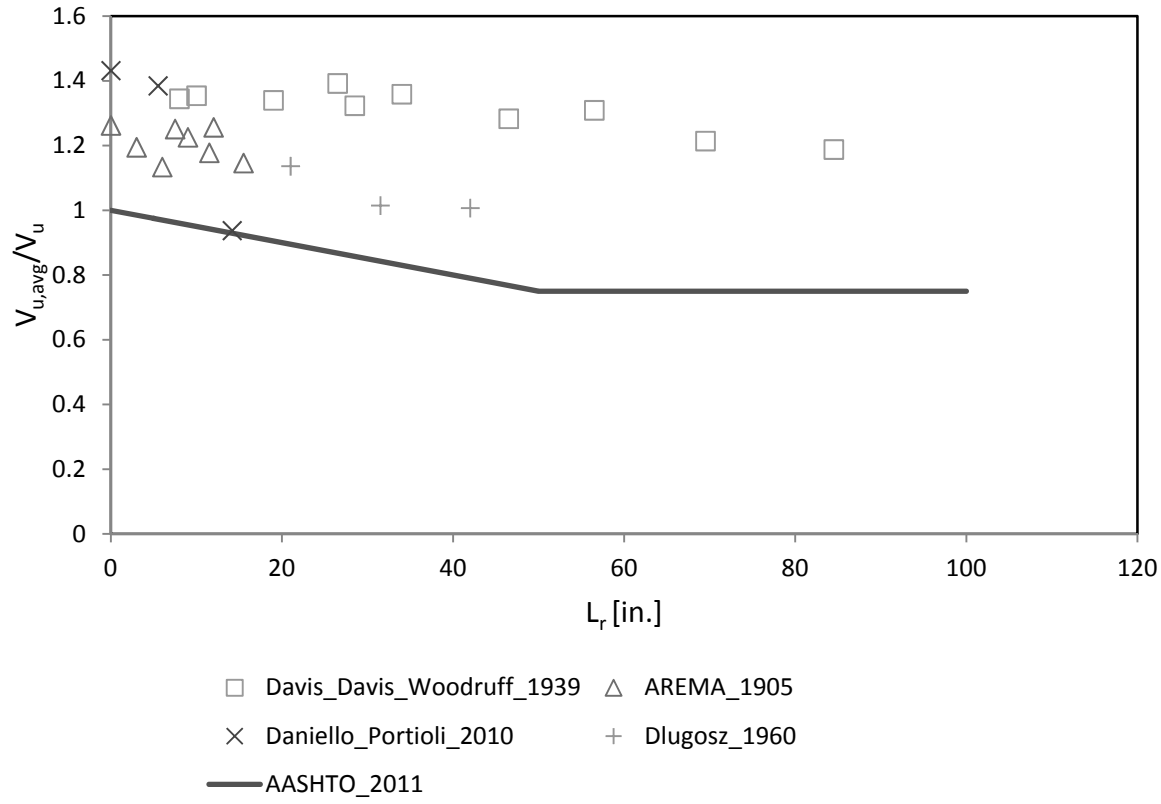
Figure 2.33 Normalized Ultimate Rivet Shear Strength vs. Joint Length for Carbon Rivets
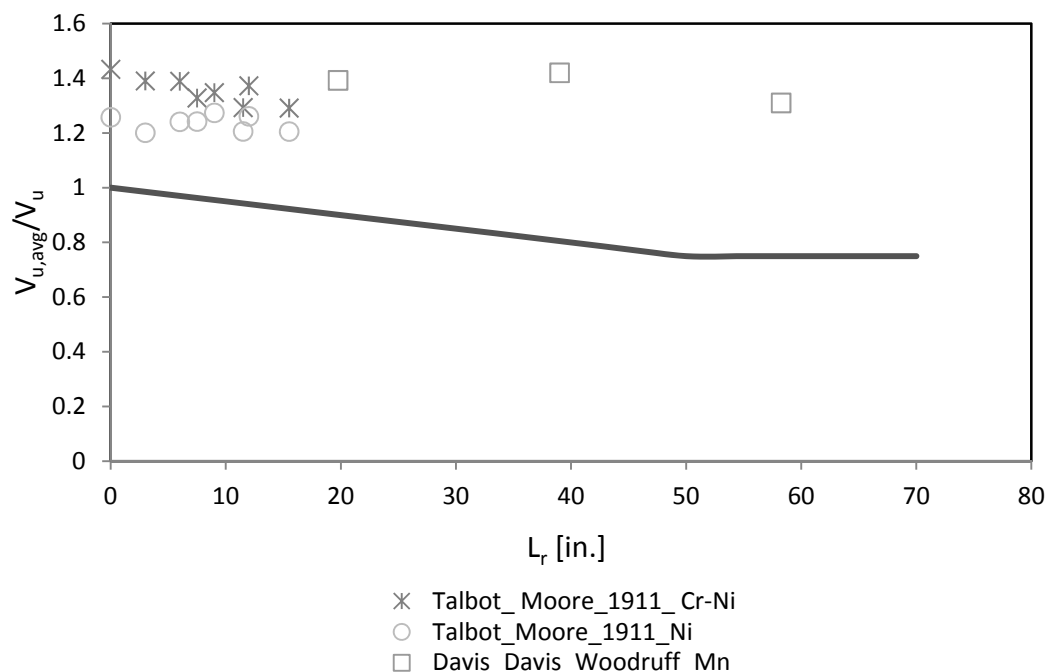
Figure 2.34 Normalized Ultimate Rivet Shear Strength vs. Joint Length for Rivets of Other Materials

The findings from this literature review demonstrate a need for more current research and an investigation of as-built riveted steel structures as opposed to fabricated test specimens (the majority of the research in this literature review was dated prior to 1970). In addition, the joint length effect and force distribution among fasteners may differ if the specimen is not loaded in tension at the ends (all splice tests were loaded in this manner). Lastly, the data from past literature does not indicate as high of a joint length effect as current AASHTO recommendations predict. This review implies that a better understanding of actual rivet shear strength and therefore connection performance could potentially improve the current design recommendations.

Chapter 3: Experimental Design and Setup

3.1 General

The objective of the experiments described in this thesis was to produce data on the effect of connection length on riveted connection strength. The test specimens were fabricated from components salvaged from two aging steel truss bridges and the available geometries constrained the testing possibilities. This required that connections be tested in a loading configuration that is different from the lap splice tests reported in the literature. This chapter describes the test specimens, the bridges they were salvaged from, the development of a test configuration that was capable of testing connections of varying length, and how the loading conditions relate to previous rivet connections tests and the connection of built-up truss members to gusset plates. The geometry of the available salvaged bridge components is discussed first as it controlled the design of the tests and the loading applied to the riveted connections.

3.2 Description of Bridges and Salvaged Bridge Components

The bridge components used in the testing program were salvaged from two steel bridges from Washington State Highway 12. The bridges were in constructed in 1931 and were in service until 2010 when they were demolished and replaced. Bridge 1 was a Pony truss with a Warren configuration and had a span 100 feet, with a 12-foot peak height. In contrast, Bridge 2 was a through truss in a Pratt configuration with a 140-foot span and a 27-foot peak height.

The guardrails were selected from each bridge as the component for testing because there was a large quantity to be salvaged, and the geometry included a long riveted connection length to support the experimental goals. Figure 3.1 depicts the original drawings of Bridge 1, where the location of the guardrail is highlighted (this portion is shown in Figure 3.2). The second bridge and guardrail details are shown in Figure 3.3 and Figure 3.4, respectively.
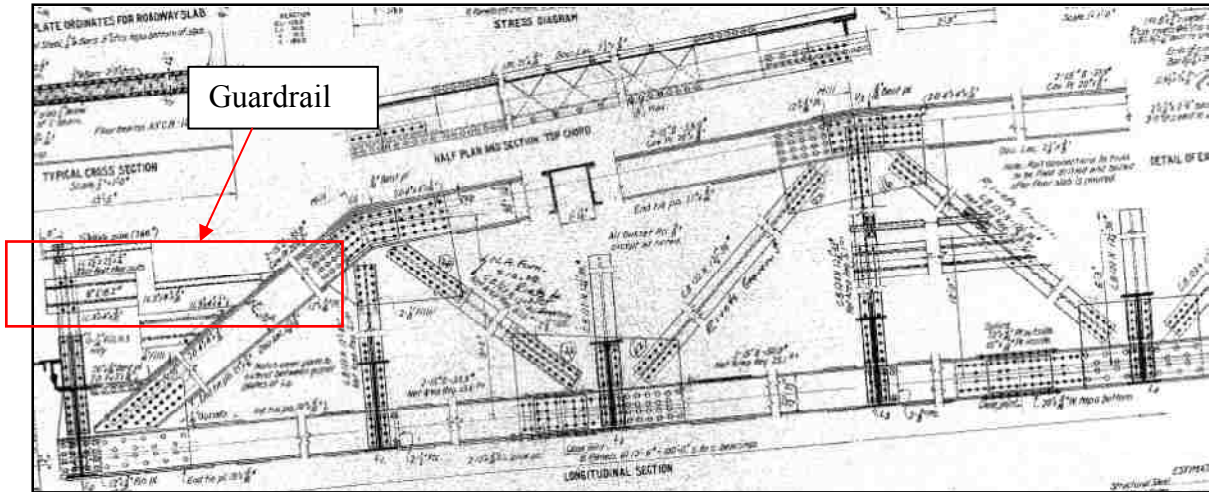
Figure 3.1 Drawing for Bridge 1
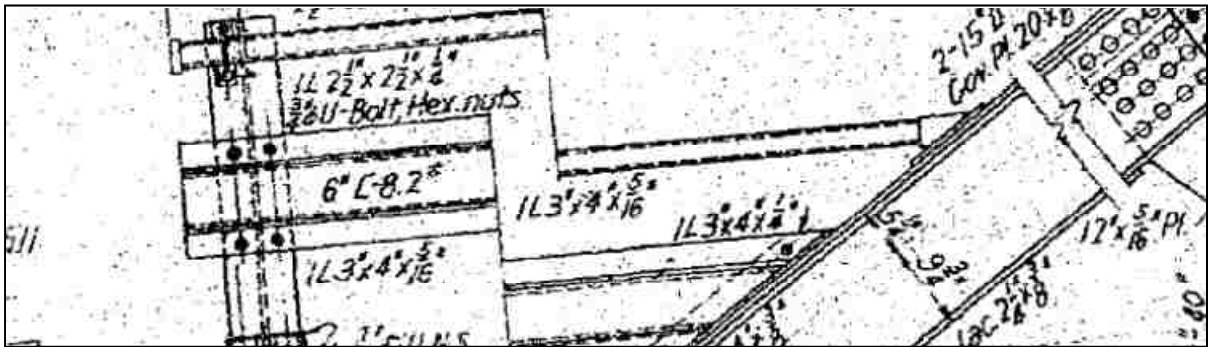
Figure 3.2 Guardrail Section from Bridge 1
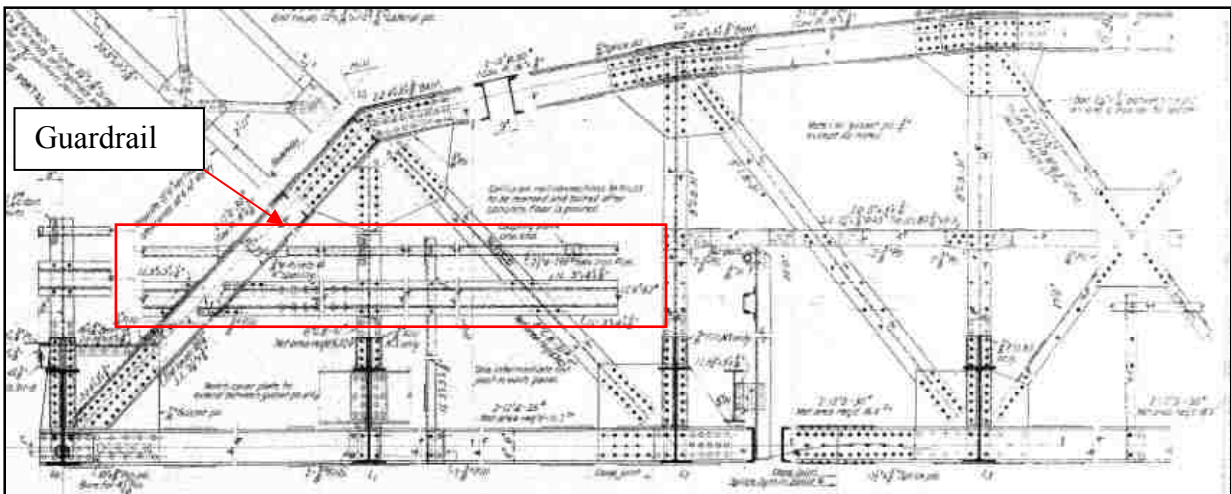
Figure 3.3 Drawing for Bridge 2
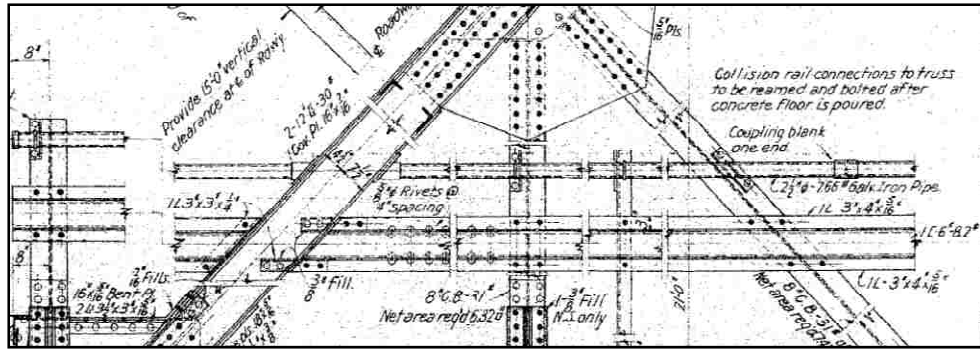
Figure 3.4 Guardrail Section from Bridge 2

The guardrails shown in Figure 3.2 and Figure 3.4 were identical. As shown, each guardrail section consisted of a C6x8.2" and L3x4x5/16" shapes connected by 5/8 in. diameter rivets spaced at 4 in. on center. The type of steel used for the channel and angle of the guardrail was likely to be A7 based on the date of construction.

In addition to the guardrail, gusset plate joints were salvaged from Bridge 1 and Bridge 2. While these joints were not used in the tests described, they may be used in future tests to verify some of the conclusions reached here. A photo of Joint U3, which was salvaged from Bridge 1, can be seen in Figure 3.5.

Figure 3.5 Joint U3 from Bridge 1

3.3 Description of Salvaged Guardrail Components

This section describes the geometry, condition, and material properties of the salvaged guardrail.

3.3.1 Geometry

Six sections of a guardrail were salvaged from Bridge 1 and Bridge 2 described in Section 3.2.

Figure 3.6 below depicts one of the original guardrail specimens. The salvaged guardrail sections were the longest of the salvaged pieces and were continuously riveted. Thus, the guardrail sections presented an opportunity to test connections of varying length with minimal test setup. The total length of guardrail salvaged was approximately 562 in. (46 ft 10 in) with the longest connection being 99 in. and the shortest being 51 in. Figure 3.7 below shows the cross section of the guardrail.

Figure 3.6 Original Guardrail Specimen
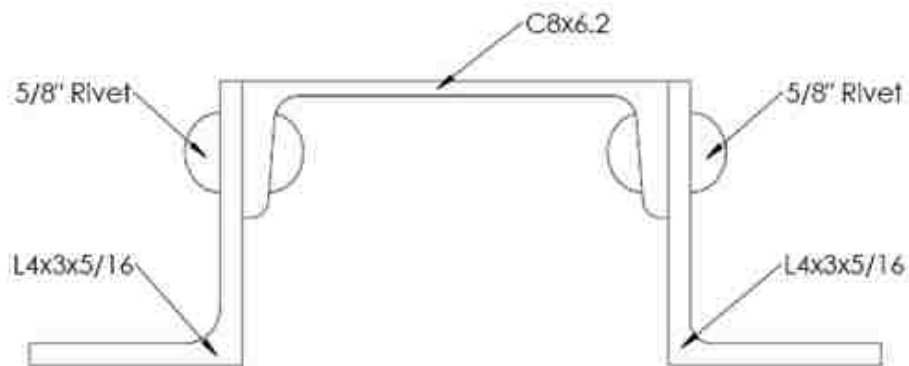
Figure 3.7 Cross Section of Guardrail Specimen

3.3.2 Condition of Salvaged Guardrail Components

All guardrail sections were professionally sandblasted to remove the many layers of paint and allow for fabrication (Figure 3.8 below depicts the guardrail specimens after sandblasting). Many small holes used to connect the guardrail to the bridge in service were present in the channel web and legs of the angles. In addition, some of the guardrails had channels or angles that were not continuous for their entire length. A few dents were also present in the channel flange and at the angle leg to channel flange connection. All of these types of imperfections were documented and considered in selecting the lengths of guardrail from which to fabricate the specimens.

Figure 3.8 Guardrail Specimens after Sandblasting

3.4   Development and Discussion of the Experimental Setup

This section describes the development of the test specimen geometry, method of loading, and discusses how the loading compares with previous testing and loading conditions in actual splice riveted connections in bridges. The last sub-section describes the expected behavior of the resulting test specimen.

3.4.1   Development of the Test Specimen Geometry

Prior to testing the rivets in the guardrail, it was necessary to modify the cross section to ensure the failure occurs in the rivets. There were many considerations in developing the test setup for the guardrail sections to accommodate the desired failure modes, the guardrail geometry, and the test machines. These are described below.

First, the guardrail cross section cannot be loaded in tension or compression in its original configuration. In tension, it is difficult to grip both ends with the channel shape on one end and the angles on the other. Furthermore, if tested as a splice connection between the angles and channels, the length would be very limited since the axial capacity of these pieces is small (see Figure 3.9). Loading the ends of the specimen in tension (similar to past research) or compression would result in failure of the connecting elements prior to developing the strength of the rivets. Since the specimens gathered for this research program are in their as-built condition, it was found to be difficult to modify their cross-sectional area to improve their strength and test them in tension or compression. Additional difficulties were found for providing stability if tested in compression and by the large eccentricity of the cross section.
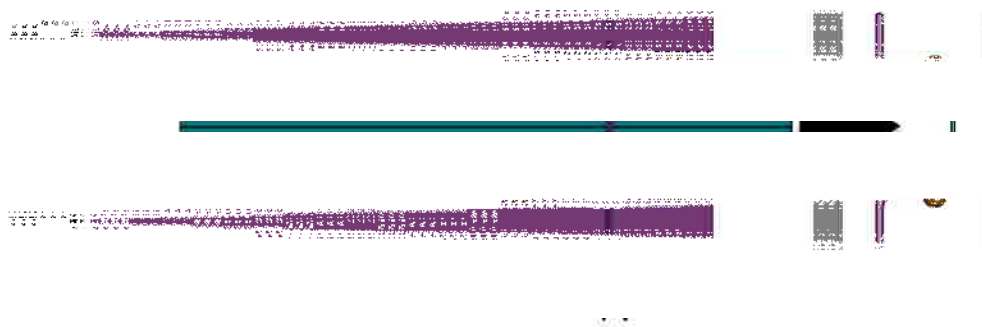
Figure 3.9 Testing Guardrail in Tension "Lap-Splice"

Therefore, an alternate form of load transfer was developed to overcome yielding of the connecting elements, global stability and eccentricity while allowing for the testing of connections of various lengths. The setup was designed to load the connection in shear rather than in tension or compression as a splice, as the connecting elements are too weak. To reduce eccentricity and improve torsional stability, the guardrail sections were cut longitudinally and placed back-to-back as shown in Figure 3.10. As shown, one of the half cross sections was flipped upside down to reduce eccentricity between the rows of rivets. To load the channels and angles in shear such that the cross sections do not fail in tension or compression, the half cross sections of guardrail in Figure 3.10 were bolted to a middle plate at the channel (see Figure 3.11a).

(a)   (b)
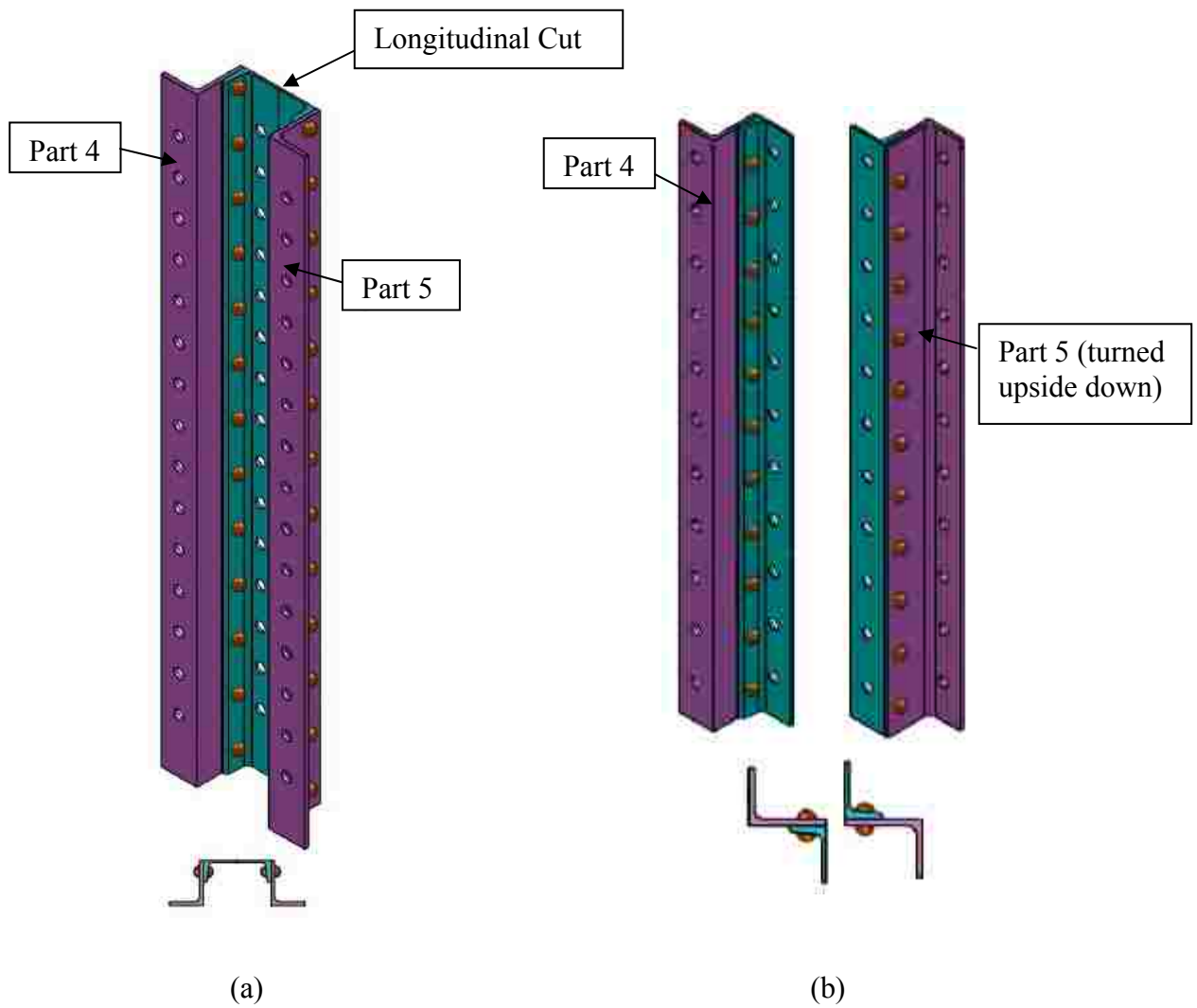
Figure 3.10 Fabrication of Guardrail for Test Specimen (a) Guardrail Prior to Longitudinal Cut (b) After Cut
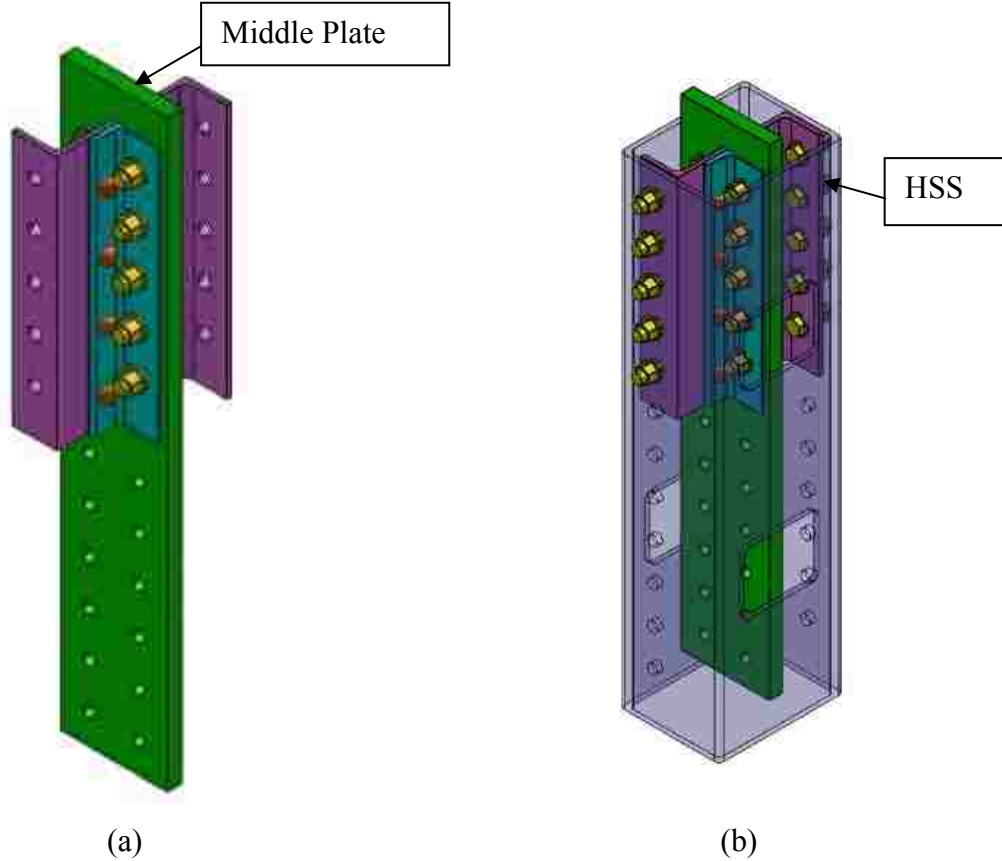
Figure 3.11 Guardrail Sections Bolted to (a) Middle Plate and (b) Hollow Structural Shape (HSS)

The angle was then bolted to a hollow structural section (HSS) as shown in Figure 3.11b. Slip critical bolted connections were designed for connection to the plate and HSS, and the shear transferred to the angles and channels can be assumed as uniform. Transferring the load in this distributed manner enables the rivets to develop their strength before failure of the connecting elements but results in a difference in loading with previous tests as discussed in Section 0 and 3.4.4. Placing the middle plate and guardrail longitudinally inside of the rectangular HSS, improved global stability and allowed for testing of connections of various lengths. The resulting configurations are described in detail in the following section.

3.4.2   Guardrail Configuration Designs

Two test configurations were designed to accommodate various connection lengths. The configuration for shorter connections was tested in a 300-kip Universal Testing Machine, denoted the "Small Baldwin," and the configuration for longer connections was tested in the 2400-kip capacity Universal Testing Machine denoted the "Baldwin." Each was designed to use the HSS tube and middle plate to enable the tests of riveted joints. Figure 3.12 and Figure 3.13 show the Small Baldwin and Baldwin test configuration with parts listed in Table 3.1 and Table 3.2, respectively.
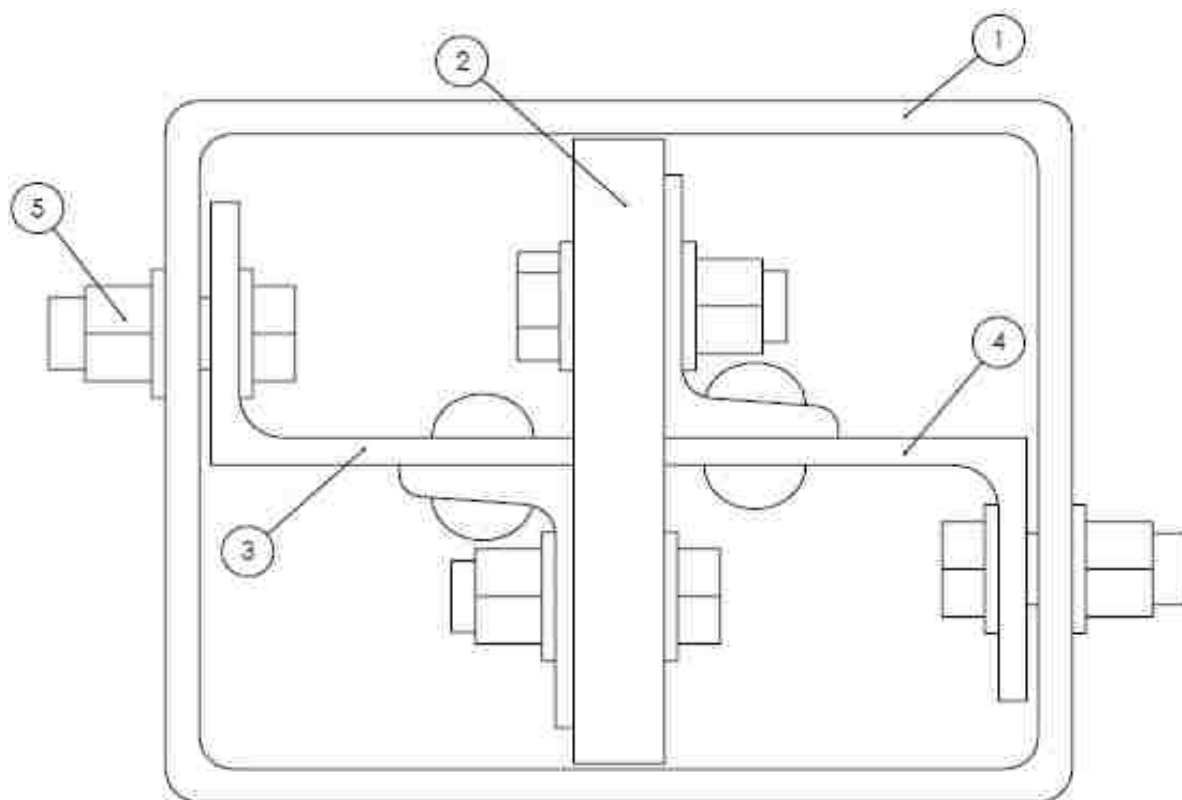
Figure 3.12 Cross Section of Small Baldwin Guardrail Configuration

Table 3.1 Small Baldwin Configuration Parts

Part No.	Name	Material	Grade [ksi]
1	HSS 10 x 8 x 3/8"	A500	46
2	PL 7 1/8 x 1"	A572	50
3	West Guardrail	A7	36*
4	East Guardrail	A7	36*
5	¾" Bolts	A490	

*Nominal strength, C6x8.2 and L4x3x5 were tested separately for tensile strength
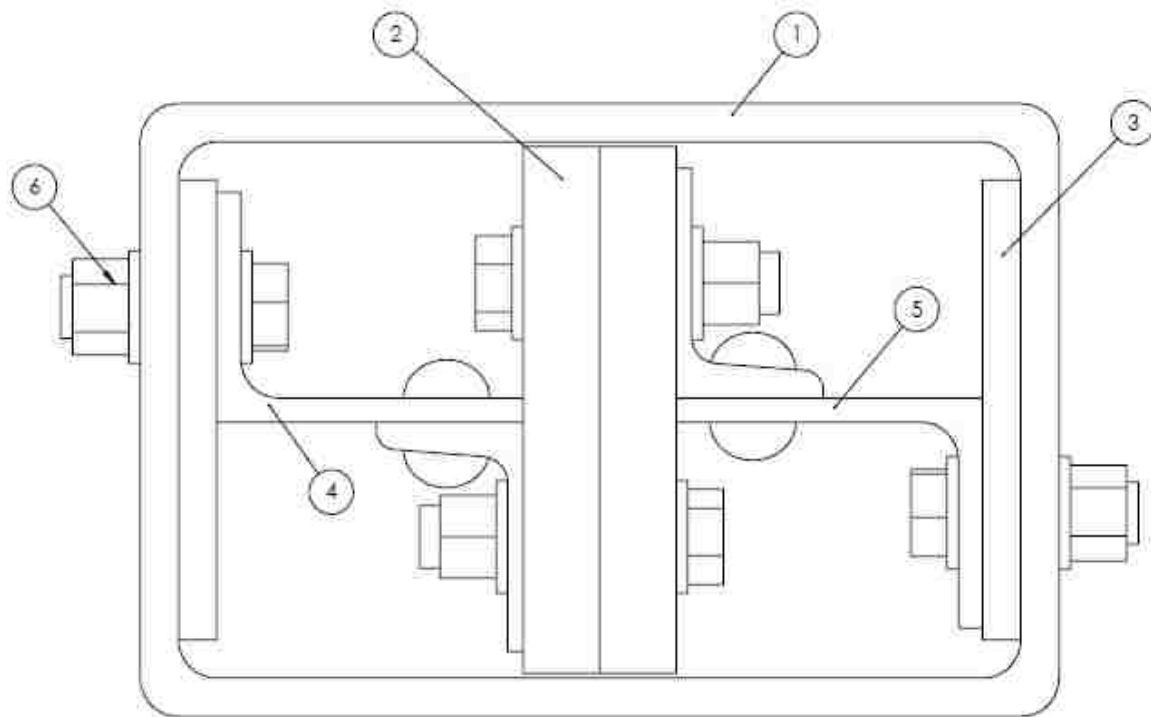
Figure 3.13 Cross Section of Baldwin Guardrail Configuration

Table 3.2 Baldwin Guardrail Configuration Parts

Part No.	Name	Material	Grade [ksi]
1	HSS 12 x 8 x 1/2"	A500	46
2	PL 6 7/8" x 1"**	A572	50
3	PL 6 x 1/2"	A572	50
4	West Guardrail	A7	36*
5	East Guardrail	A7	36*
6	¾" Bolts	A490	

*Nominal strength, C6x8.2 and L4x3x5 were tested separately for tensile strength
**Quantity: 2

There were a few differences between the two designs. First, the HSS for the Baldwin design is wider and thicker to allow for more compression capacity. Second, there are two middle plates, which are wider for the Baldwin design to allow for increased compression capacity. These differences enabled testing of longer riveted connections in the Baldwin. Lastly, the material for the shim plates in the Small Baldwin design was A36 rather than A572 for the Baldwin design, as only A36 was available for the required thickness. Shim plates were used (Figure 3.12 and Figure 3.13 Part 2), if necessary to fit the configuration together. Full sets of drawings for each configuration can be found in Appendix D.

3.4.3 Loading of Guardrail Test Configuration

The test configurations were loaded by pushing on the rectangular HSS on the bottom and top of the middle plate as shown in Figure 3.14. The load transferred through friction in the slip critical bolts to the channel (from the plate) and the angle (from the HSS) then through the rivets in shear. The configurations were designed so that the capacity of the setup was not exceeded during the testing. The setup capacities that were considered include yielding of the cross-sections, slip of the bolts that connect the plates to the channel or HSS to the angle, and bearing at the riveted connections. Sample calculations are provided in Appendix C.
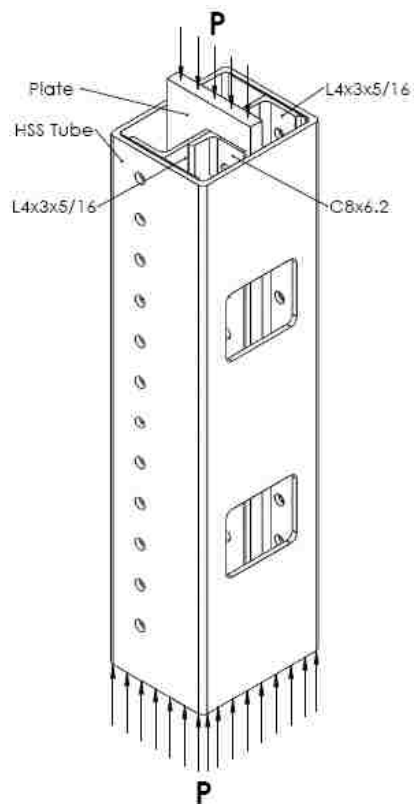
Figure 3.14 Loading of Guardrail Configuration
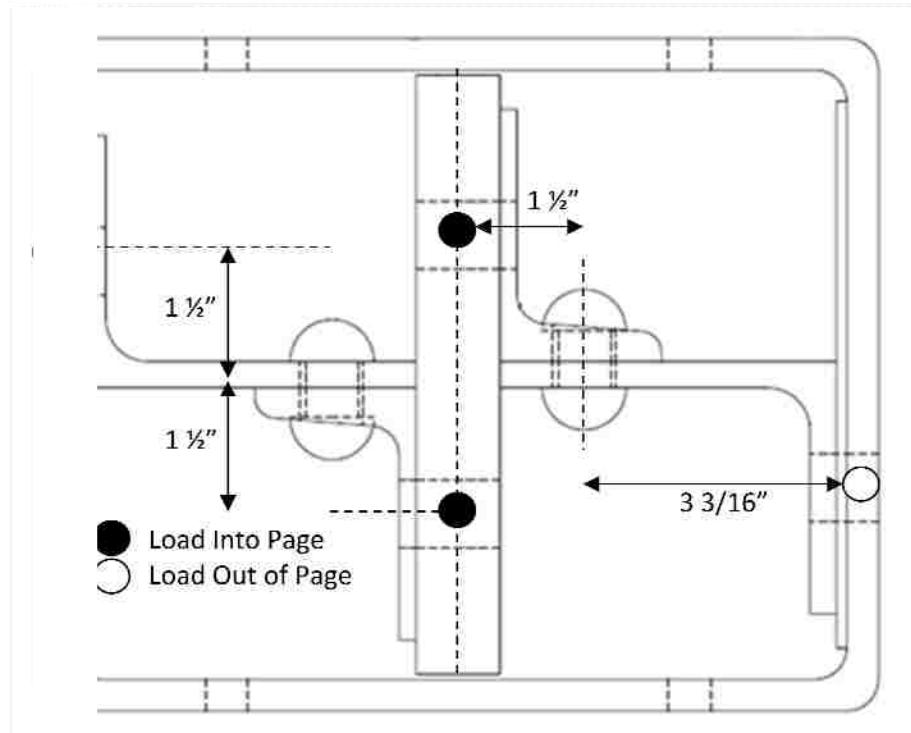
Figure 3.15 depicts the load transfer through the bolts to the rivets in plan view. The loads out of the page represent the load from the middle plate and the loads into the page come from the HSS shape. The geometry of the loading results in direct loading of the rivets in shear.
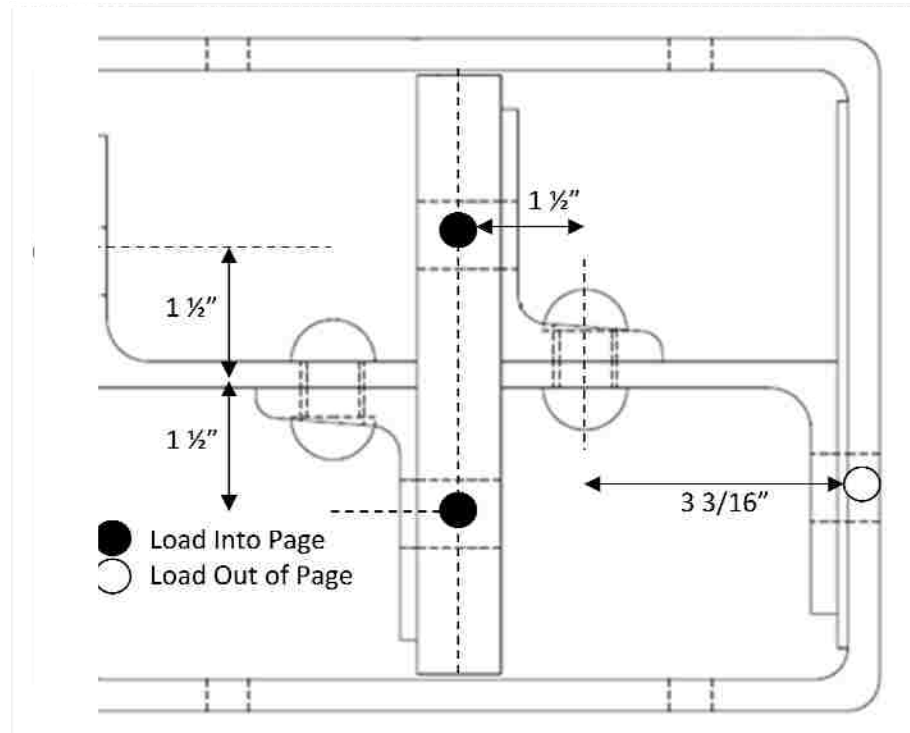
Figure 3.15 Cross Section With Load Transfer

3.4.4 Comparison with Previous Experimental Programs

In past tests, riveted connection specimens had been fabricated and tested in a lap splice configuration (see Figure 2.19). The specimen is loaded in tension at the ends (see Figure 3.16a), which places the rivets in double shear. This loading leads to higher stresses in the rivets at the ends of the connection especially when yielding occurs in the connecting elements. As shown in the literature review, some tests have demonstrated that as the connection length increases, the stresses in the rivets at the ends of the connection increase relative to the average rivet stress. For tests of longer connections, a larger net section area of the connected elements was typically used to ensure failure occurred in the rivets via shear.

The loading of the riveted connection in the guardrail test described here differs from that of previous research described in Section 2.3. Some of the lap splices contained multiple rows of rivets (see Section 2.3.6 Dlugosz (1962)), where this configuration has one row of rivets being loaded. More importantly, the rivets will be loaded in a distributed manner rather than at the ends, which could lead to different results. In the theoretical study performed by Fisher and Rumpf (1967), the spliced connection was loaded in tension at the ends creating a

fastener stress distribution as depicted in Figure 2.26, where the outer bolts have a larger stress than the middle bolts for longer connections. In contrast, in the setup for testing the guardrail components, the load is transferred to the rivets through other structural members instead of loading the rivets directly. The members are loaded through slip critical bolts along their length rather than at their ends. This creates a uniform shear load distribution due to the distributed nature of the bolted connection (see Figure 3.16b). It is expected that the nearly uniform shear stress distributions in the guardrail components will lead to more uniform stresses in the rivets.

(a)

(b)
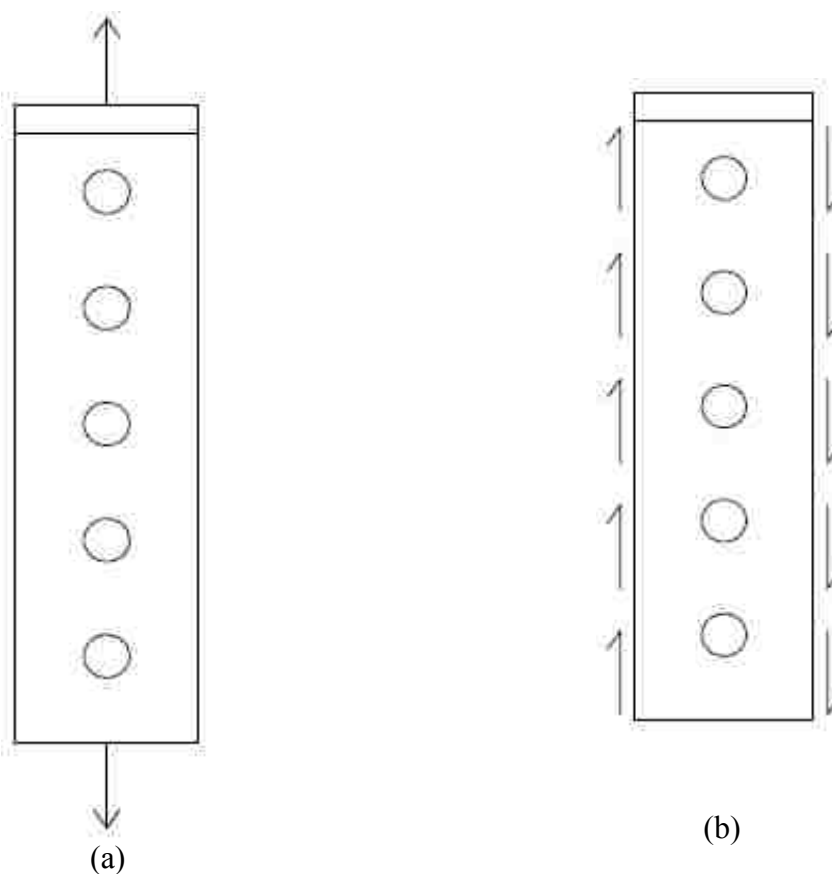
Figure 3.16 Loading Comparison (a) Fisher & Rumpf (1967) (b) Current Research Program

In steel truss bridge gusset plate connections, the load is applied to the riveted connections as a combination of a distributed shear load and a tension load at the ends (i.e. a combination of the loading from Fisher and Rumpf (1967) and the loading used here). Figure 3.17 shows a typical gusset plate connection, with the built up connecting member consisting of a channel and two plates. When the member is loaded, the shear load is transferred from the channel to the gusset plate rivets via tension load at the ends and from the plate to the gusset plate rivets

via a distributed shear load. Therefore, an investigation of riveted connection response under the loading described here provides complimentary information on connection strength.
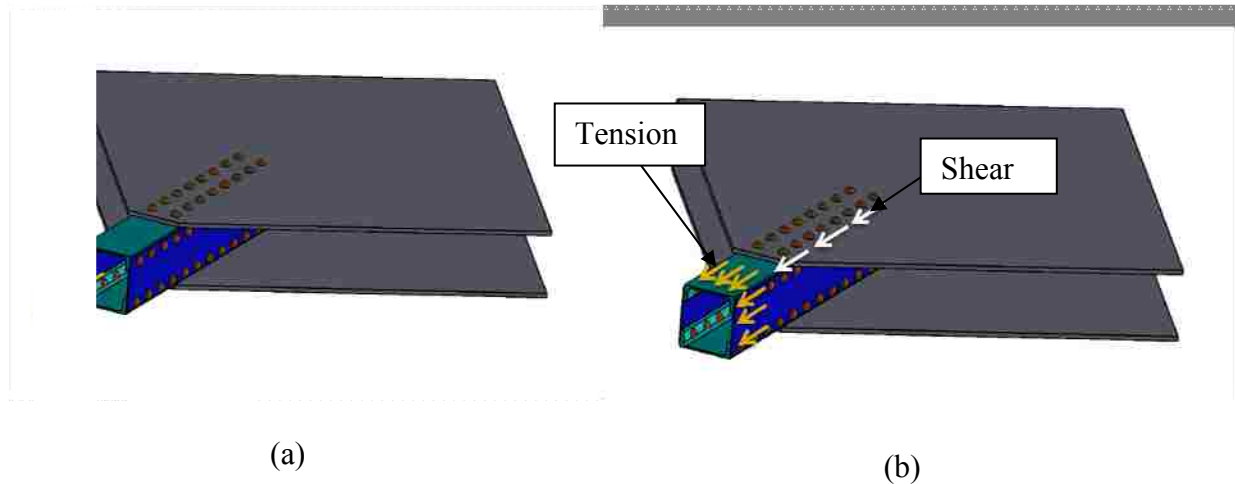
Figure 3.17 Gusset Plate Loading via Tension and Shear

3.4.5   Assessment of Yielding in Gusset Plate Connections and the Test Specimen

The following section describes the behavior of gusset plate connections based on an analysis of bridges from the 1930-1950s (similar to the test specimen) and leads to an analysis of yielding in the connecting elements of the test specimen for this experimental program.

3.4.5.1   Yielding Elements in Gusset Plate Connections

To understand the expected behavior of the guardrail configuration during testing, the geometry and material properties of three bridges from Washington State: Metaline Falls Bridge over Pend Oreille River (1950), Cle Elum River Bridge (1949), and HOH River Bridge (1930) were studied. These bridges were selected because they were constructed in a similar era as the bridges where the guardrail was salvaged. Therefore, they were likely designed using similar provisions and they were likely built with similar structural and rivet steel properties.

3.4.5.2   Description of Gusset Plate Analysis

To determine if an element in a gusset plate connection was expected to yield prior to failure of the rivets in shear, the drawings were analyzed by gathering the geometry of the connection. The following parameters were compared for a given connection:

- A_n/A_s ratio : Net Tension Area of Connecting Elements to Total Rivet Shear Area

- A_sF_u : Total Rivet Shear Area x Average Ultimate Rivet Shear Strength

- A_nF_y : Net Area of Connecting Elements x Yield Strength of Connecting Elements

- A_nF_y/A_sF_u ratio: Net Area of Connecting Elements x Yield Strength Total Rivet to Total Rivet Shear Area x Ultimate Rivet Shear Strength

- A_nF_y/A_sERY ratio: Net Area of Connecting Elements x Yield Strength Total Rivet to Total Rivet Shear Area x Effective Rivet Yield (ERY)

The yield capacity of the connecting elements (F_y), Effective Rivet Yield (ERY), and the average ultimate rivet shear strength (F_u) were assumed based on material test results (experimental from Section 4.2), values from literature (expected), and values from design standards from the time of bridge construction (nominal from ASTM standards for allowable stresses listed in Table .A.1). The connecting elements and rivet steel were assumed A7 steel from bridges constructed from 1924-1931. The nominal ERY was taken from recommendations by Olson (2010). The expected values were assumed 10% higher than the nominal values as recommended by ASTM. The experimental rivet shear strength was based on the test described in 0, where the ERY was estimated from the average rivet shear stress versus joint set plot, and the yield strength of the connecting element was assumed as the strength of the guardrail angle (section 4.2.2) which was likely A7 steel. Table 3.3 summarizes these values.

Table 3.3 Material Properties for Bridge Analysis

	Nominal	Expected	Experimental Results
Rivet F_u shear [ksi]	15	16.5	53.20
Rivet ERY [ksi]	18	19.8	36.20
Plate F_y [ksi]	33	36.3	32.59

For a gusset plate connection, the parameters listed above were calculated based on the values in Table 3.3 and the geometry of the gusset plate (A_n, A_s), which was gathered from the drawings. The net area was calculated by taking the gross area of the connecting element (angle, plate, wide flange structural shapes) and subtracting the area of the rivet holes in the connection. Figure 3.18 is an example of a gusset plate connection from the original drawings for the Cle Elum River Bridge.
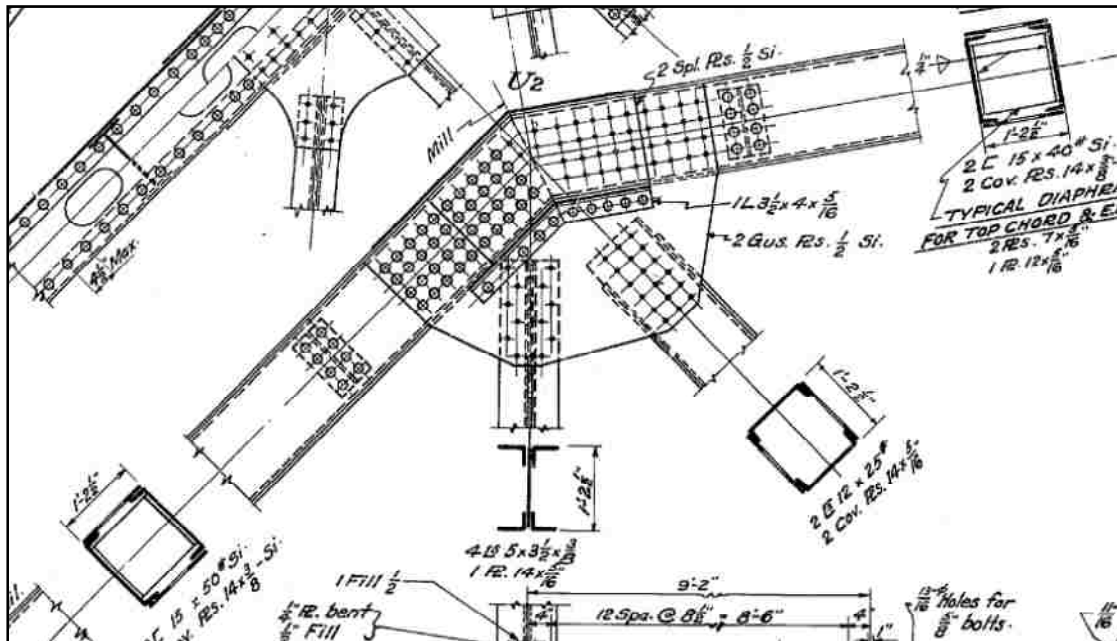
Figure 3.18 Drawing from Cle Elum River Joint U2

3.4.5.3 Summary of Connecting Element and Rivet Behavior

The results of the study for the Cle Elum River Bridge are described below. Figure 3.19 represents a schematic of the Cle Elum River Bridge including gusset plate names. Additional data measuring the parameters listed above can be found in Appendix B.
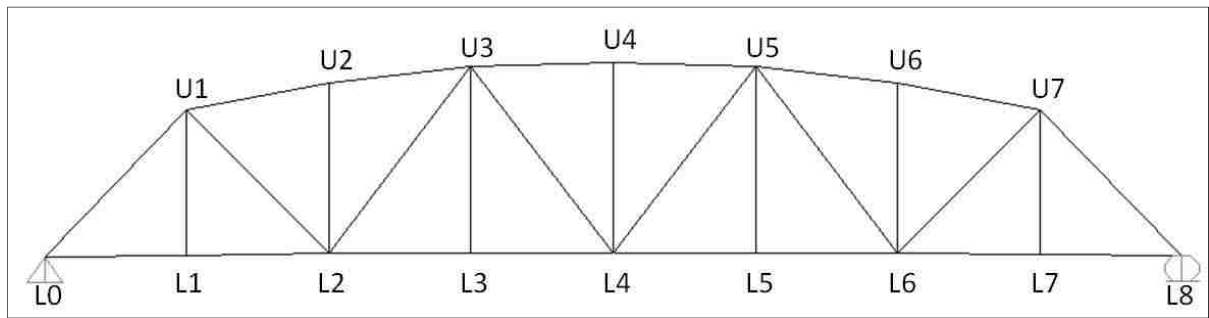
Figure 3.19 Schematic of Cle Elum River Bridge Truss

Figure 3.20 represents the A_nF_y/A_sF_u ratio for all gusset plate connecting elements (hanger, diagonal, and upper chord) using nominal values for material properties. All ratios are greater than 1.0, which suggests that failure of the rivets in shear will occur prior to yielding of connecting elements. The same relationship was found using the expected values from Table 3.3.
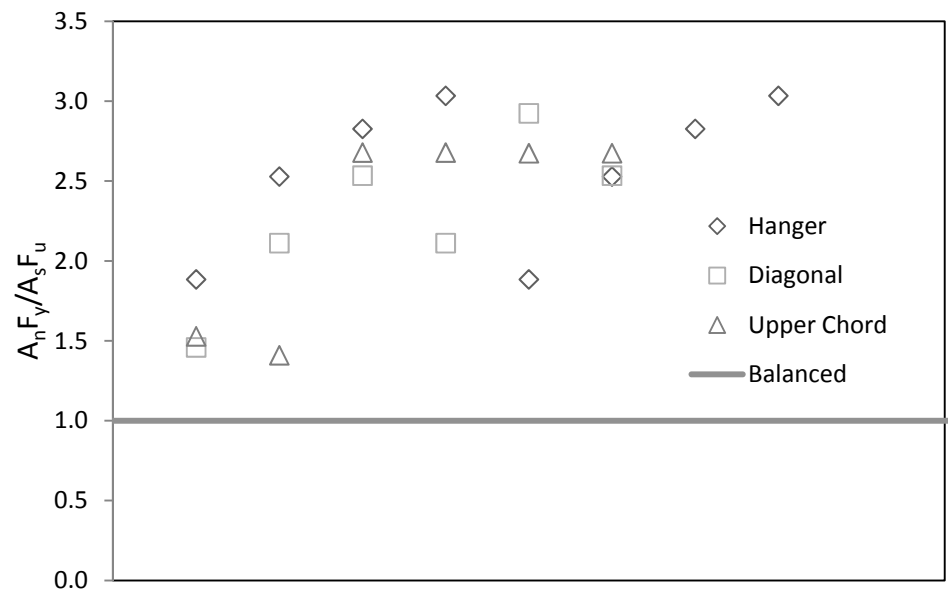
Figure 3.20 Cle Elum River A_nF_y/A_sF_u Ratio – Nominal Values

Figure 3.21 shows the A_nF_y/A_sERY ratio, which signifies the onset of non-linear behavior in the rivets. All ratios are greater than 1.0, which suggests that the connecting elements will remain elastic at the time of yielding of the connecting elements. Similar results were found using the expected values from Table 3.3.
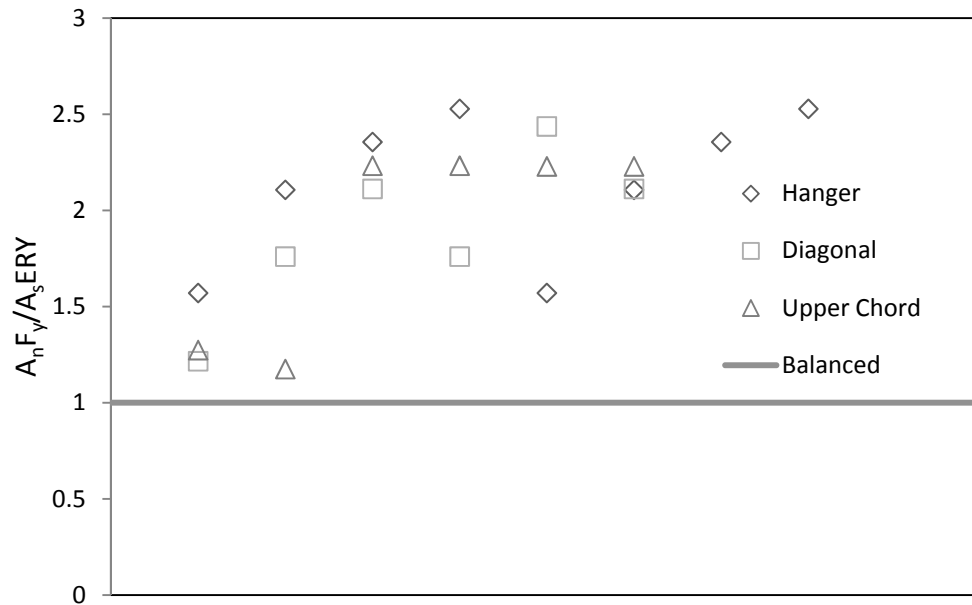
Figure 3.21 Cle Elum River A_nF_y/A_sERY Ratio – Nominal Values

When the experimentally obtained values were used, a different relationship was found (see Figure 3.22). All ratios are less than 1.0, which suggests that the connecting elements will yield prior to failure of rivets in shear. In addition, Figure 3.23 shows that the rivets could potentially behave in-elastically prior to yielding of the connecting elements.
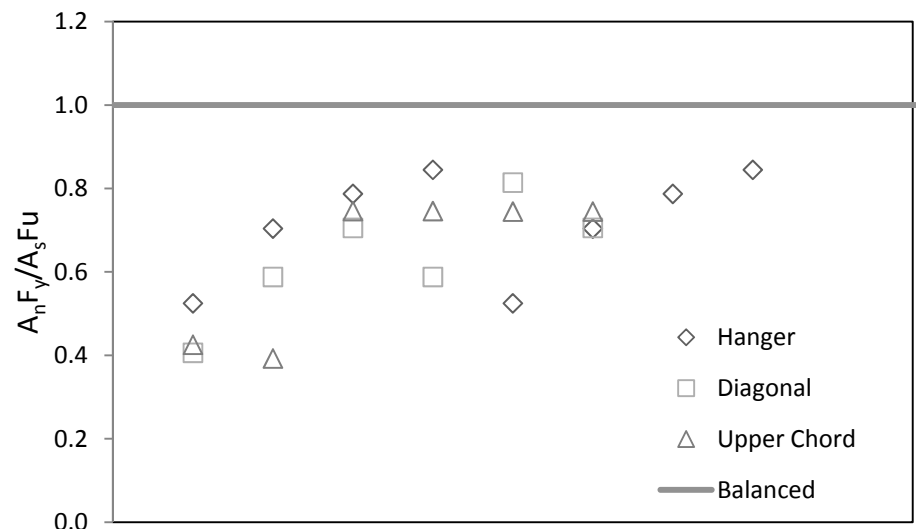
Figure 3.22 Cle Elum River A_nF_y/A_sF_u Ratio – Experimental Values
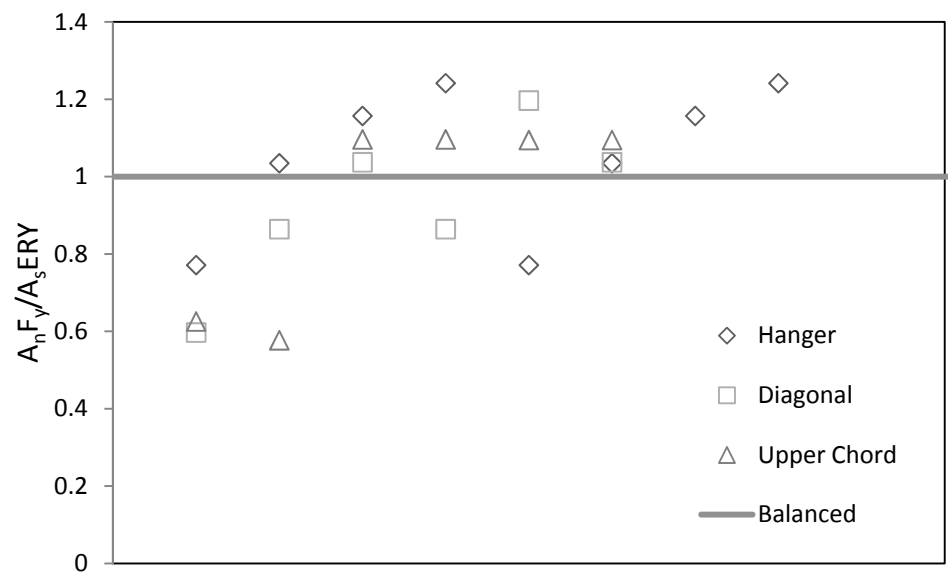
Figure 3.23 Cle Elum River A_nF_y/A_sERY Ratio – Experimental Values

The results from the other bridges (HOH River and Metaline Falls) were similar to those of the Cle Elum River Bridge. These results show that at the time of design, based on nominal and expected material properties; it was likely assumed that the connecting elements would not yield at the time of rivet failure in shear. However, actual material test results indicate that the connecting elements will yield prior to rivet failure. Therefore, the latter behavior should be expected during the testing of riveted connections in this research program.

3.4.5.4   Yielding in the Guardrail Test Configuration

The test configuration described above load the connecting elements in shear rather than tension. Nonetheless, it is appropriate to examine the likelihood of connecting element yielding in the test specimen. To do this, similar calculations as those described in Section 3.4.5.2 were performed as described below. The material properties listed in Table 3.4 are identical to those from Section 3.4.5.2, and the experimental values from the channel and angle came from coupon tests described in Sections 4.2.1 and 4.2.2. Table 3.5 gives the force required to yield the element cross section or rivet using expected, nominal, and experimental values.

Table 3.4 Material Properties for Guardrail

	Nominal	Expected	Experimental
Rivets			
F_u Shear [ksi]	15	16.5	53.2
ERY [ksi]	18	19.8	36.2
Connecting Elements			
Angle F_y [ksi]	33	36.3	32.59
Channel F_y [ksi]	33	36.3	41.7

Table 3.5 Rivet Force and Yield Force

Element	Area [in^2]	Nominal	Expected	Experimental
		Yield Force [kips]		
C6x8.2 (half)	1.20	39.44	43.38	49.83
L4x3x5/16"	2.09	68.97	75.87	68.11
		Rivet Force [kips]		
Single Rivet	0.31	4.60	5.06	16.32

The shear yielding capacity was calculated for the channel and angle along the guardrail connection (AISC J4-3). The shear force transferred from the rivets was calculated using values obtained experimentally for rivets from a different bridge of similar vintage as listed in Table 3.5. The length of the connection was assumed as the rivet length plus 4 in. The equations used to calculate the shear yield capacity are listed below.

$$R_n = 0.6 * A_g * F_y \qquad (3.1)$$

where: R_n = shear yield capacity

A_g = gross area subject to shear [in2]

F_y = yield strength of element [ksi]

$$A_g = L * t \qquad (3.2)$$

where: A_g = gross area subject to shear [in2]

L = connection Length [in.]

t = element thickness [(L4x3x6/16 t=0.3125 in., C6x8.2 t_w = 0.200 in.)

$$L = (n - 1) * s + 2c \qquad (3.3)$$

where: L = connection length [in.]

n = no. of rivets per row

s = spacing of rivets (4 in.)

c = clearance from rivet to end of element (2 in)

81

The sections of the guardrail cross section used for computing the shear area are depicted in Figure 3.24. For the calculations, the minimum thickness of each element was used, so that the shear yielding capacity was the lower bound for that element. The relationship between the shear yielding capacity of the angle and channel with the rivet force assuming experimental material properties is plotted in Figure 3.25.
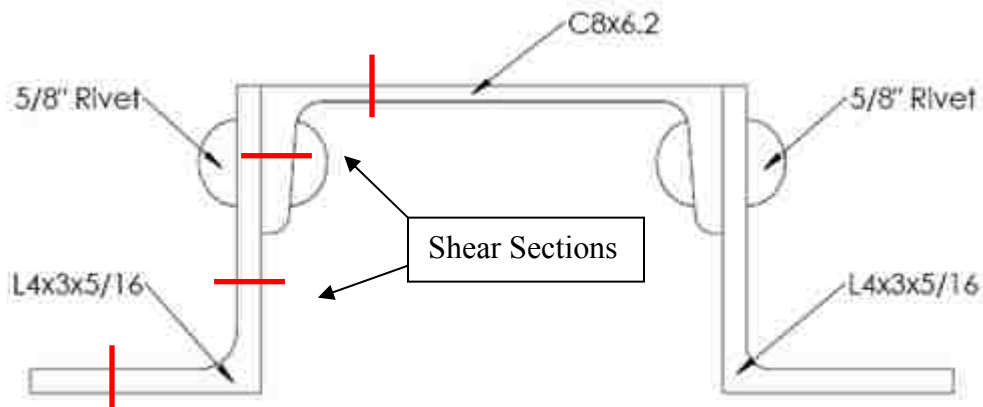
Figure 3.24 Guardrail Faces Subject to Shear
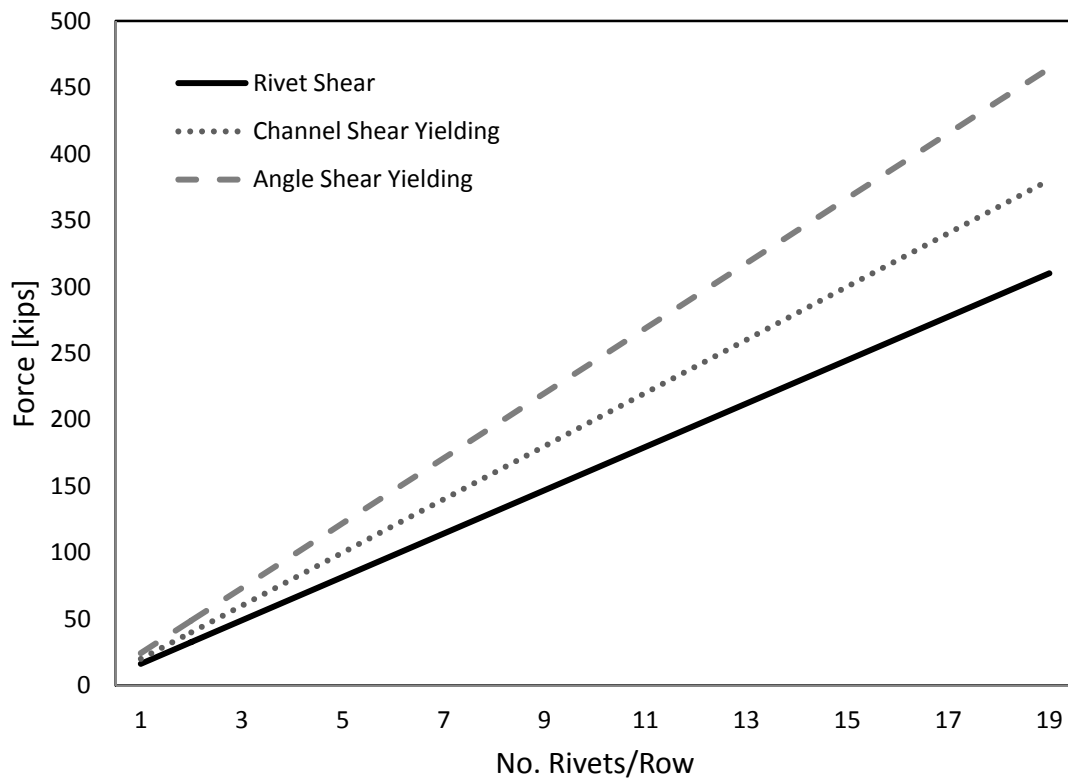
Figure 3.25 Force vs. No. Rivets/Row Shear Yielding

These results suggest that the channel and angle sections are unlikely to yield in shear with the given strength of the rivets. However, the shear capacity is close to the load that will be applied, therefore, if the rivets are stronger than the ones tested from a different bridge or if the connecting elements are weaker, there is potential for shear yielding in the channel. The results also show that shear yielding becomes less likely as the length of connection increases.

3.4.6   The Effect of Eccentricity in the Test Setup

While minimized, eccentricity in the test setup is still present as the distance from the rivets to the bolts attaching the angles and channels are not equal as shown in Figure 3.26. The distance from the bolt line to the rivets is e_1 (from the middle plate) and e_2 (from the HSS). A free body diagram of the shaded portion in Figure 3.26 of the guardrail will be analyzed to determine the effect of this eccentricity on the rivets.
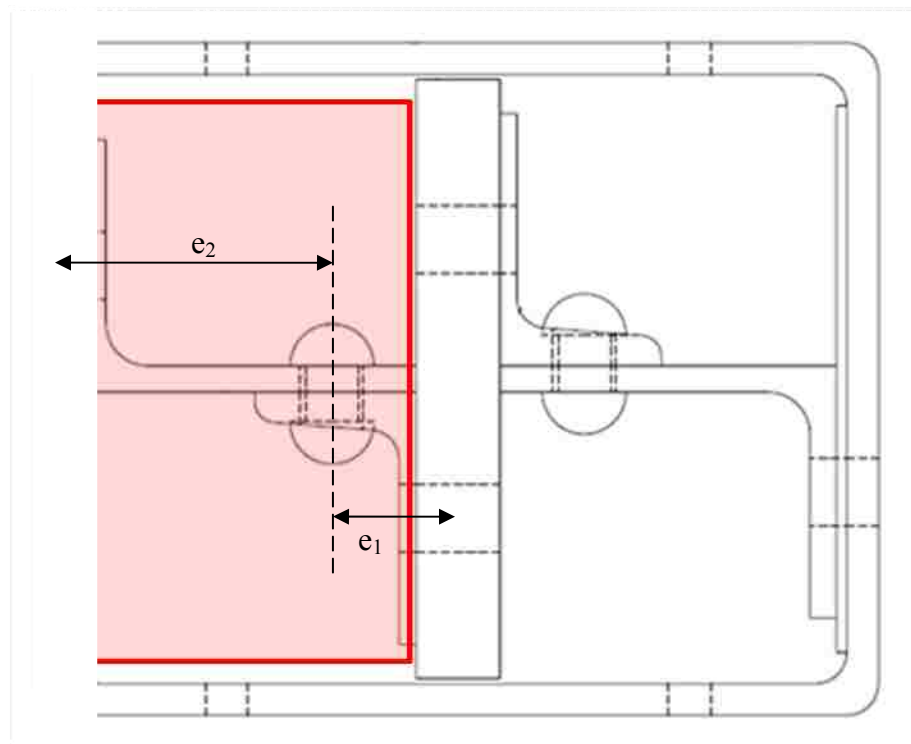
Figure 3.26 Free Body Diagram of Guardrail Configuration

The diagram below shows the distributed load from the middle plate and HSS as *P/2*, each at eccentricities of e_1 and e_2, respectively. For equilibrium, a moment from the tube (M_T) and from the plate (M_P) must be present.
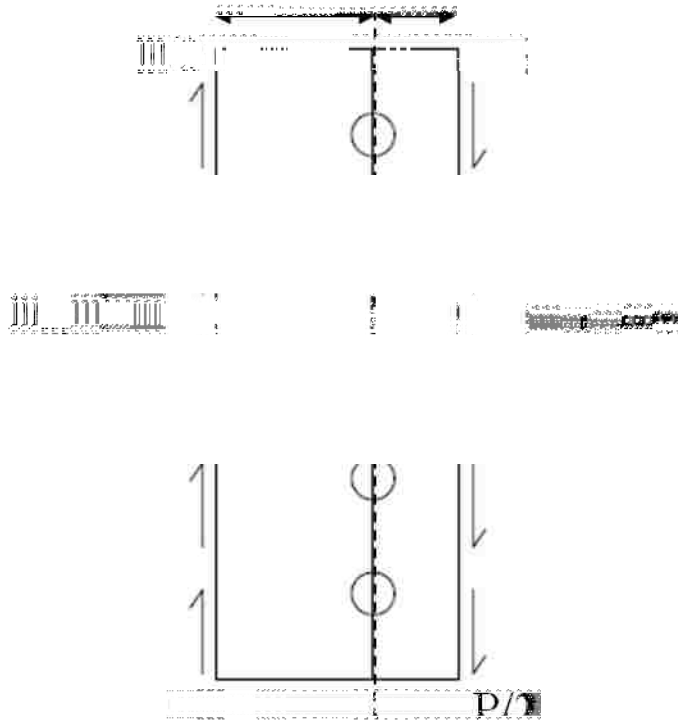
Figure 3.27 Guardrail Section Free Body Diagram

From the diagram above, the following equilibrium equation can be derived:

$$M_T + M_P = \frac{P}{2}(e_1 + e_2) \tag{3.4}$$

If the guardrail section is cut down the line of rivets giving the free body diagram of Figure 3.28, it is clear that the force in the rivets, *P/2*, and the moment in the tube must be resisted by a moment in the rivets (M_R). The corresponding equilibrium equation is given in Eq-3.5.
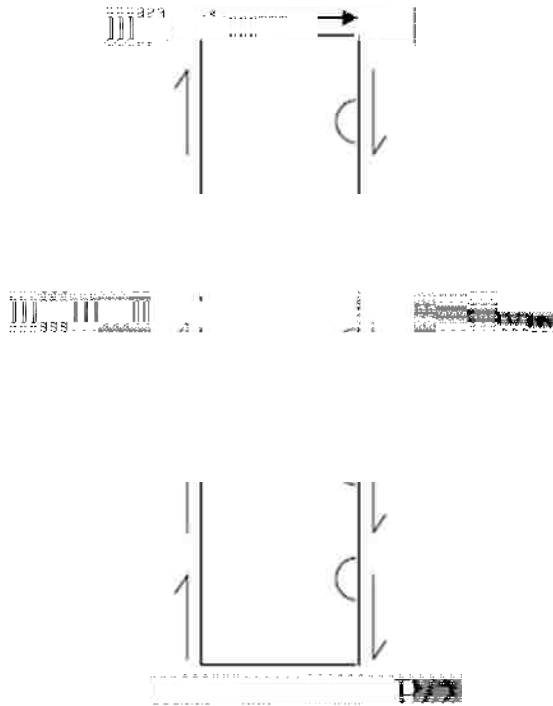
Figure 3.28 Free Body Diagram of Angle

$$M_R = \frac{P}{2} e_2 - M_T \qquad (3.5)$$

Looking at the free body diagram of the opposite side shown in Figure 3.29, gives the equilibrium equation in Eq-3.6.
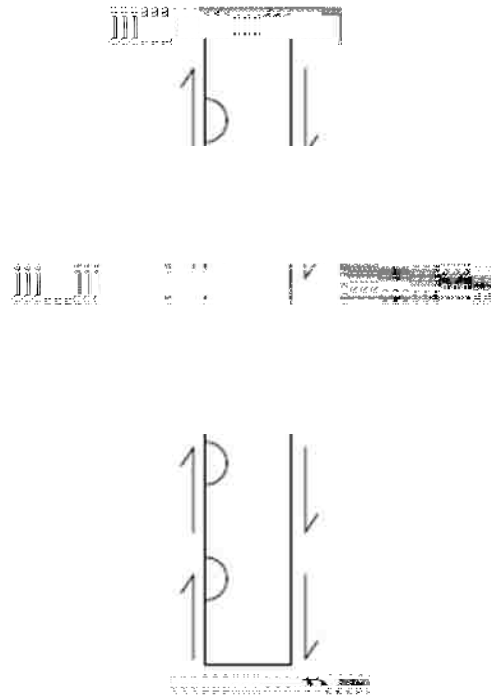
Figure 3.29 Free Body Diagram of Channel

$$M_R = M_P - \frac{P}{2} e_1 \qquad (3.6)$$

The resulting moment on the rivets (M_R) will produce a horizontal distribution of stress on the row of rivets. This effect in combination with the vertical stress, will increase the total stress on the rivets.

In order to solve the above equations for M_R, an assumption must be made about the values of M_R and M_T. Assuming that $M_T = 0$, will produce the largest value of M_R and represents the worst case for the horizontal stress in the rivets. With MT = 0, Eq. 3.5 gives the following for M_R :

$$M_R = \frac{P}{2} e_2 \qquad (3.7)$$

The corresponding horizontal shear stress on the row of rivets:

$$\sigma_h = \frac{M_R y}{I}$$

(3.8)

where: σ_h = horizontal stress in-rivet [ksi]

y = distance from centroid of rivet group to point of interest [in.]

I = moment of inertia of the rivet group [in^4]

The moment of inertia of the rivet group depends on the number of rivets per row:

$$I = 2 \sum_{n=1}^{m} A d^2$$

(3.9)

where: I = moment of inertia of the rivet group [in^4]

A = area of one rivet [in^2]

d = distance from centroid of rivet group to-rivet

m = total number of rivets in group divided by two

The horizontal stress was combined with the total stress to calculate the vertical stress distribution.

$$\sigma_v = \sqrt{\sigma_u{}^2 - \sigma_h{}^2}$$

(3.10)

where: σ_v = vertical stress in-rivet [ksi]

σ_u = ultimate strength of the rivet [assumed 62 ksi from experiment average]

The horizontal stress distribution was computed for riveted connections with 2 to 18 rivets per row for an assumed value of *P=37 kips,* which is the load that causes the ultimate vertical stress of 62 ksi in the two-rivet connection. The horizontal stress distribution is plotted from the centroid of the rivet group (see Figure 3.30). The corresponding vertical stress normalized by the ultimate strength ($\sigma_u = 62$ ksi) is plotted in Figure 3.31. The legend corresponds to the total number of rivet rows in the connection.
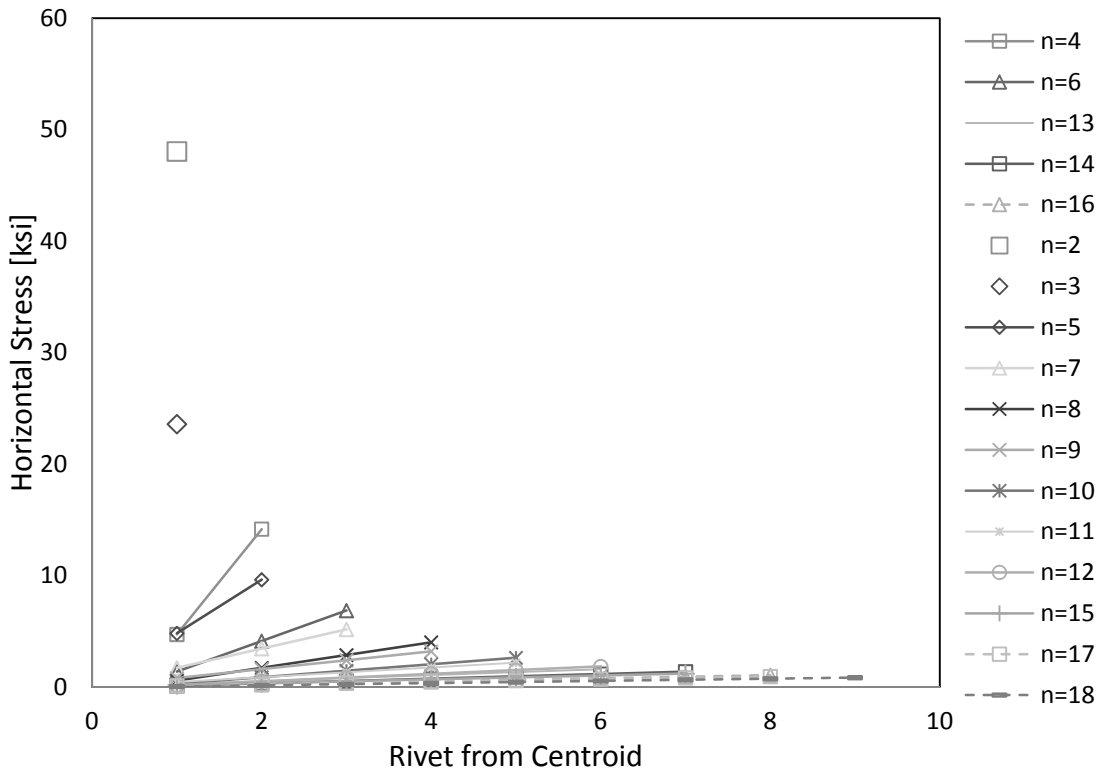
Figure 3.30 Horizontal Stress vs. Rivet from Centroid
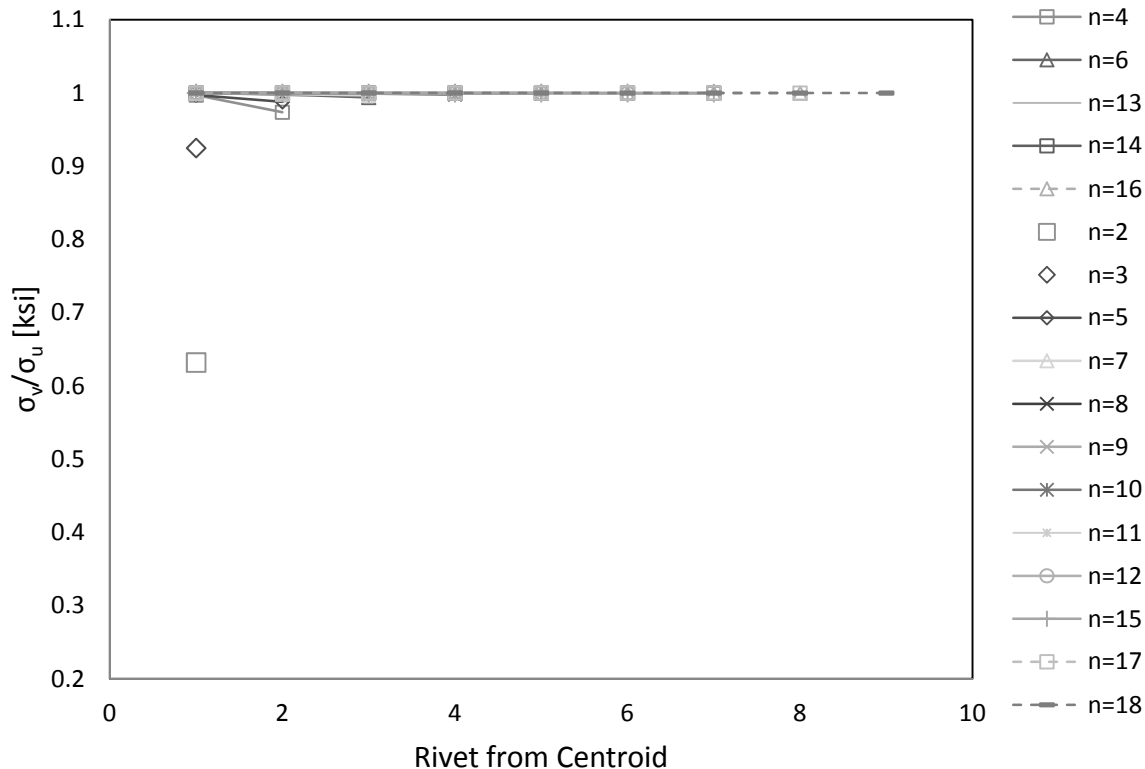
Figure 3.31 Vertical Stress vs. Rivet from Centroid for $M_T = 0$

The results show that as the connection length increases, the horizontal stress distribution becomes uniform. The graph also shows that the horizontal stress produces a large effect for riveted connections that are 8 rivets per row or less. The resulting vertical stress in the rivets does not vary for connections more than 4 rivets per row. However, this represents the worst-case scenario with respect to the possible values of M_R and M_T. In reality, a moment transferred to the tube, M_T, exists to reduce the horizontal stress on the rivets.

To investigate this effect, a value of for M_T will be assumed as half of the maximum possible value of M_T given in Eq-3.11. The corresponding value for M_R is given in Eq-3.12.

$$M_T = \frac{P}{4}e_2 \qquad (3.11)$$

$$M_R = \frac{P}{4}e_2 \qquad (3.12)$$
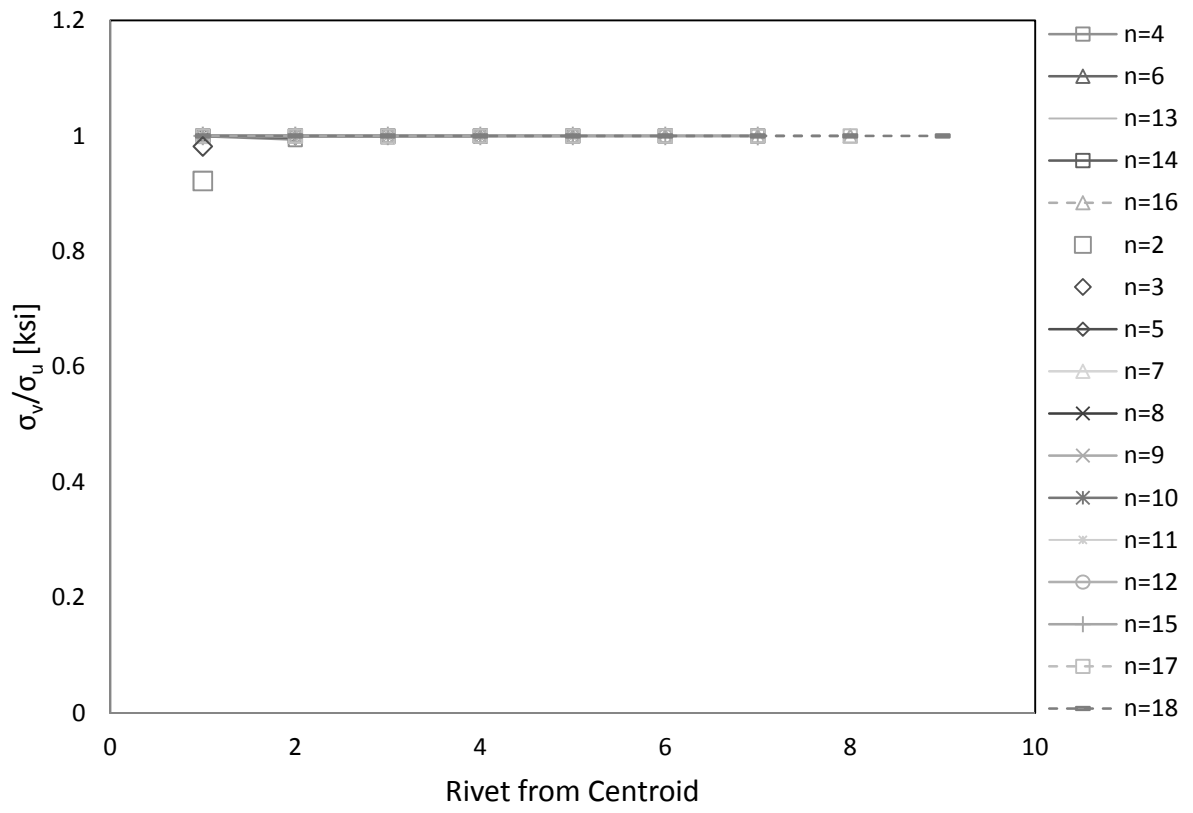
Figure 3.32 Vertical Stress vs. Rivet from Centroid for $M_T \neq 0$

Figure 3.32 shows that when M_T is not assumed as zero (was $0.25*P*e_2$ in this investigation), that the variance in the resulting vertical stress in the rivets is less than for the worst-case scenario of M_T equal to zero. Therefore, since it is unlikely M_T equals zero, there probably is not a large effect on the vertical stress in the rivets from the horizontal stress.

3.5   Specimen Assembly and Preparation

This section describes the preparation of the parts depicted in Figure 3.12. This includes the steps to assemble the guardrail configuration for testing followed by a description of the instrumentation used.

3.5.1   Specimen Preparation

Figure 3.33 depicts each part of the test setup prior to assembly for the Small Baldwin tests. The Baldwin configuration (connection lengths greater than 7 rivets) was constructed using the same steps listed below.

(a)   (b)   (c)

Figure 3.33 Test parts prior to assembly (a) Part 1 - HSS Tube (b) Part 3 - Middle Plate (c) Parts 4 & 5 - Guard Rail

The first step to assemble the connection tests was to sandblast (using fine aluminum oxide sand particles) the faying surfaces for the bolted slip critical connections to meet the AISC provisions. This included the inside of the HSS (Figure 3.12 Part 1) and the middle plate (Figure 3.12 Part 3). To improve the movement and stability of the plate inside of the tube, "feet" were welded to the inside of the HSS tube (see Figure 3.34). These feet served to keep the plate straight and prevent twisting. To minimize friction, Polytetrafluoroethylene (PTFE or Teflon) was glued to the feet and the inside of the HSS tube. Stainless steel was glued to the longitudinal sides of the plate to slide against the Teflon, and both surfaces were greased prior to testing. The guardrail pieces were labeled as "West" or "East," for consistency during testing and data analysis. In addition, horizontal lines were drawn on the guardrail to monitor local shear deformation as shown in Figure 3.35.
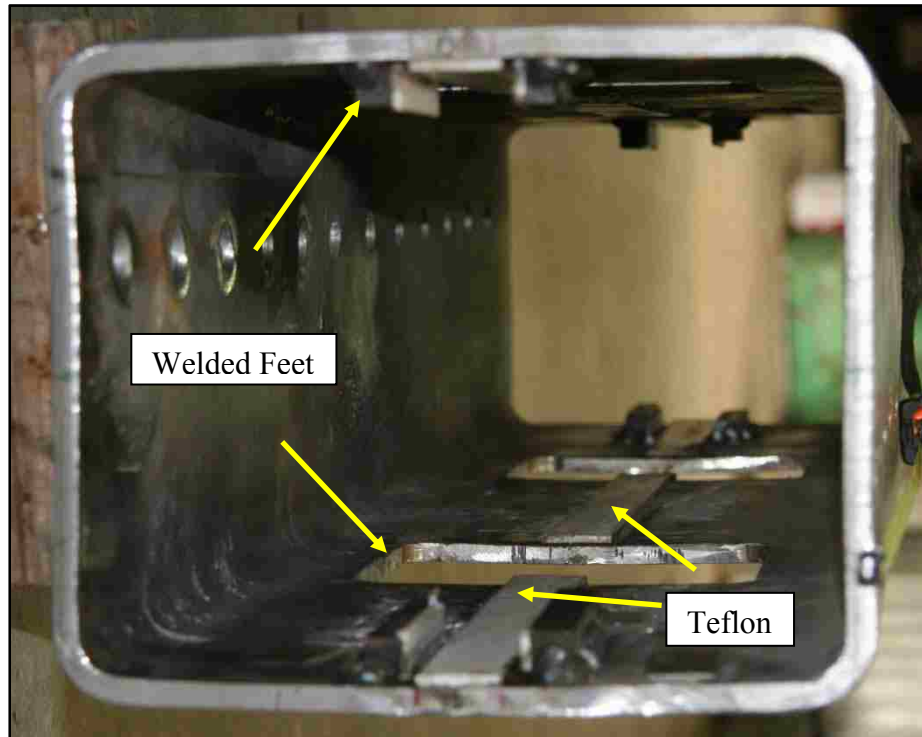
Figure 3.34 Teflon and Welded Feet on HSS Tube

(a)   (b)

Figure 3.35 Horizontal Grid on (a) West Guardrail (Part 4) and (b) East Guardrail (Part 5)

Figure 3.36 depicts the next step, which was to bolt the channel section of the guardrail onto the middle plate, and tighten the bolts with a torque wrench to meet the slip critical requirements from the AISC Steel Construction Manual (2005). This was achieved utilizing "Turn-of-Nut Pretensioning" from AISC 8.2.1. The bolts were tightened to "snug tight," such that the surfaces were clamped together without any gaps. Then the nut, bolt, and plate were marked, and the nut was turned a minimum of 120œwith a torque wrench.

Figure 3.36 Guardrail Bolted to Middle Plate

3.5.2   Instrumentation

Instrumentation was attached to the guardrail and plate prior to inserting the plate/guardrail apparatus into the HSS tube. Twenty-seven Duncan Potentiometers (pots) and nine plastic deformation strain gauges were attached for the first test. The pot numbers in

Table 3.6 are listed to "29" (as opposed to "27") because the number corresponds to the instrumentation channel in the computer, where some of the channels were used for the loading cell signal. Pots that were attached to the guardrail were first glued to a small piece of aluminum and then the aluminum was screwed on to the guardrail to ensure adhesion during the test. Figure 3.37 and Figure 3.38 depict attachment of pots to the guardrail.

Figure 3.37 Attachment to Guardrail to Measure Rivet Deformation
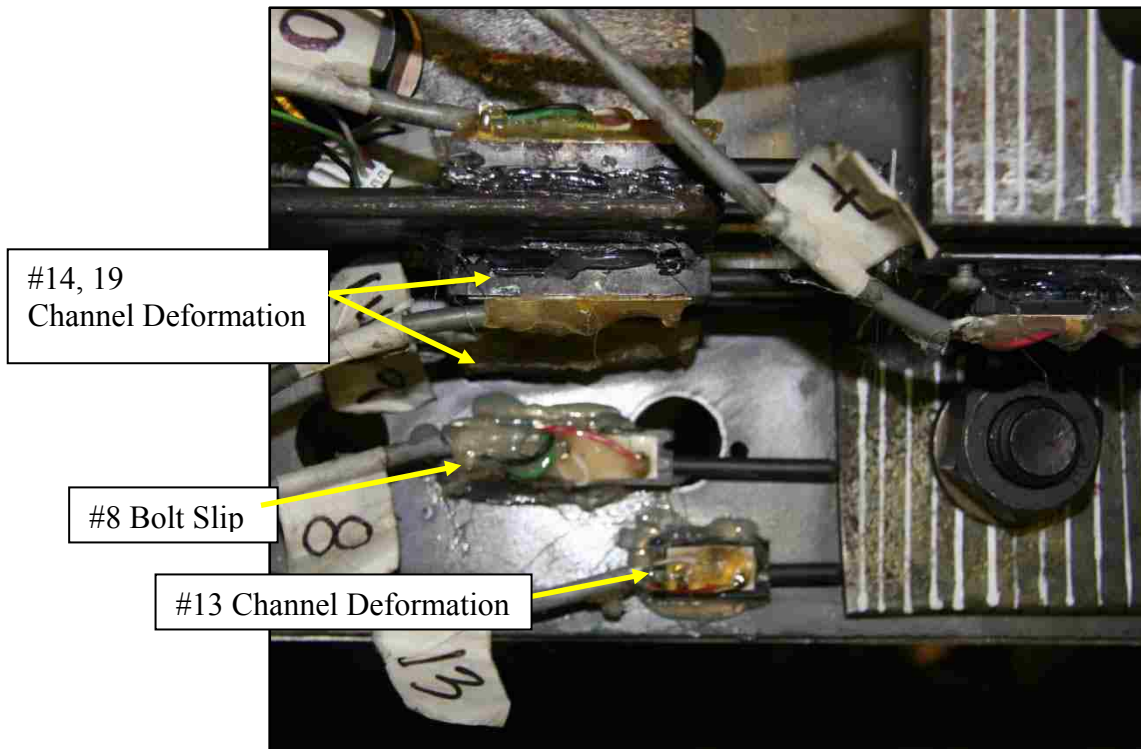
Figure 3.38 Pots Measuring Bolt Slip and Channel – Plate Deformation

Each pot is shown by number and its target deformation measurement in

Table 3.6. Figure 3.39 shows the location of the pots with respect to the cross section elements to be tested. As shown, the key deformations to be measured were the overall displacement, deformation at the angle and channel legs, bolt slip, and rivet deformation.
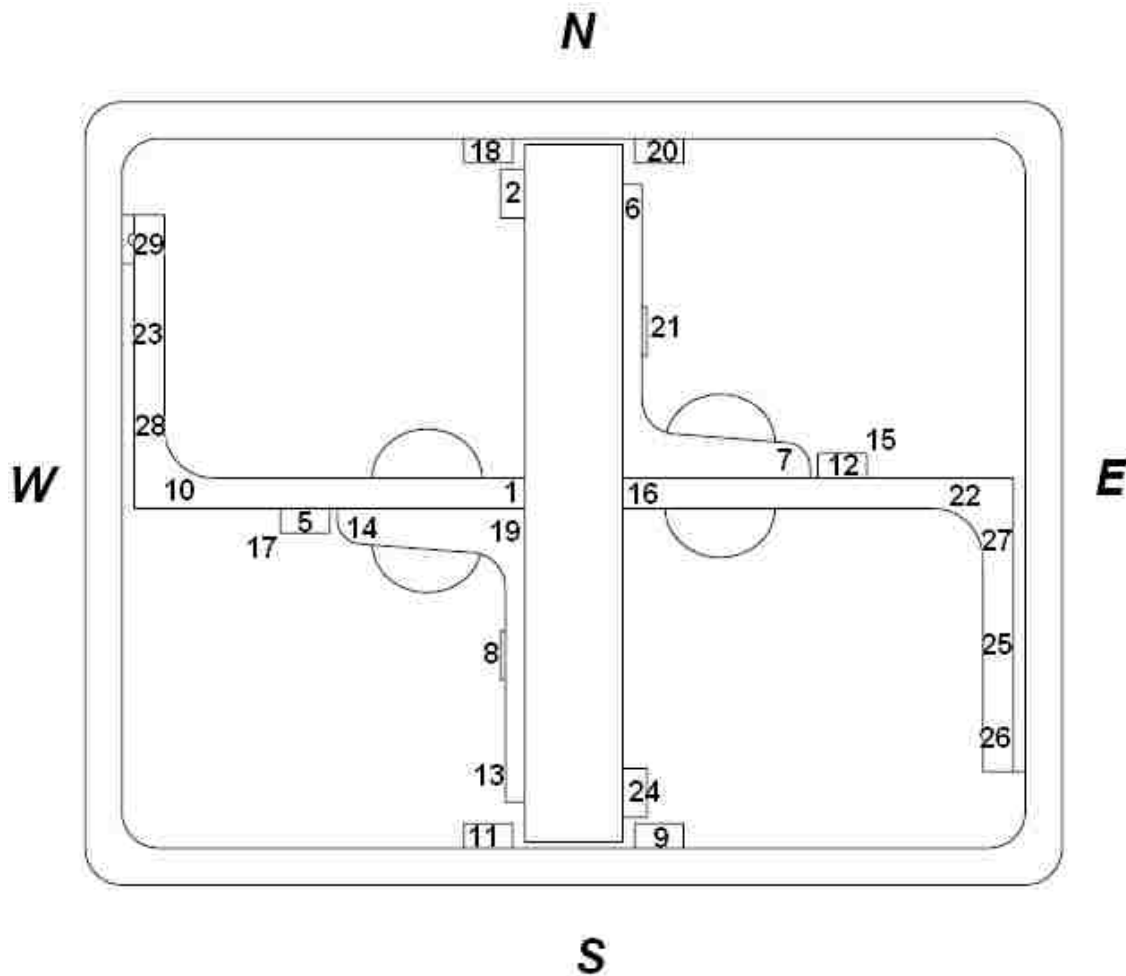
Figure 3.39 Duncan Potentiometer Layout

Table 3.6 Duncan Potentiometer Location and Measurement Descriptions

Pot	Location	Measurement
1	E Angle Bottom	E Angle (rivet faying surface) deformation
2	Outer HSS NW Top	HSS - Plate deflection "Overall"
5	W Angle Top	Rivet deformation
6	NE Plate Bottom	E Channel (bolted plate surface) deformation
7	E Channel Lower E Flange	E Channel (rivet faying surface) deformation
8	SW Plate Bottom	W Channel - Plate bolt slip
9	Outer HSS SE Bottom	Overall
10	W Angle Bottom	W Angle (rivet faying surface) deformation
11	Outer HSS SW Bottom	Overall
12	E Angle Top	Rivet deformation
13	SW Plate Bottom	W Channel (bolted plate surface) deformation
14	W Channel Lower W Flange	W Channel (rivet faying surface) deformation
15	E Angle Bottom	Rivet deformation
16	E Angle Lower W Side	E Angle (rivet faying surface) deformation
17	W Angle Bottom	Rivet deformation
18	Outer HSS NW Bottom	Overall
19	W Channel Lower E Flange	W Channel (rivet faying surface) deformation
20	Outer HSS NE Bottom	Overall
21	E Channel Bottom	E Channel - Plate bolt slip
22	E Angle Lower E Side	E Angle (rivet faying surface) deformation
23	Inner HSS NW Bottom	HSS - W Angle bolt slip
24	Outer HSS SE Top	Overall
25	Inner HSS SE Bottom	HSS - E Angle bolt slip
26	Inner HSS SE Bottom	E Angle (Bolted Surface) deformation
27	Inner HSS SE Bottom	E Angle (Bolted Surface) deformation
28	Inner HSS NW Bottom	W Angle (Bolted Surface) deformation
29	Inner HSS NW Bottom	W Angle (Bolted Surface) deformation

Strain gauges were placed within one rivet diameter of selected rivet holes to measure the local stress at the rivet hole. This measurement will help to calibrate finite element models of the test setup.

Figure 3.40 Strain Gauge Placement on East Angle

Table 3.7 describes the location of the strain gauges, where "W" stands for "West," "E" for "East," "C" for "Channel," and "A" for "Angle." The number prefix corresponds to the rivet nearest the strain gauge, where strain gauges on the angle were placed below the rivet and those on the channel were placed above the rivet. For example, "2EA" corresponds to a strain gauge that is below the second rivet on the East angle (see Figure 3.40).

Figure 3.40 Strain Gauge Placement on East Angle

Table 3.7 Strain Gauge Locations

Strain Gauge	Distance from Rivet Center [in.]
1 WC	0.910
2 WC	0.872
2 EA	1.135
3 EA	0.900
4 EA	1.065
1 EC	0.850
2 EC	1.000
3 EC	0.970
4 EC	0.800

This instrumentation was utilized for the first small Baldwin test (four-rivets), and after analysis of results, the instrumentation was simplified. For subsequent tests, strain gauges and pots to measure angle and channel deformation were not used.

3.5.3 Assembly

After attaching instrumentation, the plate and guardrail specimens, (Figure 3.12 Parts 3, 4, 5) were lowered into the HSS tube (Figure 3.12 Parts 1) using a crane (see Figure 3.41). If necessary, shim plates (Figure 3.12 Part 2) were inserted between the angle and inner HSS to maintain a uniform bearing surface for the high strength bolts.

<div align="center">(a)   (b)</div>

Figure 3.41 Assembly of Plate, Guardrail, HSS (a) East Guardrail (b) West Guardrail

Following insertion of the plate and guardrail into the HSS, bolts were attached and tightened using a torque wrench using the method described in Section 3.5.1 (see Figure 3.42).
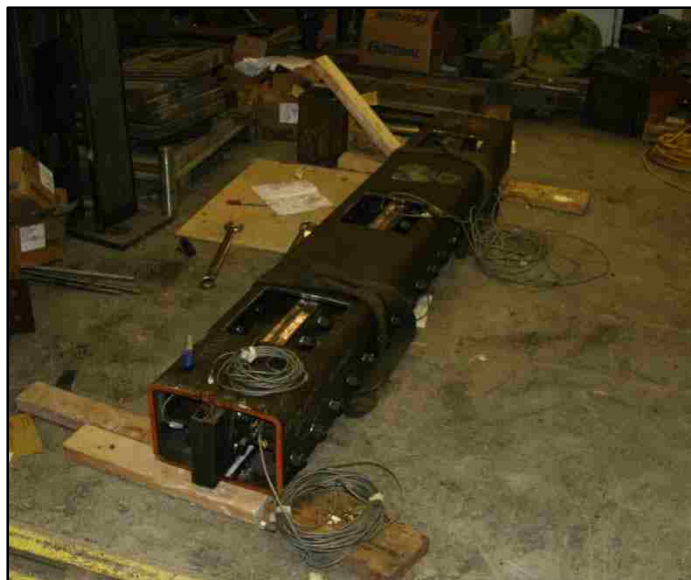
Figure 3.42 Baldwin Specimen After Attachment of Middle Plate to HSS

The last step was to attach pots to the outside of the HSS to measure the overall displacement and place the specimen into the testing machine (see Figure 3.43). Table 3.8 lists total number of rivets and bolts for each specimen tested.

Table 3.8 Test Specimens with Connection Lengths

Test Name	No. Rivets/Row	Total Rivets	No. Bolts/Row	Total Bolts
Small Baldwin				
Two-rivet (2R)	2	4	3	12
Four-rivet (4R)	4	8	5	20
Two-rivet (Four-rivet Length) (2R(4L))	2	4	5	20
Seven-rivet (7R)	7	14	10	40
Baldwin				
Eleven-rivet (11R)	11	22	13	52
Seventeen-rivet (17R)	17	34	19	76

(a)   (b)

Figure 3.43 Guardrail Configuration Prior to Testing (a) Small Baldwin (≤ 7 Rivets in Length)
(b) Baldwin (> 7 Rivets in Length)

Chapter 4: Experimental Observations

4.1 General

The following chapter describes the results of the experiments beginning with preliminary material tests followed by primary riveted connection tests. The section on material tests gives the material properties gathered as well as the stress versus strain relationships. The discussion of the riveted connection tests is divided into two sections: Small Baldwin tests for specimens 2R, 2R (4L), 4R, and 7R and Baldwin tests for specimens 11R and 17R. For each test, the overall load versus displacement relationship accompanies a description of the test observations. Photos taken during the tests and documentation of the behavior of the connecting elements are also provided.

4.2 Material Tests

This section describes material tests of the connecting elements in the guardrail beginning with the C6x8.2 channel section and the L4x3x5/16.

4.2.1 Channel C6x8.2

Two coupons (C1 & C2) were cut from the web of the channel in the guardrail in accordance with ASTM 370-10 and tested in tension using a 300-kip UTM. Figure 4.1 and Figure 4.2 below represent drawings of coupons C1 and C2, respectively, including dimensions and several thickness measurements over the gauge length (average thickness in Table 4.1).
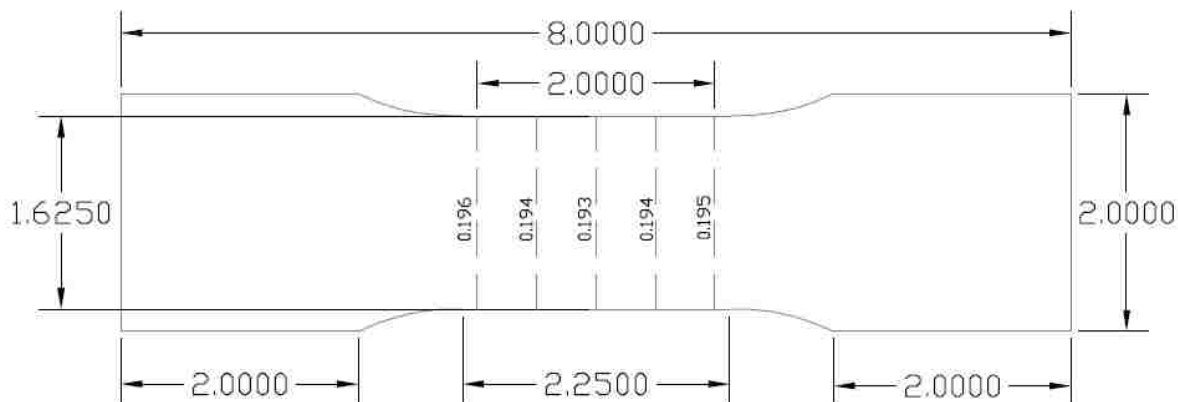
Figure 4.1 Tension Coupon C1 (all dimensions in inches)
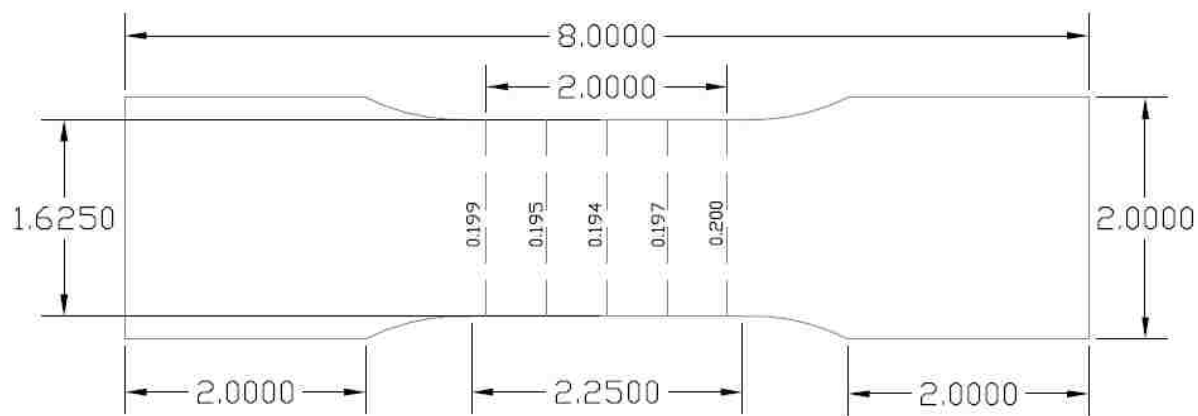
Figure 4.2 Tension Coupon C2 (all dimensions in inches)

Table 4.1 Average Gauge Thickness of Channel Coupons

Coupon Name	Average Thickness [in.]
C1	0.194
C2	0.197

The coupons were loaded to failure, Figure 4.3 below depicts the stress strain curve for coupon C2 (coupon C1 slipped from the grips during the test therefore no data is provided). The yield strength of the material was approximated assuming the 0.2% offset method, and the ultimate strength was assumed the maximum stress. Photos of the coupons after testing can be seen in Figure 4.4. The material tests measured the yield strength of the channel material as 41.70 ksi and ultimate strength as 60.68 ksi.
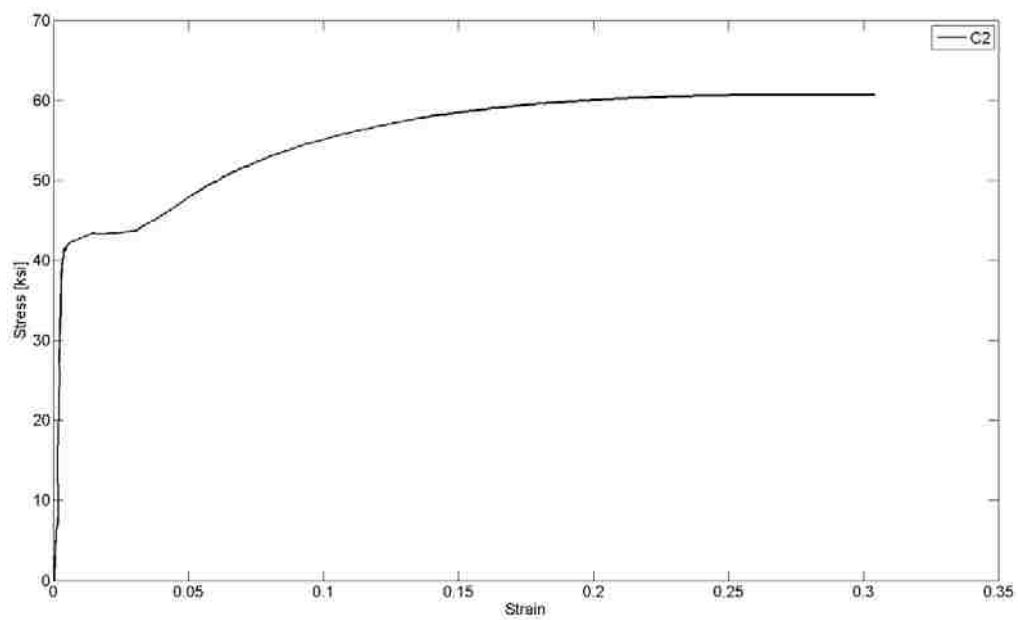
Figure 4.3 Stress vs. Strain Diagram for Channel Coupons

(a)   (b)   (c)   (d)

Figure 4.4 Channel Coupons Tension Testing (a) C1 before (b) C1 after
(c) C2 before (d) C2 after

4.2.2 Angle L4x3x5/16

The process described in section 4.2.1 was repeated for the angle section, where the coupons were cut from the shorter leg of the angle. Figure 4.5 and Figure 4.6 below represent drawings of coupons A1 and A2, respectively. Figure 4.7 below represents the stress vs. strain diagram of the angle coupon sections. Photos of the coupons after testing can be seen in Figure 4.8. The material tests measured the yield strength of the angle material as 32.59 ksi and ultimate strength as 54.25 ksi (average of A1 and A2 test results).
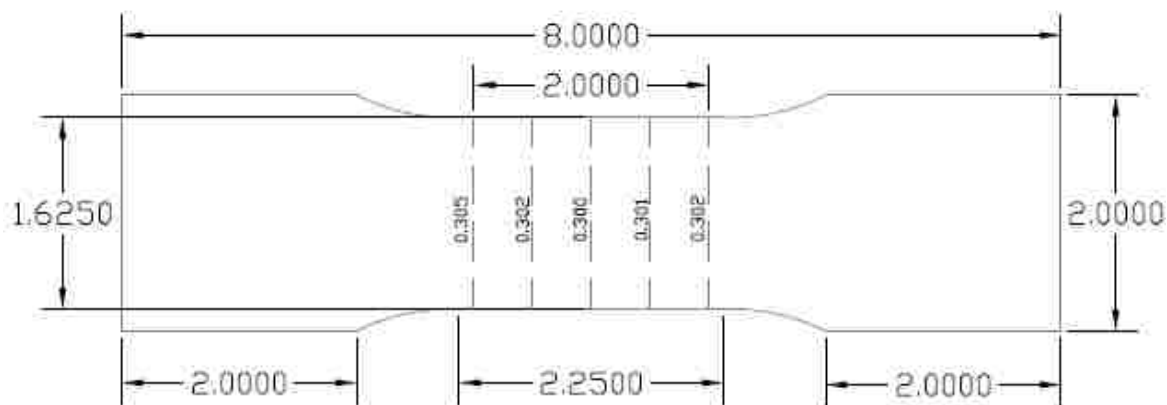
Figure 4.5 Tension Coupon A1 (all dimensions in inches)
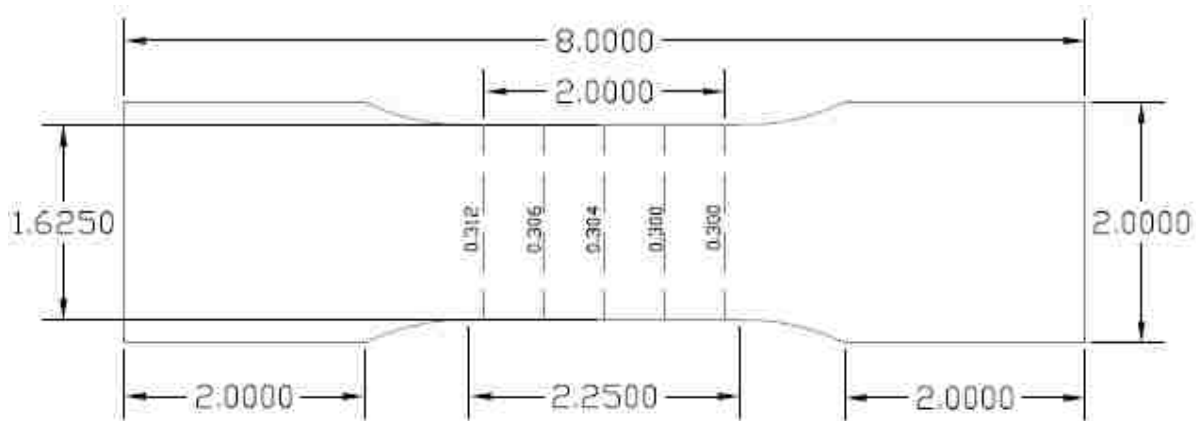
Figure 4.6 Tension Coupon A2 (all dimensions in inches)

Table 4.2 Average Gauge Thickness of Angle Coupons

Coupon Name	Average Thickness [in.]
A1	0.302
A2	0.304
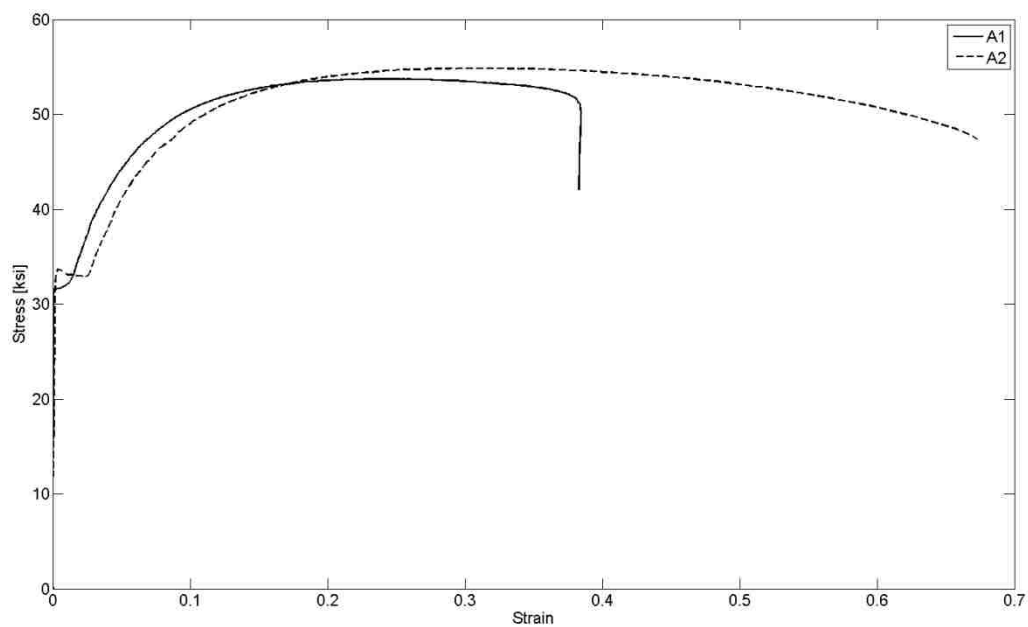
Figure 4.7 Stress vs. Strain Diagram for Angle Coupons

(a)   (b)   (c)   (d)
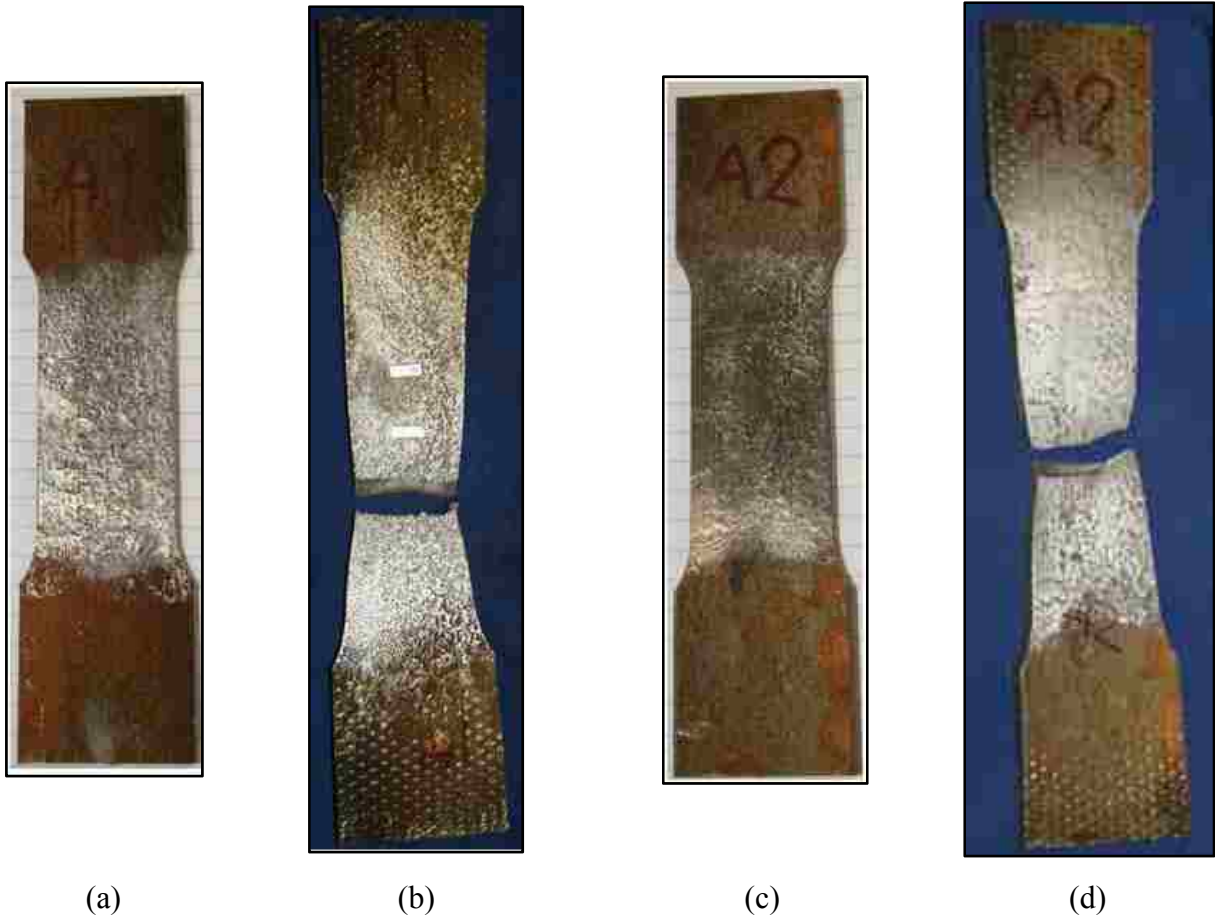
Figure 4.8 Angle Coupons Tension Testing (a) A1 before (b) A1 after
(c) A2 before (d) A2 after

4.2.3 Box Tests (Channel and Angles)

To measure the single shear strength of ¾ in. rivets were obtained from WSDOT and were from a different truss bridge built in the 1950s. Although these rivets did not come from the same bridge as the guardrail, they were used to approximate the rivet strength from a similar bridge for design of the test configuration. The connection had plates riveted to angles and it was possible to shear the rivets as shown in Figure 4.9. The test was conducted in a 300-kip UTM.
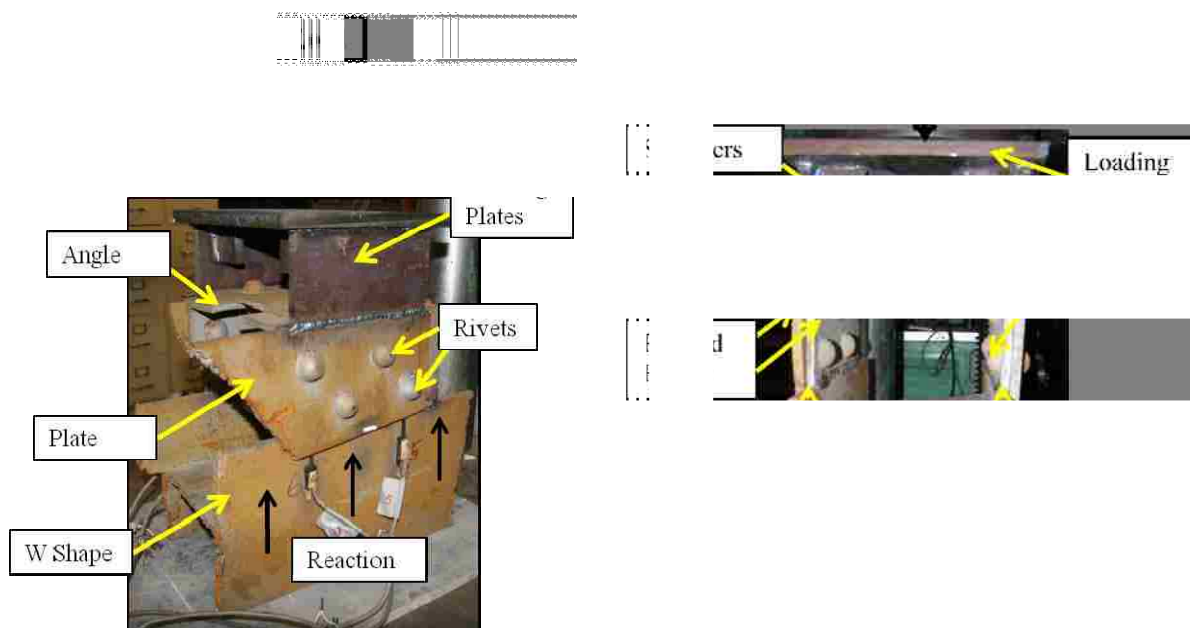
(a) Isometric View　　　　　　　　　　(b) Load Transfer

Figure 4.9 Box Test to Measure Rivet Shear Strength

As shown in Figure 4.9a the riveted connection is a built-up section consisting of two plates and two angles. Two loading plates were welded to the plates of the riveted connection to transfer the load in shear to the rivets. On top of these plates, a horizontal plate was welded to transfer the compressive load from the Small Baldwin to the riveted plates. The built up section was welded to a wide flange shape to react with the riveted plates, and the load transfer is depicted in Figure 4.9b. Plates were welded to the inside of the wide flange to act as stiffeners. Four pots were placed under the connecting elements to measure the rivet deformation. Figure 4.10 below depicts the load versus displacement curve.
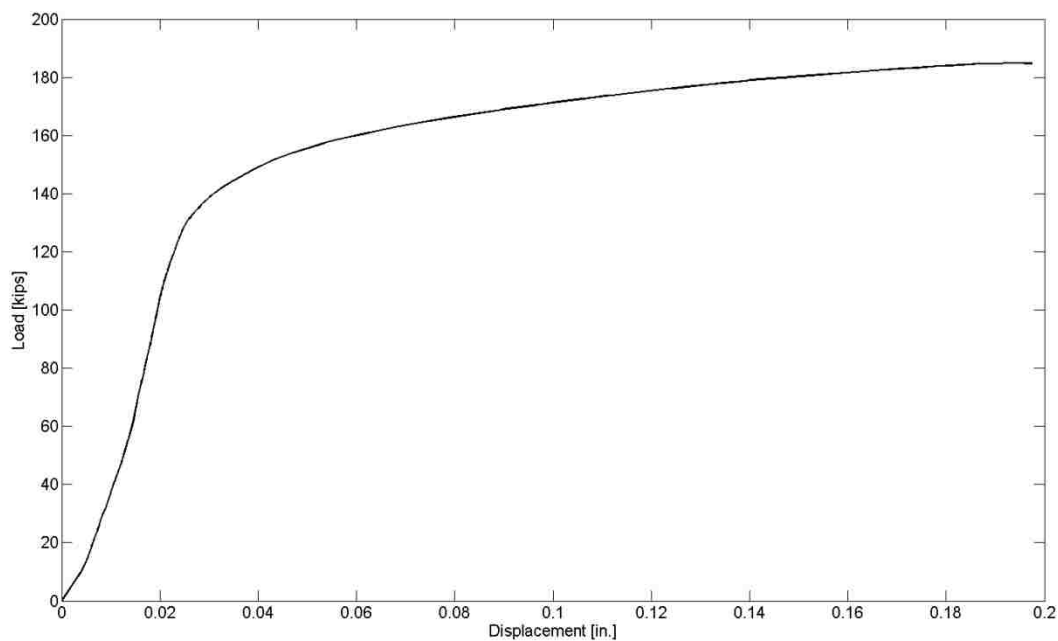
Figure 4.10 Load vs. Displacement Curve for Box Test

Eight rivets were tested in single shear, and the average ultimate rivet shear strength was estimated using the equation below:

$$F_{u,avg} = \frac{P_{max}}{n * A_v} \qquad (4.1)$$

where: $F_{u,avg}$ = average ultimate rivet shear strength [ksi]

P_{max} = maximum load during test

n = number of rivets loaded in single shear

A_v = area of one rivet cross section [in^2]

The average ultimate shear stress of the rivets was calculated to be 52.3 ksi. The average rivet stress versus displacement plot can be seen in Figure 4.11 below.
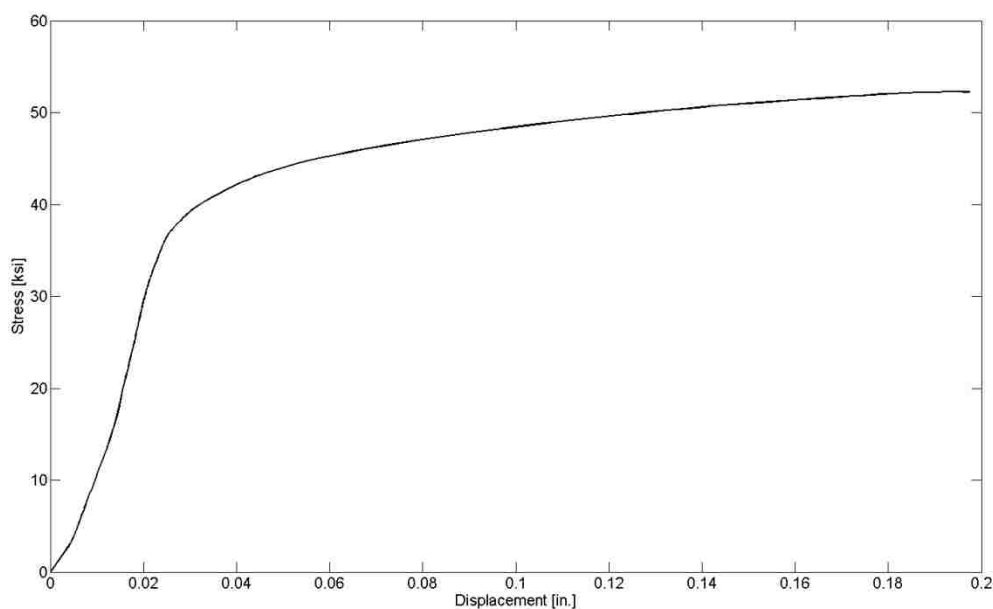
Figure 4.11 Average Rivet Stress vs. Displacement for Box Test

4.2.4   Summary of Material Tests

Table 4.3 summarizes the results of all material properties measured. These values were used to design the primary test specimens described in Section 0

Table 4.3 Summary of Material Test Results

Material Tested	Test Performed	Yield Strength [ksi]	Ultimate Strength [ksi]
Box Test	Shear Test	n/a	52.31
Coupon Test	C2 Tension	41.70	60.68
	A1 Tension	31.60	53.73
	A2 Tension	33.58	54.78

4.3　Small Baldwin Connections

This section describes the observations from each test, the overall displacement relationship, and key behavior of the connecting elements.

4.3.1　Test Specimen 4R

The test on Specimen 4R was the first performed in the Small Baldwin, with four-rivets per row for a total of eight rivets in the specimen. Five bolts were used to connect each channel to the middle plate and each angle to the HSS. The test specimen was placed in the Small Baldwin (300-kip UTM) with a loading plate welded to the top of the middle plate to ensure uniform loading (see Figure 4.12). The compression load was applied at a constant slow rate until all of the rivets fractured. This caused the middle plate to fall completely through the HSS. The loading plate was used in all Small Baldwin tests, and for all tests, the specimens were loaded until all rivets fractured.

Figure 4.12 Photo of Test 4R During Testing

During the test, the load increased linearly until approximately 0.12 in. of overall displacement. This was followed by a few drops in load (see Table 4.4), which could represent rivet or bolt slip. Due to these sudden jumps in load, some of the pots fell off that had been attached with glue. The maximum load observed was 147.7 kips, where the load proceeded to drop until the first rivet fractured at approximately 0.5 in. of overall displacement. After the first rivet fractured, the remaining rivets began to fracture in a sequence that was difficult to determine. Many loud "ping" noises were heard as rivets popped off the specimen. It is likely that rivet 3E fractured first, but this was not clear during testing (see Figure 4.14). Figure 4.13 shows the load versus overall displacement, where the displacement represents the average measurements from the pots measuring the difference in displacement between the HSS and middle plate. Table 4.4 summarizes observations made during test 4R including the approximate load and displacement at which it occurred corresponding to Figure 4.13.

Table 4.4 Test 4R Observations

Test Name: Specimen 4R		Date Performed: 11/09/2011
No.	**Approximate Load [kip] (Displacement [in.])**	**Observation**
1	120 (0.12)	drop in load
2	130 (0.2)	drop in load
3	140 (0.3)	drop in load – bolt slip noise
4	130 (0.3 to 0.4)	plateau of loading
5	0.45 in	increase in load
6	145 (0.5)	maximum load
7		load began to drop
8	130 (0.5)	rivet fracture - noise
9		reload
10	100 (0.6)	rivet fracture - noise
11		reload
12	90 (0.65)	rivet fracture - noise
13	20 (0.75)	last rivet fractured
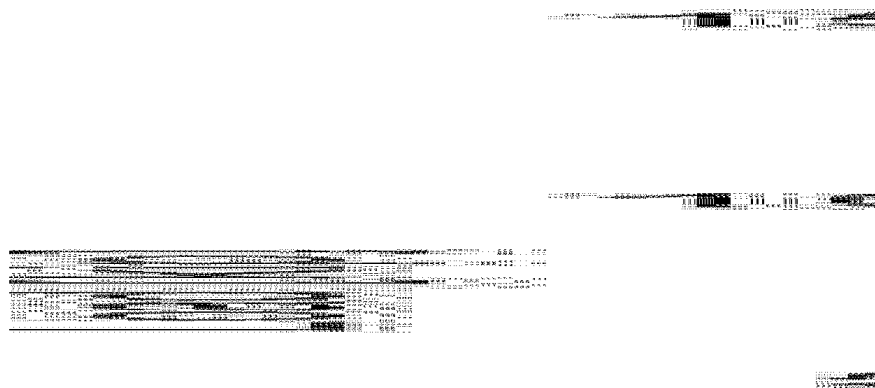
Figure 4.13 Load vs. Overall Displacement – Specimen 4R

(a)	(b)
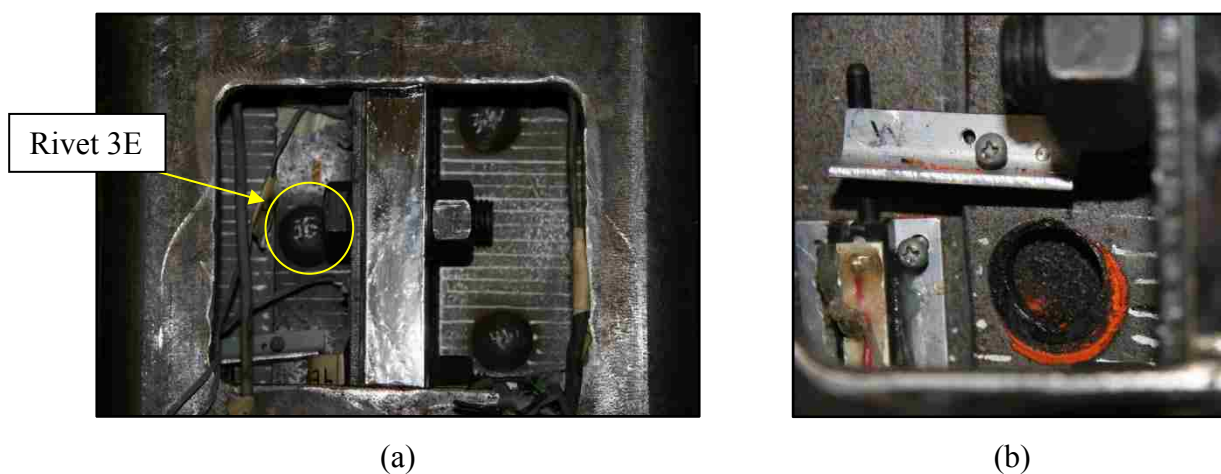
Figure 4.14 Photo of Fracture of Rivet 3E (a) Rivets Prior to Fracture (b) Rivet 3E Post Fracture

After the test, the specimen was taken apart by removing all bolts and gathering all specimen parts: West Guardrail (West Channel and West Angle), East Guardrail (East Channel and East Angle), and the fractured rivets. Photos were taken of each specimen part to compare with photos taken prior to the test. The parts were surveyed for damage such as deformation of the channel or angle legs, rivet or bolt hole deformation, or buckling, all of which was documented.

Deformation of the channels and angles was evident after the test. The angle leg that was riveted to the channel experienced some buckling near the rivets (see Figure 4.15). Rivet hole deformation was observed in the holes along the angle, where it appeared the shape of the hole deformation was different for each hole (see Figure 4.16). It appeared that the bottom holes (3E and 4E) were deformed more than the top.

Significant buckling was also observed in the flange of the east channel that is riveted to the east angle (see Figure 4.17). The bottom of the east channel web was deformed after testing, which was likely due to the large bolt spacing between the last hole and the end of the channel (see Figure 4.18). The photo of the east channel prior to testing is depicted in Figure 4.16.
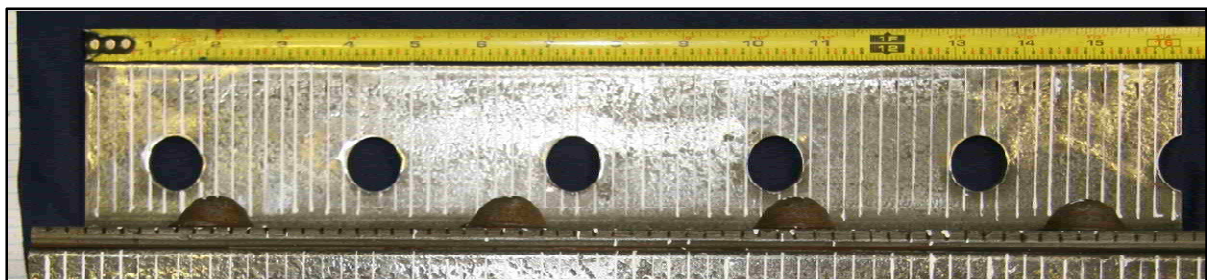
(a) Before Testing
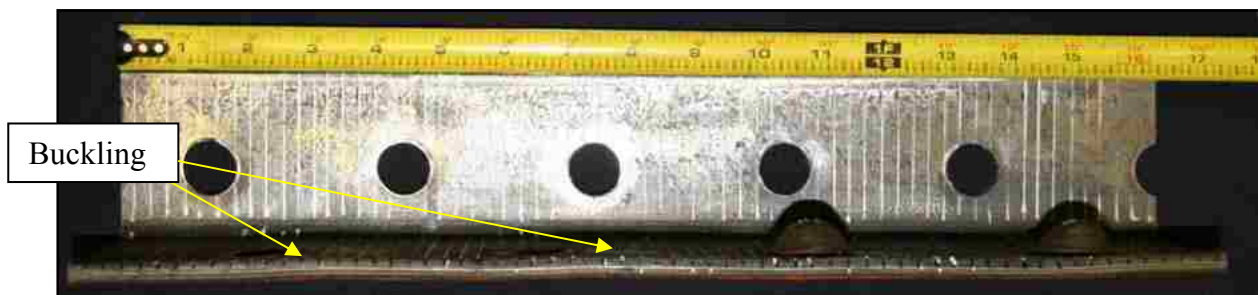
(b) After Testing

Figure 4.15 East Angle Bolted Surface – Specimen 4R
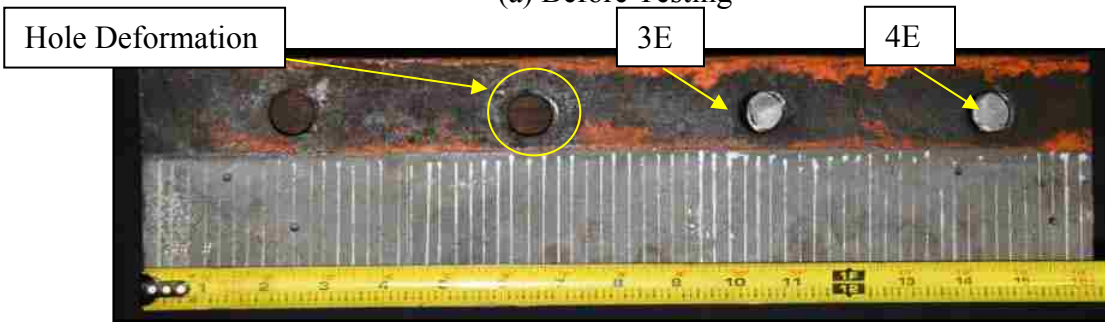
(a) Before Testing

(b) After Testing

Figure 4.16 East Angle Riveted Surface – Specimen 4R

(a) Before Testing
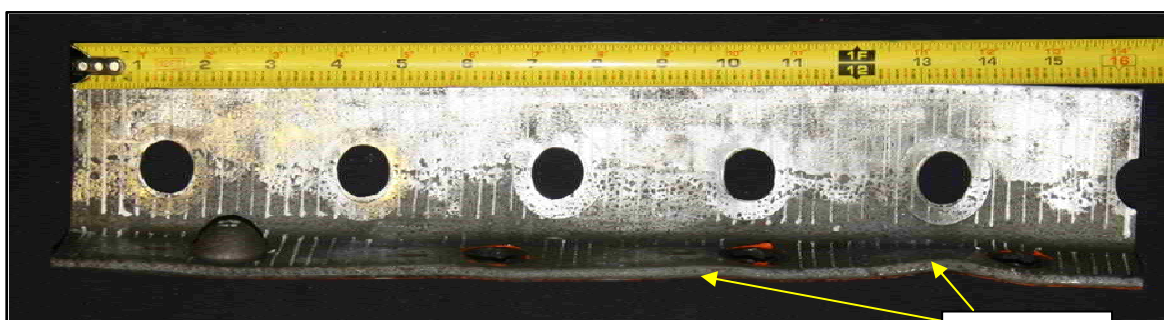
(b) After Testing

Buckling

Figure 4.17 East Channel Bolted Face – Specimen 4R

(a) East Channel Flange Faying Surface

Last Bolt Hole to Middle Plate

Deformation

(b) East Channel Flange Rivet Surface

Figure 4.18 East Channel Deformation from Last Bolt – Specimen 4R

The west angle leg that was riveted to the channel appeared to have some buckling (see Figure 4.19), but it was not as large in magnitude in the east angle. The riveted surface of the west guardrail had some rivet hole deformation, which seemed more pronounced in the bottom holes (3W and 4W) as shown in Figure 4.20. There was also some buckling of the west channel along the riveted surface (see Figure 4.21), but it was not as significant as that of the east channel. The rivet holes in the west channel experienced some deformation, where there appeared to be more near the bottom holes (see Figure 4.22).

(a) Before testing

(b) After Testing

Figure 4.19 West Angle Bolted Surface – Specimen 4R

Hole Deformation

(b)
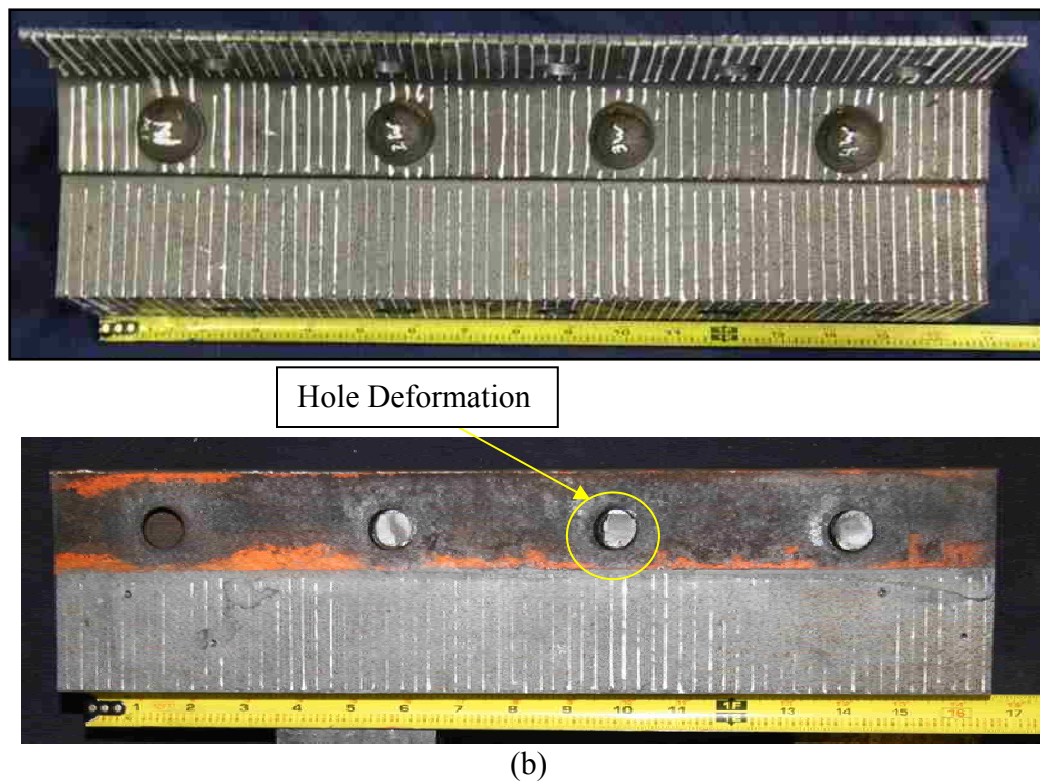
Figure 4.20 West Angle Rivet Hole Deformation – Specimen 4R

Buckling

Figure 4.21 West Channel Buckling – Specimen 4R
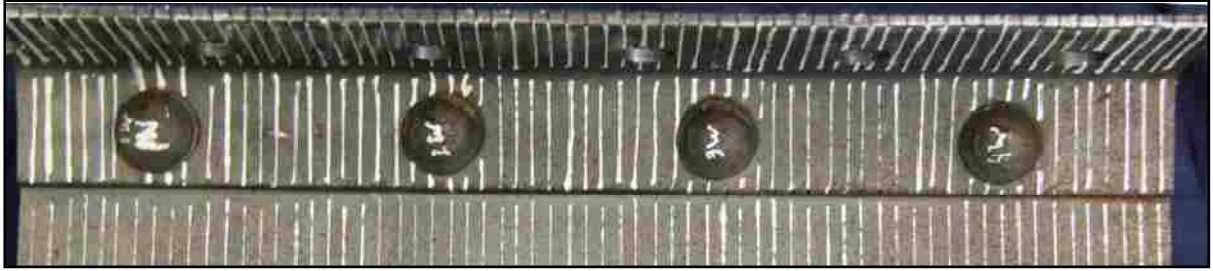
(a) Before Testing

Hole Deformation

(b) Angle After Testing
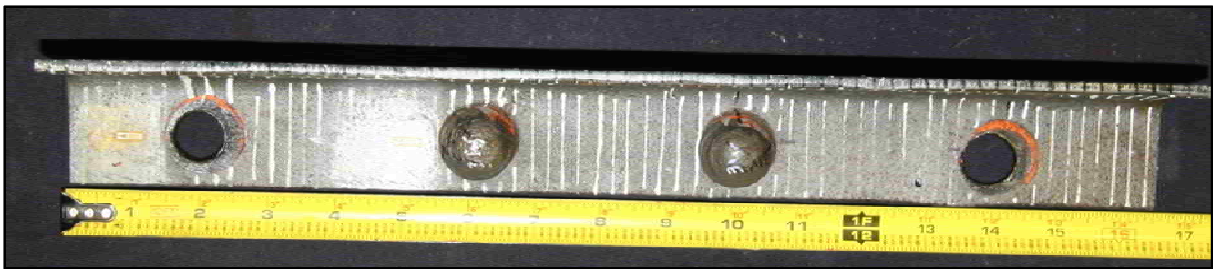
(c) Channel After Testing

Figure 4.22 West Channel Rivet Hole Deformation – Specimen 4R

The rivets that fractured and came off the specimen are shown in the photos below, where the shapes of the sheared surfaces seem more round for rivets 1E, 2E, 4W. The sheared surface for rivet 2E and 3E is oblong.

(a) All Fractured Rivets

(b) East Rivets (from left 1E 2E 3E 4E)

(c) West Rivets (from left 1W 4W)

Figure 4.23 Test 4R Fractured Rivets

4.3.2   Test Specimen 2R

This was the shortest test performed in the Small Baldwin, where there were two rivets per row for four total rivets in the specimen. Figure 4.24 depicts the specimen during testing.

Figure 4.24 Test 2R During Testing

During the test, the load increased steadily, until a few drops in load began to occur at approximately 60 kips. This likely corresponded to bolt slip. After the load reached 70 kips, the load increased steadily until a maximum of 79.3 kips (0.75 in), where the load dropped. The first rivet fracture occurred at approximately 0.8 in. of overall displacement, where the load increased again to 40 kips, and remaining rivets fractured at almost 1 in. of overall displacement. Table 4.5 lists the observations and Figure 4.25 shows the load versus overall displacement curve.

Table 4.5 Test 2R Observations

Test Name: Specimen 2R		Date Performed: 11/29/2011
No.	**Approximate Load [kip] (Displacement [in.])**	**Observation**
1	62 (0.2)	drop in load
2	65 (0.4)	drop in load
3	70 (0.5)	drop in load
4	79 (0.72)	maximum load
5		sudden drop
6		fracture noise
7	30 (0.8)	load again
8	45(0.95)	fracture noise
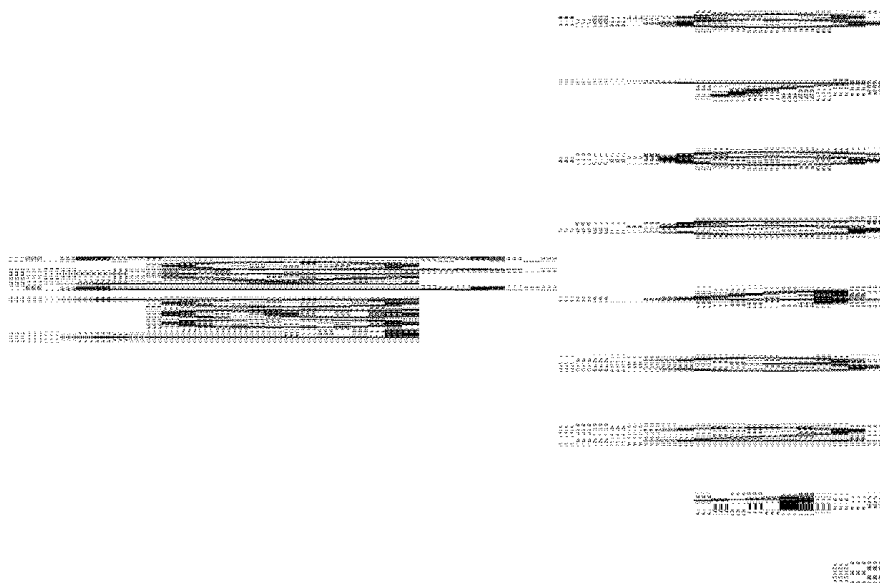
Figure 4.25 Load vs. Overall Displacement – Test 2R

Figure 4.26 shows a view through the access holes of the guardrail after testing. The rivet deformation can be seen by the gap between the bottom of the east angle and channel.
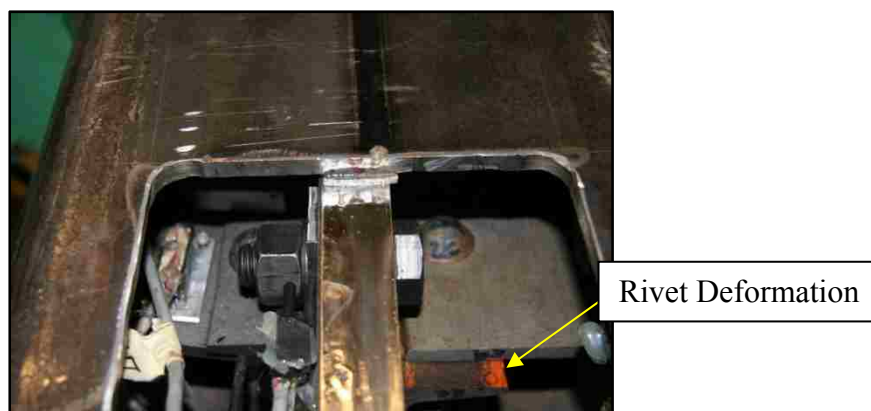
Figure 4.26 Test 2R After Testing

The following images depict the damage observed after taking the specimen apart. In the east guardrail, buckling was observed in the angle along the riveted surface as shown in Figure 4.27. The rivet hole deformation in the east guardrail is shown in Figure 4.28, where there is some deformation in both holes.
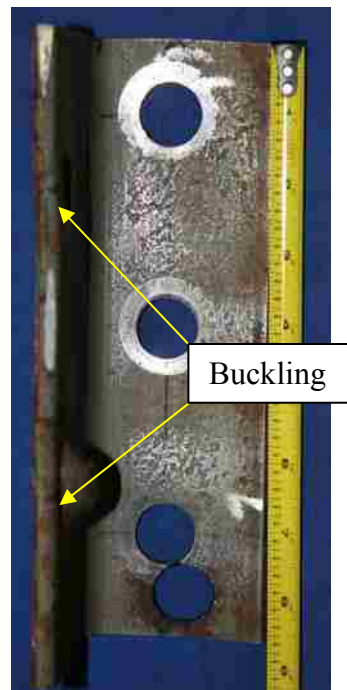
(a) Before Testing   (b) After Testing

Figure 4.27 Buckling in East Angle – Specimen 2R
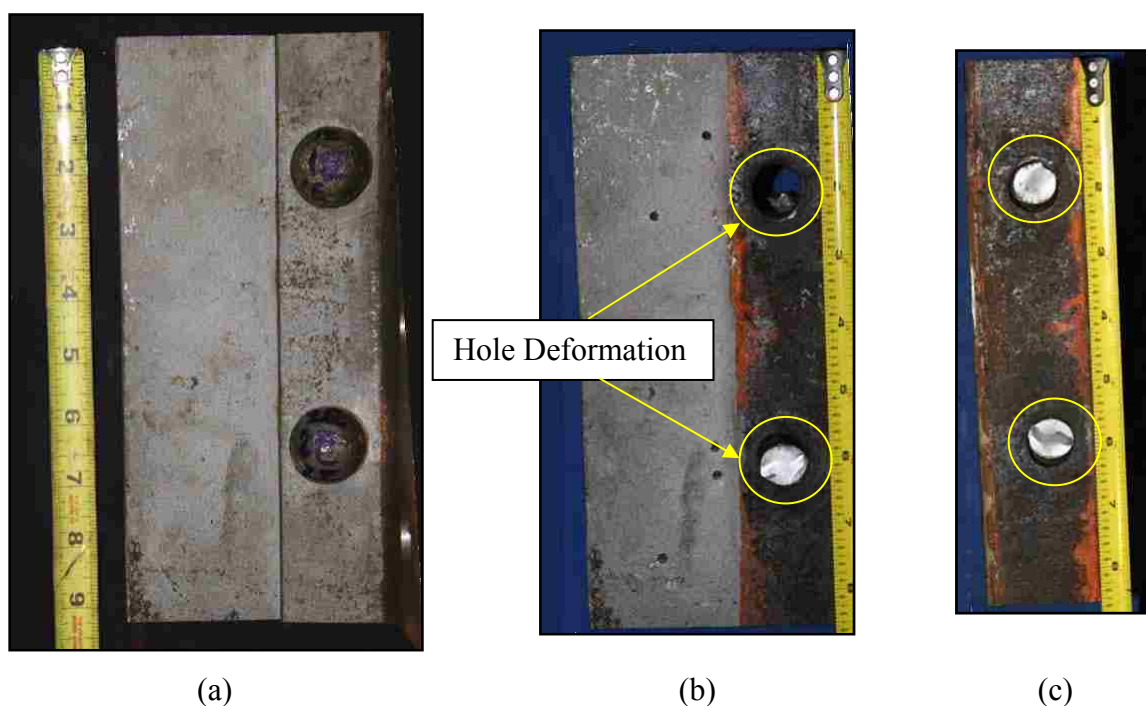
Figure 4.28 East Guardrail Rivet Hole Deformation (a) Before Testing (b) East Angle After Testing (c) East Channel After Testing – Specimen 2R

In the west guardrail, significant buckling also observed in the west angle as shown in Figure 4.29. The rivet hole deformation for the west guardrail is depicted in Figure 4.29. Both rivet holes appear to have deformed similarly. There was also significant buckling observed in the east and west channel. The images below depict the buckling along the riveted surface of the west channel. The bolt holes depicted did not deform after testing, they were re-drilled prior to testing to fit the specimen together. The fractured rivets (1E) from this test are shown in Figure 4.32.

(a) Before Testing   (b) After Testing
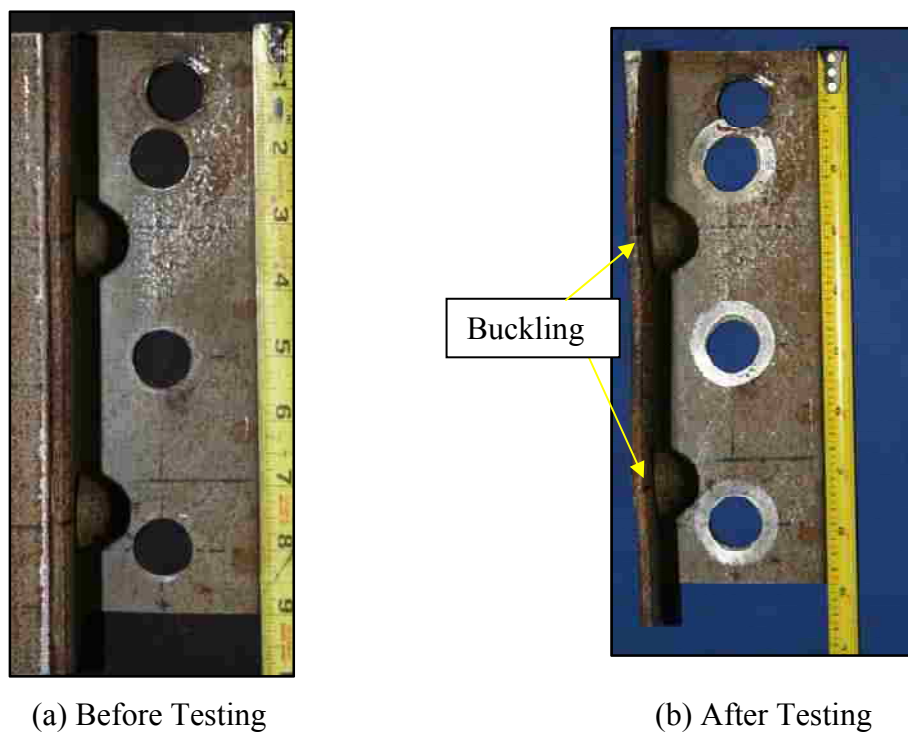
Figure 4.29 West Angle Buckling- Specimen 2R

(a)   (b)   (c)
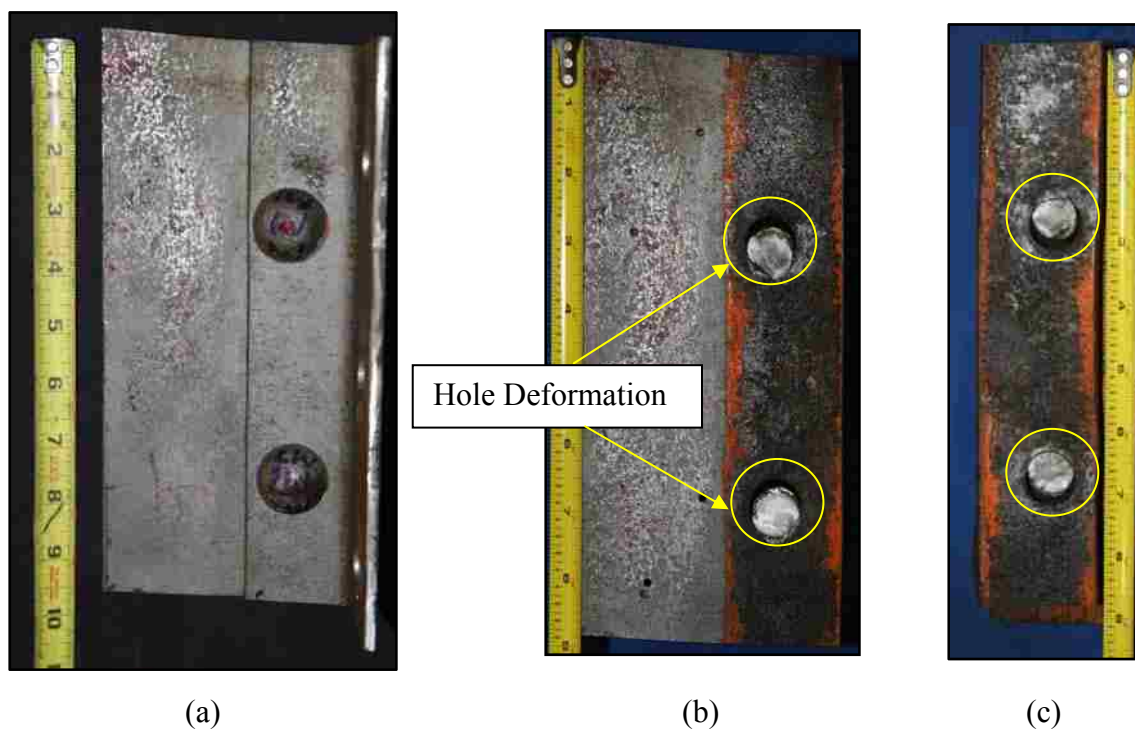
Figure 4.30 West Guardrail Rivet Hole Deformation (a) Before Testing (b) West Angle After Testing (c) West Channel After Testing- Specimen 2R

(a) Before Testing   (b) After Testing
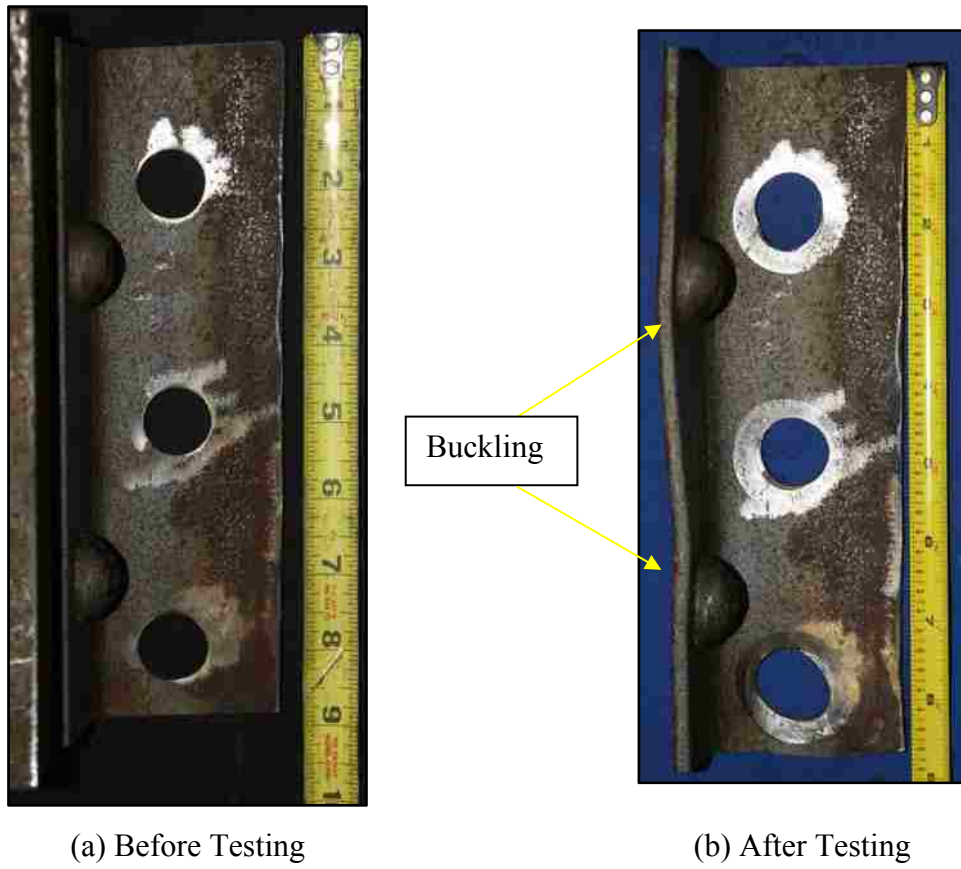
Figure 4.31 West Channel Buckling – Specimen 2R

Figure 4.32 Test 2R Fractured Rivets

4.3.3   Test Specimen 2R (4L)

Specimen 2R (4L) was a guardrail connection that had four rivets per row but with two of these removed was tested to investigate the effect of channel and angle deformation on average rivet shear strength. This test served as a comparison with specimen 2R described in Section 4.3.2. The overall displacement of the plate through the HSS tube for specimen 2R was observed to be larger than the rivet deformation measured during the test. By removing two rivets of the four in specimen 2R(4L), it was expected that the overall displacement would be closer to the rivet deformation.

Figure 4.33 Photo of Test 2R (Four-rivet Length) During Testing

The rivets were removed by drilling a small hole through the rivet head and increasing the diameter of the drill bit until the head was removed. Then a chisel and hammer were used to remove the rivet. Figure 4.34 depicts the west guardrail before and after the removal of the first (1W) and last (4W) rivets in the row. This specimen had two rivets per row for a total of four rivets in the specimen. Five bolts were used to connect each channel to the middle plate and each angle to the HSS, which will provide more resistance against bolt slip.
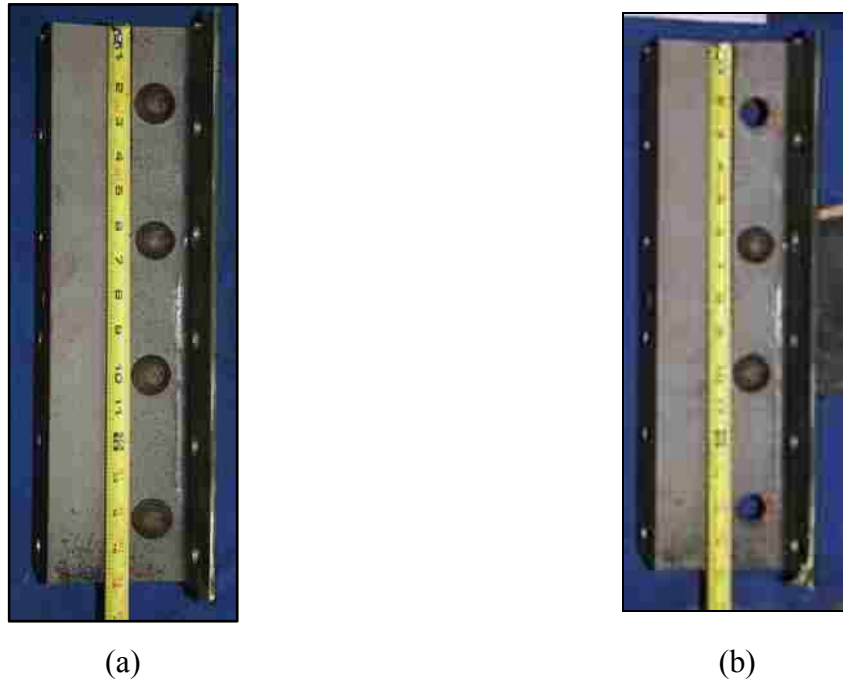
Figure 4.34 Removal of First and Last Rivet in West Guardrail (a) Prior to-rivet Removal (b) Post Rivet Removal - Specimen 2R (4L)

There were no drops in load prior to the maximum load during the test. In addition, noises were heard that might indicate bolt slip, therefore, it is unlikely that the bolts slipped. The maximum load reached was 78.12 kips corresponding to an average overall displacement of 0.262 in. (see Figure 4.35). The load proceeded to decline until reaching approximately 0.3 in. of overall displacement where the first rivet fractured, shortly followed by the fracture of the other three rivets (see observations in Table 4.6). A key observation was that the rivet deformation and overall displacement readings were close through the duration of the test, which suggests that the majority of the overall displacement lead to-rivet deformation rather than bolt slip or deformation of the connecting elements. The load versus overall displacement curve is shown in , where the curve is smooth throughout the test.

Table 4.6 Test 2R (4L) Observations

Test Name: Specimen 2R (4L)		Date Performed: 12/13/2011
No.	**Approximate Load [kip] (Displacement [in.])**	**Observation**
1		smooth loading - close to rivet displacement
2	78 (0.25)	load begins to drop
3	60 (0.3)	first fracture
4		reload
5	63(0.35)	next fracture
6	40 (0.4)	final fracture
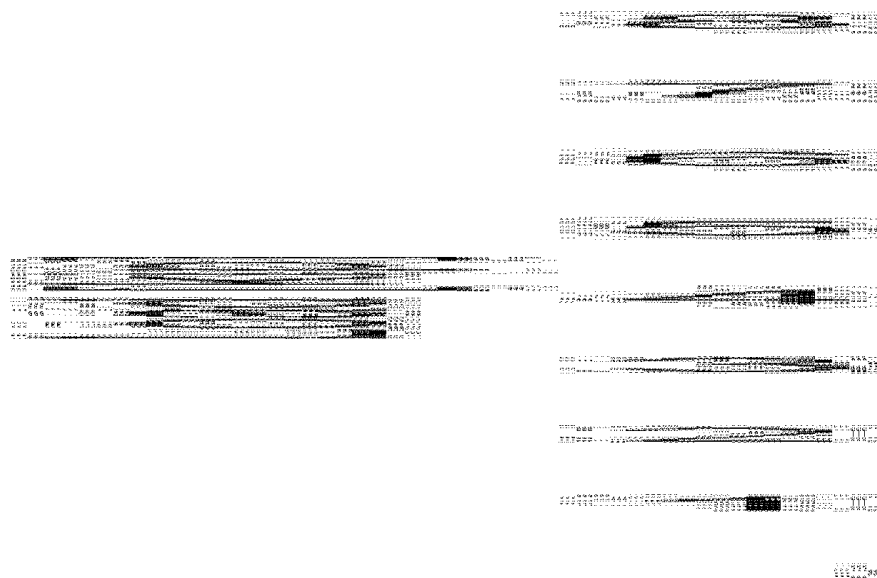
Figure 4.35 Load vs. Overall Displacement – Test 2R (4L)

In contrast to the previous tests, there was less damage observed in the channel or angles after taking the specimen apart. Figure 4.36 below depicts some buckling of the channel that was riveted to the angle in the east guardrail. Some buckling was also observed in the west angle along the riveted surface as shown in Figure 4.37. Rivet hole deformation was observed in both guardrails in the middle test 2R (2W, 3W, 2E, and 4E). The deformation appeared to be more in the top rivet (2W and 3W). Figure 4.38 and Figure 4.39 depict the rivet hole deformation. The fractured rivets are shown in Figure 4.40. Extensive rivet deformation is clear in the figure, which includes rivets 2W, 2E, 3W, and 3E. The rivets appear to have similar oval shapes.

(a) Before Testing

(b) After Testing

Figure 4.36 Buckling in East Angle Riveted Surface - Specimen 2R (4L)

(a) Before Testing
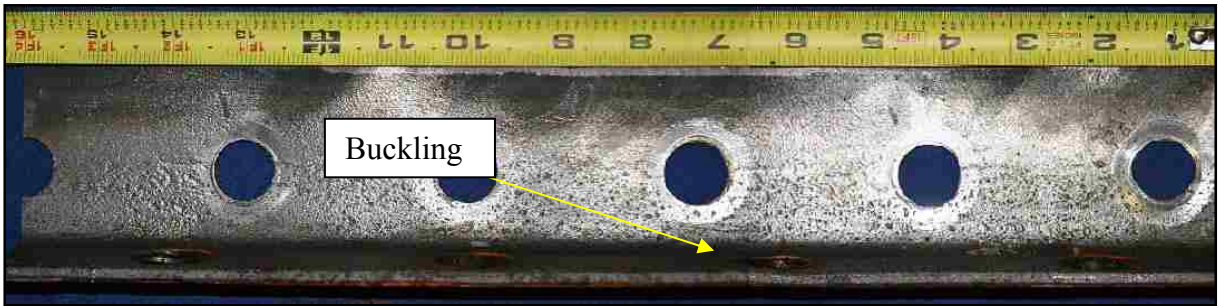
Buckling

(b) After Testing

Figure 4.37 Buckling in West Angle Riveted Surface - Specimen 2R (4L)

(a) Prior to Testing

Hole Deformation
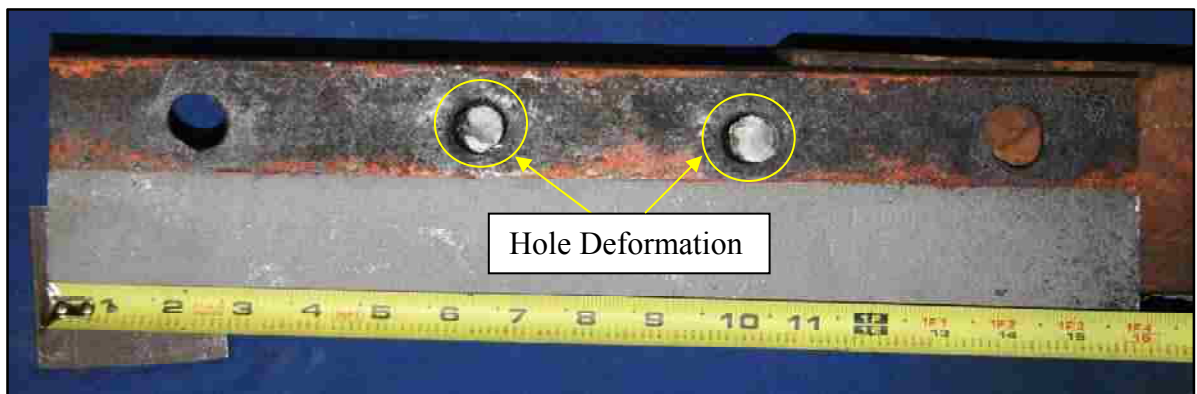
(b) Angle After Testing

Hole Deformation

(c) Channel After Testing

Figure 4.38 Rivet Hole Deformation in West Guardrail - Specimen 2R (4L)

(a) Before Testing

(b) Angle After Testing

(c) Channel After Testing

Figure 4.39 Rivet Hole Deformation in East Guardrail - Specimen 2R (4L)

Figure 4.40 Fractured Rivets – Specimen 2R (4L)

4.3.4   Test Specimen 7R

The longest connection tested in the Small Baldwin was specimen 7R which had seven rivets per row and fourteen rivets total. Ten bolts were used to connect the specimen to the plate and tube. Figure 4.41 below depicts the specimen during testing.

Figure 4.41 Photo of Specimen 7R

At the beginning of the test, the loading was smooth up until the maximum load; there were no drops in load or bolt-slip like noises. This suggests that bolt slip was unlikely to have occurred. The maximum load reached was 261.72 kips at 0.220 in. of overall displacement. The first rivet fractured at an approximate overall displacement of 0.25 in., where the remaining rivets proceeded to fracture subsequently (observations listed in Table 4.7). It was difficult to observe which rivet fractured first, as most of the rivet holes were not visible through the access holes. Figure 4.42 depicts the specimen after testing, where the east channel has displaced past the east angle.

East Channel Displacement
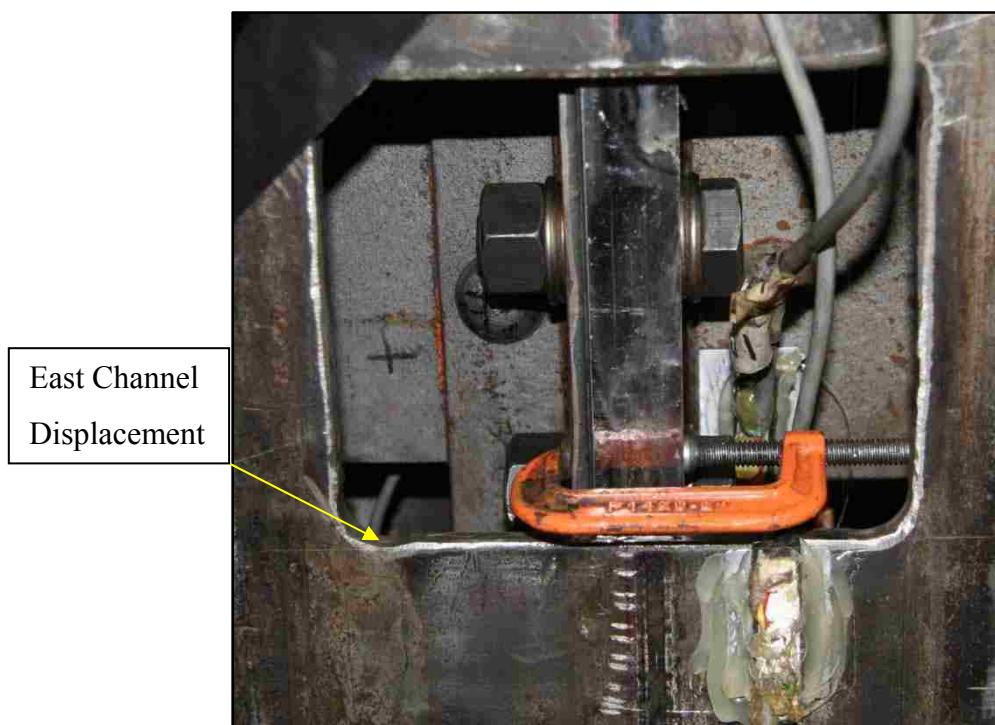
Figure 4.42 Specimen 7R After Testing Lower North Access Hole

Table 4.7 Test 7R Observations

Test Name: Specimen 7R		Date Performed: 02/18/2011
No.	Approximate Load [kip] (Displacement [in.])	Observation
1		smooth loading
2	260 (0.2)	load begins to drop
3	200 (0.25)	first fracture
4		reload
5	120(0.30)	next fracture
6	80(0.30)	next fracture
7	20 (0.4)	final fracture
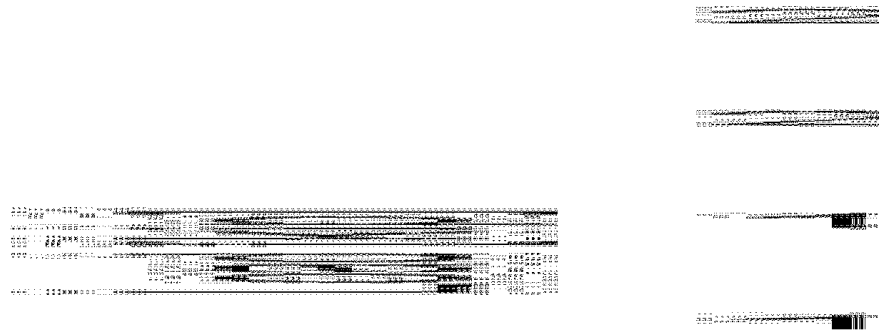
Figure 4.43 Load vs. Overall Displacement – Specimen 7R

The following photos depict the damage observed after taking the specimen apart. Some buckling was observed in the west angle along the riveted surface as shown in Figure 4.44. There was also some buckling in the west channel, which is shown in Figure 4.45. Figure 4.46 shows the hole deformation in the west guardrail. There was some deformation in the west channel along the bolted surface prior to testing. However, this was flattened when the bolts were tightened to slip critical.

(a) Before Testing

Buckling

(b) After Testing

Figure 4.44 West Angle Buckling- Specimen 7R

(a) Before Testing

Buckling

(b) After Testing

Figure 4.45 West Channel Buckling– Specimen 7R

(a) *Before Testing*

Deformation Prior to Testing

Hole Deformation

(b) West Angle After Testing

Hole Deformation

(c) West Channel After Testing
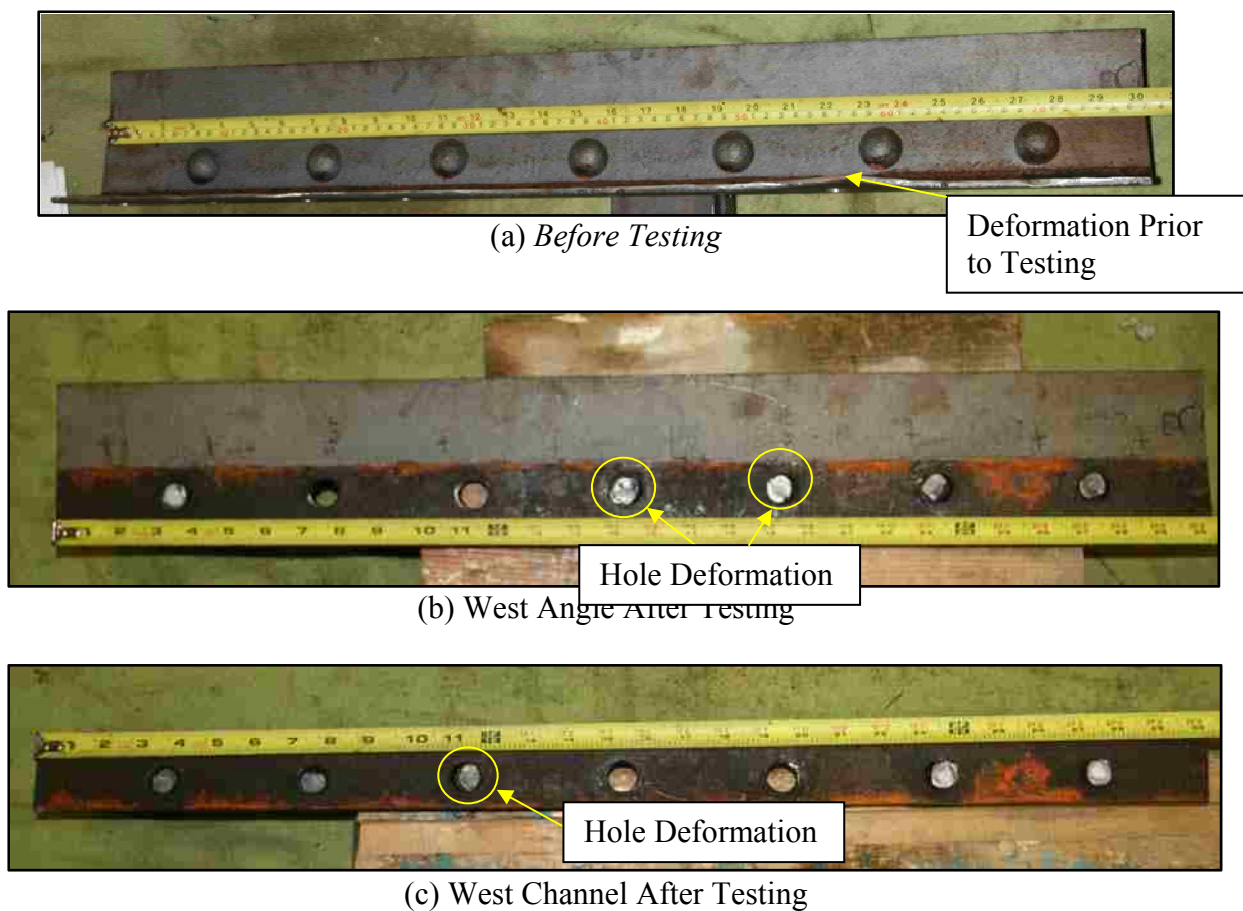
Figure 4.46 West Guardrail Hole Deformation – Specimen 7R

In the east guardrail, there was buckling observed in the east angle (Figure 4.47) and east channel (Figure 4.48) along the riveted surface. Figure 4.49 shows the rivet hole deformation in the east guardrail. There was also some deformation in the channel prior to assembly, but this was removed when the bolts were tightened to snug. There appears to be more rivet hole deformation at the bottom of the angle (right side of Figure 4.49b) and in the holes at the top of the channel (left side of Figure 4.49c).

(a) Before Testing
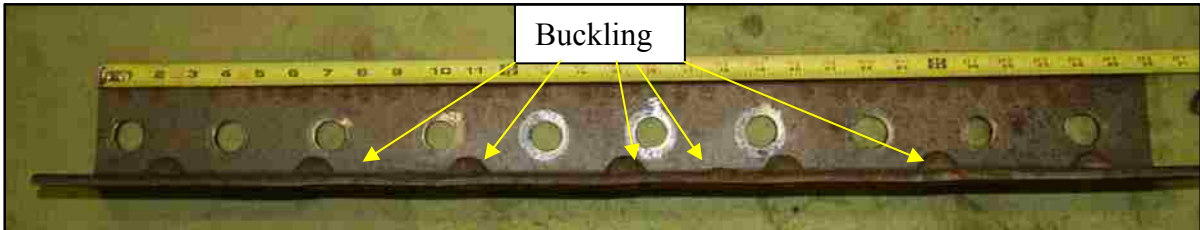
(b) After Testing

Figure 4.47 East Angle Buckling – Specimen 7R
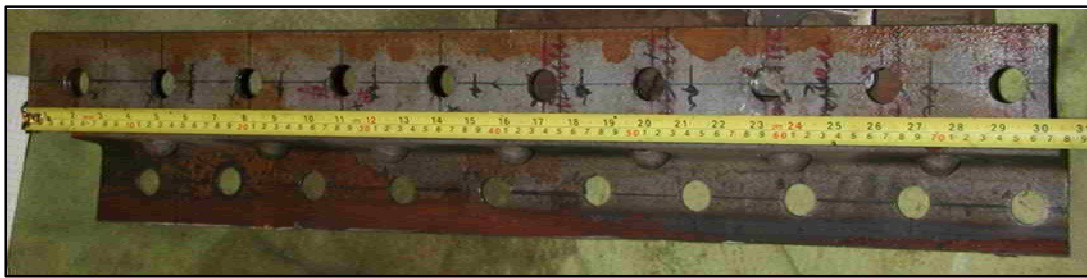
(a) Before Testing

(b) After Testing

Figure 4.48 East Channel Buckling- Specimen 7R

(a) Before Testing

(b) East Angle After Testing

(c) East Channel After Testing

Figure 4.49 East Guardrail Rivet Hole Deformation – Specimen 7R

4.4   Connections Tested in the Baldwin

The following section describes the test observations and gives the load versus overall displacement results for the tests performed in the Baldwin (Specimen 7R and Specimen 11R). Loading for tests in the Baldwin was displacement-control. However, the newly installed controller software was unable to achieve the target slow velocity required for the test. To get around this, small increments of displacement were used as the loading. However, the controller was unable to achieve the target displacement consistently and often overshot it before correcting back to the target. The data collected was filtered to represent the upper envelope of the load-displacement curve.

For the tests in the Baldwin, a channel was bolted to the crosshead with a 1 in. thick plate welded inside of it, to apply the axial load uniformly to the middle plates in the test specimen. Figure 4.50 shows the loading channel bolted to the Baldwin crosshead.
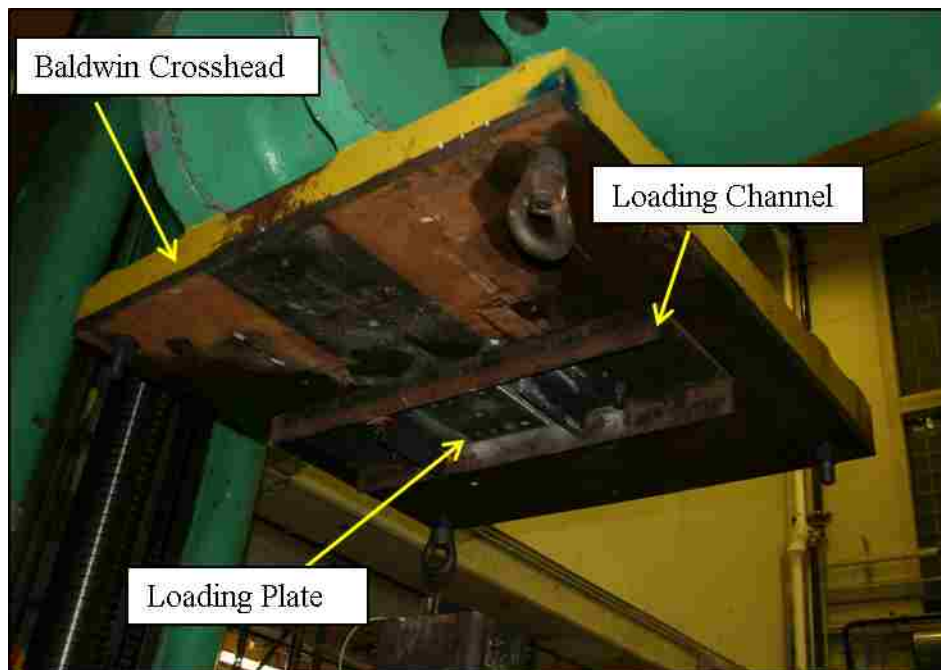
Figure 4.50 Loading Channel for Baldwin Tests

4.4.1 Test Specimen 11R

This test included eleven rivets per row for a total of 22 rivets in the specimen and thirteen bolts were used to connect the specimen to the plate and tube. This test started on 01/28/2012; but was stopped due to concern that the strength of the HSS shape near the access holes might be insufficient. The HSS was modified by adding four 3" x ½" stiffening plates to the HSS at the access holes increasing the yield capacity to 700 kips. Then testing was resumed on 01/30/2012.

It was determined that the yield capacity of the HSS 12x8x1/2 at the access holes was 423.2 kips and the expected rivet capacity was 415 kips (assuming 63 ksi for average ultimate rivet shear from previous test results). Figure 4.51 shows the HSS from specimen 11R with the added reinforcement.

(a)   (b)

Figure 4.51 Specimen 11R with HSS Reinforcement (a) Prior to Reinforcement (b) After Reinforcement

The load versus overall displacement curve is shown in Figure 4.52. Eight pots measured the overall displacement, where the x-axis displacement represents the average measurement of these pots. As discussed above, the Baldwin controller regularly overshot the target displacement and slightly unloaded at each displacement increment. As a result, the curve represents the outer envelope of the data.
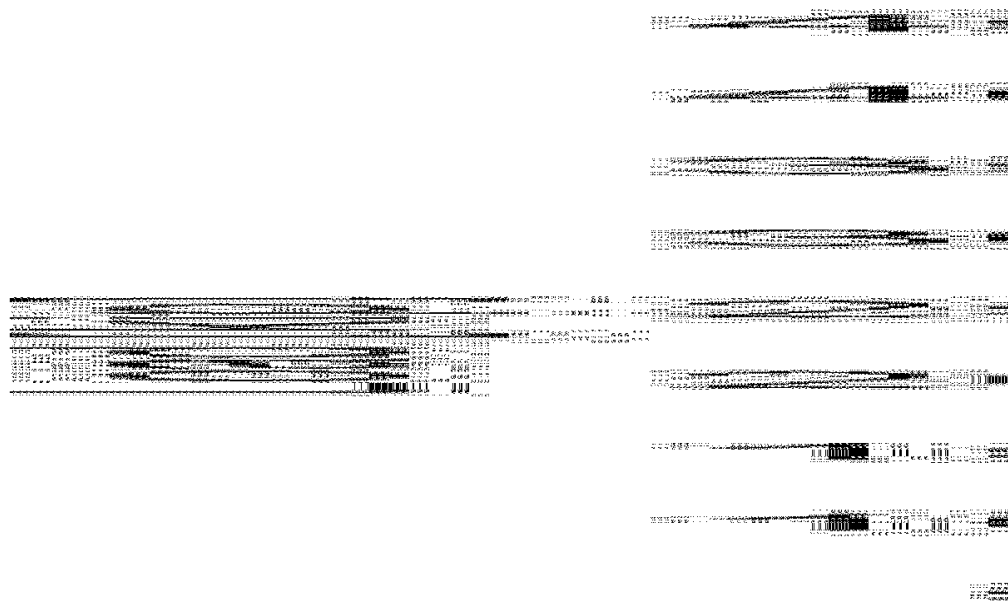
Figure 4.52 Load vs. Overall Displacement – Specimen 11R

During the test, there were a few observations of slip prior to reaching the maximum load. The first occurred at 170 kips, followed by a slip at 270 kips, which were likely bolt slips. Another slip occurred at approximately 350 kips, and was accompanied by a loud bang. However, the specimen continued to resist additional load after that. The maximum load was 422.7 kips, where the first rivet fractured at 0.65 in. of overall displacement. Since the Baldwin test was controlled by displacement, the test could be paused to see which rivet fractured first. Rivet 10E was found to fracture first in this case. In addition, the access holes were large enough to observe the possible order of rivet fracture. After the first fracture, the load increased, and the remaining rivets fractured simultaneously at approximately 0.9 in. of overall displacement. Table 4.8 lists the observations during the test. Figure 4.53 depicts the view through the access holes of the fractured rivets.

Table 4.8 Test 11R Observations

No.	Approximate Load [kip] (Displacement [in.])	Observation
Test Name: Specimen 11R		Date Performed: 01/30/2012
1	170 (0.05)	bolt slip
2	270 (0.10)	bolt slip
3	350 (0.30)	slip with loud noise
4	423.5 (0.60)	maximum load
5	370 (0.65)	first rivet fracture 10E
6	150 (0.70)	load decrease
7	160 (0.90)	remaining rivets fractured

(a) South Side   (b) North Side

Figure 4.53 Fractured Rivets After Test - Specimen 11R

The following photos depict the damage observed after taking the specimen apart. In the west guardrail, some buckling of the angle along the riveted surface was observed uniformly along the full length as shown in Figure 4.54. There was also buckling observed in the west channel along the riveted surface as shown in Figure 4.55. The rivet hole deformation in the west guardrail is shown in Figure 4.56, where the holes appear to have deformed uniformly.

The fractured rivets in the west guardrail are shown in Figure 4.57, which include 1W, 2W, 3W, 4W, 5W, 8W, 9W, 10W, and 11W. Figure 4.60 shows the rivets that fractured in the east section of the guardrail, which includes 1E, 3E, 4E, 5E, 6E, 7E, 10E, and 11E. There

was rivet hole deformation observed in the east guardrail as shown in Figure 4.58. Buckling of the east channel observed along the riveted surface as shown in Figure 4.59.

(a) West Angle Before Testing
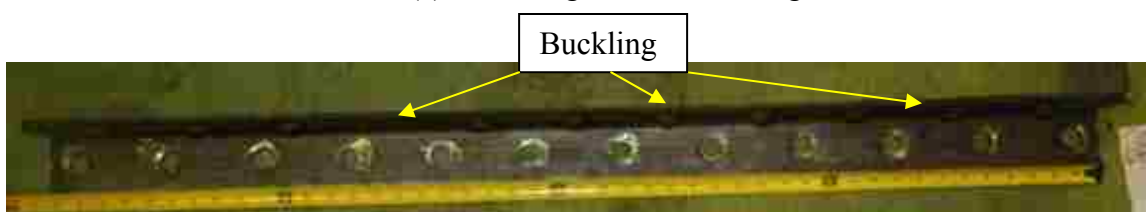
(b) West Angle After Testing

(c) West Angle After Testing

Figure 4.54 West Angle Buckling – Specimen 11R

(a) West Channel Before Testing
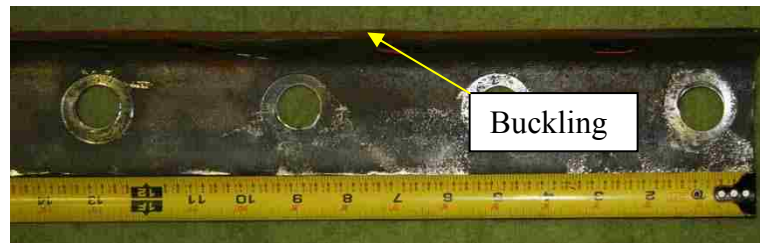
(b) End of Channel After Testing
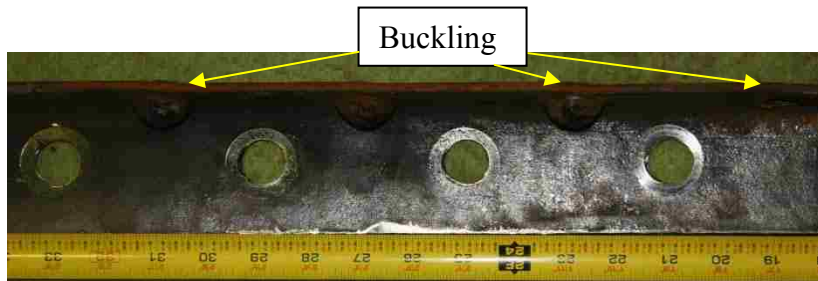
(c) Middle of Channel After Testing

Figure 4.55 West Channel Buckling – Specimen 11R

(a) West Guardrail Before Testing

(b) West Angle After Testing

(c) West Channel After Testing

Figure 4.56 West Guardrail Rivet Hole Deformation – Specimen 11R

(a)

(b)

Figure 4.57 West Guardrail Fractured Rivets - Specimen 11R

(a) Before Testing

(b) East Angle After Testing

(c) East Channel After Testing

Figure 4.58 East Guardrail Rivet Hole Deformation – Specimen 11R

(a) Before Testing
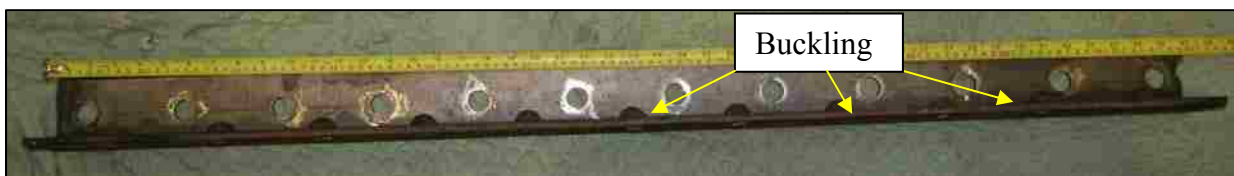
(b) After Testing

Figure 4.59 East Channel Buckling – Specimen 11R

(a)   (b)

Figure 4.60 East Guardrail Fractured Rivets - Specimen 11R

4.4.2   Test Specimen 17R

This test was the longest connection tested in this experimental program. The total length was 17 rivets per row (70 in. total with clearances), where 18 bolts were used to fasten each channel to the plate and the angle to the HSS for 72 bolts total. Prior to testing, the HSS was reinforced at the bottom to increase its yield capacity. Two ¼ in. thick plates were welded to each side of the HSS along the shorter side (see Figure 4.61). The added area of five square inches increased the yield capacity to 929.2 kips.
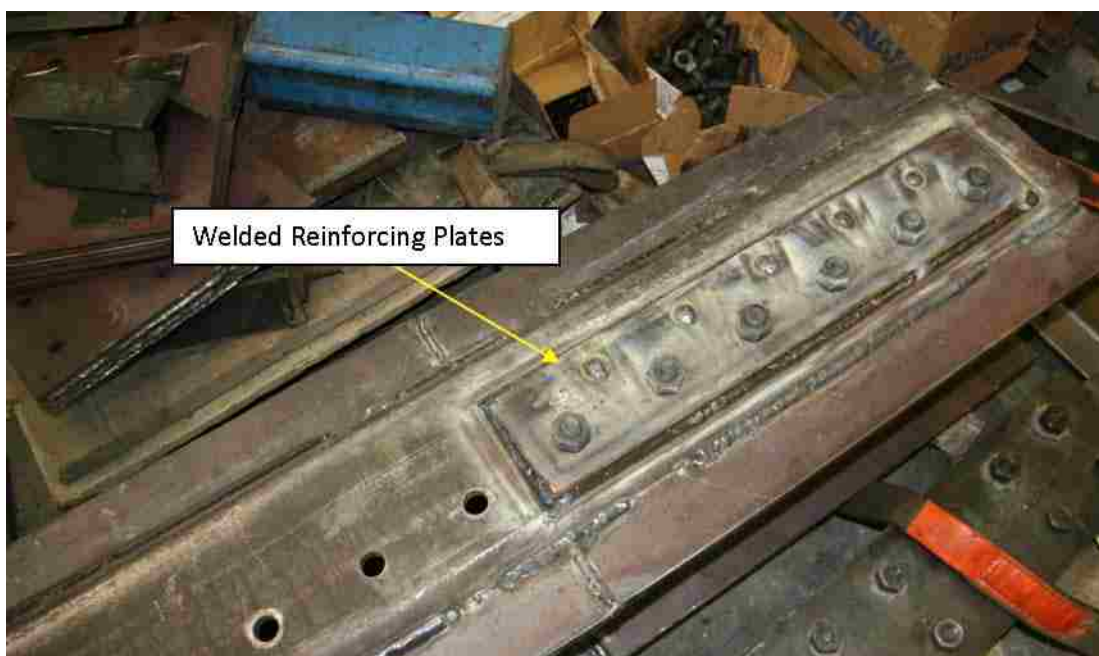
Figure 4.61 HSS Reinforcement for Specimen 17R

The loading in this test was smoother compared to test of specimen 11R because improvements were made in operating the displacement control of the Baldwin. The specimen loaded elastically until approximately 70 kips, where there were several drops in load back down to 70 kips until 100 kips was reached. The load continued to increase with displacement until 300 kips where several drops in load down to approximately 100 kips occurred until 500 kips was reached. After 500 kips, the load increased steadily until the maximum was reached (649.3 kips at an average overall displacement of 0.465 in). The first rivet fractured (16W) at approximately 630 kips or 0.5 in. of overall displacement. The load increased slightly and then dropped down to 500 kips where the remaining rivets fractured simultaneously. Observations are listed in the table below, and the load versus overall displacement for test 17R is shown in Figure 4.62. The load versus displacement graph

shown in Figure 4.62 represents the upper envelope of the load due to several load drops that occurred during the test.

Table 4.9 Test 17R Observations

Test Name: Specimen 17R		Date Performed: 02/10/2012
No.	**Approximate Load [kip] (Displacement [in.])**	**Observation**
1	70 - 100	several drops in load - bolt slip
2	300-500	several drops in load with some noise - bolt and/or-rivet slip
3	580 (0.4)	drop in load
4	650(0.45)	maximum load - first rivet fracture 16W
5	630(0.5)	reloading of specimen
6	450(0.55)	remaining rivets fractured
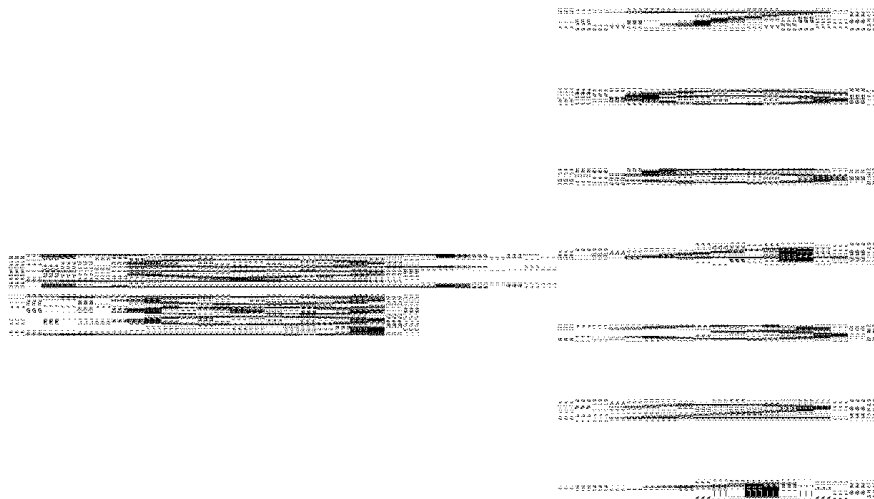
Figure 4.62 Load vs. Overall Displacement – Test 17R

After the test was complete, the specimen was taken apart, and the following damage was observed. Similar to previous tests, there was buckling in the west channel along the riveted surface as shown in Figure 4.63. The rivet hole deformation for the west guardrail is shown Figure 4.64, where the shape of the deformed hole is similar along the length of the channel. The rivet hole deformation in the west angle is shown in Figure 4.65. The fractured rivets are shown in the Figure 4.66, and they include 1W, 3W, 4W, 5W, 6W, 8W, 9W, 10W, 12W, 14W, 15W, 16W, and 17W.

(a) Middle of West Chanel Prior to Testing
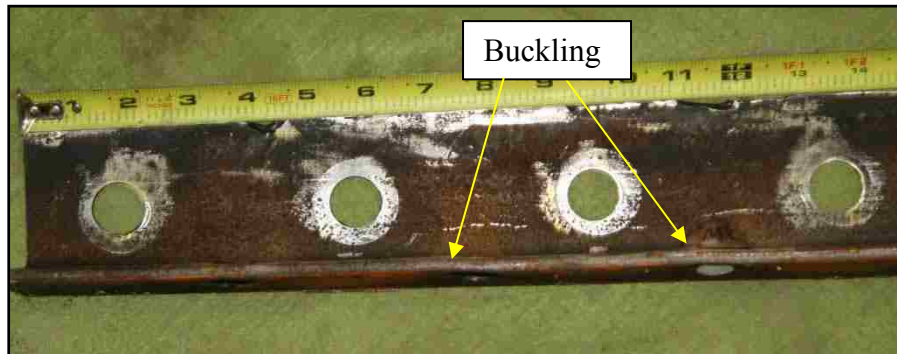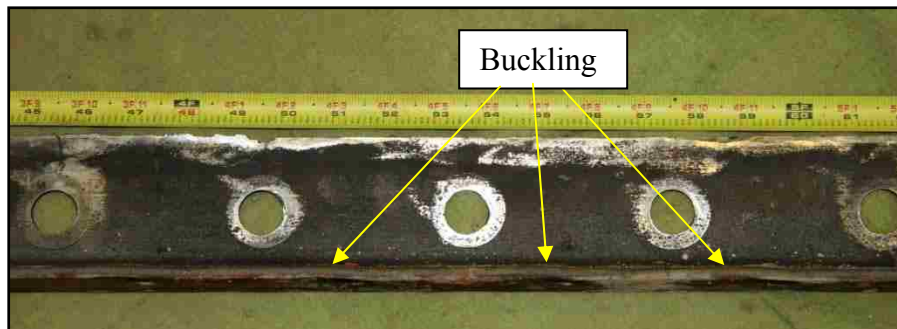
(b) Top of Channel

(c) Bottom of Channel

Figure 4.63 West Channel Buckling – Specimen 17R

(a) West Channel Prior to Testing

(b) Top of Channel

(c) Middle of Channel

(d) End of Channel

Figure 4.64 West Channel Rivet Hole Deformation- Specimen 17R

(a)

(b)

(c)

Figure 4.65 West Angle Rivet Hole Deformation – Specimen 17R

Figure 4.66 West Guardrail Fractured Rivets – Specimen 17R

The damage observed in the east guardrail is depicted in the photos below. Buckling of the east channel was also observed along the entire length, except in the last inch of the channel (right side of Figure 4.67c). Deformation of the rivet holes in the east channel as shown in Figure 4.68, where the hole deformation was uniform along the length. The corresponding rivet hole deformation in the east angle is shown in Figure 4.69. Some buckling was also observed in the east angle along the riveted surface as shown in Figure 4.70.

(a) East Channel Prior to Testing
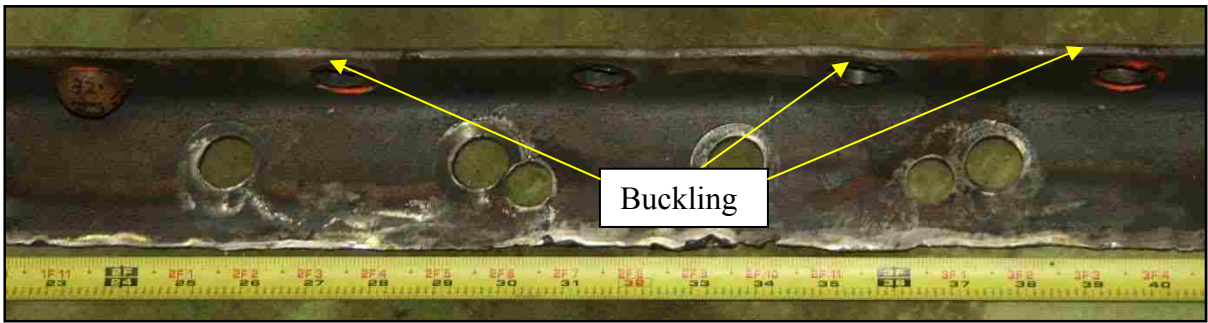
(b) Middle of Channel
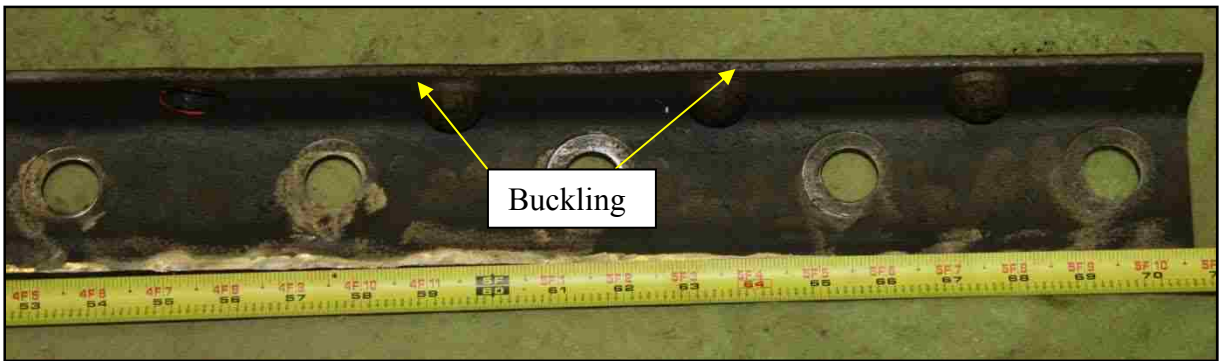
(c) End of Channel

Figure 4.67 East Channel Buckling – Specimen 17R

(a) Top of Channel

(b) Middle of Channel

(c) Bottom of Channel

Figure 4.68 East Channel Rivet Hole Deformation- Specimen 17R

(a) East Angle Prior to Testing

(b) Top of Angle After Testing

(c) Middle of Angle After Testing

(d) Bottom of Angle After Testing

Figure 4.69 East Angle Rivet Hole Deformation – Specimen 17R

(a) East Angle Prior to Testing
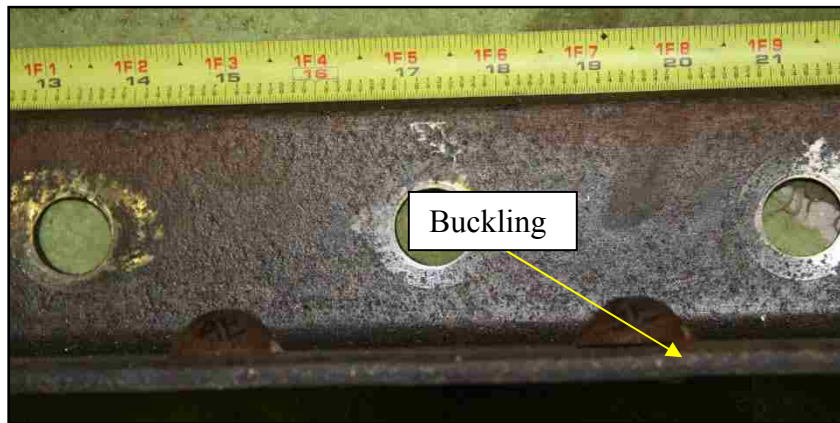
(b) Top of Angle After Testing
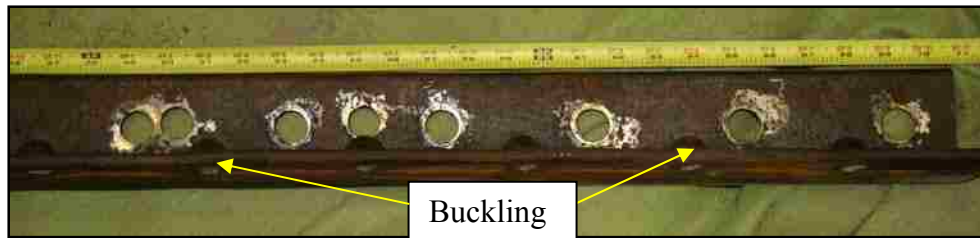
(c) Bottom of Angle After Testing

Figure 4.70 East Angle Buckling – Specimen 17R

Chapter 5: Analysis and Discussion of Experimental Results

5.1 General

The following chapter analyzes the test results for each specimen. The first section compares the data with consideration of the effect of connection length on rivet shear strength. In addition, the relationship between the reduction factor recommended by AASHTO and the rivet shear strengths from each test is discussed. The test results are then compared to those of past experiments. The second section analyzes the rivet deformation at ultimate load for each test. The third section compares the general behavior of the test configuration under load, concerning the overall displacement, rivet deformation, bolt slip, and approximate shear deformation. The last section discusses the strain gauge data from test specimen 4R.

5.2 Rivet Strength

This section examines the rivet strength results from the test specimens and compares them to relevant literature and current AASHTO recommendations.

5.2.1 Rivet Strength from Test Specimens

The average rivet shear stress versus rivet deformation for all of the tests performed in this test program is shown in Figure 5.1 for the west guardrail up to the ultimate rivet shear stress (specimen 17R is not included as the instrumentation failed during the test), and the east guardrail is shown in Figure 5.2. Individual load versus rivet deformation plots can be found in Appendix E.1. The rivet deformation is plotted separately for the west and east guardrail because they include different rivet groups. The rivets did not deform equally in each guardrail because some of the bolts connecting the middle plate to the channel and the HSS to the angle slipped. Since slip occurred in different bolts connecting the west and east guardrail at different times, the load transfer was not steady throughout the test, causing a difference in the rivet deformation.

Figure 5.1 show that all of the tests perform similarly in the elastic portion of the curve up to approximately 30 ksi. The onset of yielding appears to occur at a lower load for the shorter connections, with the exception of test 2R (4L). For this specimen, the majority of the overall displacement was concentrated in the rivet deformation rather than the yielding of the connecting members, thus yielding of the rivets occurred at a lower rivet deformation. In

addition, as a result, test 2R (4L) experienced the largest rivet deformation at ultimate load. The average ultimate rivet shear stress is lowest for test 4R, where the ultimate load was reached at a lower value of rivet deformation. The largest ultimate stress was measured from test 2R; however, there is little difference for all of the tests.
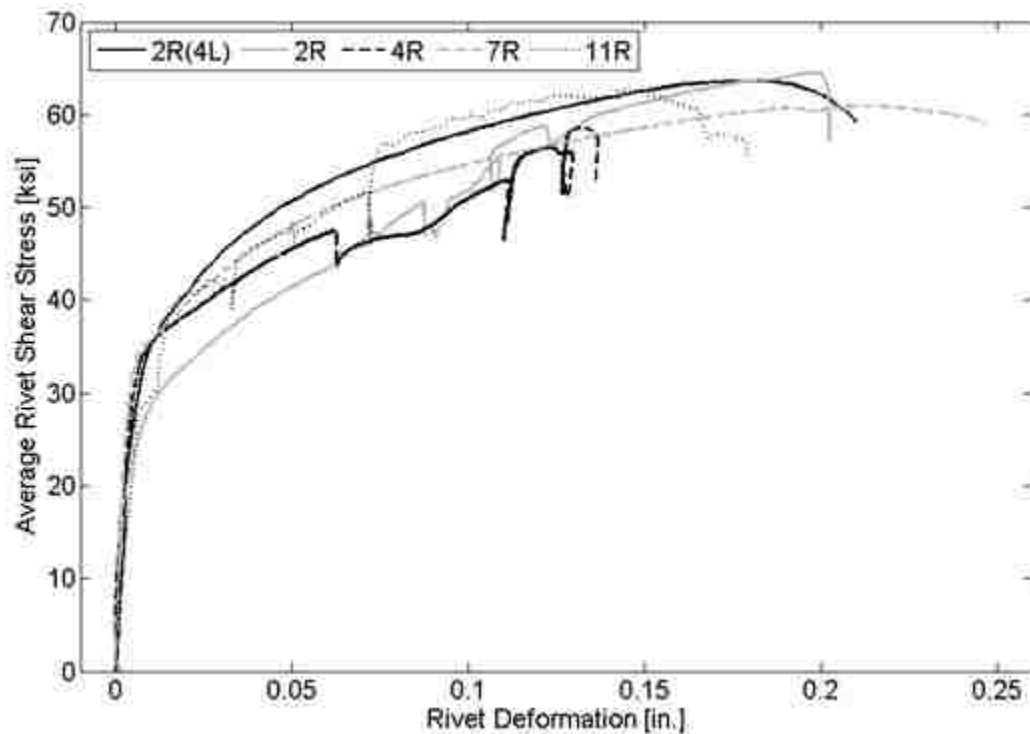
Figure 5.1 Average Rivet Stress vs. Rivet Deformation Ultimate Load - West Guardrail

Figure 5.2 shows that the initial elastic stiffness is higher for the longer tests. This is likely because the specimen is stiffer because the connection reaches the full length of the HSS, and there are more bolts attached to the middle plate and HSS. However, this difference in behavior of the test configuration did not affect the average ultimate rivet shear strength. The onset of yielding in the rivets appears to occur at lower average rivet shear stress for the shorter connections. The rivet deformation at ultimate load does not show a trend with connection length.
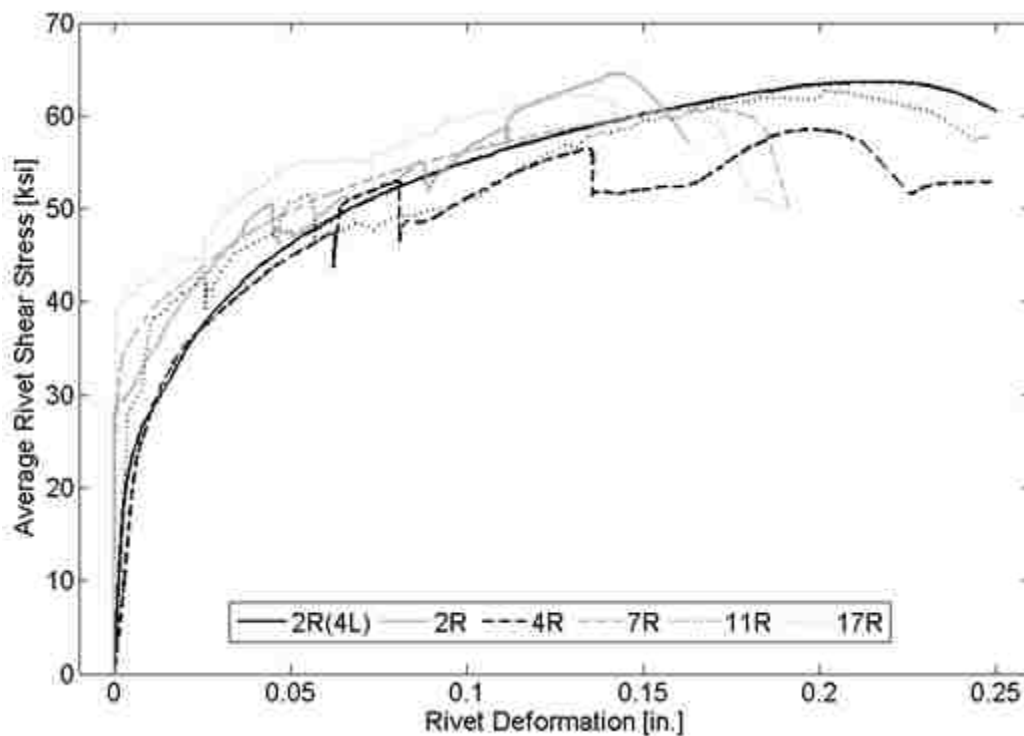
Figure 5.2 Average Rivet Stress vs. Rivet Deformation Ultimate Load - East Guardrail

The ERY was also computed for the east and west guardrail for all of the test specimens (see Table 5.1). The average ERY for all of the specimens was 35.2 ksi with a standard deviation of 3.2 ksi. The stages were not as clear as shown in Figure 2.30, but the method of estimating ERY was followed as closely as possible to that of Davis et al. (1939). The pots measuring west rivet deformation came off during test 17R; therefore, the ERY could not be calculated. The ERY was plotted versus the connection length in Figure 5.3 where it is shown that as connection length increases, the ERY ranges from 30 – 40 ksi, but is not a function of connection length.

Table 5.1 ERY for West and East Guardrail

Test Name	ERY [ksi]	
	W	E
2R	29.24	37.85
4R	37.1	35.53
2R (4L)	34.27	29.98
7R	34.75	34.34
11R	36.93	37.82
17R	-	39.43
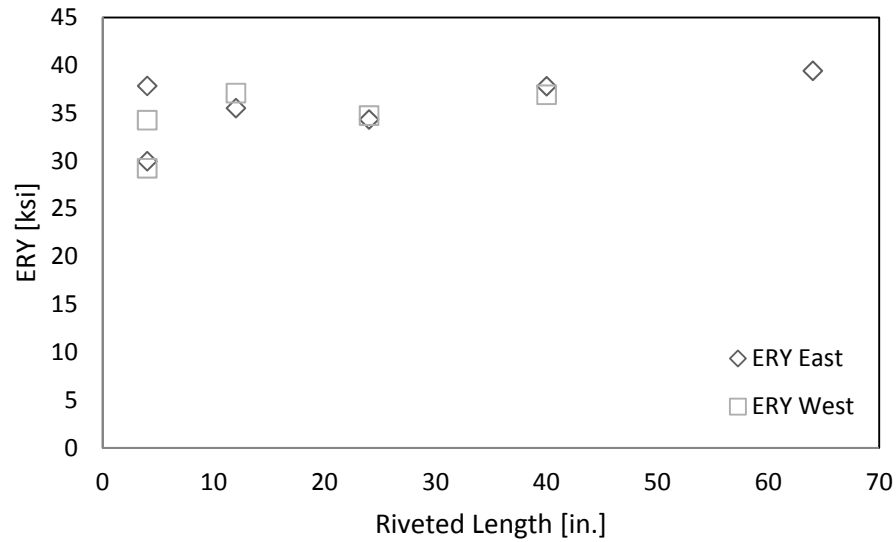
Figure 5.3 ERY vs. Riveted Length

The average ultimate rivet shear stress was compared for all of the tests. It was computed using the following equation.

$$v_u = \frac{P_{max}}{n_r A_r}$$ (5.1)

where: v_u = average rivet shear stress [ksi]

P_{max} = ultimate load [kips]

n_r = total number of rivets in test configuration

A_r = area of one rivet [in²]

The table below summarizes the average ultimate rivet shear strength ($V_{u,avg}$) in comparison to the maximum load (P_{max}), the riveted length (L_r), the total length (L), and the number of rivets per row. The data shows that the average ultimate rivet shear stress does not vary significantly with the connection length. The average of $V_{u,avg}$ for all of the tests was 62 ksi, with a standard deviation of 2.1 ksi.

Table 5.2 Summary of Ultimate Rivet Shear Strength and Connection Length

Test Name	No. Rivets /Row	L [in.]	L_r [in.]	P_{max} [kips]	$V_{u, avg}$ [ksi]
Two Rivet	2	8.5	4	79.30	64.62
Four Rivet	4	16.5	12	143.74	58.56
Two Rivet (Four Rivet Length)	2	16	4	78.13	63.67
Seven Rivet	7	30	24	261.72	60.93
Eleven Rivet	11	46	40	422.73	62.63
Seventeen Rivet	17	71	64	649.27	62.24

The average ultimate shear strength as shown in Figure 5.4 does not vary with connection length. A trend line was added to show that the average ultimate shear stress can be approximated as constant for the connection lengths (the correlation coefficient, R^2, was very small, which indicates low correlation between $V_{u,avg}$ and L_r).
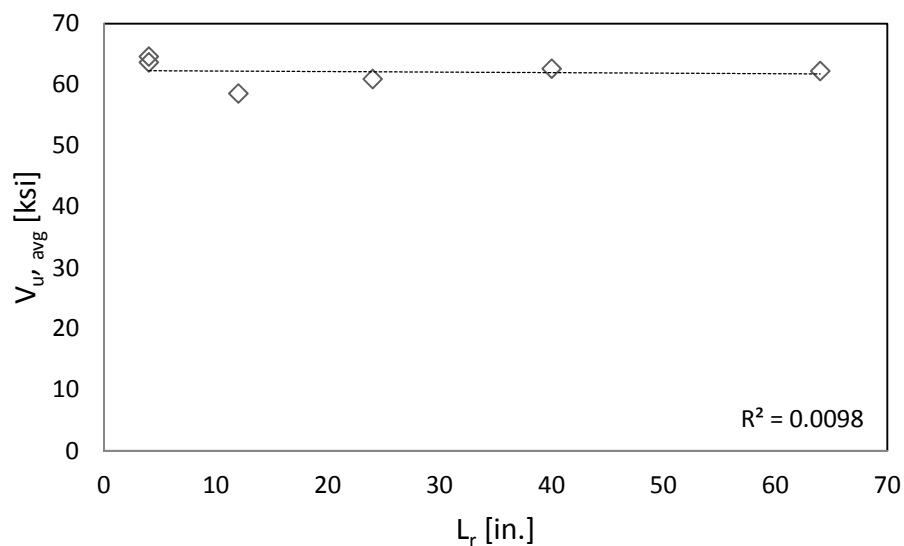
Figure 5.4 Average Ultimate Rivet Shear Stress vs. Riveted Length

The average rivet shear strength was normalized with the average rivet shear strength from test 2R, which was chosen as a basis for comparison because it was the shortest riveted length (see Figure 5.5). This plot also shows that the average rivet shear strength is a weak function of the connection length.
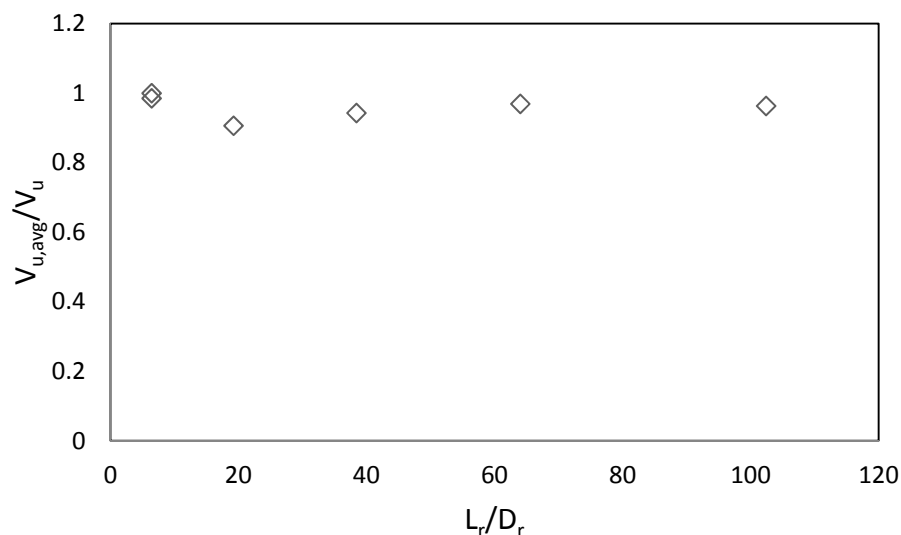
Figure 5.5 Normalized Average Ultimate Shear Strength vs. Riveted Length/Rivet Diameter

5.2.2   Comparison to AASHTO Recommendations

The results show that for this loading mechanism, the average rivet strength in shear is not a function of the connection length. However, the AASHTO specification described in Section 2.4.2 recommends a reduction factor for longer connections. The shear strength of the rivets was calculated using AASHTO's equation (see Table 5.3). The third column gives the results of this test program, the fourth column computes the rivet shear strength using AASHTO's equation and assuming a rivet shear strength equal to that of Specimen 2R (4L). Figure 5.6 shows the rivet strength versus connection length for this test program compared to AASHTO recommendations. This shows the difference between the expected connection length effect and lack of length effect observed in this test program.

Table 5.3 Rivet Shear Strength – AASHTO Reduction Factor

Test Name	L_r [in.]	Experiment $V_{u,avg}$ [ksi]	AASHTO V_u R_n/A_r [ksi]
2R	4	64.6	62.4
4R	12	58.6	59.8
2R(4L)	4	63.7	62.4
7R	24	60.9	56.0
11R	40	62.6	50.9
17R	64	62.2	47.7
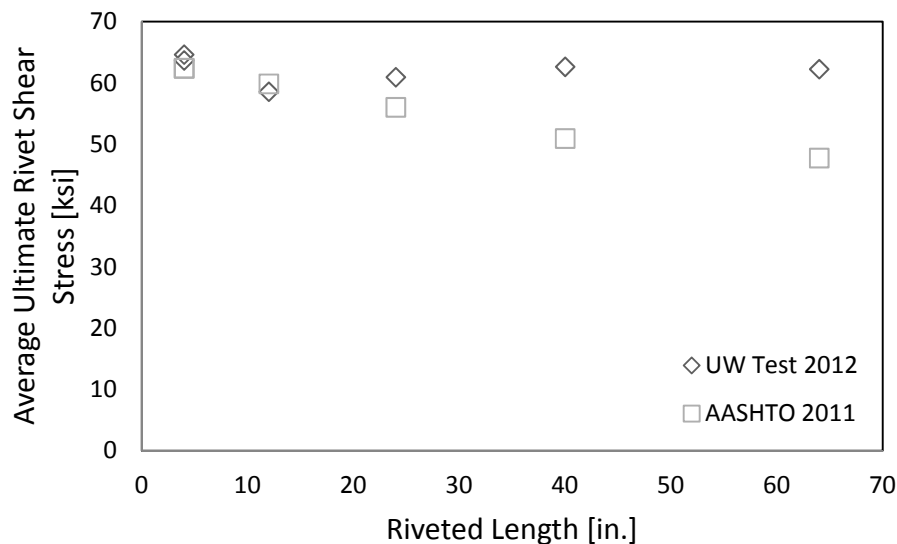
Figure 5.6 Ultimate Rivet Shear Strength vs. Riveted Length – AASHTO Reduction Factor

5.2.3   Comparison to Literature

The results from experiments described here were compared to those in the relevant literature where connection length effect was investigated. Table 5.4 below gives the average rivet shear strength from lap splice tests and includes the results of this test program. Besides connection length, the tests in the literature also incorporated other parameters such as rivet material, rivet grip, rivet pitch, splice type, and rivet diameter, which affected strength. The standard deviation of the data for each test is less than 3.0 ksi for all tests except D'Aniello et. al (2010) where the rivet diameter varied. The standard deviations are close to that of the UW Test Program where the diameter, connection type, grip, and pitch were not varied. Therefore, these average strengths for each test can provide a basis for comparison, and they show that the strength from this experiment is still larger than the literature. This is likely because tests from previous literature had a different loading mechanism, where they were all loaded in a lap splice configuration.

Table 5.4 Comparison of Experiment Results to Literature

Literature	$V_{u,avg}$ [ksi]	Std Dev [ksi]	Rivet Dia. [in.]
AREMA 1904	48.25	2.3	0.875
Talbot & Moore 1911	56.56	1.8	0.875
	52.84	2.5	0.875
Davis, Davis, & Woodruff 1939	55.17	2.7	0.875
	75.10	2.5	0.875
Dlugosz 1960	40.67	2.8	0.875
Roeder, Leon, & Preece 1994	56.59	1.7	0.750
D'Aniello, Portioli, Fiorino, & Landolfo 2010	53.04	6.7	varies (0.630-0.860)
UW Test Program 2012	62.11	2.1	0.625

All of the data was plotted from previous experiments and compared to this test program and current AASHTO recommendations (see Figure 5.7). The results of the current test program were normalized by the rivet strength from the shortest test, which was test 2R (4L) for this research, as a tensile rivet test was not performed. In contrast, the data from literature was normalized by the shear strength approximated as 67% of the rivet tensile strength. As a result, the normalized shear strength for this test program is much lower than past experiments. For shorter connections, the strength decreases linearly as AASHTO would predict. However, for longer connections there is a small decrease in strength, but not as much as the AASHTO reduction factor calculates. For shorter connections, this shows more of a length effect predicted from literature than what was observed in this test program, but for longer connections, the data is similar. Concerning the experimental results as a whole, AASHTO reduces the strength of the connection more than necessary for longer connections, but the factor is reasonable for shorter connections.
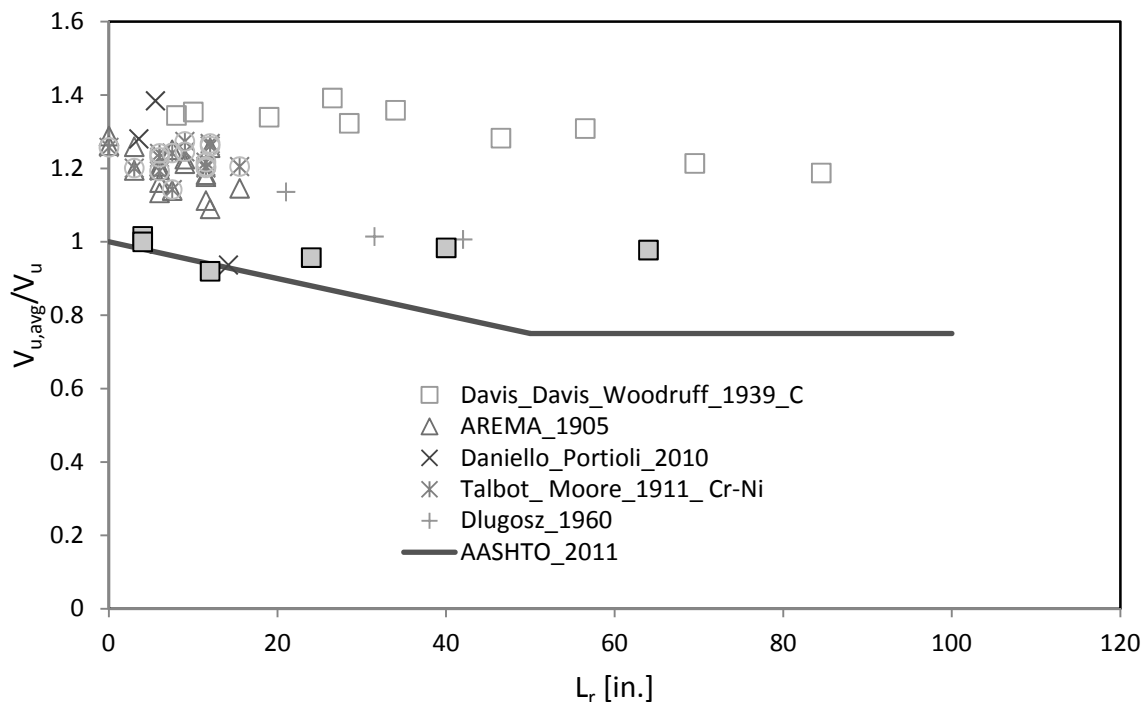
Figure 5.7 $V_{u,avg}/ V_u$ vs. L_r–Comparison to Previous Tests

As shown in the literature review, other factors (rivet diameter, pitch, grip, and material) were studied in past experiments. To isolate the impact of connection length, the data from this test program was plotted with data for carbon steel rivets with a low grip (as shown in Figure 5.8.) because the rivets in this test program were made of the same material and had a grip of only 0.7 in. This plot shows a similar trend to that of Figure 5.7; where there is not as much of a decrease in rivet shear strength as connection length increases for past experiments and this experiment.
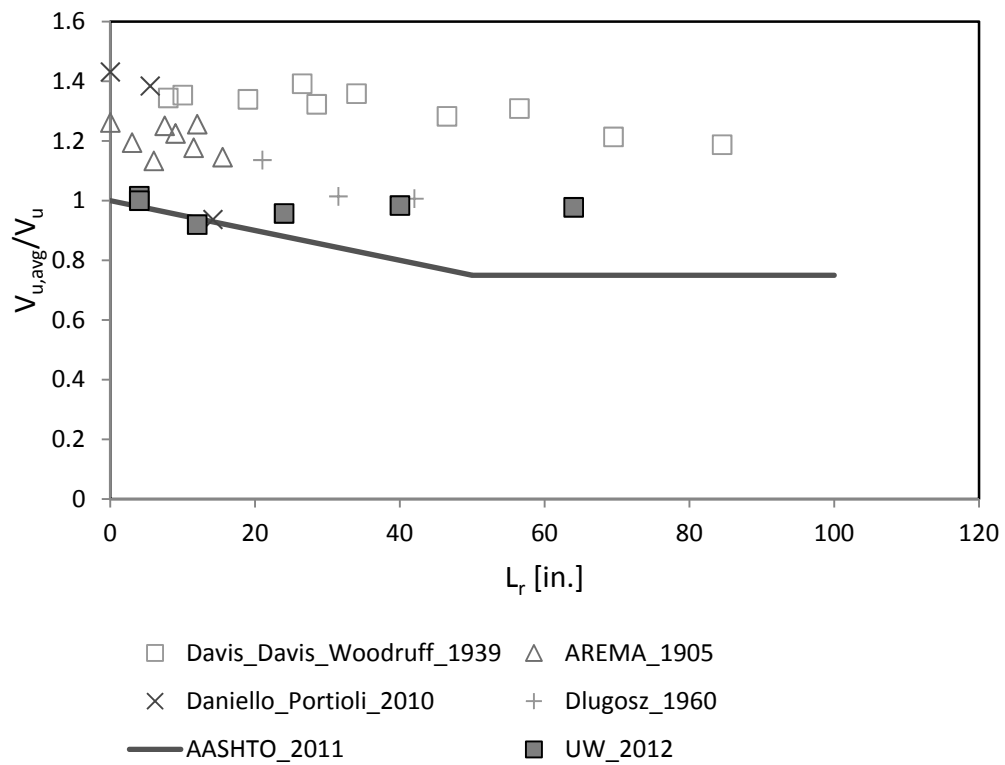
Figure 5.8 $V_{u,avg}/V_u$ vs. L_r for C-Steel Rivets with Lower Grip

5.3   Rivet Deformation

Another key measurement was the rivet deformation at ultimate load, which should not vary significantly between test specimens. The average ultimate rivet shear stress was plotted versus the rivet deformation at ultimate (see Figure 5.9). This shows that the rivet strength does not vary significantly with rivet deformation experienced at ultimate load.
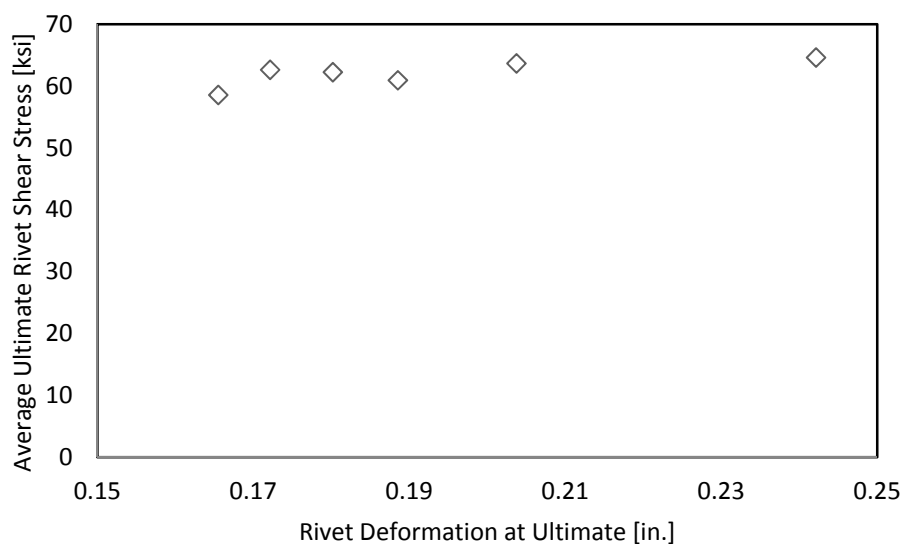
Figure 5.9 Average Rivet Shear Stress vs. Rivet Deformation at Ultimate Strength

Another parameter that was compared was the rivet deformation at ultimate load (see Figure 5.10) versus connection length. This curve shows that the rivet deformation at ultimate load decreases as the connection length increases for this test configuration. This could be because more deformation in the connecting elements was observed in the shorter connections. Therefore, the pots measuring rivet deformation at the angle-channel interface captured this deformation in addition to rivet deformation, which causes the rivet deformation to appear larger at shorter connections. It is likely that if the instrumentation were able to measure only the rivet deformation and not the connecting elements along the row of rivets, the measured rivet deformation would be the same.
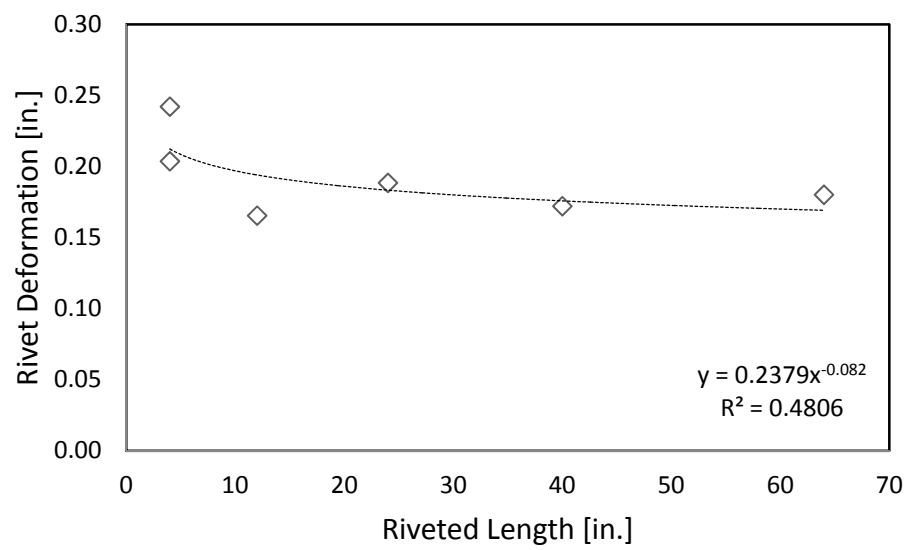
Figure 5.10 Rivet Deformation vs. Riveted Length

5.4 Components of Overall Specimen Deformation

This section discusses the three components of overall specimen deformation: rivet deformation, shear deformation of connecting elements, and bolt slip. The first sub-section compares these components for each test. The second sub-section discusses bolt-slip and the final section compares the overall displacement for each test.

5.4.1 Comparison of Deformation Components for Specimen Tests

During the test, in addition to rivet deformation, the guardrail also experienced shear deformation and bolt slip at the HSS and plate interfaces. The bar graph below (Figure 5.11) summarizes the fraction of overall displacement that each type of deformation contributed for all of the tests. For tests 2R, 2R (4L), and 4R, the shear deformation was approximated by the measurements from the pots. In contrast, for tests 7R, 11R, and 17R, the shear deformation was not measured using pots but approximated as the difference between the overall displacement and the sum of the rivet deformation and bolt slip. As a result, the fraction of overall displacement for specimens 2R, 2R (4L), and 4R will not add to 1 because of some percent error in the pot measurements, whereas specimens 7R and 11R will add to 1 by default. Individual load versus displacement plots for shear deformation and bolt slip can be found in Appendix E.3.

The graph shows that for test 2R(4L) almost all of the displacement lead to rivet deformation, with negligible shear deformation and less than 10% lead to bolt slip. Overall, the shear deformation seems to decrease as the connection length increases. The bolt slip seems consistent in all tests, where Specimen 17R experienced the most except for Specimen 11R. This specimen did not experience as much bolt slip as Specimen 17R, which could be because in Specimen 11R, less plates were bolted to the HSS. In addition, the two middle plates were bolted to Specimen 17R for their full length, whereas Specimen 11R was only bolted to 50 in. of the middle plates and bolts were placed in the remaining holes. The bolt slip may have been less for Specimen 11R and Specimen 2R (4L) because they were the shortest connections for their respective testing machines. The percentage of the displacement that lead to rivet deformation appears to decrease as the connection length increases for the tests where shear deformation was measured and not approximated, as this

is not true for Specimen 11R. A breakdown of each type of deformation for each specimen test can be found in (Table E.1–Table E.12 in Appendix E).
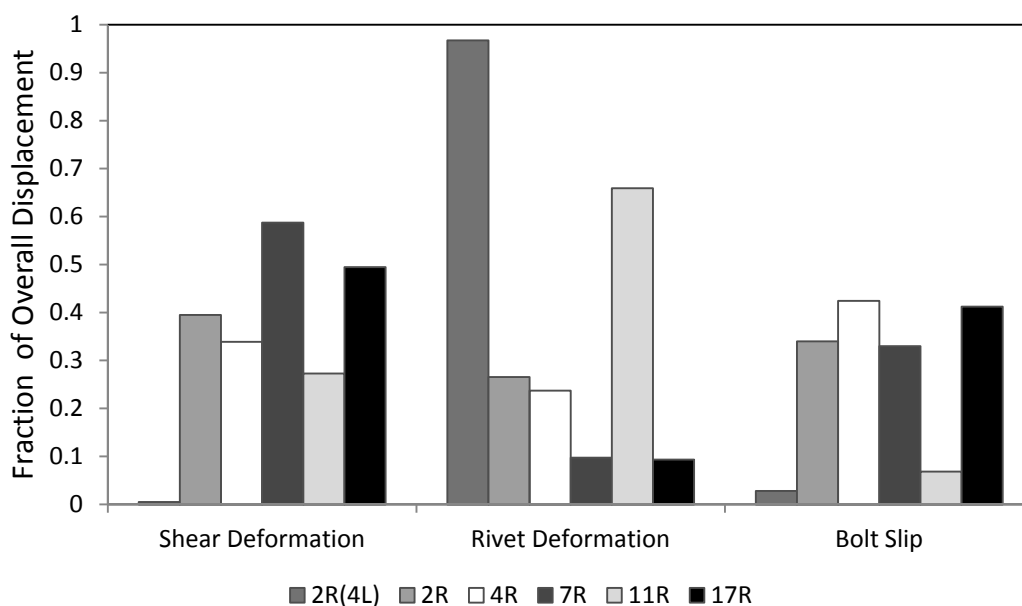
Figure 5.11 Comparison of Overall Specimen Displacement

5.4.2   Bolt Slip

The data in Figure 5.11 shows that bolt slip occurred in all of the tests. Therefore, the load at which slip first occurred was estimated for the HSS-Angle (HSS-A) and Plate-Channel (PL-C) interfaces for all tests. This was compared to the bolt slip capacity computed per AISC (sample calculation in Appendix C) and plotted against the connection length (see Figure 5.12). The data shows that at the HSS-A interface, the ratio between load at first slip and the calculated slip capacity decreases as the connection length increases. This suggests that the bolts performed better for the shorter tests. At the PL-C interface, the performance also decreases as the connection becomes longer. Note that the connections greater than 40 in. were tested in the Baldwin , which included shim plates and some reinforcement at the HSS. There were also two middle plates in the Baldwin test setup, where the Small Baldwin test setup had one middle plate. The number of faying surfaces in the Baldwin test setup could account for the lower loads at bolt slip for these tests.
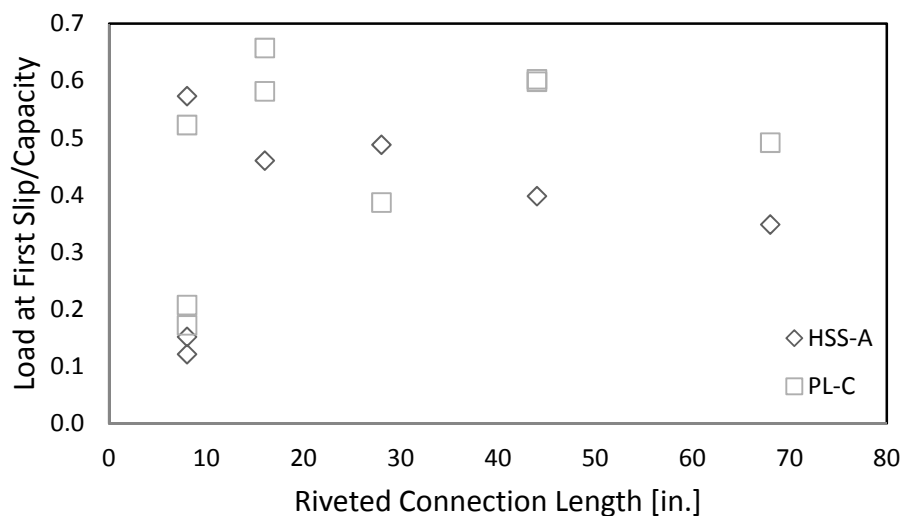
Figure 5.12 Load at First Slip/Slip Capacity vs. Riveted Connection Length

The bolts were all tightened using the turn-of-the-nut method; therefore, it is unlikely that they slipped due to loss in pre-tension. Factors that may have contributed could be the condition of the faying surfaces, the number of surfaces being clamped, and the initial gap between the surfaces.

All surfaces were sandblasted prior to testing, however, the surface may not have had sufficient roughness. The equipment and sand provided likely did not have the capability to create the proper surface. In addition, the Baldwin tests had a small gap between the shim plate and the guardrail at the HSS-A interface prior to attachment of the bolts. This was necessary to ensure that the specimen could be assembled. This gap was closed as the bolts were tightened to snug, however, this could have caused some friction loss during load transfer.

5.4.3 Overall Displacement of Test Configuration

The overall displacement of the test configuration was also plotted versus the riveted length (see Figure 5.13) to understand the behavior of the test configuration. The overall displacement of Specimen 2R (4L) was less than the other tests because the majority of the deformation took place in the rivets. The first three data points (not including Test 2R (4L)) under 40 in. were tested in the Small Baldwin and the remaining two data points were tested in the Baldwin. The data (not including Specimen 2R (4L)) shows that longer test specimens experienced less overall displacement for a given test machine setup, which suggests that more deformation of the connecting elements occurred in the shorter connections.
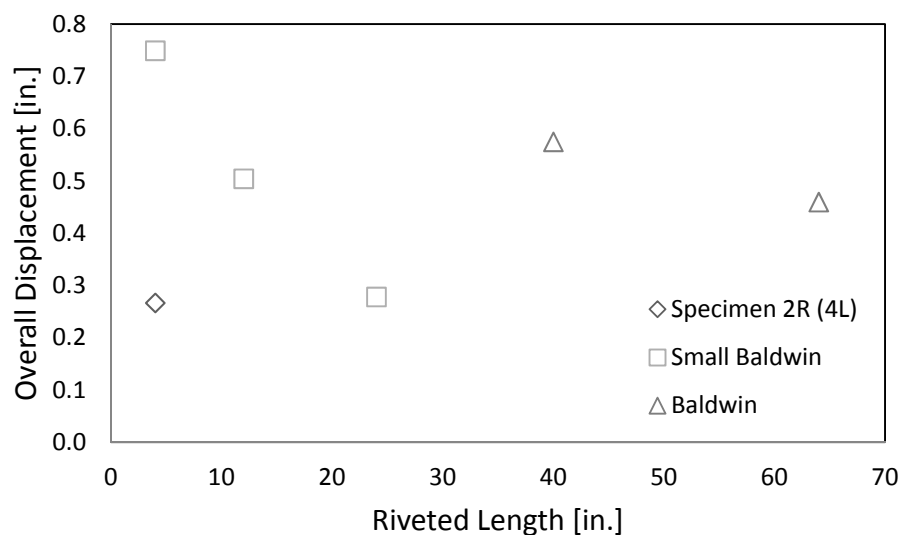
Figure 5.13 Overall Displacement vs. Riveted Length

The ratio of the rivet deformation to overall displacement at ultimate load represents the ability of the test configuration to isolate the behavior of the rivets. Figure 5.14 shows the average ultimate shear strength plotted versus this ratio. A low ratio attributes the overall displacement to the other deformations that occurred in the tests, which were bolt slip and shear deformation of the connecting elements. However, the plot shows that these other deformations did not affect the resulting strength of the rivets.
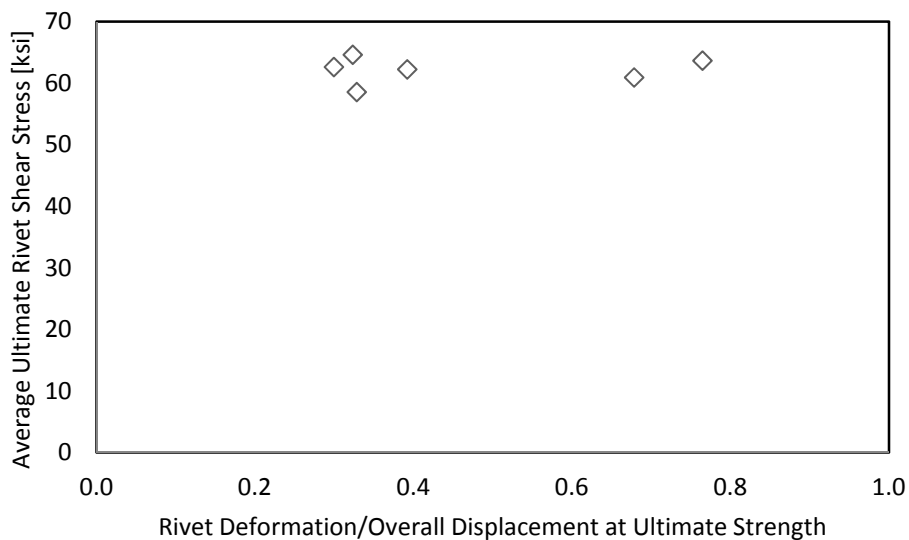
Figure 5.14 Average Ultimate Shear Stress vs. Rivet Deformation

The rivet deformation was normalized by the overall displacement and plotted versus the riveted length normalized by the total length (see Figure 5.15) to determine if there was an impact on specimen performance. This curve shows that as the proportion of riveted to total length increased, the ratio between rivet deformation to overall displacement decreased. This is likely due to the amount of deformation in the connecting elements for the shorter connections and the bolt slip that occurred in the longer connections. For shorter connections, there was less bolt slip, but more shear deformation and for longer connections, there was less shear deformation and more bolt slip.
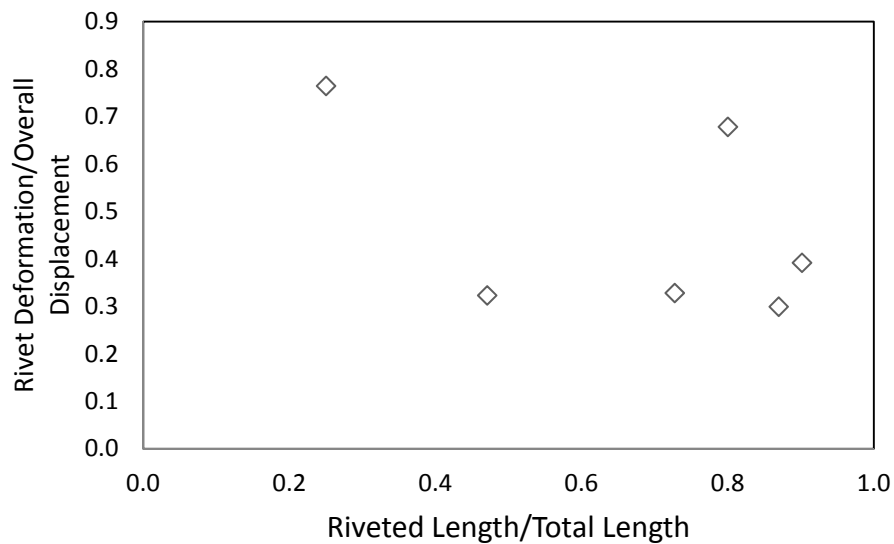
Figure 5.15 Rivet Deformation/Overall Displacement vs. Riveted Length/Total Length

The ratio of rivet deformation to overall displacement was plotted versus the ratio of rivets to bolts (see Figure 5.16) to determine if the bolted length affected the performance of the test configuration. As the ratio of rivets to bolts increases, the ratio of rivet deformation to overall displacement decreases. This suggests that less of the deformation lead to rivet deformation if there were less bolts. Therefore, increasing the number of bolts would ensure the majority of the overall displacement leads to rivet deformation.
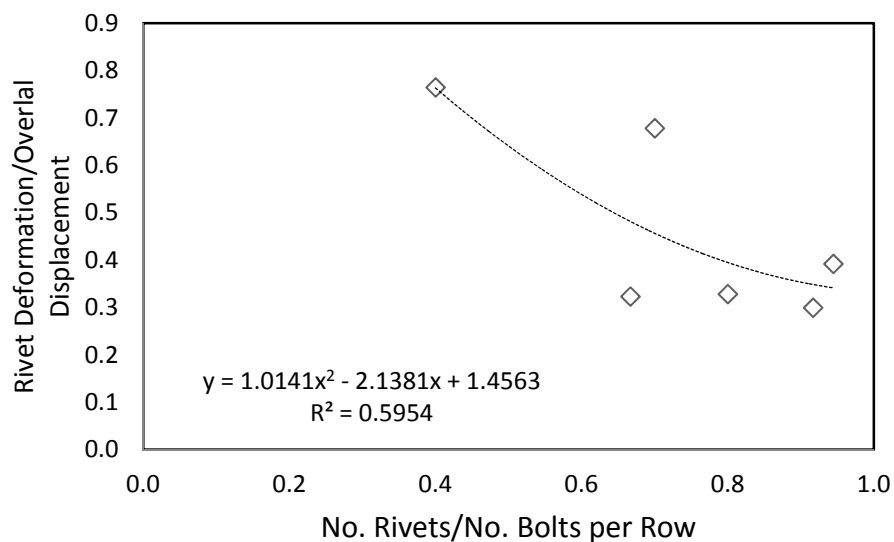
Figure 5.16 Rivet Deformation/Overall Displacement vs. No. Rivets/No. Bolts per Row

5.5   Strain Gauge Data at Rivet Holes

Strain gauges were placed below the rivets on the angles and above the rivets on the channel, therefore, the all strains measured were negative (the absolute value of the strain is plotted in the following graphs). The gauges are numbered from 1-4 which represent which rivet they were placed near where "1" is closest to the top of the middle plate and "4" would be closest to the bottom. Strain gauges could not be placed near all rivets because they were attached after the guardrail was bolted to the middle plate, so there was not sufficient space to prepare all surfaces. Figure 5.17 shows the strain distribution for the rivets in the west channel at fractions of 0.6, 0.8, and 1.0 of the ultimate load. The graph suggests that there is more strain at the 2nd rivet than the 1st rivet after the load exceeds 60% of the ultimate load. Figure 5.18 shows this relationship for rivets in the east angle and suggests that there is more strain at the 3rd rivet than the 2nd rivet, followed by the 4st rivet at all ratios of ultimate load.. Figure 5.19 depicts the strain distribution in the east channel and suggests that there is more strain at the 4th rivet than the other rivets which, appear relatively uniform at all loads. This data shows that the strain at the end rivets is larger in the east channel, but larger in the inner rivets for the west channel and east angle. This shows that there is not a significant strain distribution for this connection length. However, it was difficult to place the strain gauges at the exact same distance from the center of the rivet because the location is unclear as only the rivet head is visible.
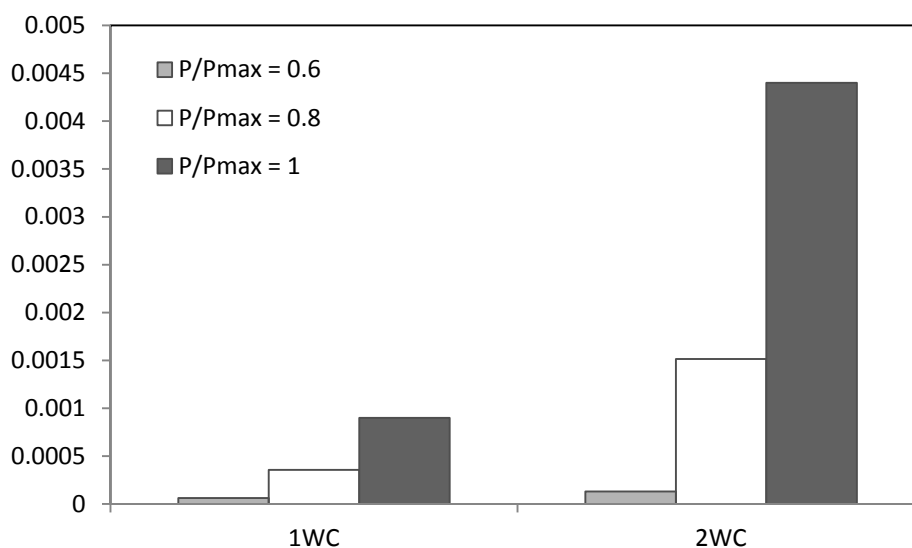
Figure 5.17 Strain Distribution in West Channel – Test 4R
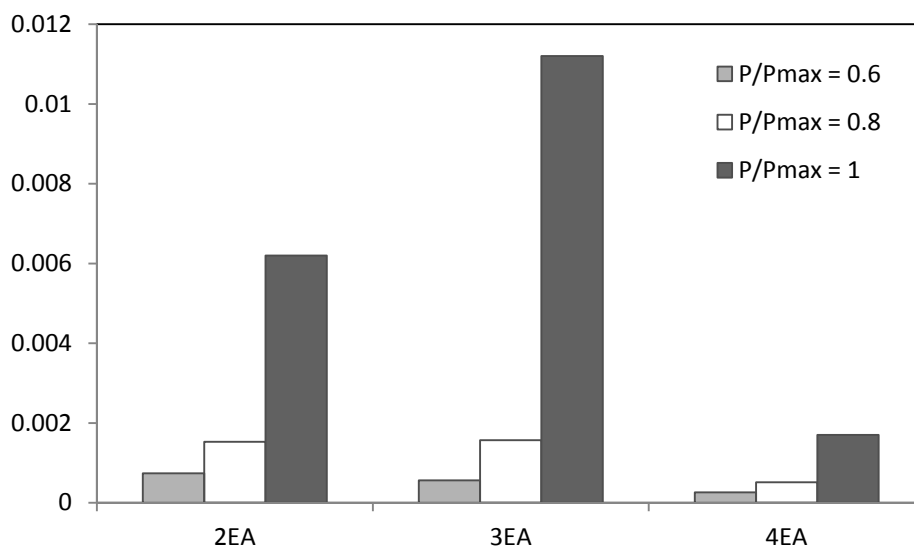
Figure 5.18 Strain Distribution in East Angle – Test 4R
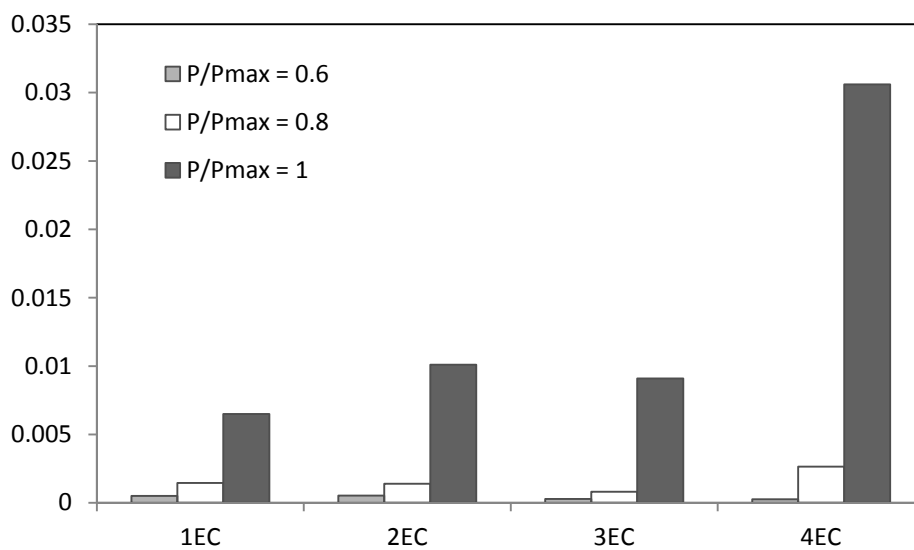
Figure 5.19 Strain Distribution in East Channel – Test 4R

Table 5.5 summarizes the strain gauge data. The corresponding yield strains were calculated from the material tests, and compared to the strain at ultimate load. All of the strain gauges except SG1WC (below 1st rivet in west channel) show that the material has yielded at the ultimate load. This is consistent with the expected behavior described in Section 3.4.5.4. However, the gauges were placed approximately 1 in. from the center of the rivet, and the strain could be high due to the local stress at the rivet hole. This data was used to calibrate finite element models of the test configuration, but were not used for subsequent tests.

Table 5.5 Summary of Strain Gauge Data

Strain Gauge	Strain at Ultimate Load	Distance from Rivet Center [in.]	ε_{ya} 0.00112 $\varepsilon > \varepsilon_y$?	ε_{yc} 0.00144
SG1WC	-0.0009	0.910	NO	
SG2WC	-0.0044	0.872	YES	
SG2EA	-0.0062	1.135	YES	
SG3EA	-0.0112	0.900	YES	
SG4EA	-0.0017	1.065	YES	
SG1EC	-0.0065	0.850	YES	
SG2EC	-0.0101	1.000	YES	
SG3EC	-0.0091	0.970	YES	
SG4EC	-0.0306	0.800	YES	

Chapter 6: Conclusions and Recommendations

6.1 Summary

Several components were salvaged from two steel truss bridges in Washington State that were in service from 1931-2010. These components provided an opportunity to investigate the actual strength of the riveted connections, compare to past experimental data and current recommendations, and potentially improve current load rating procedures for steel bridges.

Past experiments on riveted joints investigated the effect of joint length, rivet and plate material, rivet grip, pitch, and diameter, and different splice types on average rivet strength. The data showed that some other types of metal alloys had larger rivet shear strengths than typical carbon-steel rivets. The strength of the rivets showed a slight decrease as connection length increased. Overall, the rivet strengths from past experiments were still 1.5 – 2.0 times the current recommendations provided by AASHTO.

A test setup and experimental program was developed to test as-built riveted connections of various lengths. The loading mechanism, which applied load to the rivets in a distributed manner, was different from past research, where the load was applied at the ends of the connections. Riveted connections tested here had 5/8 in. diameter rivets with a 4 in. center-to-center spacing, and 2 to 17 rivets per row corresponding to a connection length of 4 in. to 64 in.

The test configuration was loaded in compression and utilized bolts to transfer the load to the riveted joint, which was then loaded in shear. This loading mechanism allowed testing of longer connections, as opposed to loading the connection at the ends, which would not enable the rivets to reach their strength prior to failure of the connection cross section. Under this loading, the riveted connection was subject to a distributed shear load and experienced shear deformation of the rivets and the connecting elements. The bolts connecting the specimen to the setup also slipped under load, which was not anticipated, but was an outcome in all of the tests.

The ratio between the rivet deformation and the overall displacement of the test apparatus was the lowest for shorter connections. This indicates that more deformation of the connecting elements occurred in shorter connections and less in longer connections. However, this deformation was observed in all tests. In addition, the rivet hole deformation appeared more uniform in longer connections, which is different than the hole deformation behavior in bolted connections and riveted connections tests reported in the literature. In shorter connections, there was also more deformation at the ends of the connecting elements where the load was transferred.

6.2   Conclusions

The strength of the riveted connection did not vary significantly between the test specimens of different lengths, which is contrary to current AASHTO design recommendations. For each test, the average rivet shear stress and Estimate Rivet Yield (ERY) were calculated. The average rivet shear strength for all of the tests was 62 ksi with a standard deviation of 2.1 ksi and the ERY varied from $30 - 40$ ksi.

These results and those from past experiments show that the reduction factor provided by AASHTO (2011) for longer connections may not be necessary. When the connection length factor (R_2) was plotted with experimental results from the literature, a length effect was not observed for longer connections, however, for shorter connections the strength decreased linearly as AASHTO predicted. In this test program, a decrease in average shear strength was not observed for short or long connections. Even though the loading mechanism was different for past experiments and this testing program, the complete set of data show that the factor is not needed. In addition, the reduction factor is based on a tension lap-splice configuration, which is not completely representative of typical gusset plate connections. Besides shear loading transmitted to the rivets through tension in a riveted joint, the shear load is also transmitted through shear lag, which represents the loading mechanism of this test program.

Current AASHTO recommendations from 2010 suggest rivet shear strength of 34.5 ksi for bridges constructed prior to 1936. This value is still much less than the results of this test program (62 ksi), and similar to the conclusions from Olson (2010), the AASHTO recommendation appears closer to the ERY (35.2 ksi). Past research on riveted connections

in a lap splice configuration of a similar rivet grip and material, gave an average rivet strength that was less than the results of this test program because of the difference in loading mechanism.

6.3   Recommendations

When connections were loaded in a distributed manner, a length effect on rivet shear strength was not observed. In addition, past experiments loaded in a tension lap-splice configuration only exhibited a length effect for shorter connections but not for connections longer than 50 in. Therefore, it is not recommended to continue the use of the reduction factor provided by AASHTO (2011) when calculating riveted joint strength. The need for such reduction factor depends on more than just connection length. It could also depend on the geometry of the gusset plate connecting elements, the shear lag factor or loading mechanism, and potentially other factors.

For further research with this test configuration, the issue of bolt slip could be investigated to determine how to create the appropriate surface. In addition, instrumentation could be added to measure the deformation of each individual rivet in the connection rather than the average of the displacement at the ends of the connection.

A testing program on as-built riveted connections and parametric study should investigate how shear lag or loading mechanism and connection geometry affects the distribution of shear stress in the rivets. This will further investigate if a connection length effect exists in riveted connections by simulating realistic loading mechanisms and connection geometries.

References

AASHTO, American Association of State Highway and Transportation Officials. (2011). The manual for bridge evaluation. Washington, D.C.: AASHTO.

American Institute of Steel Construction . (2005). *Steel Construction Manual.* American Institute of Steel Construction .

AREMA. (1905). Tests of riveted joints. *American Railway Engineering and Maintenance-of-Way Association* (pp. 272-484). Chicago: Press of the Blakely Printing Company.

ASTM. (2011). Standard test methods and definitions for mechanical testing of steel products. *A370-10* . Conshohocken, PA: ASTM International.

Brockenbrough, R. L. (2002). *AISC Rehabilitation and Retrofit Guide.* Chicago: American Institute of Steel Construction.

D'Aniello, M., Portioli, F., & Landolfo, R. (2011). Experimental investigation on shear behaviour of riveted connections in steel structures. *Engineering Structures , 33*, 516-531.

Davis, R. E., Woodruff, G. B., & Davis, H. E. (1939). Tension tests of large riveted joints. *Transactions of the American Society of Civil Engineers , 105* (2084), 1193-1299.

Dlugosz, S. W. (1962). *Static tension tests of long riveted joints.* Bethlehem: Lehigh University.

FHWA. (2009). Load rating guidance and examples for bolted and riveted gusset plates in truss bridges. *Publication No. FHWA-IF-09-014* . Federal Highway Administration.

Fisher, J. W., & Rumpf, J. L. (1967). *The analysis of bolted butt joints.* Bethlehem: Fritz Engineering Laboratory.

Fisher, J. W., & Yoshida, N. (1970). Large bolted and riveted shingle splices. *Journal of the Structural Division , 96* (9), 1903-1018.

Fisher, J. W., Yen, B. T., & Mann, J. E. (1987). *Fatigue and fracture evaluation for rating riveted bridges.* Transportation Research Board, National Cooperative Highway Research Program Report 302.

Kulak, G. L., Fisher, J. W., & Struik, J. H. (1987). *Guide to design criteria for bolted and riveted joints.* New York, NY: John, Wiley & Sons.

Munse, W. H., & Cox, H. L. (1956). The static strength of rivets subjected to combined tension and shear. *University of Illinois, Bulletins of the Engineering Experiment* (437).

Olson, A. (2010). *Triage evaluation ofgusset plates in steel truss bridges.* University of Washington.

Roeder, C. W., Leon, R. T., & Preece, R. F. (1994). *Strength, stiffness, and ductility of older steel structures under seismic loading.* Seattle: University of Washington.

Talbot, A. N., & Moore, H. F. (1911). Tests of nickel-steel riveted joints. *University of Illinois, Bulletins of the Engineering Experiment , 7* (49), pp. 1-53.

Wilson, W. M., Bruckner, W. H., & McCrackin, T. H. (1942). Tests of riveted and welded joints in low-allloy structural steels. *University of Illinois, Bulletins of the Engineering Experiment* (337).

Appendix A   ASTM Historical Standards

The following table gives the nominal strengths of rivet and structural steel from the time of construction for the bridge, from which the test specimen was salvaged. These values were used in Section 0.

Table .A.1 Historical Summary of ASTM Specifications for Rivet Steel in Bridges (Brockenbrough, 2002)

Date	Specification	Yield Point [ksi]	Tensile Strength [ksi]
1900	A7	30	50/60
1901-1904	A7	1/2 Tensile Str.	50/60
1905-1908	A7	Record Value	50
1909-1913	A7	Record Value	50
1914-1923	A7	1/2 Tensile Str.	46/56
1924-1931	A7	1/2 Tensile Str. ≥ 25	46/56
1932	A141-32T	1/2 Tensile Str. ≥ 28	52/62
1933	A141-32T	1/2 Tensile Str. ≥ 28	52/62
1934-1938	A141-33	1/2 Tensile Str. ≥ 28	52/62
1939-1948	A141-36 A141-39	1/2 Tensile Str. ≥ 28	52/62
1949	A141-49T	28	52/62

Table A.2 Historical AISC Allowable stresses for Rivets – ASD* (Brockenbrough, 2002)

AISC Spec. Year	Type of Rivet	Tension [ksi]	Shear [ksi]	Bearing [ksi]
1928	A9	13.5	13.5	
1936	A141	15.0	15.0	32.0/40.0**
1949	A141	20.0	15.0	32.0/40.0**
1963	A141	20.0	15.0	1.35Fy
	A196 & A406	27.0	20.0	1.35Fy
1969	A502 Grade 1	20.0	15.0	1.35Fy
	A502 Grade 2	27.0	20.0	1.35Fy
1978	A502 Grade 1	23.0	17.5	1.50Fu
	A502 Grade 2 or 3	29.0	22.0	1.50Fu
1989	A502 Grade 1	23.0	17.5	1.20Fu
	A502 Grade 2 or 3	29.0	22.0	1.20Fu

*ASD Nominal strength before driving
**Lower value for single shear, higher for double shear

Table A.3 Historical Summary of ASTM Specifications for Structural Steel in Bridges (Brockenbrough, 2002)

Date	Specification	Yield Point [ksi]	Tensile Strength [ksi]
1905-1908	A7	Record Value	60 desired
1909-1913	A7	Record Value	60 desired
1914-1923	A7	1/2 Tensile Str.	55/65
1924-1931	A7	1/2 Tensile Str. ≥ 30	55/65
1932	A140-32T	1/2 Tensile Str. Or 33 min	60/72
1933	A7-33T	1/2 Tensile Str. ≥ 30	55/65
1934-1938	A7-34	1/2 Tensile Str. ≥ 33	60/72
1939-1948	A7-39	1/2 Tensile Str. ≥ 33	60/72
1949	A7-49T	1/2 Tensile Str. ≥ 33	60/72

Appendix B   Bridge Study

The results of the study on the Cle Elum Bridge are depicted in the figures below for the key parameters studied. The nominal strength of the materials were used in Figure B.1, Figure B.2 - Figure B.4 used the expected values, and Figure B.5 depicts the results with experimental values. The results show that the nominal and expected values experience rivet shear failure prior to yielding, whereas the experimental values experience yielding prior to the development of the rivets' shear strength.
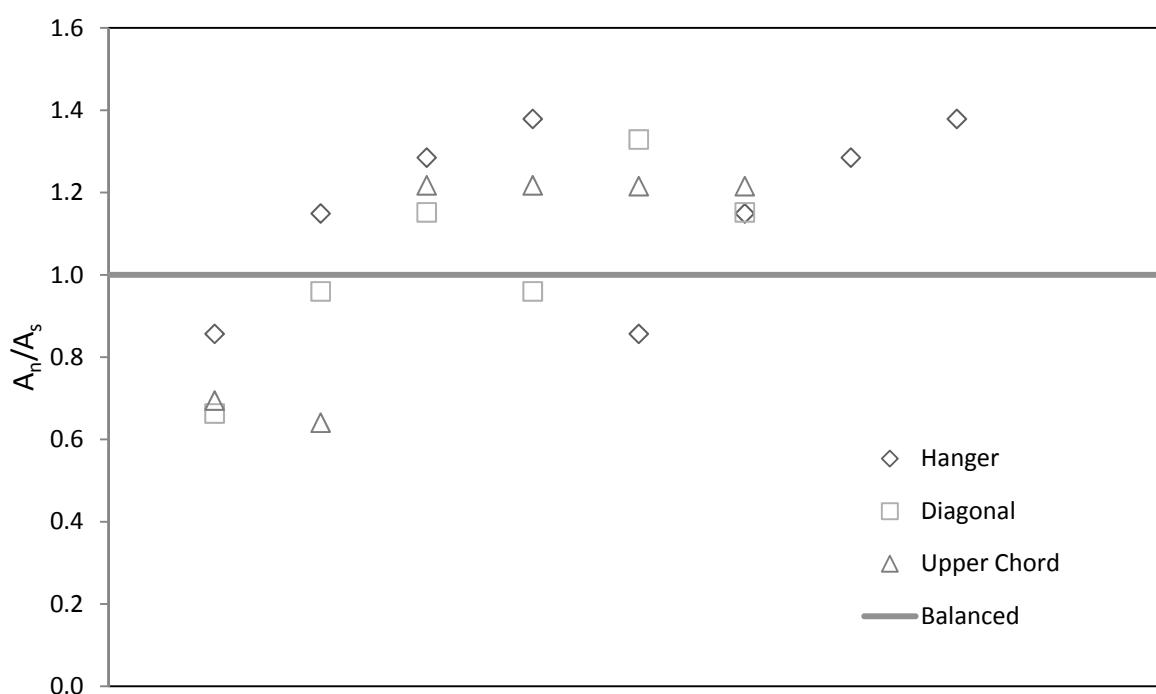
Figure B.1 Cle Elum- A_n/A_s Ratio – Nominal
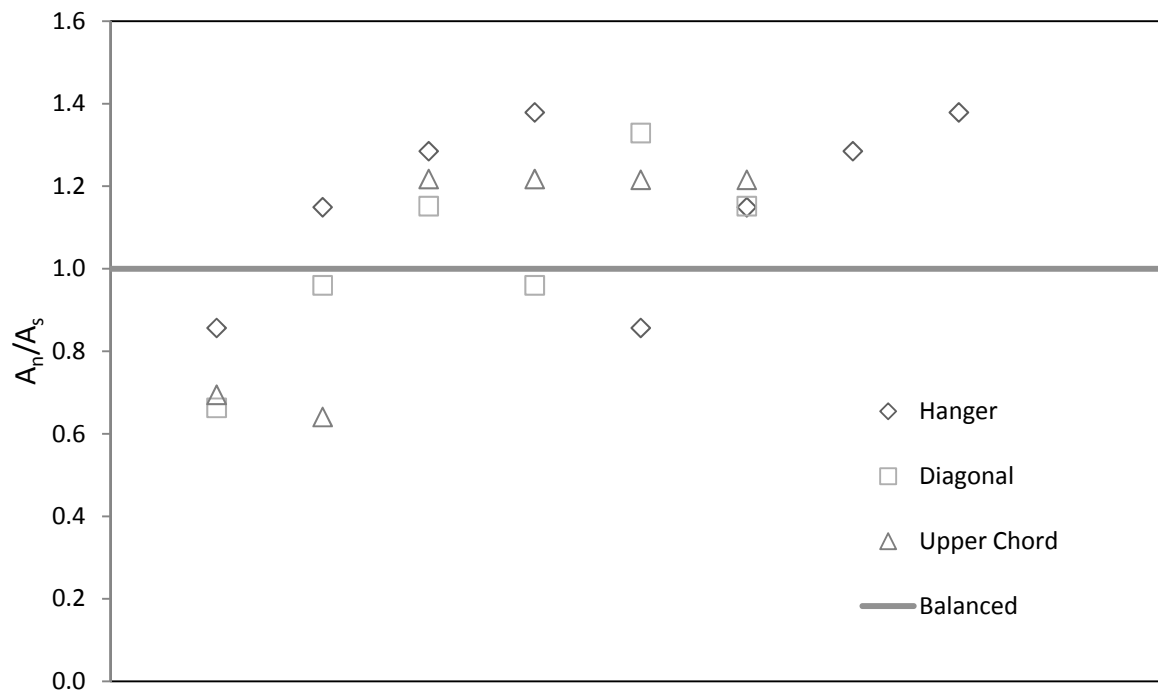
Figure B.2   Cle Elum - A_n/A_s Ratio – Expected
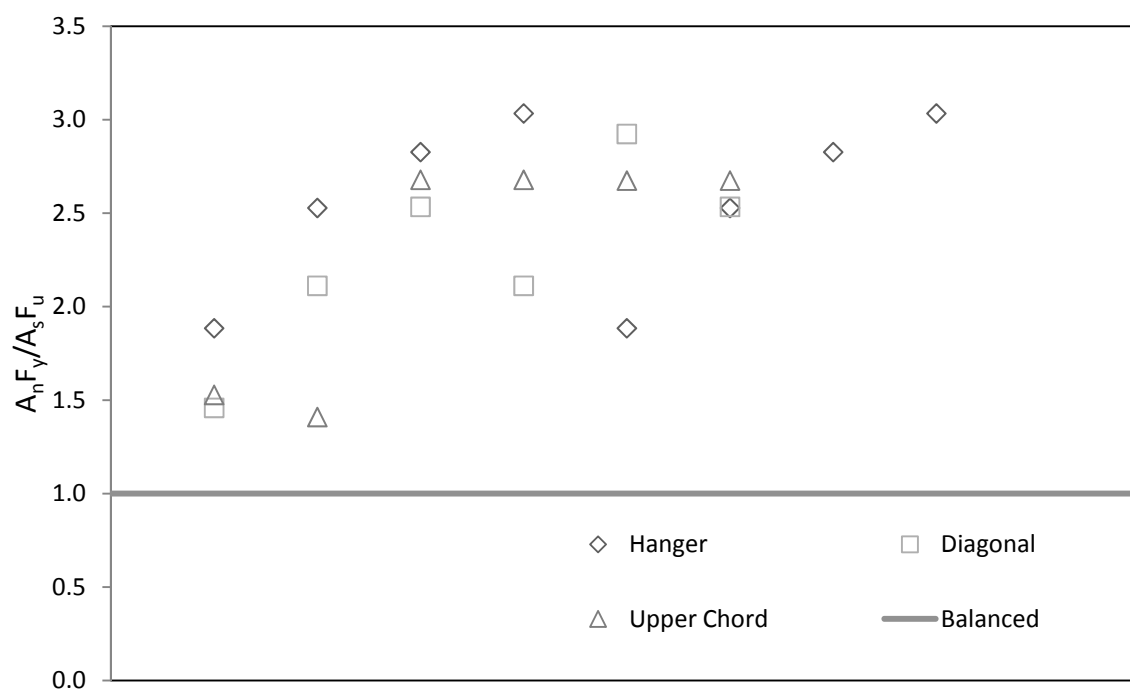
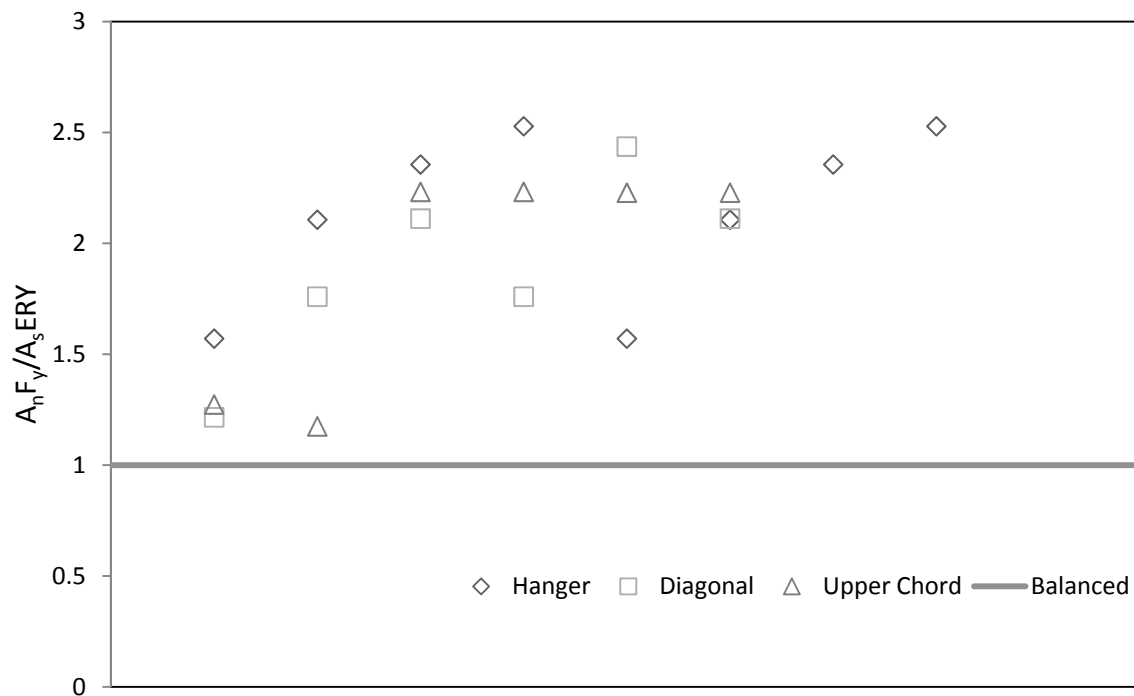*Figure B.3   Cle Elum - A_nF_y/A_sF_u Ratio – Expected*
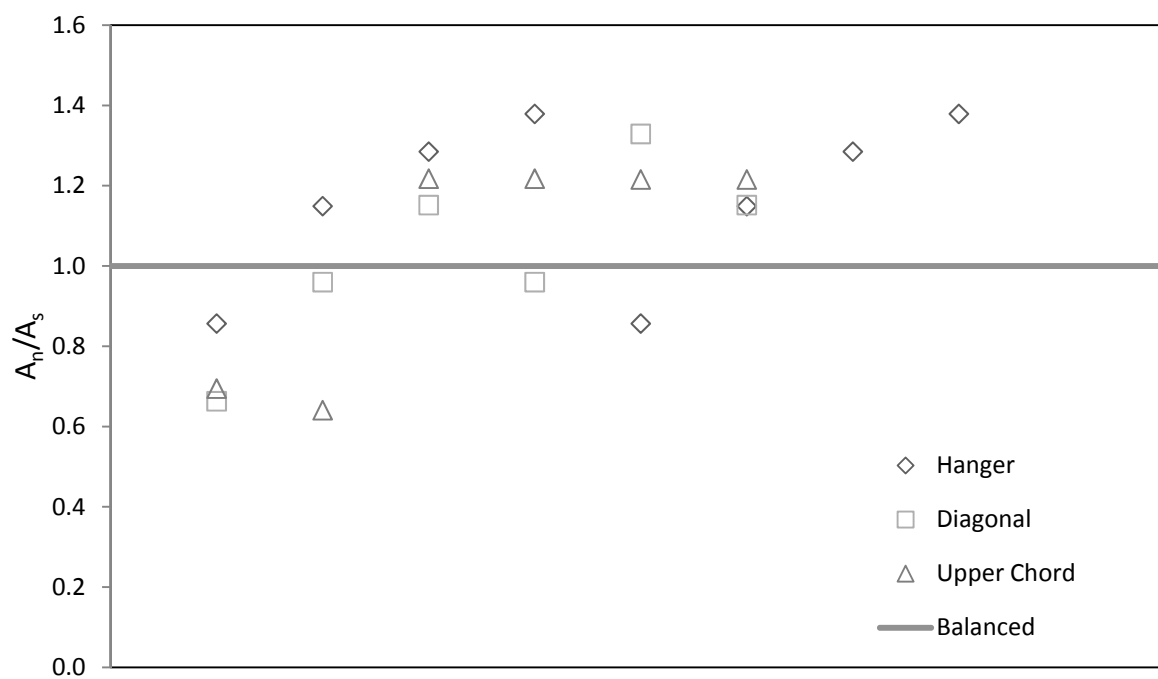
Figure B.4   Cle Elum - A_nF_y/A_sERY Ratio – Expected

Figure B.5   Cle Elum - A_n/A_s Ratio – Experimental

Appendix C   Sample Calculations for Test Specimen Design

Sample Calculation: Small Baldwin Specimen 7R

Dimensions and Material Properties

Bolts - A490	Angle	Channel	Rivets
$d_b := 0.75in$	$t_u := 0.3125in$	$t_{cw} := 0.2in$	$d_r := \frac{5}{8}in$
$F_v := 60ksi$	$F_{ya} := 32.59ksi$	$F_{yc} := 41.7ksi$	$v_{ur} := 52.3ksi$
$A_b = 0.442 \cdot in^2$	$F_{ua} := 54.25ksi$	$F_{uc} := 60.68ksi$	$A_r = 0.307 \cdot in^2$
			$n_r := 7$
			$s_r := 4in$

Plate	HSS		
$t_p := 1in$	$h_{HSS} := 10in$	$I_{xHSS} := 169in^4$	$E := 29000ksi$
$b_p := 7.125in$	$b_{HSS} := 8in$	$I_{yHSS} := 120in^4$	
$A_p = 7.125 \cdot in^2$	$t_{HSS} := 0.375in$		
$F_{yp} := 50ksi$	$A_{HSS} := 11.8in^2$		
	$F_{yHSS} := 46ksi$		

Strength of Rivets

$$P_u := v_{ur} \cdot 2 \cdot n_r \cdot A_r = 224.636 \cdot kip \qquad \text{Design for } 1.2P_u$$

Check Bolt Shear AISC (J3-6)

$$m := 1$$

$$n_v := \frac{1.2P_u}{F_v \cdot A_b \cdot m} \qquad n_v = 10.169$$

$$n_v := 12$$

$$R_{n.v} := F_v \cdot A_b \cdot n_v \cdot m$$

$$R_{n.v} = 318.086 \cdot kip$$

Slip Critical Connection (AISC J3-8)

$$\phi_{sc} = 0.85$$

$$\mu = 0.50 \qquad \qquad \text{Class B surface (unpainted blast-cleaned steel)}$$

$$D_u = 1.13 \qquad \qquad \text{multiplier}$$

$$h_{sc} = 1.00 \qquad \qquad \text{hole factor}$$

$$N_s = 1 \qquad \qquad \text{number of slip planes}$$

$$T_b = 35 kip \qquad \qquad \text{Table J3-1}$$

$$n_s = \frac{1.2 P_u}{\mu \cdot D_u \cdot h_{sc} \cdot T_b \cdot N_s} \qquad \qquad n_s = 13.632$$

$$n_s = 14$$

$$R_{n.sc} = \mu \cdot D_u \cdot h_{sc} \cdot T_b \cdot N_s \cdot n_s$$

$$R_{n.sc} = 276.85 \cdot kip$$

Spacing

$$n = \max(n_s, n_v) \qquad \qquad n = 14$$

$$clear = 2in$$

$$L_b = (n_r - 1) \cdot s_r + 2clear = 28 \cdot in$$

$$s_b = \frac{L_b}{\frac{n}{2}} \qquad \qquad s_b = 4 \cdot in$$

$$s = 3in$$

$$n_b = \frac{L_b - 2 \cdot clear}{s} + 1 = 9 \qquad \qquad \text{bolts per row}$$

Check the connection as a bearing connection

Check Bearing on the Angle (AISC J4-10)

$$d_h = d_b + \frac{1}{16} in$$

First bolt

$$L_e := 1.5 in$$

$$L_{c1} := L_e - 0.5 \cdot d_h \qquad\qquad L_{c1} = 1.094 \cdot in$$

$$R_{n1} := min(1.2 L_{c1} \cdot t_a \cdot F_{ua}, 2.4 \cdot d_b \cdot t_a \cdot F_{ua}) \qquad\qquad R_{n1} = 22.251 \cdot kip$$

Other bolts

$$L_{c2} := s - d_h \qquad\qquad L_{c2} = 2.188 \cdot in$$

$$R_{n2} := min(1.2 L_{c2} \cdot t_a \cdot F_{ua}, 2.4 \cdot d_b \cdot t_a \cdot F_{ua}) \qquad\qquad R_{n2} = 30.516 \cdot kip$$

$$R_{n.brg} := 2\left[R_{n1} + (n_b - 1) \cdot R_{n2}\right] \qquad\qquad R_{n.brg} = 532.752 \cdot kip$$

Re-Check Strength

Check Bolt Shear AISC (J3-6)

$$R_{n.v} := F_v \cdot A_b \cdot 2 \cdot n_b \cdot m = 477.129 \cdot kip$$

Slip Critical Connection (AISC J3-8)

$$R_{n.sc} := \mu \cdot D_u \cdot h_{sc} \cdot T_b \cdot N_s \cdot 2 \cdot n_b = 355.95 \cdot kip$$

Strength Check

$$R_n := min(R_{n.sc}, R_{n.brg}, R_{n.v}) \qquad\qquad R_n = 355.95 \cdot kip$$

$$StrengthCheck := \begin{vmatrix} "OK" & if & 1.2 P_u \le R_n \\ "NOT\ OK" & otherwise \end{vmatrix} \qquad\qquad StrengthCheck = "OK"$$

Check Spacing and Edge Distances

$L_e = 1.5 \cdot in$ $s = 3 \cdot in$

Minimum Spacing

$$s_{min} = \left(2 + \frac{2}{3}\right) \cdot d_b \qquad s_{min} = 2 \cdot in$$

$MinSpace := \begin{vmatrix} \text{"OK"} & \text{if } s \geq s_{min} \\ \text{"NOT OK"} & \text{otherwise} \end{vmatrix}$ $\qquad MinSpace = \text{"OK"}$

Maximum Spacing

$$s_{max} = min(24 \cdot t_a, 12in) \qquad s_{max} = 7.5 \cdot in$$

$MaxSpace := \begin{vmatrix} \text{"OK"} & \text{if } s \leq s_{max} \\ \text{"NOT OK"} & \text{otherwise} \end{vmatrix}$ $\qquad MaxSpace = \text{"OK"}$

Minimum Edge Distance

$L_{e.min} := 1.125in \qquad$ AISC Table J3.4

$MinEdge := \begin{vmatrix} \text{"OK"} & \text{if } L_e \geq L_{e.min} \\ \text{"NOT OK"} & \text{otherwise} \end{vmatrix}$ $\qquad MinEdge = \text{"OK"}$

Maximum Edge Distace

$$L_{e.max} = min(12 \cdot t_a, 6in) \qquad L_{e.max} = 3.75 \cdot in$$

$MaxEdge := \begin{vmatrix} \text{"OK"} & \text{if } L_e \leq L_{e.max} \\ \text{"NOT OK"} & \text{otherwise} \end{vmatrix}$ $\qquad MaxEdge = \text{"OK"}$

Final Bolt Design

Total Bolts: $\qquad 2 \cdot n_b = 18$

Per edge: $\qquad n_b = 9$

Spacing: $\qquad s = 3 \cdot in$

Edge Distance $\qquad L_e = 1.5 \cdot in$

Capacity $\qquad R_n = 355.95 \cdot kip$

Check Yielding of Middle Plate and HSS

$$P_{yHSS} = A_{HSS} \cdot F_{yHSS} = 542.8 \cdot kip \qquad\qquad 1.2 \cdot P_u = 269.563 \cdot kip$$

$$P_{yp} := A_p \cdot F_{yp} = 356.25 \cdot kip$$

$$PlateYield := \begin{vmatrix} \text{"OK"} & \text{if } 1.2 \cdot P_u \le P_{yp} \\ \text{"NOT OK"} & \text{otherwise} \end{vmatrix} \qquad\qquad PlateYield = \text{"OK"}$$

$$HSSYield := \begin{vmatrix} \text{"OK"} & \text{if } 1.2 \cdot P_u \le P_{yHSS} \\ \text{"NOT OK"} & \text{otherwise} \end{vmatrix} \qquad\qquad HSSYield = \text{"OK"}$$

Check Buckling of Middle Plate and HSS at the Ends

Plate

$$I_{xp} = \frac{b_p \cdot t_p{}^3}{12} = 0.594 \cdot in^4 \qquad I_{yp} = \frac{t_p \cdot b_p{}^3}{12} = 30.142 \cdot in^4$$

$$r_{xp} = \sqrt{\frac{I_{xp}}{A_p}} = 0.289 \cdot in \qquad r_{yp} = \sqrt{\frac{I_{yp}}{A_p}} = 2.057 \cdot in$$

$$K := 0.5$$

$$L := 4in \qquad \text{Distance from last bolt hole to top of Middle Plate}$$

Weak Axis Controls Buckling

$$\frac{K \cdot L}{r_{xp}} = 6.928 \qquad \frac{K \cdot L}{r_{yp}} = 0.972 \qquad F_e := \frac{\pi^2 \cdot E}{\left(\frac{K \cdot L}{r_{yp}}\right)^2} = 3.027 \times 10^5 \cdot ksi \qquad 4.71\sqrt{\frac{E}{F_{yp}}} = 113.432$$

$$F_{cr} := \begin{vmatrix} F_{yp} \cdot 0.658^{\frac{F_{yp}}{F_e}} & \text{if } \frac{K \cdot L}{r_{yp}} \le 4.71\sqrt{\frac{E}{F_{yp}}} \\[4mm] 0.877 \cdot F_e & \text{otherwise} \end{vmatrix} \qquad\qquad F_{cr} = 49.997 \cdot ksi$$

$$P_n := F_{cr} \cdot A_p = 356.225 \cdot kip$$

$$StrengthCheck := \begin{vmatrix} "OK" & if & 1.2P_u \leq P_n \\ "NOT OK" & otherwise \end{vmatrix} \qquad StrengthCheck = "OK"$$

HSS

$$r_{xHSS} := \sqrt{\frac{I_{xHSS}}{A_{HSS}}} = 3.78 \quad r_{yHSS} := \sqrt{\frac{I_{yHSS}}{A_{HSS}}} = 3.189 \cdot in$$

$$K := 0.5$$

$$L := 5in \qquad \text{Distance from last bolt hole to bottom of HSS}$$

Weak Axis Controls Buckling

$$\frac{K \cdot L}{r_{xHSS}} = 0.661 \quad \frac{K \cdot L}{r_{yHSS}} = 0.784 \quad F_e := \frac{\pi^2 \cdot E}{\left(\frac{K \cdot L}{r_{yHSS}}\right)^2} = 4.657 \times 10^5 \cdot ksi \quad 4.71\sqrt{\frac{E}{F_{yHSS}}} = 118.261$$

$$F_{cr} := \begin{vmatrix} F_{yHSS} \cdot 0.658^{\frac{F_{yHSS}}{F_e}} & if & \frac{K \cdot L}{r_{yHSS}} \leq 4.71\sqrt{\frac{E}{F_{yHSS}}} & F_{cr} = 45.998 \cdot ksi \\ 0.877 \cdot F_e & otherwise \end{vmatrix}$$

$$P_n := F_{cr} \cdot A_{HSS} = 542.778 \cdot kip$$

$$StrengthCheck := \begin{vmatrix} "OK" & if & 1.2P_u \leq P_n \\ "NOT OK" & otherwise \end{vmatrix} \qquad StrengthCheck = "OK"$$

$$F_{cr} = \begin{vmatrix} F_{yHSS} \cdot 0.658^{\dfrac{F_{yHSS}}{F_e}} & \text{if } \dfrac{K \cdot L}{r_y} \leq 4.71 \sqrt{\dfrac{E}{F_{yHSS}}} & F_{cr} = 45.997 \cdot ksi \\ 0.877 \cdot F_e & \text{otherwise} \end{vmatrix}$$

$$P_n = F_{cr} \cdot A_{HSS} = 542.769 \cdot kip$$

$$StrengthCheck = \begin{vmatrix} \text{"OK"} & \text{if } 1.2 P_u \leq P_n \\ \text{"NOT OK"} & \text{otherwise} \end{vmatrix} \qquad StrengthCheck = \text{"OK"}$$

Check Shear Yielding of Channel

Shear Stress in Channel at Ultimate Load

$$A_{shear} = t_{cw} \cdot L_b$$

$$\tau = \dfrac{\dfrac{P_u}{2}}{A_{shear}} \qquad \tau = 20.057\ ksi$$

$$R_n = 0.6 \cdot F_{yc} = 25.02\ ksi$$

This shows that the channel will likely be near its yield capacity in shear at the time the rivets reach their strength

Appendix D   Test Specimen Design Drawings

D.1   Design for Specimens Tested in the Small Baldwin

The drawings for each part of the specimens tested in the Small Baldwin are shown in the following set of drawings. These were used in the fabrication and assembly of each test specimen.
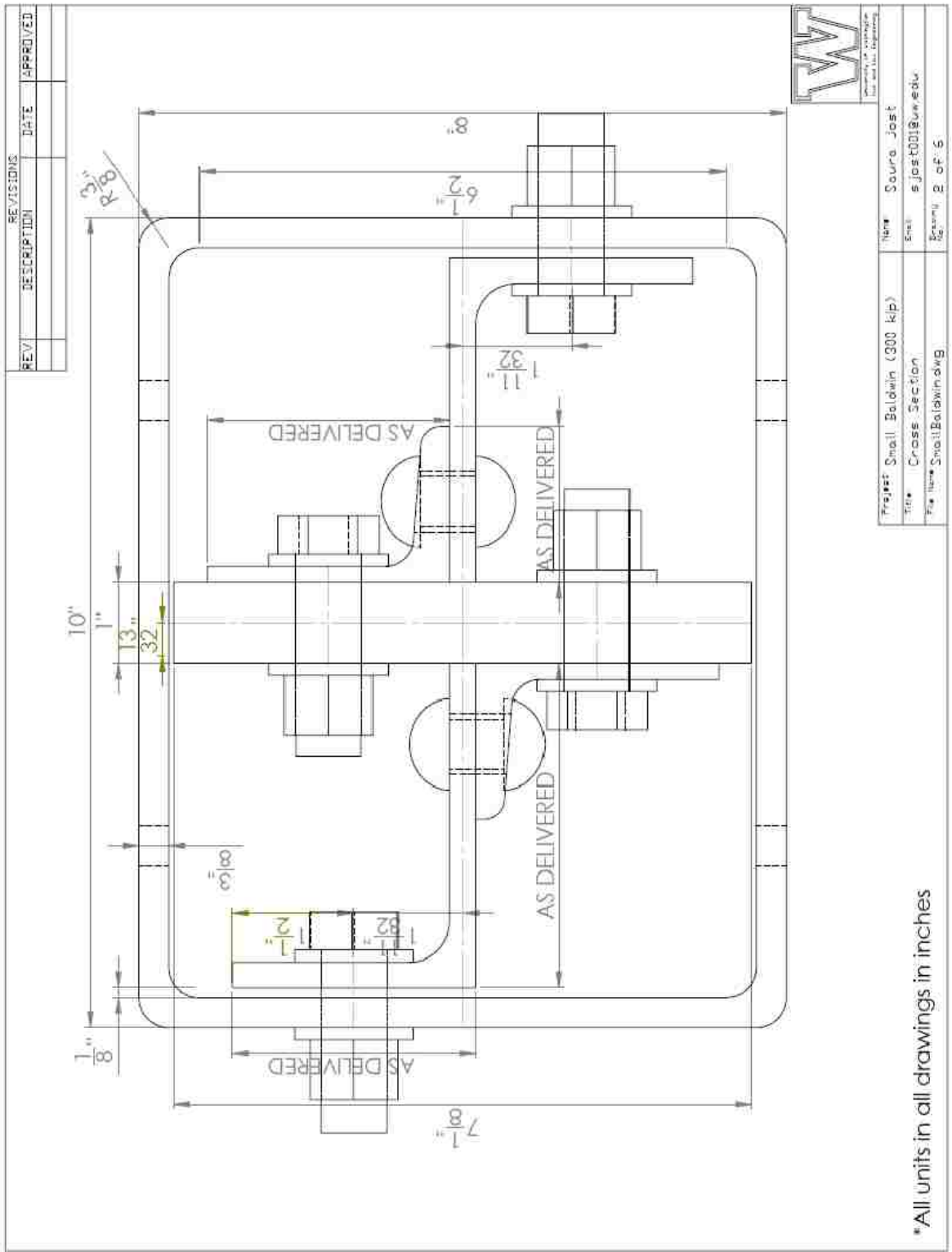
Small Baldwin (300 kips) - 2,4,7 rivets
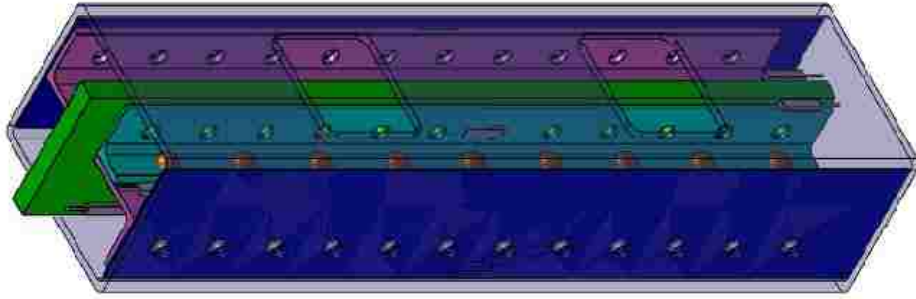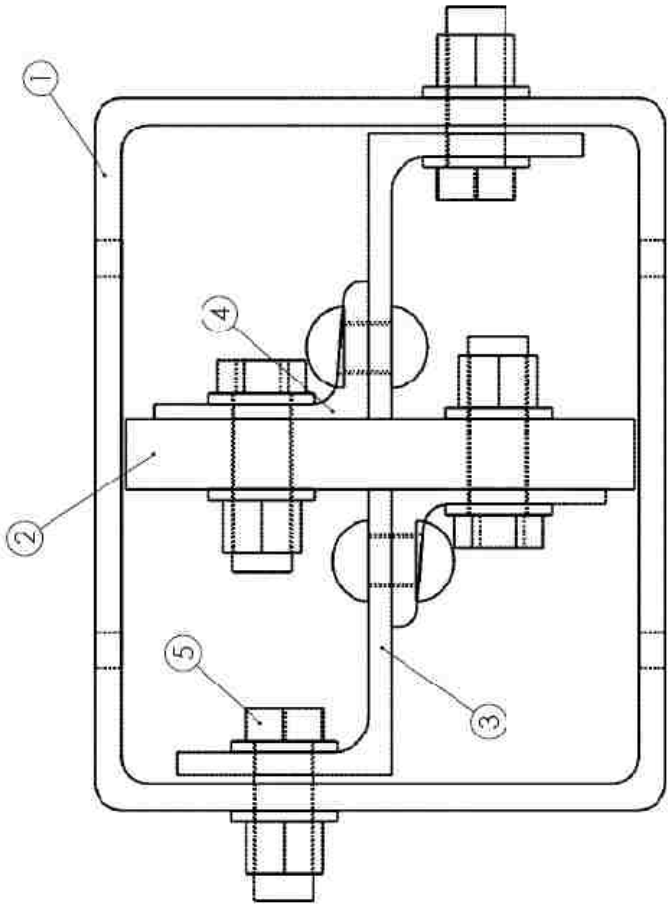
Note: There are a total of 3 designs for rivet connection lengths of 2,4,7 rivets. Each design will use the same HSS 10x8x3/8 (part 1), Plate 1 shims (part 2 (x2 plates)), and Plate 2 (part 3). The channel and angle configurations (CL 1 & CL 2) will change with connection length.

1. HSS 10 x 8 x 3/8 - ASTM A500
2. Plate 2 - A572 Grade 50
3. Channel (C6x8.2) & Angle (L4x3x5/16) Configuration 1 (CL 1) also parts 6,8,10,12,14,16 - PROVIDED BY UW
4. Channel (C6x8.2) & Angle (L4x3x5/16) Configuration 2 (CL 2) also parts 7,9,11,13,15,17 - PROVIDED BY UW
5. A490 3/4" Structural Bolts - PROVIDED BY UW

*All units in all drawings in inches

Part 1

Top View

Front View

Back View

Right/Left View

Top View
10"
8"
$6\frac{7}{2}$"
$1\frac{11}{32}$"
$2\frac{21}{32}$"
$1\frac{11}{32}$"
$2\frac{21}{32}$"

Right/Left View
5"
6"
5"
$5\frac{1}{2}$"
9"
9"
$R\frac{1}{2}$"
Access Hole Detail
Same Access Hole Detail as above

Front/Back View
2"
$\frac{13}{16}$"
12@3"
39"
4"

205

Part 3

Top View

Side View

Top View

Side View

Part 4

Right View

Part 3

RIVETS ALREADY IN PLACE

REVISIONS
REV | DESCRIPTION | DATE | APPROVED

Part 4

Top View

Side View

Top View

Side View

Right View

Right View

Part 4

Part 3

D.2 Design for Specimens Tested in the Baldwin

The drawings for each part of the specimens tested in the Baldwin are shown in the following set of drawings. These were used in the fabrication and assembly of each test specimen.

Baldwin - 11 and 17 rivets
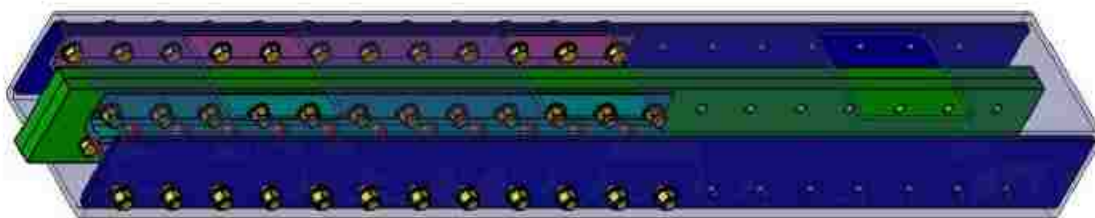
Note: There are a total of 2 designs for rivet connection lengths of 11 and 17 rivets. Each design will use the same HSS 12x8x1/2 (part 1), Plate 2 (part 2 (x2 plates)), and Plate 1 shims (part 3 (x2 plates)).. The channel and angle configurations (CL 1 & CL 2) will change with connection length.
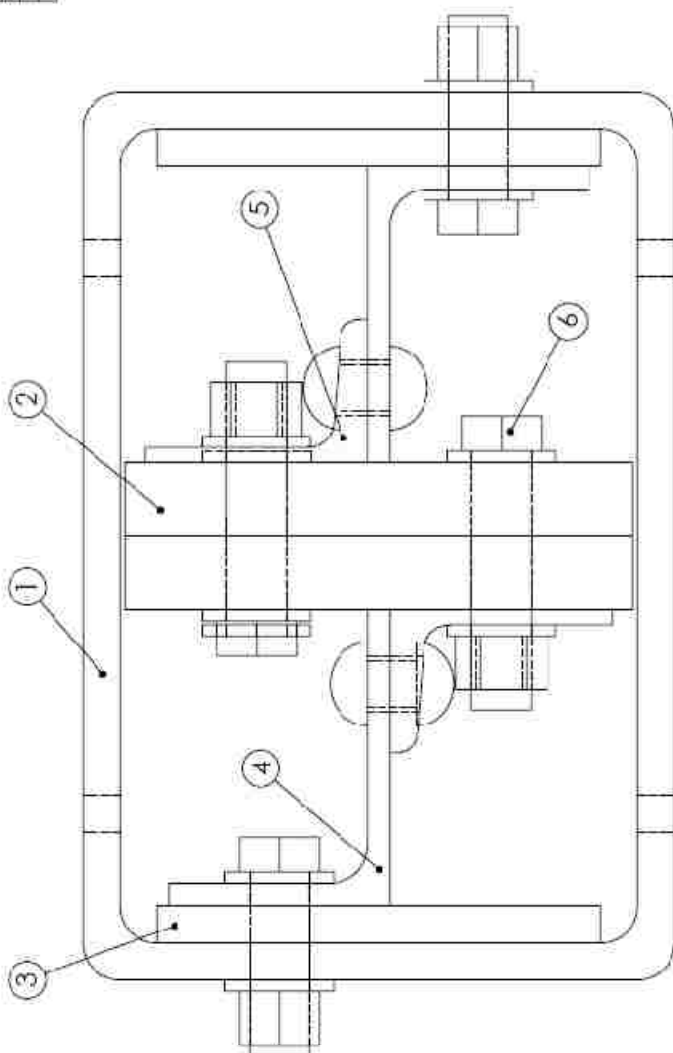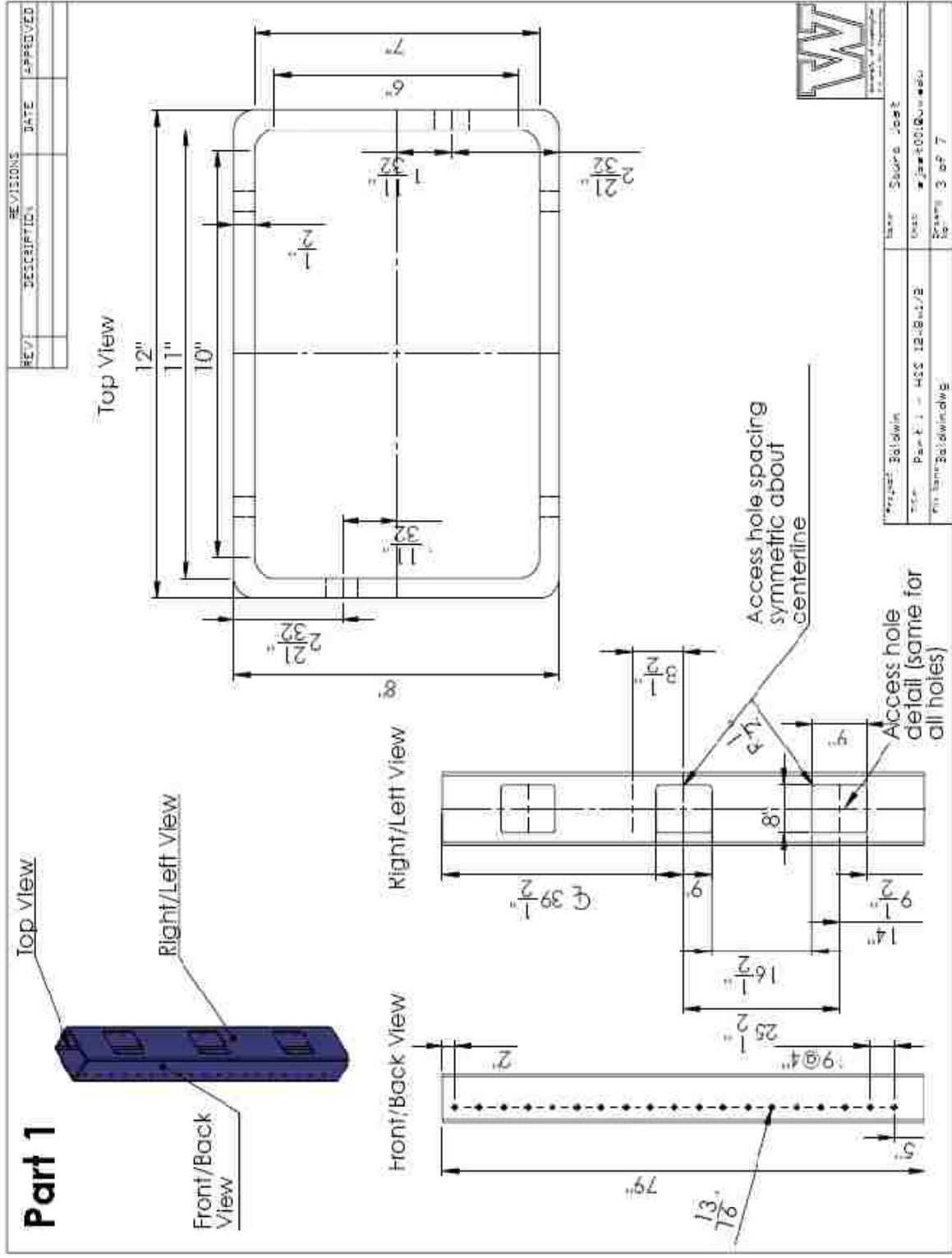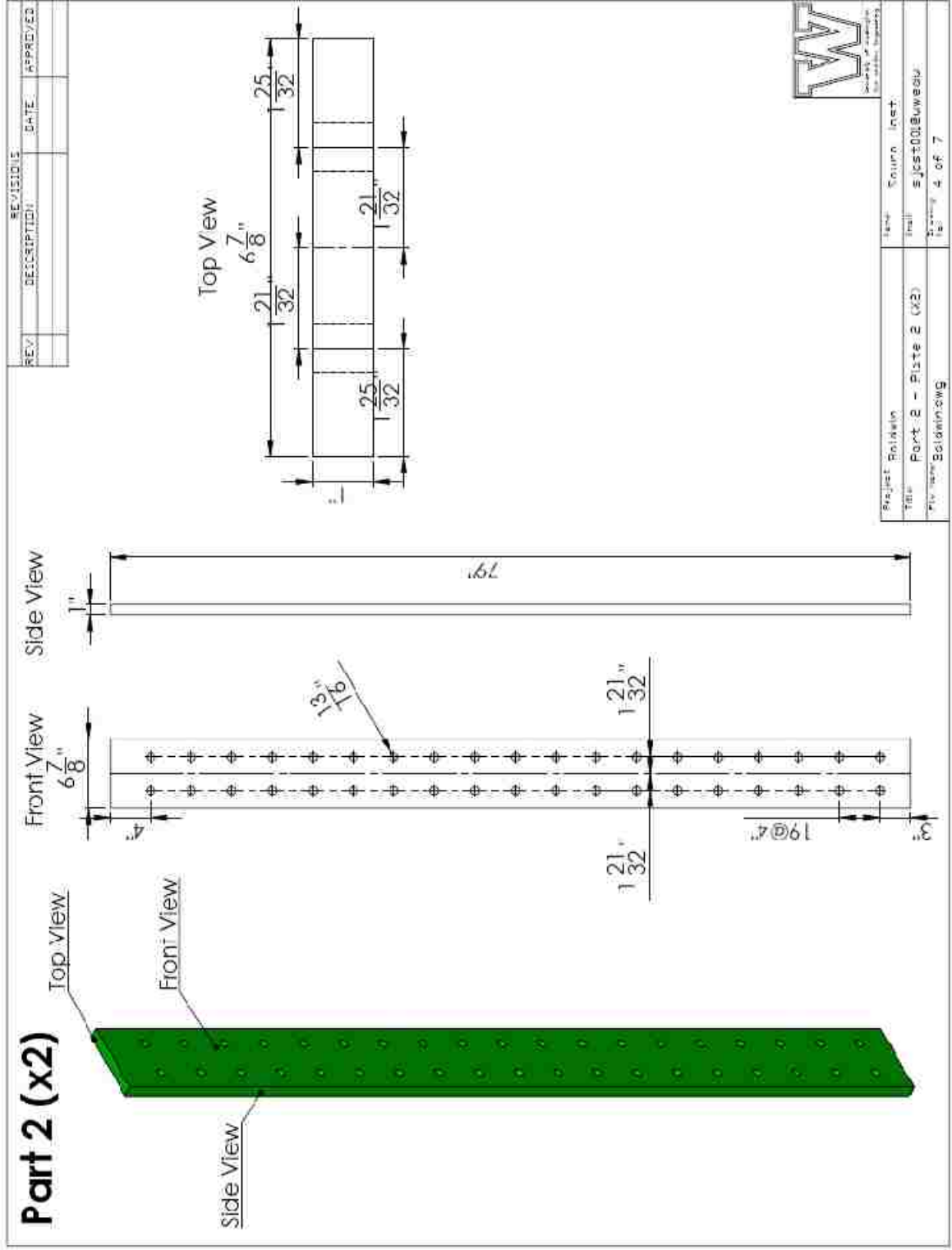
1. HSS 12 x 8 x 1/2 - ASTM A500
2. Plate 2 - A572 Grade 50(x2)
3. Plate 1 (shim)- A572 Grade 50 (x 2)
4. Channel (C6x8.2) & Angle (L4x3x5/16) Configuration 1 (CL 1) PROVIDED BY UW
5. Channel (C6x8.2) & Angle (L4x3x5/16) Configuration 2 (CL2) PROVIDED BY UW
6. A490 3/4" Structural Bolts - PROVIDED BY UW

*All units in all drawings in inches

Top View

Right/Left View

Front/Back View

Part 1

Top View

Right/Left View

Front/Back View

Access hole spacing symmetric about centerline

Access hole detail (same for all holes)

213

Part 2 (x2)

Part 3 (x2)

Top View

6"

$1\frac{21}{32}$"

$1\frac{11}{32}$"

$\frac{1}{2}$"

Side View

$\frac{1}{2}$"

79"

Front View

$\frac{13}{16}$"

19@4"

2"

5"

Top View

Front View

Side View

215

Part 4

Top View

Side View

Right View

Part 5

Right View

Part 4

Top View

Side View

AS DELIVERED

AS DELIVERED

AS DELIVERED

AS DELIVERED

$1\frac{1}{2}$"

$1\frac{1}{2}$"

Ø $\frac{13}{16}$"

$1\frac{1}{2}$"

$1\frac{1}{2}$"

2"

3"

19@4"

77"

77"

2"

2"

REVISIONS
REV | DESCRIPTION | DATE | APPROVED

Project: Baldwin
Title: Part 4 — CL 1
File Name: Baldwin.dwg

Name: Saura Jost
Email: sjost001@uw.edu
Drawing No: 16 of 3

Part 5
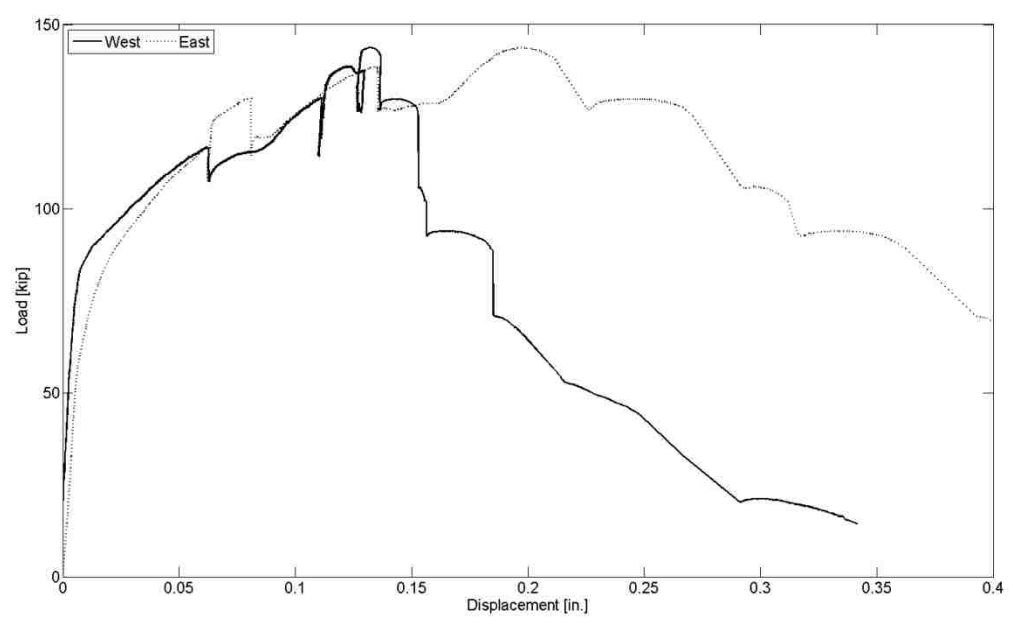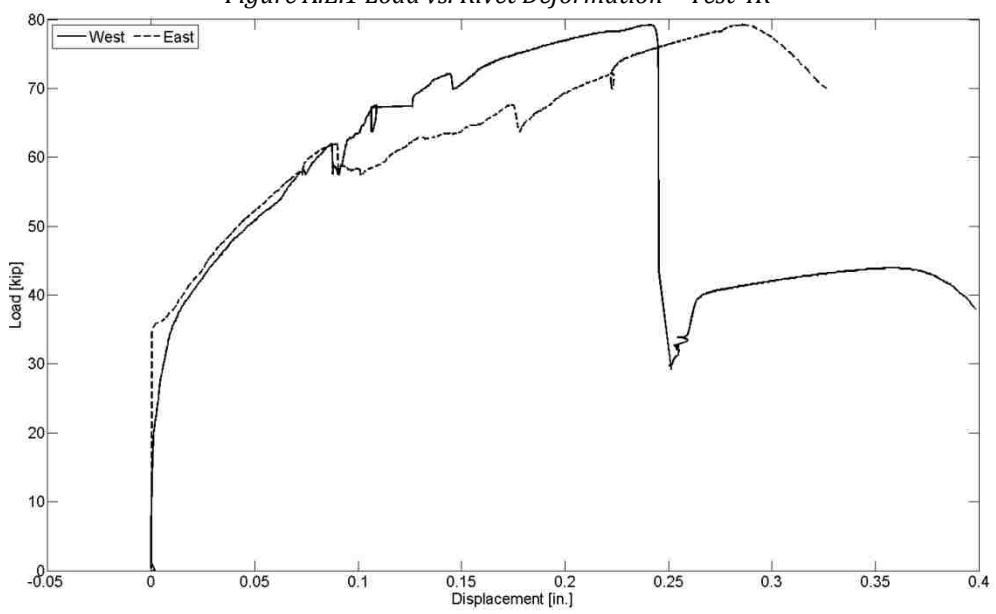
Appendix E   Additional Test Specimen Data

E.1   Load versus Rivet Deformation Plots

The load versus rivet deformation plots for each test are given in this section, where "West" represents the rivets in the west guardrail and "East" represents those in the east guardrail.

Figure A.E.1 Load vs. Rivet Deformation – Test 4R
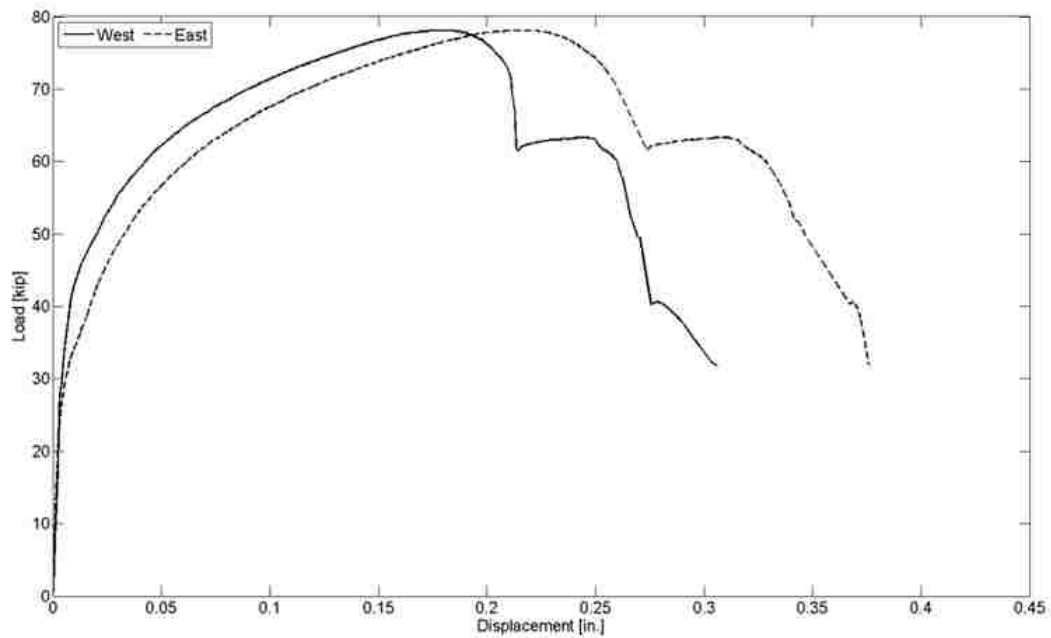

Figure A.E.2 Load vs. Rivet Deformation – Test 2R

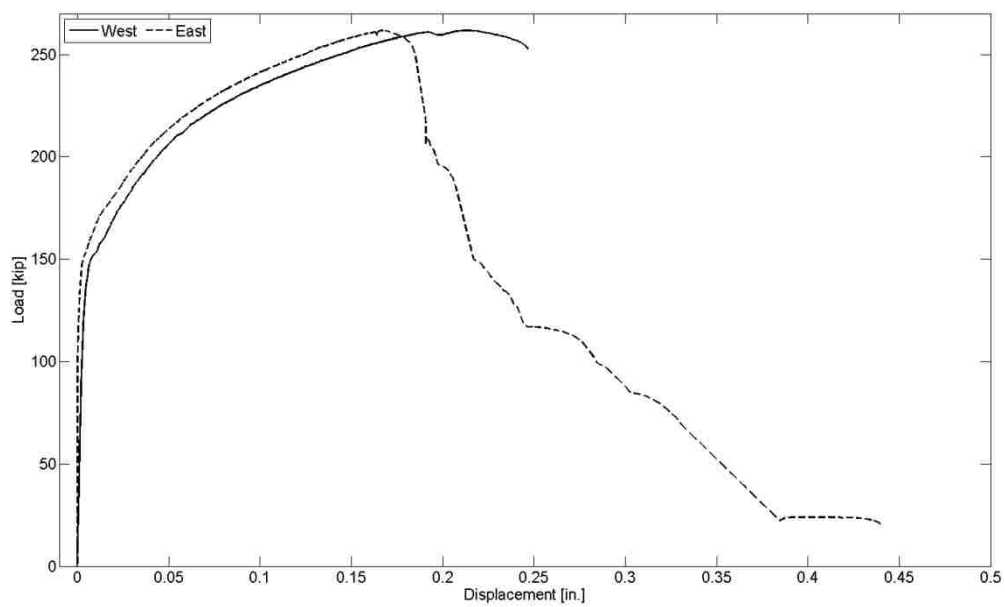*Figure E.3 Load vs. Rivet Deformation– Test 2R (4L)*

Figure E.4 Load vs. Rivet Deformation – Test 7R
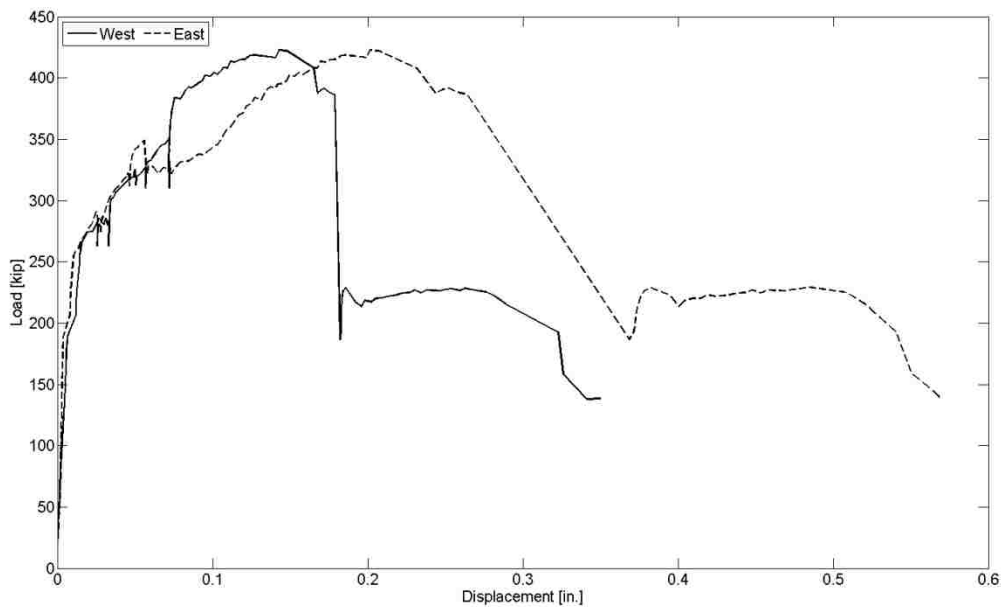
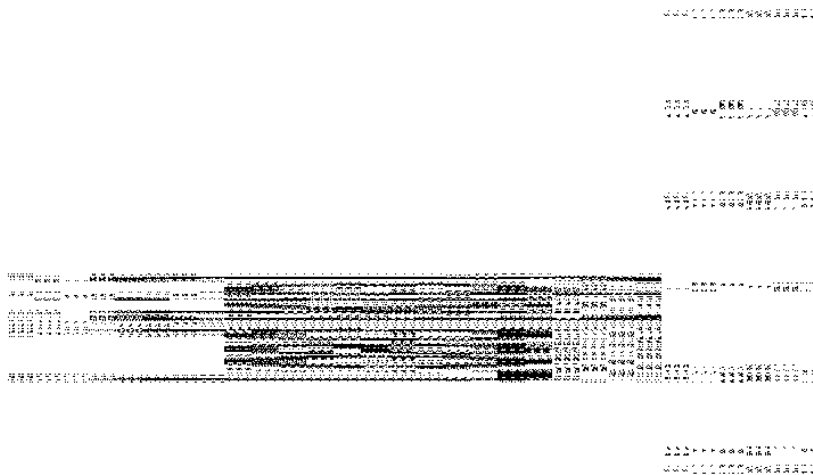*Figure E.5 Load vs. Rivet Deformation – Test 11R*

Figure E.6 Load vs. Rivet Deformation – Test 17R

E.2   Summary of Other Displacements

In this test setup, there were several displacements and deformations measured by the pots. Ideally, the overall displacement would represent the sum of such deformations. The values from the pots measuring rivet deformation, angle and channel deformation, and bolt slip, were summed to determine if this was equal to the overall displacement. They were calculated at the ultimate load and done separately for the west and east guardrail. This would account for the deformations occurring in the specimen aside from rivet deformation and improve the understanding of the test configuration behavior. The measurements were taken at the ultimate load because the pots did not function well throughout the test, therefore, the load versus shear deformation plots did not provide useful data and were not included.

For Test 4R, the overall displacement for the west guardrail was 0.5104 in. The deformation from the west channel to the angle was approximated as the difference between Pots 10 and 13 (as depicted in Figure 3.39) because they were both measured relative to the middle plate and the resulting calculation was 0.134 in. This accounts for the shear deformation at the WC-Plate interface, the net deformation at the riveted surface between the angle and channel, and the shear deformation at the angle. This value was added to the shear deformation of the WA-HSS face, which was approximated as the difference between Pots 29 and 23. This value is 0.190 and listed in row 2 of Table E.1 as shear deformation.

Table E.1 West Guardrail Deformations – Test 4R

West Guardrail		Fraction
Overall Displacement	**0.510**	of Sum
Shear Deformation	0.190	0.34
Rivet Deformation	0.133	0.24
Bolt Slip	0.238	0.42
Sum	**0.560**	
Percent Error	9.8	

Table E.2 East Guardrail Deformations – Test 4R

East Guardrail Overall Displacement	**0.498**	Fraction of Sum
Shear Deformation	0.281	0.47
Rivet Deformation	0.198	0.33
Bolt Slip	0.114	0.19
Sum	0.593	
Percent Error	19.1	

Table E.3 West Guardrail Deformations – Test 2R

West Guardrail Overall Displacement	**0.749**	Fraction of Sum
Shear Deformation	0.296	0.39
Rivet Deformation	0.199	0.27
Bolt Slip	0.254	0.34
Sum	0.749	
Percent Error	-0.125	

Table E.4 East Guardrail Deformations – Test 2R

East Guardrail Overall Displacement	**0.749**	Fraction of Sum
Shear Deformation	0.099	0.13
Rivet Deformation	0.286	0.38
Bolt Slip	0.106	0.14
Sum	0.491	
Percent Error	-34.4	

Table E.5 West Guardrail Deformations – Test 2R (4L)

West Guardrail Overall Displacement	**0.272**	Fraction of Sum
Shear Deformation	0.022	0.10
Rivet Deformation	0.185	0.85
Bolt Slip	0.012	0.05
Sum	0.218	
Percent Error	-19.6	

Table E.6 East Guardrail Deformations – Test 2R (4L)

East Guardrail Overall Displacement	0.261	Fraction of Sum
Shear Deformation	0.001	0.00
Rivet Deformation	0.223	0.97
Bolt Slip	0.006	0.03
Sum	0.230	
Percent Error	-11.9	

Table E.7 West Guardrail Deformation- Test 7R

West Guardrail Overall Displacement	0.273	Fraction of Overall Displacement
Rivet Deformation	0.211	0.77
Bolt Slip	0.027	0.10
Sum	0.237	
Percent Error	-13.0	
Approx. Shear Deformation	0.035	0.13

Table E.8 East Guardrail Deformation- Test 7R

East Guardrail Overall Displacement	0.283	Fraction of Overall Displacement
Rivet Deformation	0.166	0.59
Bolt Slip	0.023	0.08
Sum	0.190	
Percent Error	-33.0	
Approx. Shear Deformation	0.093	0.33

Table E.9 West Guardrail Deformation – Test 11R

West Guardrail Overall Displacement	0.523	Fraction of Overall Displacement
Rivet Deformation	0.143	0.27
Bolt Slip	0.345	0.66
Sum	0.488	
Percent Error	-6.8	
Approx. Shear Deformation	0.036	0.068

Table E.10 East Guardrail Deformation – Test 11R

East Guardrail Overall Displacement	**0.626**	Fraction of Overall Displacement
Rivet Deformation	0.202	0.32
Bolt Slip	0.068	0.11
Sum	0.270	
Percent Error	-56.9	
Approx. Shear Deformation	0.356	0.56

Table E.11 West Guardrail Deformation – Test 17R

West Guardrail Overall Displacement	**0.459**	Fraction of Overall Displacement
Rivet Deformation	0.227	0.49
Bolt Slip	0.043	0.09
Sum	0.270	
Percent Error	-41.2	
Approx. Shear Deformation	0.189	0.41

Table E.12 East Guardrail Deformation – Test 17R

East Guardrail Overall Displacement	**0.460**	Fraction of Overall Displacement
Rivet Deformation	0.133	0.29
Bolt Slip	0.174	0.38
Sum	0.307	
Percent Error	-33.3	
Approx. Shear Deformation	0.153	0.33

E.3   Load versus Bolt Slip Plots

The pots that measured bolt slip at the HSS-Angle and Channel-Plate interfaces functioned moderately during the test, however, in the data analysis, only the values at the ultimate load were used. The following figures show the load versus bolts slip plots when the pots gave some data.
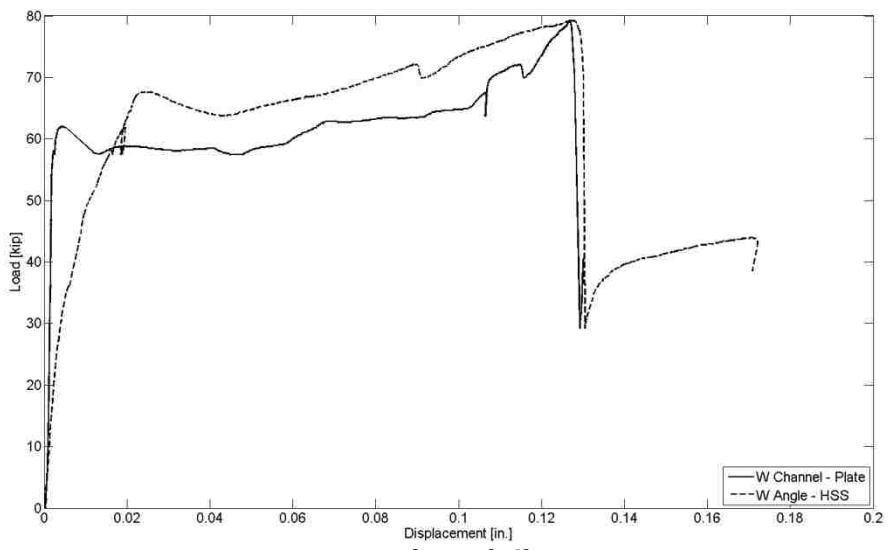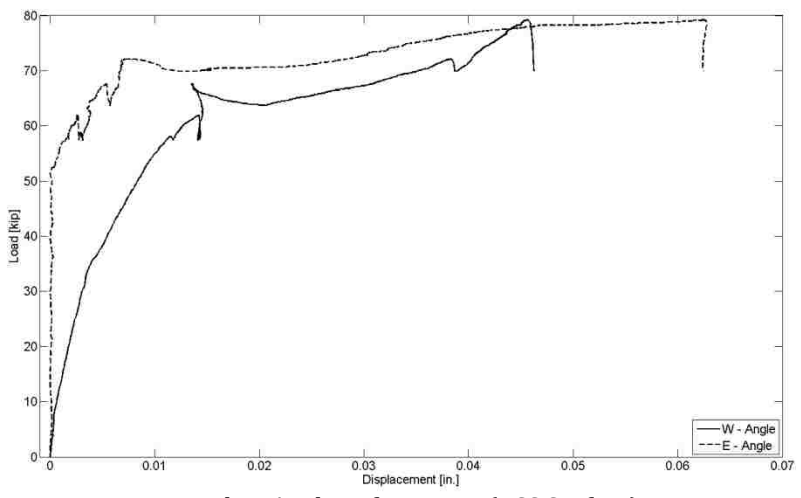

Figure E.7 Load vs. Bolt Slip – Test 2R

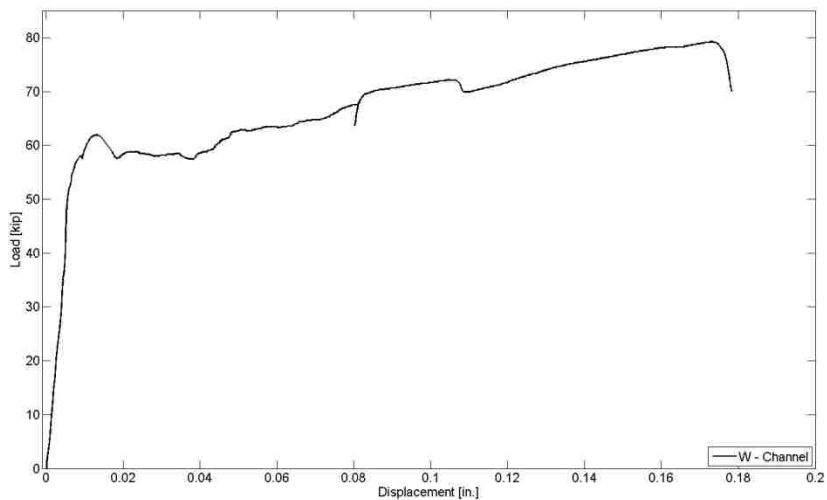*Figure E.8 Load vs. Angle Deformation (HSS Surface) – Test 2R*

Figure E.9 Load vs. Channel Deformation (Plate Surface) – Test 2R
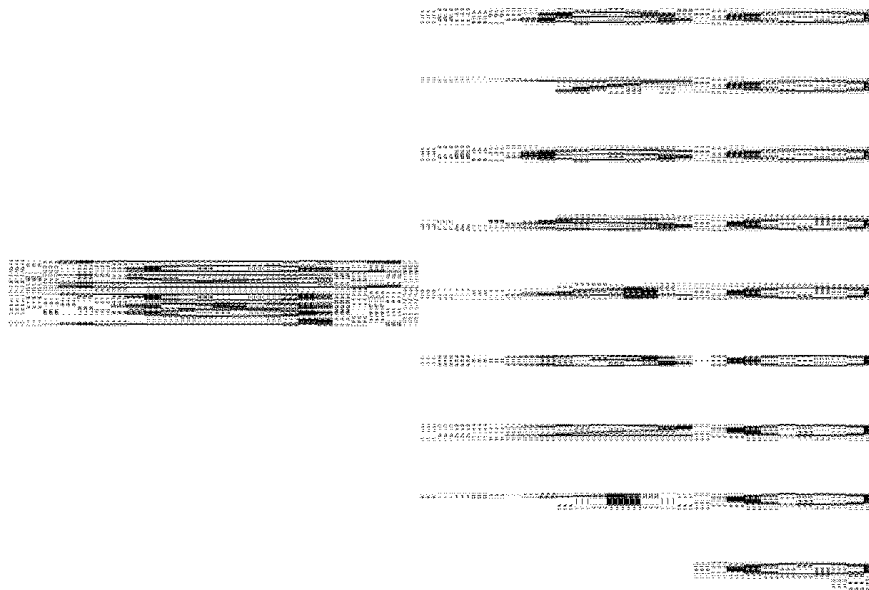
Figure E.10 Load vs. Bolt Slip – Test 2R (4L)
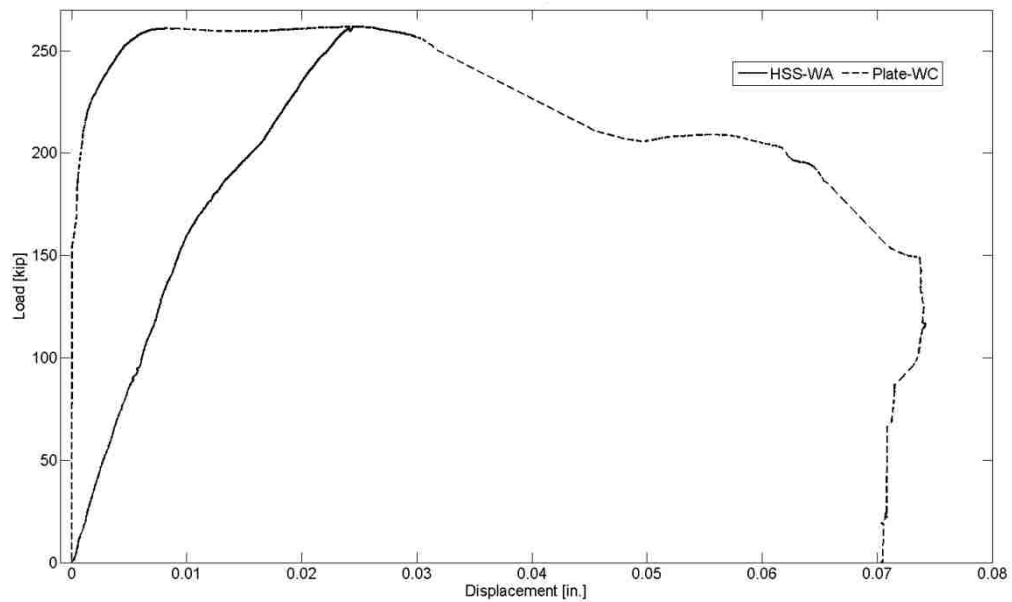
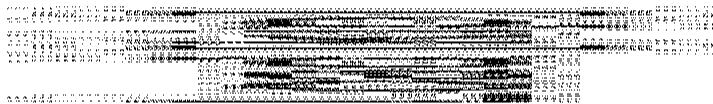*Figure E.11 Load vs. Bolt Slip – Test 7R*

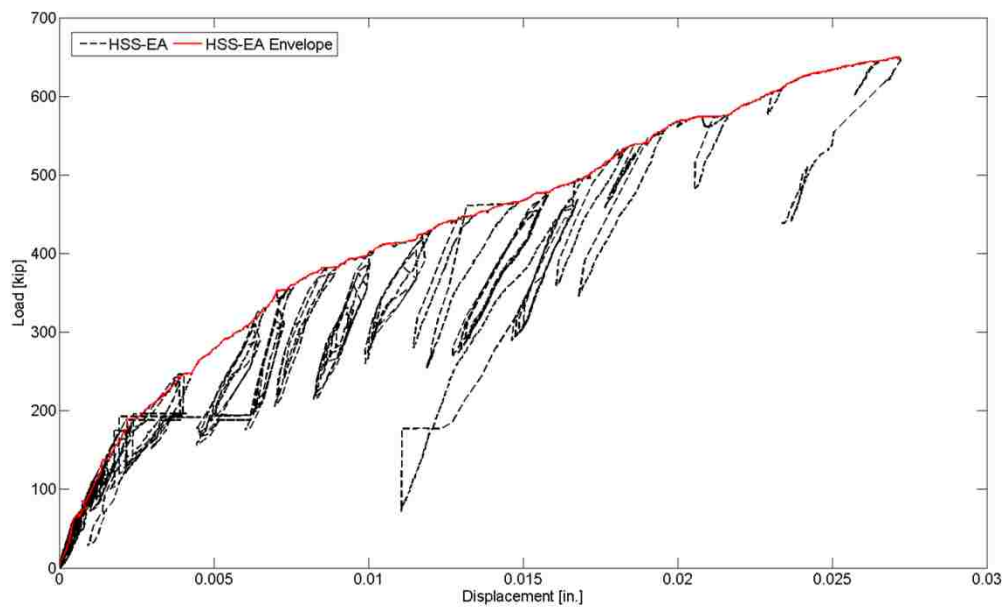*Figure E.12 Load vs. Angle Bolt Slip – Test 11R*

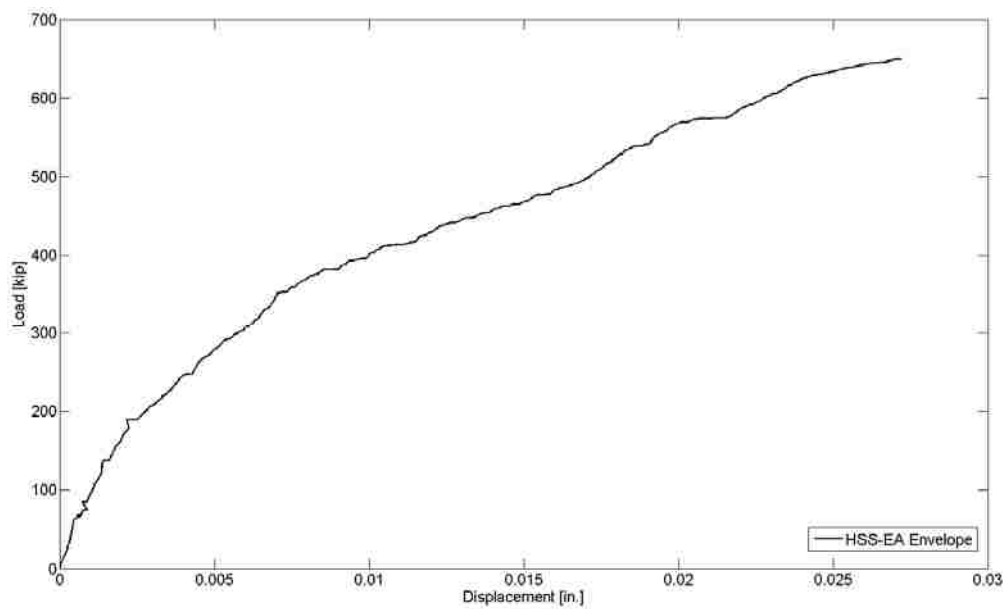*Figure E.13 Load vs. Angle Bolt Slip – Test 17R*
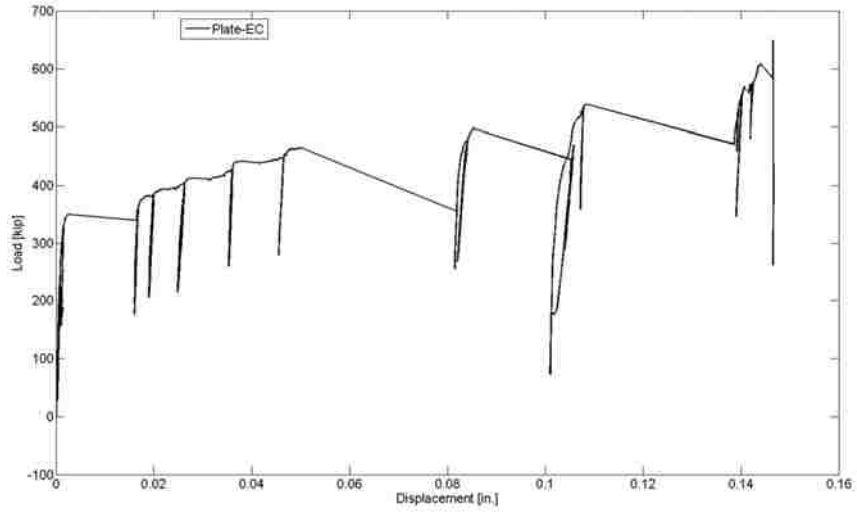

Figure E.14 Load vs. Angle Bolt Slip Envelope – Test 17R

Figure E.15 Load vs. Channel Bolt – Slip Test – 17R